ANALYSIS OF SURFACE MOUNT TECHNOLOGY SOLDER JOINTS

A Thesis submitted for the degree of Doctor of Philosophy

by

Ip Kee HUI

BSc, MSc, MIEAust, CPEng

Department of Materials Engineering, Brunel University

1996

Acknowledgments

First of all, I would like to thank Professor Brian Ralph of Brunel University for his guidance and supervision. His experience and academic knowledge have contributed much to the approach of the project. His advice on the presentation format and use of English in the thesis has enabled me to complete the project on time.

I would also like to express my gratitude to various departments and persons in the City University of Hong Kong. Thanks go to the Department of Manufacturing Engineering and Department of Applied Science, in which I performed most of the investigations. Special thanks are directed to Mr. D. F. Hung, technician in the Applied Science Department, for his generous help and advice on the topic of Scanning Electron Microscopy, and Miss S. Lee, technician in the Manufacturing Engineering Department, for her constant assistance in setting up equipment for the experiments.

Lastly, I would like to show appreciation to my family for the support and encouragement given. In particular, thanks go to my wife, Ivy, for her endurance of my long working hours throughout the entire project.

Abstract

The factors determining the quality of surface mount technology (SMT) solder joints are numerous, and complex. The exploration of these factors, and how they may affect the reliability and quality of the joints can only be achieved through continuous research. In this project, essential areas of SMT joints were selected for study and analysis, with the intention of providing additional design and process guidelines for the production of quality SMT joints.

In the infrared reflow process, one of the common defect phenomena is the occurrence of tombstoning; that is after soldering only one end of the component is soldered while the other is lifted up, assuming a position like a tombstone. The initiation of tombstoning during reflow was analysed based on the forces acting on the component. A model was developed to predict the initiation of this phenomenon. The model shows that, under vibration-free conditions, the surface tension of the molten solder is the source of the force causing the initiation of tombstoning. The contact angle, which varies with the length of the printed circuit board solder land, has a significant effect on the value of the surface tension acting as a force pulling upward on the component. The model further shows that tombstoning initiation is due to the combined effects of the surface tension; the weight of the component; the dimensions of the component; the length of the solder underneath the component; and the length of the solder protruding from the end of the component. Selected components were used as examples for predicting the conditions of initiation, and these conditions were further substantiated by a series of experiments.

Another area of study was a method which directly pulled the components off printed circuit boards and this was used as a means for testing the bond quality of surface mount technology leadless chip solder joints. Components D7243, CC1206, RC1206, RC1210, and CC1812 were selected for this study. It was found that the ultimate tensile force which breaks a component off the printed circuit board has the potential to be used as a parameter for measuring the quality of the solder joint. The effect of solder thickness on the strength of a joint has also been investigated. The shape of joints soldered by two methods, wave soldering and

infrared reflow, were compared. Joints at the two ends of a component produced by infrared reflow were found more uniform than the ones produced by wave soldering. A recommendation is made here for the wave soldering approach in achieving uniform solder joints. The effects of solder shape on the joint strength were further investigated by finite element analysis. A convex joint was found marginally more robust than a concave joint.

Two aspects of the internal structure of SMT solder joints were investigated, void content and copper/tin intermetallic compounds. The voiding conditions of wave-soldered and infrared reflow joints were compared. No voids were found in all specimens that were produced by wave soldering. However, there were always voids inside joints produced by infrared reflow. Microhardness tests indicated that the hardness of compounds at the copper/solder interface of infrared reflowed joints is lower than that in the wave-soldered joints. It is considered that the lower hardness of the interfacial region of the infrared reflowed joints is due to the presence of voids. Scanning electron microscopy was used to study the formation of copper/tin intermetallic compounds for joints produced by infrared reflow. The results show that Cu_6Sn_5 was the only compound with a detectable thickness. Other compounds such as Cu_3Sn, were virtually not found at all. Aging of the joints at 100^0C, shows that both the Cu_6Sn_5 and the overall interfacial thickness grew with time.

One of the important areas which had been overlooked previously and was studied in some details was the effects of solder paste exposure on the quality of solder paste. The characteristic changes of solder paste due to exposure were investigated in three areas, weight loss, tackiness, and rheology. The evaporation of low boiling point solvents was considered as the main contribution to the loss in the weight of the solder paste. The weight loss against exposure time was found to follow an exponential behaviour. A method was designed to evaluate the tackiness changes of solder paste due to exposure. It was found that the decay of tackiness against exposure time can be expressed by a power law. It is recommended that solder paste manufacturers should provide the necessary characteristic constants so as to enable the characteristics to be calculated after a specific exposure. The rheological changes of the solder paste as a result of exposure were also investigated. The

implication on the printability of the solder paste due to these changes was studied and discussed.

Abbreviations

PCB	printed circuit board
SMT	surface mount technology
TAB	tape automated bonding
DIP	dual-in-line package
QFP	quad flat pack integrated circuit
IR	infrared
WS	wave soldering
R	rosin
RMA	mildly activated rosin
RA	fully activated rosin
cpm	citations per million
IPC	Institution for Interconnecting and Packaging Electronic Circuits
SOT	small outline transistor
SOIC	small outline integrated circuits
FEA	finite element analysis
RH	relative humidity
IMC	intermetallic compound
SEM	scanning electron microscopy
EDX	energy-dispersive x-ray analysis
UV	ultra-violet
SE	secondary electrons
PLCC	Plastic leaded chip carrier
CFCs	Chlorofluorocarbons

List of Figures

List of Tables

Contents

Chapter 1

Introduction

1.1 EVOLUTION OF ELECTRONIC PACKAGING

Over the past few decades, the demand for miniaturisation was one of the prime movers in the advancement of the electronics industry. The trend of requiring smaller and more compact products is expected to continue. Miniaturisation, so far, has been able to advance through three technological achievements; the components, the means of interconnection (mainly printed circuit boards - PCBs), and the methods of assembly. The electronic components, roughly, have gone through three eras of development [1]:

Vacuum Tube Era	1920-1950
Transistor Era	1950-Mid 1960s
Integrated Circuit Era	Mid 1960s-Present.

As a result, the size of the components is smaller, the functional capability per unit volume of component is bigger, and the leads of components are much denser. Correspondingly, these continuous changes in component configuration and design also have generated a demand for change in the interconnection techniques. Since Dr. Paul Eisner invented the first PCB in 1936 [2], the technologies available for the fabrication of PCBs are getting more complicated and sophisticated. PCBs can be divided into three groups; single-sided, double-sided, and multi-layer. Nowadays, technology is available for the fabrication of up

to 80 layers and 0.1 mm fine track boards. As far as the multi-layer boards are concerned, four and six layers are most commonly used. The majority of PCBs are made of laminates of copper and epoxy; although ceramic substrate boards are also available. In association with the advent of component and interconnection technologies, is the beginnings of new assembly technologies. Through-hole technology has been the dominant method for connecting components to PCBs for a long time. The use of surface mount technology (SMT) started only about fifteen years ago, and it is getting more popular. The other type of assembly technology, tape automated bonding (TAB), which emerged just recently would still take sometime before it is mature and will be employed for mass production.

1.2 SURFACE MOUNT TECHNOLOGY

Due to the low melting point, relatively high strength, and good electric conductivity of tin-lead solder, it has long been used as the material for bonding components to PCBs in the electronics industry. Sometimes other materials such as silver, nickel, gold, indium and antimony are added to serve specific purposes [3,4,5]. Through-hole technology is the conventional method used for soldering in the electronics industry. The PCBs employed for the through-hole soldering consist of plated through-holes which mainly serve two purposes; one is to provide interconnections between different layers of the circuit of the substrate, and the other is to accommodate the leads of the components. Previously, the components used were those with either axial or radial leads. Dual-in-line (DIP) packages, developed later were to meet the needs of higher circuitry density. The through-hole technology of soldering basically follows the steps below:

- insertion of component onto the PCB;
- clinching of component leads;
- soldering by passing through solder bath;
- cleaning of soldered assembly.

Fig. 1.1 shows components soldered by the through-hole method. However, with the

advent of the microprocessor and the growth of computer technology, circuit complexity has grown to a point that through-hole technology can no longer meet the requirements. Nowadays, it is very common that an integrated circuit has over 100 leads, and the through-hole technology which is limited by the distance between the centres of two adjacent holes (2.54 mm), becomes very inefficient. The SMT is a technology developed to overcome some of the limitations and problems with the through-hole technology.

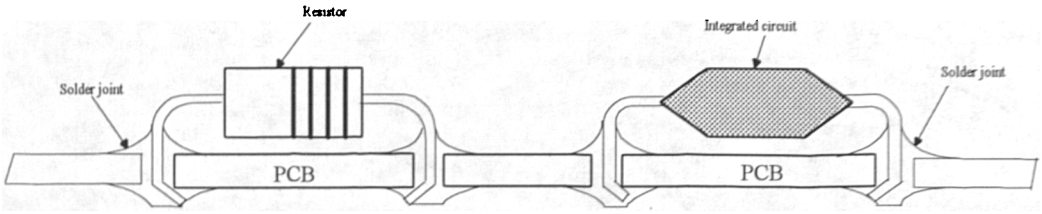

Fig. 1.1 Through-hole technology solder joints

Unlike the through-hole technology, components with SMT are soldered directly on the surface of the PCB, Fig. 1.2. In SMT, basically there are two methods of soldering. The first method, Fig. 1.3, follows the operational sequence of screen printing, component placement, reflow, and cleaning. In the screen printing operation, through the apertures of a metal stencil or a screen, solder paste is printed onto the predetermined pad positions of the PCB. The solder paste is a mixture of the metal powders (mainly tin-lead), flux, and solvent vehicles. Components are placed onto the printed positions usually by machines. The tackiness of the solder paste holds the components in place for further possessing. Heat is then applied to the board which activates the flux and turns the paste into solder. Different means are available for the application of heat to the board. In a mass production process the most common ones are the infrared reflow (IR) and the vapour phase reflow. In both of these two heating processes, a specific temperature profile has to be used for a particular configuration of boards to give a consistent and desirable quality product. A laser technique has also been employed for this heating purpose more recently. The advantage of laser soldering is that the laser is focused only on the joints and this avoids thermal shock to sensitive components and boards [4], but the draw-back is that it is a slow process as each

joint has to be heated up individually [6]. The residue from the flux after reflow is usually removed by washing, although some non-clean pastes are available on the market.

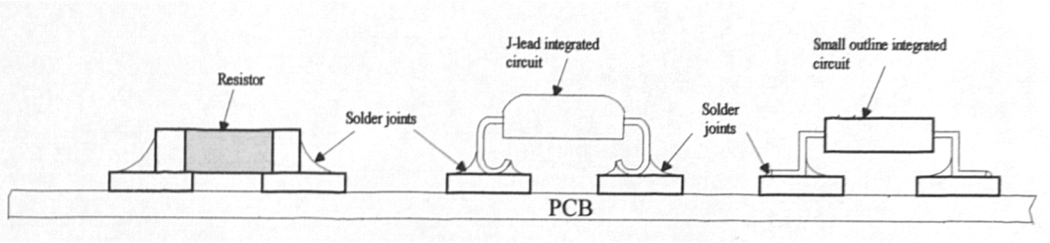

Fig. 1.2 Surface mount technology solder joints

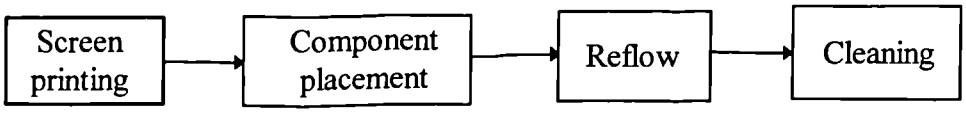

Fig. 1.3 SMT reflow process

The second method, Fig. 1.4, which is widely used in Japan, follows the operational sequence of adhesive dispensing, component placement, curing, wave soldering, and cleaning. Usually, in this process, dispensing of adhesive and placement of components are both performed by machines, only very small batches and rework are performed manually. The viscosity and tackiness of the adhesive should be able to hold the components in position during the transport of the board for the next operation. The adhesive is then cured by the application of heat, or UV light, or a combination of the two [6,7]. The board is then inverted and passed through a solder bath. The cleaning operation is carried out in the same way as in the first method. Comparing with through-hole technology, SMT has more problems in cleaning because its component configurations which stop the cleaning liquid from accessing some hidden areas to perform an effective cleaning.

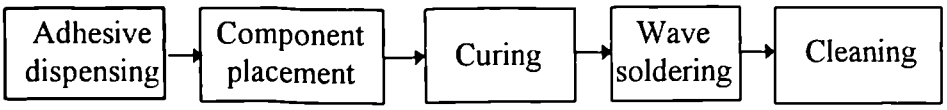

Fig 1 4 SMT wave soldering process

The term interconnectivity is defined as the number of electric connections that can be realised per unit area on the PCB [2]. SMT provides great improvements in this respect. Since components of SMT are soldered on the surface of the boards, the lead size and pitch can be much smaller as compared to those of the through-hole technology. For instance, in a 100 pin quad flat pack (QFP) integrated circuit, the pin width and the pitch are only 0.2 mm and 0.65 mm respectively [8]. With the introduction of SMT, the limitations imposed by the hole size and the lead diameter of through-hole technology are completely eliminated The reduction in component size and the increase in the interconnectivity of SMT also result in an overall reduction in material usage and costs. Automation is particularly suitable for SMT, which, on the other hand is more suitable for mass production In addition, SMT possesses other benefits, these include better circuit performance, improved shock resistance, and increased factory space utilisation [7].

1.3 OBJECTIVES AND INVESTIGATION

Although SMT is being used widely in manufacturing, as it is a relatively new technology, there are still large areas requiring further understanding and exploration. Comparing to the through-hole technology, SMT has far more process variables. A small change in any one of these variables is sufficient to alter the quality and reliability of the product [4]. Because of this, the chance of producing a defective product is higher and the job of providing a consistent process control is more difficult in SMT. To overcome these problems and to make SMT more effective, more understanding about the relation between the process variables and the product quality is desirable. Furthermore, for through-hole technology, the effects of PCB design on the quality of solder joints are much less severe.

However, for SMT, the PCB land geometry and orientation have a much higher impact on the reliability and quality of the joints [9,10,11], and this is another area in SMT worthy of more detailed investigation.

The project described in this dissertation has performed research in some of the essential areas of SMT. The objective is to provide scientific analyses and answers to the problems related to these selected areas. A summary of the work is given below:

- SMT quality increases the packaging density in the electronics industry, but on the other hand, it has introduced a new range of defects, many of their causes and methods of remedy are still not yet known. One of these defects is tombstoning, which occurs when one end of the component lifts up leading to an open-circuit. An analysis as to the causes of this type of defect is given, and at the same time, by taking into consideration such factors as surface tension of the molten solder, PCB land design, component weight, and component geometry, a model has been developed for the prediction of the occurrence of tombstoning for leadless chips. This model has been verified by a series of experiments. This part of the study is self-contained and described in Chapter 3.

- Because there was a lack of a quick and direct method for SMT solder joint reliability testing, the feasibility of using a pulling test for this purpose was studied. A test method was designed, and was used to test a range of selected components. The strength of concave and convex joints were compared and analysed by the use of finite element analysis (FEA). The effects of solder thickness of a joint were also investigated. Chapter 4 covers this part of the investigation.

- The characteristics of solder joints produced by the two most common methods, IR reflow and wave-soldering (WS) were investigated. The geometry of these two types of joints were compared in some detail. The formation and the resulting quality of different shapes of joints were analysed. Chapter 5 reports this part of the investigation.

- It is recognised that if a solder paste is exposed to the atmosphere for too long, its

quality would be impaired. However, exactly what sort of changes are taking place during exposure, what characteristics are affected by the exposure, and how the changes in characteristics would affect the printing, the subsequent operations, and the final quality of the joints still need investigation. A systematic study of these effects is given in Chapter 6.

- Chapter 7 looks at the intermetallic compounds formed in SMT solder joints. Both conventional light microscopy and scanning electron microscopy were used for this part of the investigation.

Chapter 2

Literature Search

2.1 INTRODUCTION

The aims of this literature search are mainly to:

- appreciate SMT and its existing difficulties;
- identify the topics where research would be valuable and necessary;
- have a full picture of the past work related to the research topics selected;
- ensure that the specific selected research work has not been performed by others..

Since the research did not touch upon the operations of placing components and cleaning of assembly boards, no literature search was performed in these two areas. The literature search on the printing operation was mainly concentrated on the use of metal stencils because this technique is more widely applied and was used for performing part of the experiments in this project. Moreover, as IR is the most common reflow method in SMT and was used in this project, as far as the reflow process literature search was concerned, it was mainly concentrated on the IR method. The information obtained from the literature search is presented under four headings: *solder paste, stencil printing, defects and reliability, and intermetallic compounds at joints.*

2.2 SOLDER PASTE

Solder paste is basically a mixture of the alloy powder, flux, and a vehicle. The alloy powder after reflow becomes the solder of the joints. The majority of the alloy powder used is from the tin-lead system, although other alloys are also used. There are a variety of fluxes being used in commercially available solder pastes. The common ones are rosin (R), mildly activated rosin (RMA), and fully activated rosin (RA). R is the weakest whilst RA is the one with the highest flux strength among the three. R flux contains only rosin without the presence of an activator. RMA and RA contain rosin and an activator system. The activator for RA and RMA fluxes usually is halide [12], however for RMA, the halide content is less than 0.5 %. The most common type of flux used in the electronics industry is the RMA. There are other types of flux such as those containing synthetic resins, but because of their corrosive nature, these are not being used in the electronics industry. The flux serves several functions: removal of oxide films on the metal surfaces and the powder, removal of contaminants in the joints, and to lesser extent, it acts as a heat transmitter. The flux acts as a cleaning agent of the joint surfaces to allow good solder wetting [13]. The vehicle comprises the solvents added to provide the necessary rheology and to activate the flux. The use of which type, or group, of solvents varies from manufacturer to manufacturer. One basic requirement is that the solvent has to be compatible with the flux. It is expected that the vehicle has significant effects on the quality aspect of the joints, but so far, little information has been published. This opens up a major area for future investigations. In general, the vehicle consists of glycols, and hygroscopic products [14]. The types, and the relative amount of alloy powder, flux, and vehicle used, are the major factors determining the characteristics of the solder paste. It was found that the characteristics of the solder paste are directly related to the problems which occur in the printing, component placement, and even reflow operations of SMT.

2.2.1 Powder Content

The powder content of a solder paste can be verified by the method specified by the

Institute f r Interconnecting and Packaging Electronic Circuits (IPC) [15] The powder content usually ranges from 85°o to 90°o It has been found that the percentage of alloy present determines the shape and strength of the resulting joints An increase in the alloy c ntent results in a higher strength and a larger fillet size [16,17] This is because after the reflow, f r a particular thickness of paste printed, paste with an increased powder content w ll g ve a larger s zed and hence a str nger joint Fig. 2.1 shows the fillets of a gull-wing and a leadless ch p The amount f alloy also affects the rheology, and the printability of

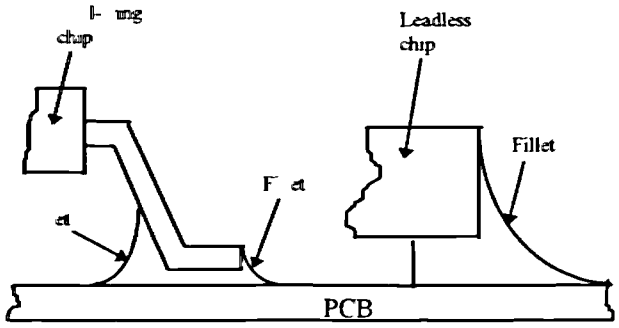

Fig 2 1 Fillets of gull-wing and leadless chips

the paste An increase in the alloy content in a fixed volume of paste gives a corresponding ncrease in the paste viscosity [18,19] This increases the difficulty of the paste to pass through the fine screen or stencil A paste with a high alloy content requires a larger printing pressure, and also increases the chance of clogging For this reason, the damage rate to the screen is higher Stein, *et al* [20], discovered that with the same mesh size of powders in the pastes, the paste with an 85°o alloy content printed more easily than the one with 90°o. also, it printed for longer without drying out. If tackiness is to be maintained in a situation that the lag time between printing and attachment of components is long, solder paste with a low alloy content is required [3,21] Since the amount of alloy and the amount of flux and solvent in the paste are interrelated, a decrease in alloy content would result in an increase in the flux and solvent content It was reported that paste with a low alloy content resulted in more v ids and slumps [17,19,22]. Slumping is a phenomenon where the paste spreads ut of its printed position Fig 2 2 shows a slump condition. Large slumps might eventually lead t bridging between two adjacent leads Warwick and Steen

[23], consider that a high alloy content and a small powder size both reduce the powder spacing which in turn causes an increase in viscosity. This paper further pointed out that the alloy content was the most important factor for controlling slump and an increase in alloy content produced less solder balls. This is further supported by the findings by Stein, *et al.* [20]. Solder balling is a type of defect that occurs during soldering, where satellites of solder are carried away by the flux and become adhered to the periphery of a joint, Fig. 2.3. If the amount and size of the balls are large, bridging of circuits may result. However, better solder wettability was found with a decrease in the alloy content. The increase in the flux content thus increasing the oxide removal strength, explains the better wettability phenomenon [24].

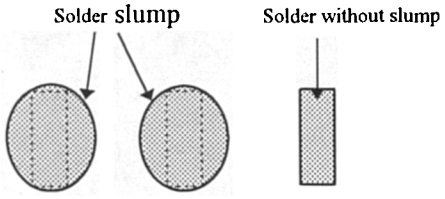

Fig. 2.2 Solder slump

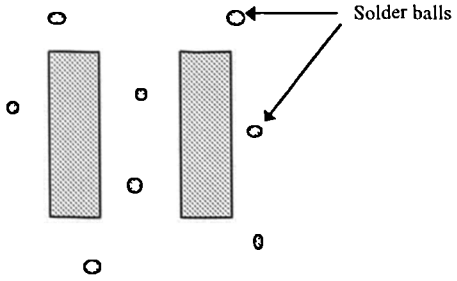

Fig. 2.3 Solder balls

2.2.2 Powder Morphology

Shape and size of the powder particles are also quality determining factors for SMT joints. The powder size is usually specified by its mesh size. Powders designated as -200+325, for instance, means that the powders can pass through a 200 mesh but not a 325 mesh. Powders designated only by a maximum size, such as -325, means that no particles are larger than the mesh size of 325. Solder powders are available in various sizes, e.g. -325, -270, -250, and -200 [25]. The approximate dimensions for various meshes are shown in Table 2.1 [6]. There are different ways of analysing the shape of powders. Scanning

Mesh count (per 25.4 mm)	Wire diameter (μm)	Mesh opening (μm)
200	41	86
250	41	61
270	36	58
325	28	51

Table 2.1 Dimensions of various meshes

electron microscopy and an image analyser are particularly useful for this purpose. A number of papers have been published relating the powder morphology to the quality of joints. The findings may be summarised as follows:

- The size and shape affect the printability of the paste. Small and spherical powders pass through the screen and stencil more easily [23]. Irregular and elongated particles cause clogging to the printing device and to syringes [19,26]. However, a small powder size reduces the paste inter-particle spacing, causing viscosity to increase [18,22,23]. It has been recommended that for paste which is to be applied by screen printing, the solder particles should be spherical and with sizes from 15 to 55 μm. For paste applied by stenciling, slightly larger and more irregular particles can be used [25]. The ideal particles for printing are uniform in size and spherical in shape, and the screen opening should be at least three times the size of the particles to avoid blockage [26,27].

- Powder morphology is strongly related to the amount of solder balls Fine powders are more easily flushed away by the melting flux during heating and thus form solder balls more readily Stein *et al.* [20], showed that very fine particles (less than 10 μm) may be carried away by the melting flux from the printed locations before the solder melts and coalesces. Solder ball formation is also related to the surface area of the particles. Small and irregular particles give larger t tal powder surface area, which means larger oxide content, and as a result this increases the likelihood of solder ball formation [4,17,19,21,28] Warwick and Steen [23], found that solder balling and solderability are correlated with alloy content, powder size and storage time of the paste.
- Small and spherical powders print better, but on the other hand they increase the likelihood of giving slumps Irregular and elongated particles inter-lock with each other and do not flow as smoothly as the spherical particles. This inter-locking characteristic inhibits the spread of the paste and reduces the degree of slumping [3,22,24].

2.2.3 Rheology

Solder paste is a non-Newtonian, thixotropic, and pseudoplastic fluid. It exhibits a yield point Non-Newtonian behaviour implies that a solder paste when subjected to shear does not flow in a laminar manner [12]. Thixotropic means that the solder paste will change its viscosity over time at a constant shear rate, furthermore, the shear rate-shear stress curve is in the form of a hysteresis loop. The thixotropic nature of solder paste is exemplified by Figs 2 4(a) and (b). Pseudoplastic implies that the paste viscosity would drop when subjected to shearing, but when a shear force is removed the viscosity would recover over time [22]. The thixotropic nature of solder paste is undesirable as it causes the viscosity to change and becomes unpredictable after different degrees of agitation due to mixing, handling, or printing. A knowledge of the viscosity of the paste is considered as one of the important factors to result in good quality of print. However, its pseudoplastic nature helps in recovering the viscosity, otherwise the low viscosity of the paste would persist and generate defects such as slumps and bridges. A number of viscometers can be used for measuring the viscosity of solder paste. The common ones are the Brookfield,

Ferranti-Shirley, and Malcom. The viscosity of a fluid is defined by the relation between the shear stress and the shear rate, and is in the form of:

Viscosity Shear stress/Shear rate.

The common viscosity unit is Pa.s. The reciprocal of viscosity is the fluidity [29]. The viscosity of solder paste during application is believed to behave as shown in Fig. 2.5, [16,18]. During stirring, squeegeeing, and screening there is a drastic drop in the viscosity.

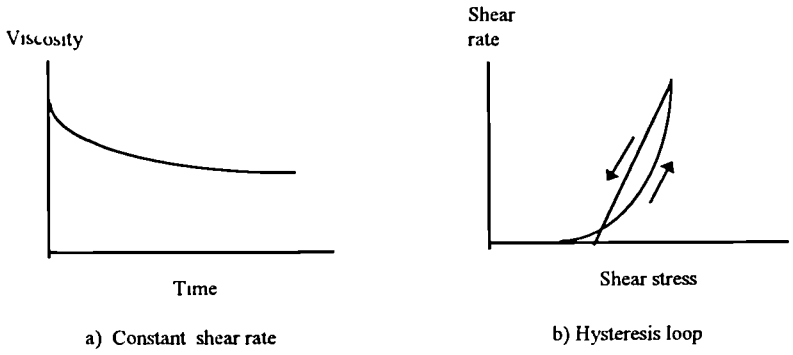

Fig. 2.4a-b Thixotropic behaviour of solder paste

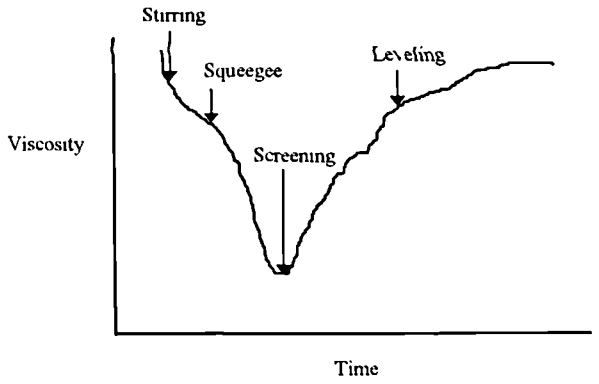

Fig. 2.5 Solder paste viscosity change during printing

At the stage of leveling, when the shear stress is removed, there would be a rapid recovery in the viscosity. The viscosity determines the printing quality, and it is directly affected by printing speed, leveling time, and printing environment. Viscosity versus shear rate is usually expressed in logarithmic form, and has been found to have a linear relation. In the Malcom system, the thixotropic index (T) is expressed by the slope of the line, and the hysteresis characteristic is expressed by the non-recovery rate (R), [23], where

$$T \quad \log(\text{viscosity at } 1.8\ s^{-1}/\text{viscosity at } 18\ s^{-1})$$

$$R = \frac{\text{viscosity at } 6\ s^{-1} \text{ (increasing shear)} - \text{viscosity at } 6\ s^{-1} \text{ (decreasing shear)}}{\text{viscosity at } 6\ s^{1} \text{ (increasing shear)}}$$

Parekh, [17], used the term shear sensitivity factor to define the slope of the viscosity versus shear rate log-log graph. In this paper, Brookfield viscosity measurements were used, and they indicated that to provide a good printing quality, solder paste with a suitable sensitivity factor is important. When the sensitivity factor is too high the paste could thin down too rapidly and lead to printing defects like slumps, solder balls, and bridges. But, on the other hand, if the sensitivity factor is too low, especially with a high initial viscosity, a lot of difficulties would be encountered during printing. As mentioned before, the viscosity of solder paste is affected by the powder morphology and the metal content [18,19,22,23]. Evans and Beddow [22], found that thixotropy fluctuated with alloy content experimentally. At similar thicknesses, pastes with low alloy content exhibited greater thixotropy. The logarithmic scale of shear rate versus shear force exhibited a power law relation. The age of the solder paste and the process environment are also factors determining the rheology. The viscosity decreases with an increase in temperature [12]. Warwick and Steen [23], showed that the viscosity increased with storage time.

2.2.4 Tackiness

Tackiness is how long the paste can maintain its ability to hold the components in position. It is very common in industry that there is a time lag in between the placement of components and the reflow operation. It is crucial that the paste possesses the correct tackiness so that the components will not be shifted off position before reflow takes place. Tackiness is considered to be affected by solvent, flux, and particle size. The ambient temperature and humidity also play an important role [17]. Gutllaume *et al.* [14], discovered that humidity plays a major role in maintaining the tackiness. The tackiness can be preserved longer if the printed paste is kept in a dry atmosphere. Tackiness can be measured by following the IPC standard [15]. Other methods are also available for this purpose [12]. Warwick and Steen [23], reported that the tack force increased as a function of time after printing up to a maximum value. This peak tack force was independent of the age of the paste and alloy content. However, there was an indication that it increased as the powder size was reduced. The tack time, defined by Warwick and Steen as the time required to fall from the peak tack force to 0.5 g mm $^{-2}$, was found to be directly related to the storage time. It fell progressively through-out the storage of the paste. No relationship between the tack time and particle size was found. Morris, [30], did a fairly comprehensive investigation on this aspect. It was found that the tack force, the force required to pull the test probe out of the solder paste, increased with the preload, and the increase was more profound with a longer dwell time, Fig. 2.6. This suggests that a slight force is desirable to

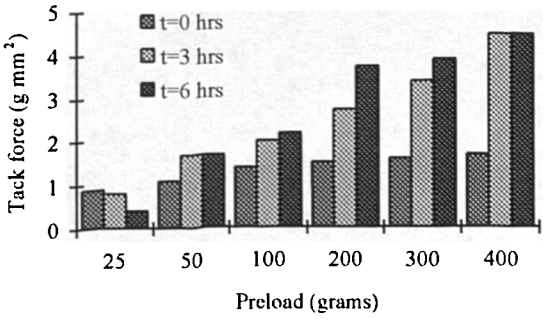

Fig. 2.6 Tack force versus preload

push the component into the paste during component placement. Morris [30] found similar behaviour to that reported by Warwick and Steen [23], that the tack force increased with the deposit age then decreased after reaching the peak, and in addition, the paper reports that the tack force was also a function of the paste deposit depth, as indicated in Fig. 2.7.

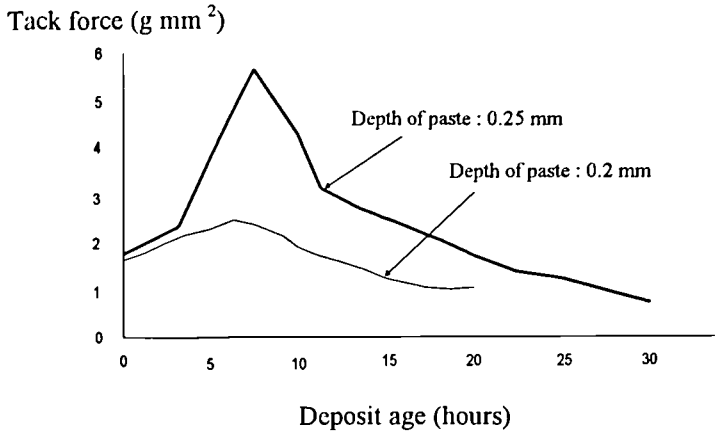

Fig. 2.7 Effects of paste age and depth on tackiness

2.3 STENCIL PRINTING

There are two common methods of depositing solder paste on PCBs, screen printing and stencil printing. Usually stencils are made of stainless steel or brass foil. For large scale production, a stencil is preferable because it lasts much longer and prints better. The goal of stencil printing is to deposit equal and the right amount of solder onto the pads of a particular device. The printed solder paste should sit squarely on the pads and with constant thickness. Markstein [31] considered that the success of a print depends upon the following factors:

- solder paste viscosity
- solder paste particle size
- solder paste particle shape
- solder paste vehicle rheology

- susceptibility of solder paste to slump
- solder paste percent alloy content
- flux type and activity
- thixotropic index
- susceptibility of paste to thixotropic breakdown when worked repeatedly
- stencil thickness
- stencil material
- stepped or uniform thickness stencil
- aperture size
- aperture shape
- aperture arrangement
- aperture aspect ratio
- whether sidewalls are electropolished
- snapoff distance
- squeegee pressure
- squeegee speed
- squeegee angle
- squeegee blade cross section
- squeegee hardness
- squeegee material
- solvent evaporation or absorption when exposed to air
- ambient temperature
- ambient humidity
- stencil/board registration
- registration repeatability
- unidirectional of dual-directional printing
- stencil cleaning frequency

Missele [32] holds similar opinions on the factors determining the success of stencil printing, only all the above are grouped under five major categories, solder paste

characteristics, solder stencil characteristics, printing machine, squeegee, and setup. A lot of the information presented in these two papers [31,32] are only conceptual opinions which need further scientific studies.

Morris, [33], did some investigations on the stencil printing of solder paste for fine-pitch SMT. The paper suggests that the diameter of the largest particle should not be larger than one-half of the smallest dimension being printed. For a 0.102 mm thick stencil, the largest solder sphere should be less than 0.051 mm. Stencils with a special configuration, but of different thicknesses, 0.102 mm and 0.152 mm, were employed for carrying out the printability test for six solder pastes. It was found that the pastes reached an equilibrium viscosity approximately after ten prints. The 0.102 mm (4 mil) thick stencil produced finer minimum pad widths than the 0.152 mm (6 mil) stencil. It is believed that the smaller wall surface area of the 0.102 mm stencil makes it better for finer prints. Markstein [31] recommends that the aspect ratio, that is the ratio of the stencil thickness to the aperture width should be 1:1.5, or less. A trapezoidal shape aperture for ease of paste release, and matted stencil surface to facilitate the rolling of the paste are also recommended. While it is important to have the viscosity low enough to ensure ease of flow through the aperture, it is equally important to maintain a suitable viscosity to allow the paste being held in place so that slump or bridging does not occur. Morris [33] found that pastes with higher thixotropy values can print finer patterns, and pastes with higher resistance to flow from rest, which measured by their yield points, are less likely to bridge due to slump at room temperature. These characteristics are indicated in Fig. 2.8 and Fig. 2.9 (from Fig. 6 and 7 respectively of Morris' paper), where A,C,D,E,F,G are the six pastes with different thixotropy and yield stress values. Printings may be performed with the PCB pads' long axes parallel or perpendicular to the squeegee travel direction. It was found the latter gave more slumps due to greater deposition volume. Since it is realised that the quality of prints is related to the aspect ratios, with different pad widths on a single board that may vary from 3.2 mm to 0.35 mm, the most desirable stencil is the one with varied thickness. Stepped stencils were reported to be used and produced desirable printing results [31,33].. Stepped stencils can either be manufactured by etching or by lamination of foils. Usually stainless steel and brass are used as stencil materials, but beryllium-copper and nickel-plated copper are also

occasionally used.

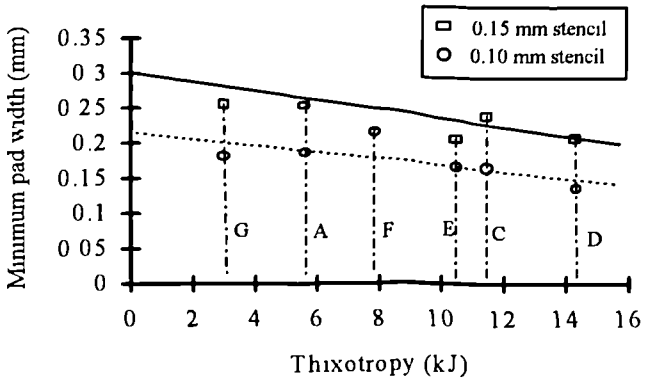

Fig. 2.8 Relationship between minimum pad width and thixotropy

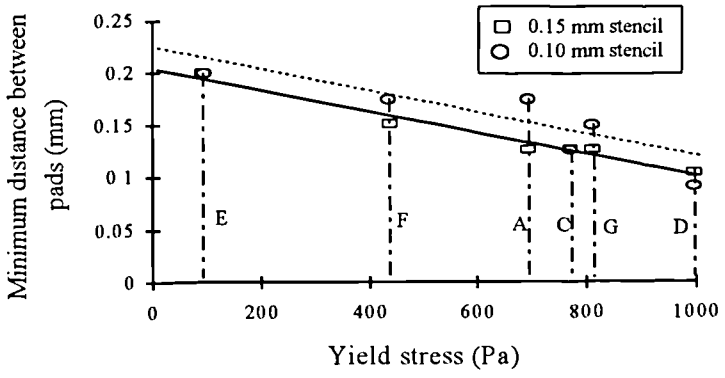

Fig. 2.9 Relationship between minimum pad separation and yield point

Squeegees for stencil printing, conventionally are made of polyurethane with a hardness ranges from 75 to 95 on the Shore "A" scale. However, for stepped stencils, it

was found that hardness ranges from 75 to 85 perform better, because a softer material allows the squeegee to follow the stepped contour of the stencil. Square and rectangular cross-sectioned squeegees are more commonly used, Fig. 2.10. Both were found to give desirable print quality, while the rectangular ones were found to possess a better ability to follow the topographical variations. This is due to the fact that the pressure of a rectangular squeegee is from the bending, as compared to a square one which is directly from the vertically applied force. Printing defects and solder paste evenness are always an area of concern. Mannan *et al.* [34], compared the performance of squeegees made of different materials. Metal, composite, and polyurethane squeegees were used in the investigation. With controlled printing conditions, the heights of the printing deposits were measured, and the level of defects for a variety of aperture widths, lengths, and pitches were recorded. It was found, as expected, that the harder the squeegee material the less was the scooping, Fig. 2.11. The metal gave a more constant height of print for all the apertures than the composite and the polyurethane. Due to the difference in support to the squeegee in printing, perpendicular prints resulted in higher deposits than parallel prints, Fig. 2.12. The difference in deposit heights was considered mainly come from the scooping. Mannan *et al.* [35], went further by developing a model for the prediction of the amount of scooping. The model took into consideration of factors like squeegee material, printing speed, force applied, and the non-Newtonian properties of the solder paste. As has been mentioned before, there is a difference in the perpendicular and parallel printed solder paste heights. The paper suggests an empirical formula showing the relationship between the scooping depths of perpendicular and parallel prints, as Equation 2.1.

$$\Lambda_{perp} = \Lambda_{par} (1-e^{n/v}) \qquad (2.1)$$

where Λ_{perp} = perpendicular scooping depth

Λ_{par} = parallel scooping depth

v = squeegee speed

n = constant.

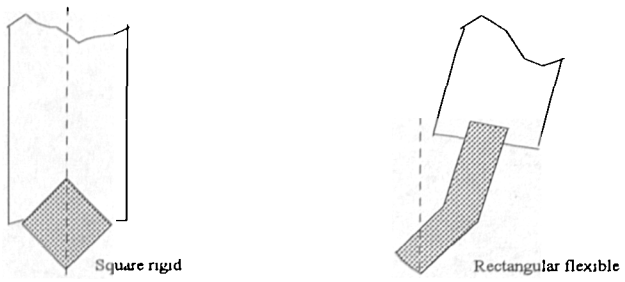

Fig. 2.10 Squeegee geometry

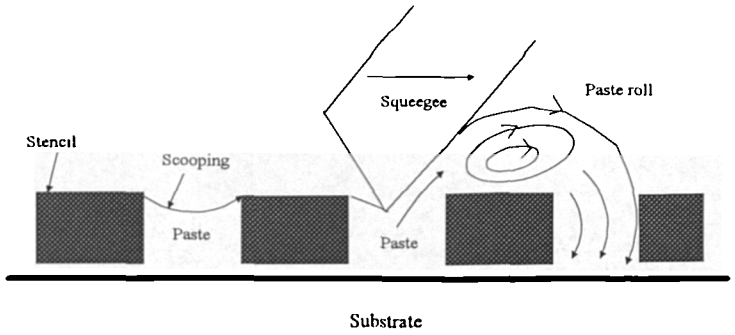

Fig. 2.11 Formation of scooping

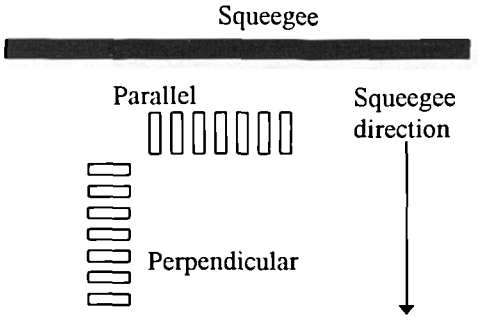

Fig. 2.12 Perpendicular and parallel prints

Considering Equation 2.1, if the ratio n/v is positive, the term $e^{n/v}$ is also positive and its values must be in the range of 1 to ∞. On the other hand the values in the bracket $(1- e^{n/v})$ become zero or negative which makes the equation invalid. So, for a valid equation the value in the bracket $(1- e^{n/v})$ must be positive and this can only be true if the constant "n" is negative since "v" cannot be negative. In this case, the term $(1- e^{n/v})$ is always less than one and positive. Furthermore, from the equation it can be seen that the scooping of a perpendicular print is smaller than that of a parallel print since Λ_{perp} is smaller than Λ_{par}. Further information which can be deduced from the equation is that the printing speed "v" is a determining factor on the difference in thickness between the perpendicular and the parallel prints. An increase in the printing speed would result in a larger paste thickness difference. For components like the QFP, with leads orientated both perpendicular and parallel to the printing direction, a discrepancy in the thickness of solder paste deposited is normally expected. In the same paper, Mannan, *et al.* [35] proposed another equation, Equation 2.2, for the calculation of the paste height:

$$H = (H_t - \Lambda)(1 + v_p/v) \tag{2.2}$$

where v is the printing speed, v_p is the average paste velocity underneath the squeegee, Λ is the depth of squeegee deformation, and H_{st} is the stencil thickness. Without going into details of the derivation, the paper further proposes Equation 2.3 for the calculation of the perpendicularly printed scooping:

$$\Lambda_{perp} = \varepsilon \left(\frac{Q - bv}{B} - pv - d \right) \tag{2.3}$$

where ε is a squeegee material property constant, bv is the pressure on the squeegee from the paste above the stencil, pv is the pressure per unit width of paste below the squeegee, Q is the loading force on the squeegee, B is the horizontal squeegee length, and d is the pressure due to the paste trapped between the squeegee and the end aperture wall. The equations given were mainly based on a force analysis in printing, not much consideration has been given to the dynamic effects and the flow behaviour of the paste. The analysis

based on which the model developed was much simplified. Due to the complexity of the printing process, the validity and accuracy of the above equations need further verification. Landis and Notman [36], considered that a good deposit of solder paste should satisfy the following conditions:

$$F_1 >> F_2 + F_3$$

where F_1 is the adhesive force of the solder paste onto the PCB

F_2 is the shear stress applied to the paste by the walls of the stencil

F_3 is the cohesive force of the paste as it separates from the stencil during snapoff.

This proposition was based on the belief that the adhesive force of the solder paste on the PCB should be stronger than the other pulling forces imposed on the paste during the removal of the stencil, so that defects like smears would not occur.

2.4 DEFECTS AND RELIABILITY

In through-hole technology, the leads of electronic components are firstly clinched, then soldered to the boards. On some rare occasions, the leads are even twisted first then soldered. By contrast for SMT, the components are connected basically only by the solder, there is no other additional mechanism as there is in the through-hole technology for connection reinforcement. Therefore, SMT assemblies are more vulnerable in terms of reliability. Since the soldering method of SMT is totally different from that of the through-hole technology, the knowledge, such as the causes of failure, failure mechanism, causes of defects, quality and reliability standards, and methods of carrying out reliability tests, that are inherited from the through-hole technology are inapplicable to the SMT case. In realising its importance and urgency, studies on the defects and reliability of SMT joints have been increasing. Frear and Yost [37], did a literature survey on papers which contain the key words *solder, failure, and reliability*. The survey was carried out in five databases. Duplicate entries were removed. The number of citations in a given year were divided by the total number of papers recorded in the five databases that year, and expressed in

citations per million (cpm). It was found that the number of papers had increased roughly from 9 cpm to 65 cpm, between the years 1968 and 1993. Even with such a large volume of papers published, due to the fact that SMT is a relatively new technology and combined with its complexity, there are still areas which need further investigation and improvement.

2.4.1 Effects of Heating Process

In a broad sense, the type of defects and reliability problems generated are closely related to the process operations employed. The heating history in soldering is a significant factor determining the nature of any defects. There are a number of methods available for the application of heat for SMT soldering, namely hot plate, laser, hot-air reflow, vapour phase reflow, IR reflow, and wave-soldering. The last three methods are found to be the most beneficial and suitable for mass production. Furthermore, IR reflow and wave-soldering will be looked at in more detail here as these two processes have been employed for the research described in this dissertation.

2.4.1.1 Vapour Phase

Vapour phase reflow uses the latent heat of vaporisation of the condensing vapour. The fluid developed for this purpose normally is a long-chain perfluorocarbon blend that consists of only carbon and fluorine. A typical structure is as Fig. 2.13 :

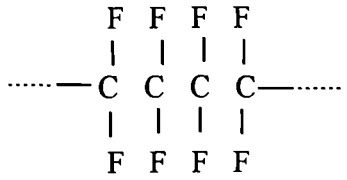

Fig. 2.13 Perfluorocarbon chain.

The fluid contains no chlorine atoms thus it does no harm to the ozone layer [38]. It is an

inert fluid which does not react with other materials. In the entire heating process the saturated vapour forms a protective shield to isolate the assembly from the atmosphere thereby prevents oxidation. The oxidation-free environment allows this process to produce clean boards which only require minimum subsequent cleaning [39]. During reflow the assembly is simply immersed in the saturated vapour and heated for the required duration. Heat is being transferred from the condensing vapour to the surface of the board, land pattern, and the components. Since the fluid boils at a constant temperature, vapour phase reflow is considered as having the best temperature consistency and uniformity among the available heating methods. This makes the process independent of the geometry of the parts being processed, and most suitable for assemblies with a mixture of components and with different positions and orientations. In the early use of vapour phase reflow, parts were submerged in the vapour bath directly, this caused thermal shock and created thermal cracks to the joints as well as to the components. It was shown that the temperature rates of rise could exceed 50 Ks^{-1} [40]. Warping of the assemblies was another common defect phenomenon. Nowadays, to reduce the effects of thermal shock, the vapour phase bath is normally equipped with a preheat zone using vapour or infrared as means of heating. With the preheat zone, parts can be brought up to the required temperatures gradually. Fig. 2.14 shows a typical temperature profile for vapour phase reflow. It is recommended that the temperature ramping rate for preheat is between 2 to 3 Ks^{-1}, the liquidus time should be controlled to 45 to 60 s to minimise component stress and allow solder joint formation, and the cooling rate after reflow again should be 2 to 3 Ks^{-1} [40]. The temperature profiles for both vapour phase and IR reflow have to satisfy the following requirements:

- the initial heating rate is low to provide time for solvent evaporation, and gradual heating of the assembly,
- at the flux activation stage there is proper time and temperature for the flux to complete the cleaning. It would be ideal if the cleaning activity is completed just at the time when the solder particles start to melt,
- the phase at temperatures above the liquidus line is not too short therefore to allow the complete melting of the alloy particles to form the fillet, and the out-gassing of the remaining solvent and flux residues. On the other hand, it is important that this phase is

not too long or the temperatures are too high as both would cause damage to the components and the PCB.

- the cooling has a ramping rate about the same as the initial heating rate. A cooling rate less than 3 Ks^{-1} is recommended. A quick cooling rate would result in a slightly stronger joint, but it should not be too fast, because it may lead to brittleness or cracks [41].

The common defects associated with an improper vapour phase temperature profile are cracks on both joints and components, dry joints, and wicking. Usually there are fewer and smaller gas inclusions because of the oxygen-free heating conditions. However, due to the rapid heating conditions of vapour phase reflow, tombstoning and lifting are more frequently found compared to when IR reflow has been used [6].

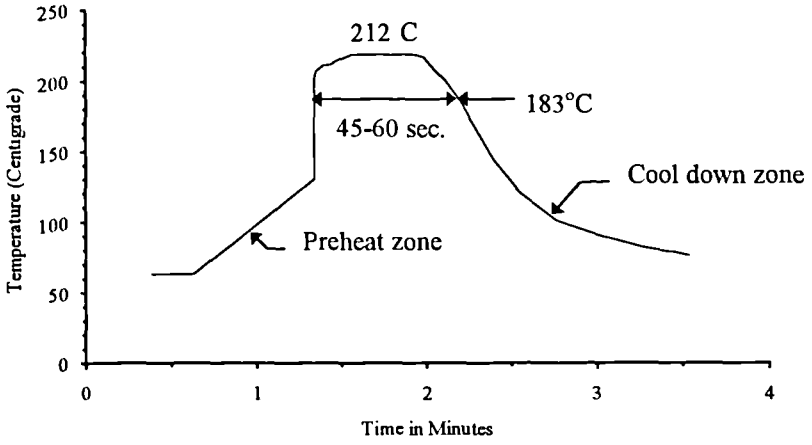

Fig. 2.14 Vapour phase temperature profile

2.4.1.2 Infrared

IR reflow is the most common method used in SMT soldering. Compared with vapour phase reflow, it is a cheaper process, because of the higher cost of the inert fluid used in vapour phase reflow. The basic requirements of an IR temperature profile are the

same as in the vapour phase case. However, because it employs a different heating mechanism, the exact shapes of the two are totally different. The early developed IR reflow ovens used short-wavelength emitters as heat source. Short-wavelength IR is difficult to control and adjust. The new generation IR reflow ovens employ long-wave, convergent systems [42]. The advantage with a long-wave system is that a large variety of materials absorb its heat energy at about the same rate. This allows materials like plastics, ceramics, solder paste, and tin/lead plating to be processed with minimum heat disparity. A typical new generation of IR reflow oven uses long-wavelength emitters as heat sources built into four zones. The first three zones are for preheating and the last one is for reflow. A heat source is located both above and below the conveyor which carries the assemblies through the entire process. Each zone can be individually controlled and adjusted so that the temperature profile can be easily changed to meet the needs of a particular assembly configuration. In some systems, to provide an even and effective heat transfer, forced convection is used. With some hands-on experience, a desirable temperature profile can be obtained easily by adjusting the conveyor speed, zone temperatures, and air-draught rate. To provide a consistent quality of solder joints, it is important that the same temperature profile is used on boards with the same configuration [43]. It is advisable to check the profile at least twice a day, once in the morning and once in the afternoon, as the ambient temperature also has changing effects on the profile. Some papers recommend a specific temperature profile just on the basis of the alloy composition in the paste. It is necessary to point out here that the alloy composition should not be the only factor in determining the profile, other factors such as solvent and flux should also be taken into consideration. The temperature profile should vary with the board configuration and the paste type. With a particular oven setup, components at different locations on a board are subjected to different heating profiles. The difficulty is to have the hottest and coldest joints on the same board both reflowed to the required quality. Nowadays, there are many types of solder pastes on the market, each requires a specific profile to achieve its optimum heating conditions. No-clean solder pastes with a low solid content and little activation require totally different forms of temperature profile. It is recommend that for all IR reflow temperature profiles, the maximum temperature rise rate is between 2 to 4 Ks^{-1}. With reference to Fig. 2.15, the profile for a paste with RMA flux can be divided into four stages

[44,45,46]:

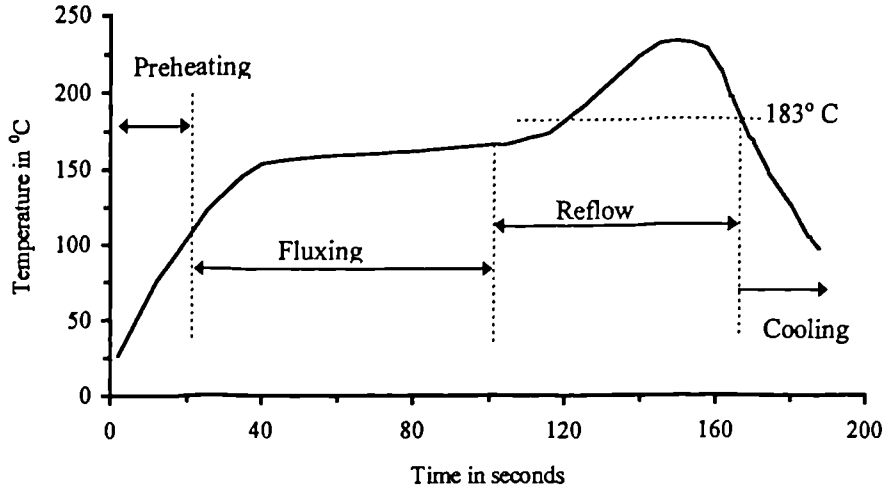

Fig. 2.15 IR reflow temperature profile

- *Preheat:* At this stage the assembly is gradually brought to a temperature of about 100° C. One of the objectives of this stage is to reduce or eliminate the thermal shock of a part when it enters the reflow zone. The majority of the solvent in the paste is evaporated at this stage. The heating rate cannot be too fast otherwise the volatile out-gassing of the solvent would increase the amount of voids in the solder joints. The dominating physical phenomena are diffusion among the particles, and the liquid-gas transformation of the solvent.
- *Fluxing:* The temperatures range roughly from 100 to 170° C. Activation of the flux is the dominating activity during this stage although some of the solvent residues continue to be evaporated. The fluxing time should be about 60 s. The upper temperature of the range and the fluxing time vary with the flux type. At this stage, the flux is melted first then floods the joint. The functions of oxide removal and prevention of further oxidation by the flux are the main activities of this stage. The fluxing time and the rate of temperature rise are the two critical parameters which need to be controlled properly. A high heating rate leads to rapid out-gassing of the flux resulting in voids, spattering of particles, and incomplete deoxidation. The flux may not be able to escape

completely and its residues form voids after cooling if the fluxing time is too short. On the other hand the fluxing time cannot be too long either since this may burn out all the flux well before entering the reflow stage. At the same time, the viscosity of the flux is continuously reducing and the flux serves as a heat transfer medium among the particles. The evaporation and the melting of the flux lead to repacking of the particles and a reduction of the overall volume. This stage further increases the temperature of the part so as to minimise the degree of thermal shock when entering the reflow zone.

- *Reflow*: For most solder paste, reflow at temperatures just above the liquidus line, 183° C., is insufficient. The common peak temperatures used are in between 200 and 230° C. The alloy particle composition is one of the factors determining the choice of the peak temperature for reflow. Insufficient reflow time and peak temperature result in dry-joints. However, the dwell time above the liquidus line cannot be too long, and the peak temperature cannot be too high, as either would lead to grain and intermetallic compound growth which increase the brittleness of the joint. The other problem with a long dwell time and a high peak temperature is cracking of the electronic components. Minimum-maximum values of dwell time are 40 to 60 s. Above the liquidus temperature, the particles change from a mushy state to bulk melting, this is then followed by wetting and spreading. This wetting and spreading mechanism of the molten solder determines the geometry of and the defects in the joint. For components that are slightly misplaced, the surface tension of the molten solder has the effect of bringing them back to position. Since most of the heat is transmitted by radiation, shadowing can be a source of defects in reflow. The possible visual defects associated with the reflow process are dry joints, tombstoning, bridging, solder balls, and wicking [47].
- *Cooling and Solidification:* The rate of cooling at this stage affects the quality of the joint in terms of strength and fatigue resistance. A fast cooling, results in a finer grain size and this improves the fatigue endurance. But the other extreme is that, too fast a cooling may lead to thermal stresses and resulting cracks in the joints and components. A slow cooling rate giving a large grain size reduces the net grain boundary area and has the effect of increasing the brittleness of the joint. It is essential to treat this stage as of equal important to the preceding three. An improper cooling after reflow is likely to

lead to a significant number of problems. A phenomenon named supercooling was found on eutectic solder [48]. The effects of this characteristic on the quality of the joints deserves further investigation.

2.4.1.3 Wave-Soldering

Wave-soldering of SMT components is inherited from the through-hole technology. In through-hole technology, components are mounted on the top side of the board, component pins on which solder is deposited are round and small in diameter, therefore there are no major problems in terms of thermal shock and solderability. However, when wave-soldering is employed for SMT components, the components are totally immersed into the bath, and there is a high probability of this resulting in thermal cracks in the components. To overcome this, preheat should be provided and properly controlled. The bottom preheat temperature should exceed 140° C. The peak temperature of the wave is determined by the solder type; for a 60Sn40Pb solder this should be limited to 232 $\pm$2° C. Low soldering temperatures between 232°C and 243°C can be used to reduce the sudden temperature rise effects, but on the other hand, the reduction in temperature increases the surface tension of the solder which increases the likelihood of bridging [49]. Component dwell time in the wave should not exceed 10 s, e.g. 7 s for small outline transistors (SOTs). It was recommended that the absolute maximum temperature difference between preheat and wave is 100°C [40]. In fact, many SMT components were never designed for the wave-soldering process; the geometry of components is very often a hindrance to solderability. Unlike components for the through-hole technology, the immersed part of a SMT component is not all wettable, which further increases the difficulties in wetting. There are two reasons why the wave-soldering process is still being used for SMT. One is because wave-soldering facilities may be already available in the factory and it is therefore cheaper to convert the process for SMT applications than to bring in a new process, like IR reflow [50]. Another, and very often dominant reason, is that wave-soldering can handle boards with mixed SMT and through-hole technology components.

Thermal cracks, solder skips, and solder bridges are the three most common defects

in wave-soldering. To a large extent, these three types of defect limit the application of wave-soldering for some SMT components. Heat-sensitive components like chip inductors, electrolytic capacitors, and potentiometers cannot be submerged into the solder wave [42]. Small outline integrated circuit (SOIC) packages are particularly intolerant of a long immersion time in hot solder; it was reported that there were significant number of failures after exposure for only more than 3 s. Solder skips are joints not soldered, or only partially soldered. This defect is closely related to the soldering mechanism of wave-soldering. Shadowings are considered to be the main cause. Components with a large body height difference, and positioned close to each other usually lead to solder skips. Passive components with their long axes aligned parallel to the flow direction definitely increase the chance of solder skipping. The problems of solder skips can be overcome by the use of double wave soldering. Over these two waves, the first is a turbulent wave which breaks up the surface tension and at the same time provides vertical pressure to the solder so that solder can access to the hidden parts, the second is a laminar wave which rounds up the shape of the joint [51]. Electrovert [52] argued that a single Omega wave performs even better in preventing solder skips. The working principle of this system is to employ an electromagnetic transducer to vibrate an element located in a defined position. The laminar nature of the surface tension of the solder is broken down by the vibration, and by controlling the vibration amplitude an optimum condition is achievable [10], as indicated in Fig. 2.16. Electrovert [52], reported in a specific test that, up to 55% reduction in solder skips and 45% reduction in overall defects were found as compared to a double wave system. Modifying the PCB pattern, such as by extending the solder pads of SOIC also has effects of reducing the amount of solder skips. Solder bridges have been the most common reliability problem in wave-soldering of SMT devices. In fact, the surface tension of solder in the process is the major cause of bridging, which stops this soldering method being used on fine pitch SMT packages. QFPs with 80 pins and above are almost impossible to wave-solder without bridges. Reliability in bridging by wave-soldering is much lower than that by reflow processes. The common methods suggested to improve the solder bridging yield in wave-soldering are :

- *To reduce the surface tension of molten solder* [53]. This can be achieved by increasing

the temperature and improving the cleanliness of the solder.

- *To provide dummy pads or solder thieves* [10,11]. Bridges usually occur with the last leads. Thus for soldering a SOIC, if dummy pads or solder thieves are provided at the ends of each row of pads, any bridges which may occur will not affect the function of the circuit. The provision of the additional pads is exemplified by Fig. 2.17 and Fig. 2.18.

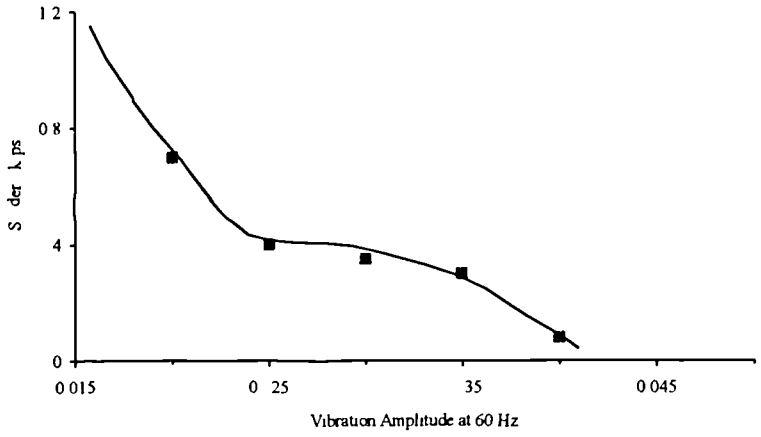

Fig. 2.16 Effects of vibration amplitude on solder skips by an Omega wave

- *To avoid putting components too close to each other* [50]. Although this contradicts the main objective of SMT, which is to increase the interconnectivity.
- *To use a hot air-knife* [50,51]. A stream of precisely controlled hot air is used to remove the excess solder on the leads. Lowell and Sterritt [49], even claimed that with the introduction of this technique, wave-soldering can handle fine pitch chips comparable to a reflow process.

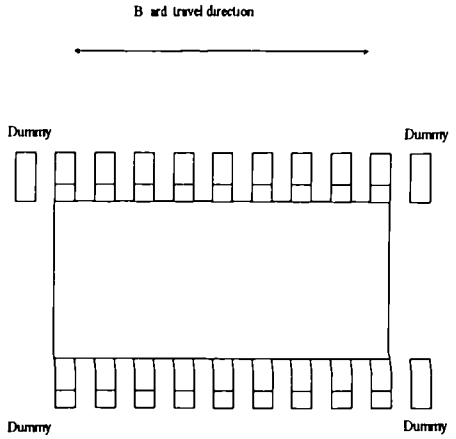

Fig. 2.17 Dummy pads to reduce bridges

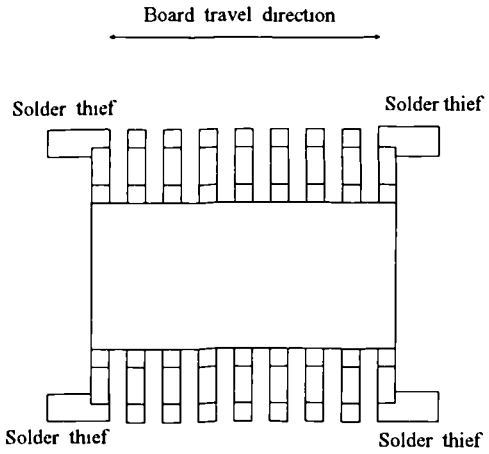

Fig. 2.18 Addition of solder thieves to reduce bridges

Schouten [54] studied the wetting mechanism of wave-soldering by analysing its capillary behaviour. The paper looks at the solderability problems with SMT components during wave-soldering. When a part is pushed in a pot of molten solder, it can be wettable or non-wettable. The meniscus shape of the two conditions are shown in Fig. 2.19. For a conventional component, only the metal leads are immersed, and the solderability is high. For a SMT component, the entire body which is partially metallised and partially made of

plastic, is immersed. The non-wettable plastic together with the body height, increase the wetting difficulties. The wetting conditions may be as shown in Fig. 2.20. Schouten [54] is one of the few authors who have analysed the wetting of SMT components in wave-soldering from a theoretical view point. The analysis was based on the Young and Laplace capillary equation [55] (Appendix A). The pressure difference across the surface of a meniscus is:

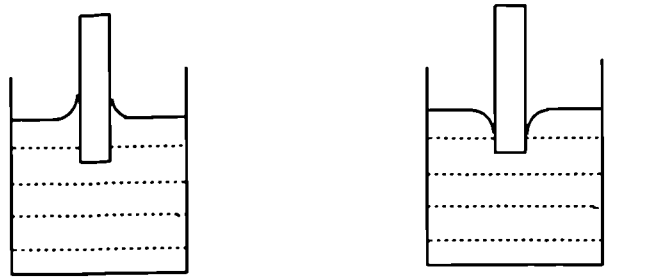

Fig. 2.19 The shapes of meniscus under wetting and non-wetting conditions

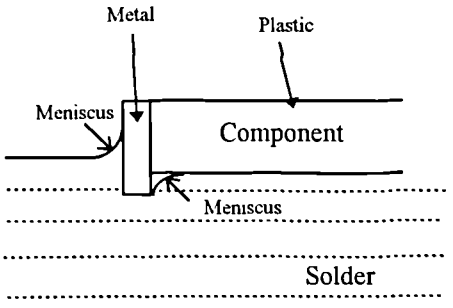

Fig. 2.20 Wetting conditions for SMT component in wave-soldering

$$\Delta P \quad \gamma\left(\frac{1}{R_1}+\frac{1}{R_2}\right)$$

where γ is the liquid surface tension

R_1 and R_2 are the radii in two surface planes which are perpendicular to each other

Referring to Fig. 2.21, in a capillary, ΔP equals the liquid height pressure, so

$$\Delta P - d.g.\Delta h$$

In a fine capillary tube, the curved surface of the liquid can be approximated to part of a sphere surface, therefore $R_1 = R_2 = R$, and

$$\Delta P = \frac{2\gamma}{R}$$

$$\Delta h = \frac{2\gamma}{d.g.R}$$

In the case of a parallel gap, i.e., R_2 = infinity, which is similar to an immersed leadless component, then

$$\Delta h = \frac{\gamma}{d.g.R} \qquad (2.4)$$

where d = liquid density

g = acceleration due to gravity

h = height of liquid column

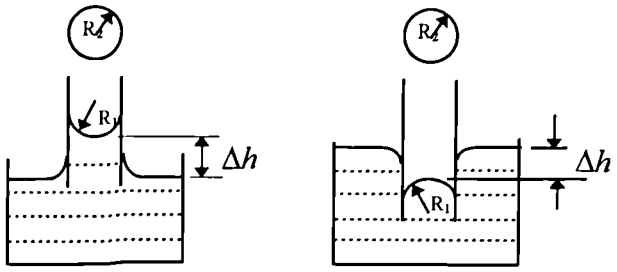

Fig. 2.21 Capillary behaviour of liquid

For 60Sn40Pb and 63Sn37Pb solders, their surface tension and density at 250^{0}C are 0.4 J m^{-2} and 8 Mg m^{-2} respectively. Equation 2.4 for these solders becomes:

$$\Delta h = \frac{5.10^{-6}}{R}$$

The physical meaning of the above equation is that a larger pressure head Δh gives a smaller R. A smaller R, on the other hand, requires a shorter metallisation both on the PCB and the component. From every respect, a short metallisation is always desirable. The physical arrangement in wave-soldering of a SMT component is shown in Fig. 2.22, in which the relation between Δh and R can be seen. The value of Δh can be increased by an increase in the depth of immersion but is always limited by the thickness of the PCB, as if the solder level is well above the top of the PCB flooding would occur. The use of board pallets has a positive effect in increasing the value of Δh, but it is necessary to make sure that there are no gaps existing otherwise flooding still occurs. It is considered that the strength and reliability of a joint is directly affected by it geometry, Liedtke *et al.* [56] had put some efforts into developing models for the prediction of wave-soldered fillet geometry of SMT components. The factors taken into consideration in the models included the dimensions of the metallisations, and the molten solder properties such as the mass density and the surface tension. The validity of these simplified models require experimental verification.

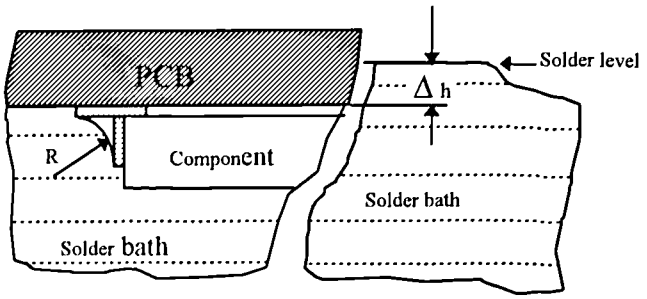

Fig. 2.22 The formation of the meniscus for a chip submerged in a solder bath

2.4.2 Tombstoning

Tombstoning is also known as drawbridging, or the Manhattan effect. It happens only on leadless chips. It is a phenomenon resulting from the movement of the chips during reflow. In a less severe case, one end of the component may be slightly lifted up leading to an open circuit. In an extreme case, one end of the component may be totally erected, giving a situation where the component stands up like a tombstone, Fig. 2.23. This is a very common defect in SMT, lowering the yield of the process. The exact causes and methods of prevention still require more intensive investigations. It would be particularly valuable if a theoretical base can be formulated, from which, process or design guidelines can be established to prevent its occurrence. Only a limited number of papers have been published on this topic; and most of these do not take an analytical approach. Most of the conclusions drawn are speculative and empirical in nature. Based on the published information [9,57,58,59], the following summarises the causes and methods of prevention:

- Unbalanced forces during wetting are considered as the main cause of tombstoning. Surface tension of molten solder is the source of these forces.
- Old solder paste has corroded particles with a high oxide content [60]. Contaminated solder has a high surface tension which raises the chance of tombstoning, or lifting.
- The force holding the component in position is insufficient. This force mainly comes

from the weight of the component and the tackiness under the component Age deteriorates the tackiness of solder paste. A higher placement force increases the tackiness and is desirable in this respect. Extended PCB metallisation underneath the component also has an effect of preventing the component from lifting.

- A high heating rate generates more vigorous component movement, which increases the dynamic effect in the formation of tombstoning. Uneven heating or shadowing may results in unbalanced surface tension over the two ends of a discrete component.
- Thick solder paste and a high component centre of gravity increase the leverage, and make the component easier to erect. Although thin solder paste reduces tombstoning, it may result in insufficient solder and affect the reliability of the joint.

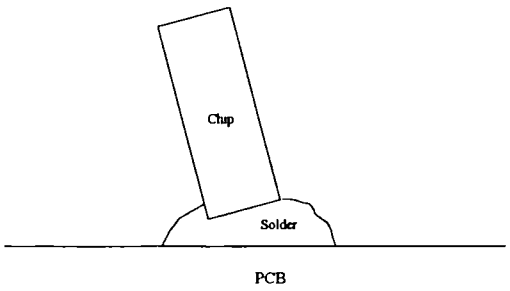

Fig. 2.23 Tombstoning of chip component

Wassink and Verguld [61], analysed the upward and downward forces of a tombstoned chip component. In their paper, liquid solder surface tension, component geometry and weight, and dimensions of the PCB metallisation are considered as the factors in sustaining the tombstoning phenomenon during reflow. The relationship between the upward moment and downward moment at different titling angles is shown. It indicates that for components R 0805 and R 1206, in many tilting circumstances the values of the two moments are very close to each other. This suggests that any disturbance would result in either the upward or downward moment predominating. The paper published by Ellis and Masada [62], incorporates the wetting properties and solder volume into the analysis. A model was developed for the calculation of the profile of the fillet, and they argue that by using the model the surface tension and the pressure at different points of the fillet profile can be computed more accurately.

2.4.3 Formation of Voids

The increase in the stress/strain level due to the presence of voids deteriorates the reliability of a joint in terms of mechanical strength, creep resistance, and fatigue resistance. Likewise, voids also impair thermal and electric conductivities. The outgassing of the entrapped flux during reflow is considered to be the source of void formation. In most cases of reflowed solder, the voids may not impose an immediate threat, but in the longer term the stress/strain concentration may lead to crack propagation, coalescence of voids, and subsequently failure of the joint. Finite element models were used to investigate the effects of voids on the reliability of SMT solder joints by Liu and Mei [63]. It was found that the stress/strain varied with the void size, and reached a maximum value at a particular radius The stress/strain of two voids interacted with each other and this interaction determined the position of the crack initiation. Hance and Lee [64], carried out a relatively comprehensive investigation of the voiding mechanism in SMT. The effects of voids on several aspects were also studied. Xie *et al.* [65] performed similar studies but emphasised the effects of voids on the strength. Barrett *et al.* [66], compared the voiding conditions of non-clean paste to that of the standard paste. The following is a summary of the findings from these three papers:

- With reference to Fig. 2.24, both the flux activity and the solderability were defined as $\log_{10}(1/S)$ by Hance and Lee [64], where S is the wetting time. Hence the smaller the S value, the higher is the flux activity or greater is the solderability. The effects of flux activity and solderability on voiding was investigated. The results were plotted on log-log scale by Hance and Lee [64]. The flux activity was varied by changing the flux activator content. It was found that a stronger flux activity resulted in less voids, and only a small amount of voids had signs of flux residues. Hance and Lee [64], argued that the flux activator was not directly responsible for the void formation, because higher flux activator did not increase the void content, but on the contrary, reduced it. Void formation was considered mainly from the outgassing of the entrapped flux, and a lesser flux entrapment meant a lower void content. In addition, the paper explains that a

higher activity of flux eliminates the oxides more rapidly and completely, therefore leaving fewer spots for the flux to adhere to, and hence, fewer voids. Flux activity also has positive effects on the size of the voids. A decrease in the flux activity results in an increase in the fraction of large voids. It is considered that large sized voids are far more harmful in terms of reliability than small sized ones. In one of the experiments, the solderability was varied by changing the treatment conditions of the copper coupons on which soldering was performed. The paper shows that an improved solderability resulted in a decrease in the void content. This phenomenon can be explained in the same way as before; a coupon with better solderability allowed the flux to clean easier and faster, hence leaving less flux residues, and subsequently less void content. It is also believed that voiding is a function of the timing between paste coalescence and elimination of metallisation oxide. The sooner the coalescence occurs the worse is the voiding.

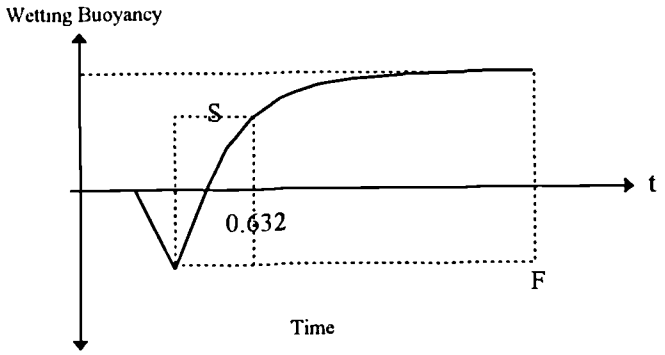

Fig. 2.24 Wetting balance curve

- With other conditions fixed, the voiding effects with different widths of paste printed were studied. It was found that the amount of voids decreased with the width. The width determined the paste coverage area. The explanation given to this phenomenon is that, a smaller coverage area gives a larger side area-to-volume ratio, and this facilitates the outgassing of the flux. This finding is particularly beneficial to components with fine pins.

- Paste with an increase in the alloy content resulted in a corresponding increase in voids [64,65]. The increase in the voids could be attributed to the increase in oxide content and the decrease in flux in the joint. The closely packed alloy particles making the gas difficult to escape was another reason resulting in more voids. This finding actually contradicts the reports [17,19,22] that have been mentioned in Section 2.2.1. Which of these is true requires further investigation. In addition, it was also found that a decrease in the particle size only had slight effects on the increase in void content. Barrett *et al.* [66], discovered that non-clean solder paste produced significantly more voids than the standard pastes. This again, might be related to the flux activity strength of the paste.
- Heating conditions determine the amount of voids. Xie *et al.* [65], employed two different temperature profiles for the reflow of the same paste. It was found that the profile with a longer heating duration produced more voids content. Preheating not necessary reduces the voids. In fact, in some cases, the contrary was found [64].
- The relation between porosity and strength can be expressed in the form of [65]:

$$\sigma - \sigma_o e^{-k}$$

where σ is the strength of material with ε volume of voids, and σ_o is the void-free strength of the material. The coefficient k is normally larger than one. The shear strength of specimens with different percentages of voids was studied. It indicated clearly that the fraction of voids had a direct effect on the strength of the joint.

2.4.4 Effects of Solder Geometry

The reliability of a joint depends heavily on two factors: metallurgical structure and shape. The literature related to the metallurgical structure is to be surveyed later. This section concentrates on information related to the shape of joints. The shape formation of solder joints has been analysed from a theoretical view point, and the effects of the shape on the mechanical strength and fatigue resistance have also been investigated [67,68]. In general, the legs of a SMT component may be in one of the three forms, as indicated in Fig.

2.25. To simulate these joints, and at the same time to carry out the necessary tests, Hoyt [69] fabricated three types of legs, butt, gull wing, and modified gull wing (the same as the J-lead in Fig. 2.25). Using a special fixture, legs were soldered on the test boards, then tensile tests were performed. Metallography was used to investigate the sites and fracture paths. The findings showed that for butt joints, failure occurred at the bottom of the leg, although evidence of cracks was also detected at the interface between the leg and the board. SEM showed that ductile fracture was the predominant failure mode for gull wing legs, this was evidenced by the cup-and-cone fracture faces in the solder. Fracture was initiated at the point with the highest stress, which was near the heel fillet. Fracture propagated close to, but not through, the intermetallic layer, and up the base of the leg. The propagation tended to pass through the Pb-rich areas. Different strain rates were used for the tests. It was found that the tensile strength increased with test speed. Among the literature searched [69,70,71], there is a common consensus on the effects of the fillet. It is agreed that the strength of a joint depends very much on the size and shape of the fillet; a large and round fillet increases the strength. When the fillet was completely removed, the strength dropped significantly. For a particular type of leg, the larger the PCB pad size the stronger the joint was found to be. This is because a large pad size gives a larger fillet size, hence a higher bond strength. The effects of stand-off height were also studied. One of the experiments [70] showed that the load to fracture value decreased from 580 N for a stand-off of 0.05mm to 490 N for a stand-off of 0.4mm. This indicated that an increase in the stand-off resulted in a reduction in the mechanical strength. The problem with these experiments was that, the specimens used did not allow a treatment of the data with the stand-off height as the only and independent variable; the joints still had the influence of the fillets though they were intended to be kept constant.. However, based on the analysed results, it is reasonable to believe that a joint with a small stand-off is more vulnerable to a tensile force. In application environments, the joints are actually more likely to be subjected to thermal fatigue. Nowadays, the stress/strain contour of a solder joint can be predicted by the use of a suitable FEA programme [72]. In conjunction with an iteration technique, FEA was used to investigate the thermal fatigue resistance of a RC 1206 solder joint [73,74]. Fig. 2.26 is the configuration on which the FEA was performed. It was found from the

analysis that a larger stand-off height gave a smaller maximum strain, and its position was near the knee of the joint. On the basis of the Coffin-Manson equation, i.e. the number-of-cycle to failure is inversely proportional to the strain, a higher fatigue life is expected for joints with large stand-off heights. In addition, joints with large stand-off heights also provide larger areas for crack propagation, and this further increases the fatigue life. The FEA also substantiates the point that the fillet is crucial for strength and fatigue resistance, and a fillet height equal to 1/3 of the height of the chip gives the maximum fatigue resistance.

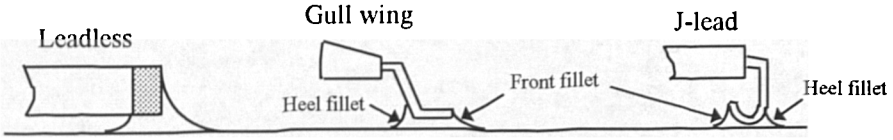

Fig. 2.25 Common legs for SMT components

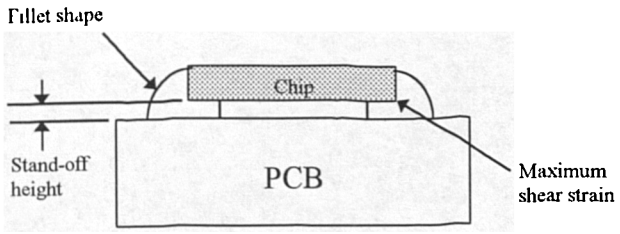

Fig. 2.26 RC 1206 chip

2.4.5 Reliability Tests

In application conditions, a SMT assembly is in fact continuously subjected to thermal cycling. In most cases, the thermal cycling is from the electric power supply which may be in the form of an on-and-off, step, or specific cycling pattern. To a lesser extent, it may be due to the change in the ambient temperature. This temperature fluctuation, either

from the heat generated internally or from the surroundings, together with the assembly made up of materials with different thermal coefficient of expansion, puts the assembly into cycling fatigue conditions. The stress/strain cycling, eventually will cause failure to the joint. It is realised that thermal fatigue failure is the predominant reliability problem in SMT, and much has been published on fatigue test methods and fatigue life prediction. Accelerated tests under different temperature conditions are by far the most common approaches [75,76,77,78,79,80]. The test method chosen very often is an analogy of the application of the assembly, and may be in the form of a) a thermal shock fatigue, b) a thermal cycling fatigue, or, c) an isothermal mechanical fatigue test. The thermal shock fatigue test is carried out by dumping the specimen between two extreme temperature chambers. Thermal cycling fatigue is either done in a temperature controlled chamber or by power functional cycling. Power functional cycling is more accurate, and its test conditions are closer relatively to the conditions of application, but on the other hand it is time consuming and costly. One of the most common accelerated tests is the one that meets the US military specification MIL-STD-883, method 1011 [74]. This method requires a thermal cycle between -55^0C and $+125^0$C, but the problem with this standard method is that it does not relate the test results directly to the SMT field of application. Isothermal mechanical fatigue produces results quickly, but should only be used for comparison. Fatigue life is considered to pass through three stages: a) crack initiation, b) crack propagation, and c) fatigue failure. Ductile fatigue failure is the failure mode found on solder joints because of the ductile nature of solders. So far, very few or no attempts have been made to measure purely the crack initiation and crack propagation of SMT joints. However, there are different methods developed for detecting the ductile fatigue failure, and the results are used as a means of measuring the reliability of solder joints. These methods basically include i) visual inspection, ii) electric resistance measurement, iii) electric discontinuity, and iv) continuous continuity monitoring [81]. Engelmaier [82], described in relative detail these fatigue testing methods, and at the same time suggested board configurations for the tests. FEA has also been used for the reliability evaluation. FEA, in principle, assumes that materials obey the law of continuum mechanics. The part to be analysed is firstly decomposed into elements. Then, by knowing the boundary

conditions, and assuming that the material's behaviour is defined by a set of algebraic equations, the stress/strain values of any region can be calculated. With the calculated stress/strain, the life of the joints can be compared or predicted. One of the advantages with FEA is that any shape of joint can be easily configured and analysed. Effects of other factors, such as temperature, can also be evaluated. Elastic and elastoplastic analyses have be performed for joints with different shapes, and in some cases the joints have been assumed to be subjected to different temperature conditions [72,73,74,76,83,84]. In FEA, the properties of materials are assumed to be isotropic. However, in reality, this is not true. FEA also has other limitations, such as the creep and stress relaxation effects of materials during an application cannot as yet be taken into consideration. The model commonly used for predicting the fatigue of solder joints is the Coffin-Manson law. The law was developed on the basis that, on a log-log scale, the strain has a linear relation with the number of cycles to failure [37,74,85,86], and is expressed in the form of:

$$\frac{\Delta\varepsilon}{2} = \frac{\Delta\varepsilon_e}{2} + \frac{\Delta\varepsilon_p}{2}$$

$$= \frac{\sigma_f}{E}(2N)^b + \varepsilon_f(2N)^c \qquad (2.5)$$

where

$\frac{\Delta\varepsilon}{2}$ total strain amplitude,

$\frac{\Delta\varepsilon_e}{2}$ $= \Delta\sigma/2E = \sigma_a/E$, elastic strain amplitude,

$\frac{\Delta\varepsilon_p}{2}$ plastic strain amplitude,

ε_f fatigue ductility coefficient (which is approximately equal to the true fracture ductility in monotonic tension),

c fatigue ductility exponent (which is the slope of the log-log, $\Delta\varepsilon_p \sim 2N$ plot),

σ_f fatigue strength exponent (which is approximately equal to the true fracture strength in monotonic tension),

b fatigue strength coefficient (which is the slop of the log-log S~N plot for high cycle fatigue)

E modulus of elasticity,

$\Delta\sigma/2$ $-\sigma_a$, stress amplitude,

N cycle-to-failure.

Since solder is a very ductile material, when it is subjected to stress, plastic deformation prevails. In these circumstances, the elastic strain value compared to that of the plastic one is much smaller and hence can be ignored. Therefore, Equation 2.5 can be reduced to:

$$N = \frac{1}{2}\left(\frac{\Delta\varepsilon}{2\varepsilon_f}\right)^{1/c} \tag{2.6}$$

From Equation 2.6 it can be seen that both ε_f and c are material constants, if the plastic strain, $\Delta\varepsilon$, can be found the fatigue life can be evaluated. In a practical sense, the difficulties with a solder joint are to locate the point with maximum strain and then measure its value. The FEA approach does provide this information. The other approach is mechanical destructive tests. Due to the nature of the application of electronic assemblies, it is very rarely that mechanical strength is the main cause contributing to reliability problems. Whichever fatigue, shear, or tensile test is performed without incorporating the thermal effects into it should only be used as a means of comparison. Cyclic bending of the assembly is commonly used as a mechanical fatigue reliability test, although vibration tests have been suggested [87]. Peel tests, as shown in Fig. 2.27, have been employed for gull-wing lead strength comparisons [66]. Leads copying the shapes of leads of SMT chips, soldered on special test boards have been used for carrying out direct pulling tests [69]. The stress of 'L' and inverted 'T' joints during a pulling test have been analysed [88]. It was found that, in terms of strength, an inverted 'T' joint was far superior to a 'L' joint. To deal with the large amount of variables in the reliability tests, Taguchi experimental design techniques were suggested to reduce the complexity and increase the effectiveness of the

tests [89,90].

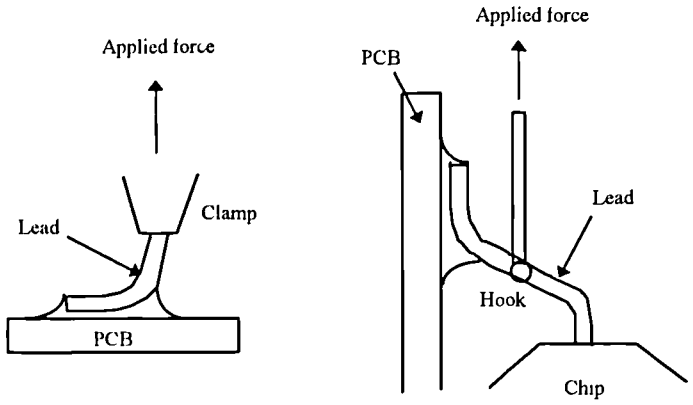

Fig. 2.27 Peel tests for gull-wing chips

2.5 INTERMETALLIC COMPOUNDS AT JOINTS

Soldering provides an inexpensive, and reliable means of joining two pieces of metal together. The most common solder used in the electronics industry is the tin-lead based solder due to its good wetting and low temperature characteristics. The surface on which solder is deposited usually is bare copper, although other materials such as a Cu-Ni-Au plated surface is also used. The presence of an intermetallic compound (IMC) at the metal/solder interface is considered to be an indication of a properly wetted joint. However, its brittle property on the other hand may have adverse effects on the reliability of the joint. How the IMC layer affects the long term reliability of the joint deserves more intensive investigation. The effects of Au and its IMC on the strength and other properties of the joints were studied [91,92,93]. In this section, a search is concentrated on the literature published on Cu/Sn intermetallic compounds, as the majority of soldering systems in the electronic industry form this type of compound.

2.5.1 Effects on Strength and Failure Behaviour

It was found that time and temperature are the two factors determining the growth of an IMC. The heating process during soldering and the subsequent service conditions of the assembly determine the thickness and composition of the compound. In a copper-solder system, only tin forms compounds with copper. The majority of the compounds formed at the copper/solder interface are either Cu_6Sn_5 (η phase) or Cu_3Sn (ε phase). In practice, it is difficult to measure the mechanical strength, the fatigue resistance, and the creep resistance of the straight IMC, and a bulk test of the joints is usually carried out. Thwaites [94] used ring and plug joints for testing. The stress/creep life at 20°C and 100°C were plotted. For comparison purpose, stresses giving a creep life of 2,000 hours were noted. It was found that the stress at 100°C was four time less than that at 20°C for most of the solder alloys tested. For 60Sn40Pb solder joints, aged at 170°C for 200 days, it was found that about one-third of the solder was converted into duplex IMC. Parent *et al.* [95] used specially designed specimens, Fig. 2.28, to perform relatively detailed studies on the effects of IMC. The solder alloy used was 63Sn37Pb. Using an Instron testing machine with the specimen mounted on a shear fixture, the steps of the specimen were fractured one after the other. The findings indicated that for the cases using 300 and 350°C as soldering temperatures, fractures were brittle in character. However, for those soldered at 230°C, a considerable amount of ductile fracture was found. Both Cu_6Sn_5 and Cu_3Sn were found by X-ray diffraction in all cases. Failures were found to begin in the Cu_6Sn_5 layer, and then extended into the bulk of the solder in all cases. The extent of failure through the Cu_6Sn_5 increased with increasing in temperature. The authors consider that the thickness of the Cu_6Sn_5 is the major effect on the strength of the joints. There were no indications that an increase in the Cu_3Sn thickness affected the strength or the extent of brittle failure in any of the tested samples. There were cases where the cracks followed the Cu_6Sn_5/Cu_3Sn interface, but these were not an exclusive phenomenon. It was considered that the interface does not represent a significantly weak point. Tensile properties of different types of solder were also studied by Quan *et al.* [96]. The results show that failure mode varied with the solder composition. For a 5Sn95Pb solder, as-processed specimens failed predominantly by a ductile mode.

However, for specimens after aging for 6 hours at 205°C, failures were again by a ductile mode but mainly through the solder/Cu_3Sn interface. Voids were found preferentially initiated in the Cu_3Sn. The tensile strength of reflowed specimens was lower than the as-processed ones. Again, both Cu_6Sn_5 and Cu_3Pb were detected in the 60Sn40Pb solder. Similar to the study by Parent *et al.* [95], it was found that failures occurred in a transgranular mode through the Cu_6Sn_5 intermetallic. This mode of failure applied to both the as-processed and reflowed specimens. The joint strength after reflow decreased to about half the strength value of the one before reflow. The decrease in strength was considered to be due to the increase and coarsening of the Cu_6Sn_5. IMC not only affects the strength, its growth also consumes solderable metallisation, and results in dewetting of the solder. Blum *et al.* [97], studied the fracture surface of solder joints. They found that fracture through the IMC was brittle in character. However, no information was given on how the experiments were performed. Kang *et al.* [98], thermally cycled silicon power transistors that were soldered to nickel-base metal. The solder alloys used were 60Sn40Pb and 5Sn95Pb. For both solders, the IMC was considered to create a structural inhomogeneity that altered the mechanical properties of the joint and shortened the fatigue life. However, ductile failures through the bulk of the joints were reported rather than through the brittle IMC layers. Keller [99], thermally cycled 60Sn40Pb joints with copper as base metal. The specimens were cycled between -40°C and 130°C. After cycling, the specimens were pulled apart at a 100 mm $minute^{-1}$ rate. It was found that for specimens before thermal cycling, failures predominantly were through the bulk, but for specimens after cycling failures were mainly through the IMC. Frear *et al.* [100], performed 60Sn40Pb solder shear tests. A mixture of failures was discovered. In shear, failures were primarily through the solder unless the IMC was thick, or the deformation rate was fast. The authors showed that when the shear rates were greater than 0.01 mm $minute^{-1}$, failures through the IMC prevailed. However, for slow shear rates, failures through the bulk of the solder were common. They found similar evidence as the other authors, that aging increased and coarsened the IMC, and resulted in lowering the strength. Frear and Vianco [101], found that the IMC was harder than both the solder alloy and the base metal. The fracture mode depended on the strength of the solder alloy. Solders with low strength gave ductile failures

through the solder, while solder of high strength, the failure depended on the thickness of the IMC. When the IMC was thin, failures were through the solder or at the solder/IMC interface. When IMC was thick, trans-IMC failures were common. The authors also observed that the fracture mode and path were affected by the degree of aging. For a 60Sn40Pb/Cu solder joint without aging, failure was by ductile fracture through the solder. Interfacial IMC played no part in the fracture behaviour. For a sample that was aged for 2 weeks at 175^{0}C, failure was completely brittle in manner and cracked through the Cu_6Sn_5. A sample aged for 3 weeks at 175^{0}C to further increase and coarsen the IMC, gave transgranular fracture again.

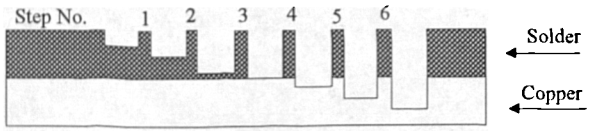

Fig. 2.28 Specimen for bond strength determination

2.5.2 Growth of Cu-Sn Intermetallic Compound

In service, an electronic assembly will often be continuously subjected to aging conditions. It was found that the IMC grows with aging time. Since, an increase in the IMC thickness is detrimental to the properties of the joint as a whole, it is crucial to understand the IMC growth mechanism. The growth rate of IMC was found to be a function of the aging time and aging temperature. The empirical formula, Equation 2.7, most commonly used for calculating the growth rate of the IMC is [37] :

$$\frac{dx}{dt} = Ax^{-n} \qquad (2.7)$$

where x is the compound thickness, n is a constant determined experimentally (n = 1/2 if the IMC grows by a diffusion-controlled mechanism, or n = 1 if it grows by interface

reaction control). A is a mobility which can be calculated if the activation energy, the universal gas constant, and the aging temperature are given. The experiments performed by Vianco *et al.* [102], showed that the IMC thickness was a function of $\sqrt{t}$ for 100Sn and 60Sn40Pb solders, where t was the number of days aged. The data exhibited a parabolic function after an initial accelerated growth rate that persisted for approximately four days. Detailed analysis indicated that for the 100Sn/Cu intermetallic, its thickness was closer to the form of $t^{0.346}$, and for 60Sn40Pb/Cu, its intermetallic thickness was closer to $t^{0.379}$. Separate growth mechanisms for Cu_3Sn and Cu_6Sn_5 were investigated. Parent *et al.* [95] showed that the Cu_3Sn thickness had a linear relation with aged time, and the rate of growth increased from 0.00347 μm minute^{-1} at 230°C to 0.0146 μm minute^{-1} at 350°C. As for Cu_6Sn_5, the thickness also grew with time and no apparent limit on the growth was detected. Vianco *et al.* [102], as expected also found both Cu_6Sn_5 and Cu_3Sn for the 100Sn/Cu and 63Sn37Pb/Cu systems after aging. The plot for the 100Sn/Cu system showed that Cu_3Sn thickness was parabolically time dependent. In the 63Sn37Pb/Cu system, the amount of Cu_3Sn also depended upon the extent of aging. On the other hand, Tu and Thompson [103], showed that Cu_6Sn_5 exhibited a linear growth rate, and that Cu_3Sn grew at the expense of Cu_6Sn_5. Mei *et al.* [104], rather than looking at the IMC growth from an empirical view point, used an analytical approach. A multiphase diffusion model was developed to analyse the growth of η phase and ε phase in solder joints..

2.5.3 Inspection Methodology

Basically the two most common metallographic methods for IMC inspection are optical microscopy and scanning electron microscopy (SEM) inspections [105]. Optical microscope inspection requires less expensive equipment, but it has limited capability. The steps for the preparation of specimens for this inspection broadly include: microsectioning, mounting, grinding, polishing, and etching. Yamada *et al.* [106], recommended a comprehensive procedure for the preparation and etching of near eutectic solder joints for IMC microscopic examination. Karlheinz and Manfred [107], compared the optical and SEM methods. This paper highlights the information that could not be revealed by the

optical approach but could be by SEM. In addition, with the use of energy-dispersive x-ray analysis (EDX), and x-ray mapping, the chemical composition of the compounds could be analysed easily.

2.6 CONCLUDING REMARKS

To ensure a good quality joint in SMT, the first step is to select a suitable solder paste. Selecting the right solder paste for the job is an art form, and it is not easy. A solder paste is characterised by a list of its constituents and parameters to facilitate selection. The more important characteristics specified are the alloy content, alloy composition, powder morphology, rheology, and tackiness. Past research has given some information about how each of these characteristics affects the performance of the solder paste. Nevertheless, the majority of the results published have been on the effects of individual characteristics, and little has been reported on the effects of interrelationships between characteristics. It was found that subsequent defects, such as slumps, bridges, solder balls, and wickings, are all related to the choice of solder paste. Solder paste is particularly deterministic to the printing quality. From understanding the rheology of the paste one can estimate its suitability for a particular printing task. Past research, to a certain extent, has been able to highlight the conflicting nature of the various characteristics for quality performance of a solder paste. For instance, a paste with fine and spherical particles is more suitable for printing and stands a higher chance of resulting in solder balling and spattering. Most of the results and comments published on the topic of stencil printing were based on experiments and observations. Very few took a theoretical approach by taking into account the printing mechanism and the solder paste properties at the same time. Extensive studies have been performed relating to the alloy powder and the flux in the solder paste. However, very little information published was about the effects of the solvent in the paste. It is expected that the printability, the tackiness, and the other properties of a solder paste, are severely influenced by the solvent. A more detailed investigation into the effects of solvent in SMT is most desirable. Speaking overall, the past studies on the solder paste have not been able to provide systematic and clear guidelines for solder paste selection.

Defects in SMT solder joints may be put into two categories: i) defects that are visually detectable from outside, and ii) defects entrapped inside the joints. The common externally detectable ones are tombstoning, bridging, solder balling, open circuit, wicking, dry joint, and insufficient solder joint. The ones that exist inside the joints and are more difficult to examine are voids, cracks, and impurity entrapments. The formation and prevention of some of these defects have been well covered by the literature cited above. However, publications on tombstoning are very limited. The reasons for its formation and methods of prevention are still not well studied. So far, the reliability tests for SMT solder joints are still confined to laboratories, and are very time consuming. In an application environment, a fast and effective method of testing which would give an indication of the quality of the joints is most desirable. Based on the literature searched, it can be seen that to establish a comprehensive reliability standard for the SMT joints is still a long way off.

The formation and the effects of intermetallic compounds in solder joints are relatively well documented. For the solder/copper system, it is found that the IMC is basically composed of two main layers, Cu_6Sn_5 and Cu_3Sn. Cu_6Sn_5 and Cu_3Sn have different effects on the reliability of a joint. There is general consensus among the authors that the IMC is brittle, and impairs the fatigue resistance. The growth of the IMC is a function of the aging time and temperature; the thicker is the IMC layer the larger is the detrimental effect. As far as the crack initiation and crack path are concerned, no unified conclusion can be drawn. Joints in which the IMC were studied in the past, primarily were produced by conventional soldering methods. Very few of the reports have touched upon SMT reflowed joints. Since, SMT reflow employs solder paste for soldering, and is a totally different approach, a study on this topic is worthwhile.

Chapter 3

Analysis of Tombstoning

3.1 INTRODUCTION

The increasing demand for smaller size electronic products has resulted in an increased application of SMT for securing components onto PCBs. SMT in the electronics industry can be divided into two main methods. The first method secures components into the desired positions by application of adhesive; the adhesive is then cured by passing through an oven, and solder is applied by passing the part through a wave-solder bath. The second method consists of screen printing solder paste, component placement, and application of heat (reflow). Each of these approaches has its merits, and the choice often depends on the types of components to be handled and the configuration of the assembly board.

SMT permits miniaturisation. However, it also introduces a range of new defects which are different from those found in the traditional through hole technology. Common defects in SMT consist of bridging, solder ball, misalignment, insufficient solder, and tombstoning (i.e. the components assuming a vertical rather than horizontal configuration) [9,57]. Tombstoning does not occur when SMT with adhesive is employed. It happens only when reflow soldering is used. The most common reflow processes are IR and vapour phase reflow. In the IR reflow process the heat is applied to the board mainly through infrared radiation [46,80]. In the vapour phase reflow process, the board is submerged in a chamber where heat is transferred to the board from the condensing vapour of a boiling liquid. The board absorbs the enthalpy of condensation, plus

heat transfer by convection. It has been found that vapour phase reflow gives components a higher chance of tombstoning [6].

3.2 TOMBSTONING PHENOMENON

The tombstoning type of defect is only associated with small SMT components without leads (leadless chips). A common phenomenon is that after the reflow process, one end of the component remains unsoldered, while proper soldering has taken place at other end so that the component lifts up at the unsoldered end. Depending on the degree of lifting, it may end up in a situation as shown in Fig. 3.1a, or the component may stand up completely as a tombstone as shown in Fig. 3.1b.

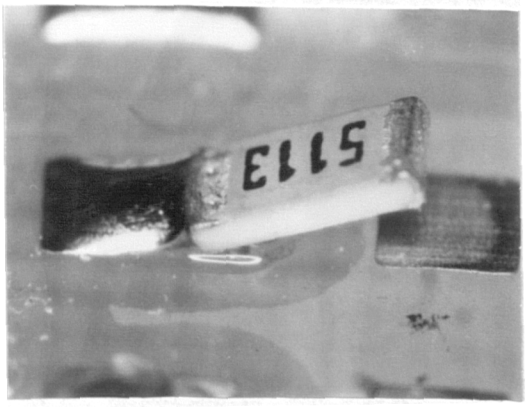

Fig. 3.1a Lifting of component

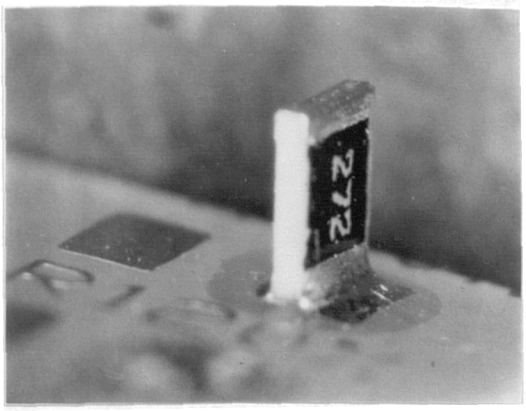

Fig. 3.1b Tombstoning of component

In the ideal situation, both ends of a leadless chip should be fully secured to the board; this requires that the soldering process over the two ends takes place simultaneously. This can be achieved only if the heat applied to the two ends is uniform. With reference to Fig. 3.2, imagine that for some reason it is impossible to heat both ends of the component simultaneously; so that the solder paste at the right has melted first, whilst the paste over the other end remains solid. In this situation, the surface tension of the molten metal results in a force that tends to pull the component upward with point 'A' as the pivot. Whether the component will lift up, and to what degree, depends on the interrelation of the geometry of the component, weight of the component, and the rate of solidification [62]. Based on the surface tension approach, Wassink and Verguld [61] have developed a model to explain how tombstoning can be sustained during the reflow process. It is realised that if uniform reflow can be achieved over the two ends, component lifting or tombstoning can be prevented [7]. To achieve this, both in the design and processing stages:

- the heat absorption rates of the two ends, which include both the component and PCB materials, should be made the same;
- the two ends should be heated up simultaneously. This can be achieved by proper orientation of the component. An example is shown in Fig. 3.3. As can be seen, at any distance traveled in the IR reflow process by the components, the temperatures at the two ends of Component A are more uniform than Component B; and
- shadowing of one end of a component due to the other part of the assembly should be avoided as far as possible during the infrared reflow process .

It is expected that the component would have passed through three stages before the completion of tombstoning:

1. the solder paste over the two ends of the component is subjected to uneven heating which causes the solder paste at one end to melt before the other;
2. the surface tension of the wetting molten solder is large enough to overcome the other forces which keep the component lying flat on the PCB, so that the component starts tilting upwards;

3. the tilting angle is further increased by the subsequent solidification process of the solder.

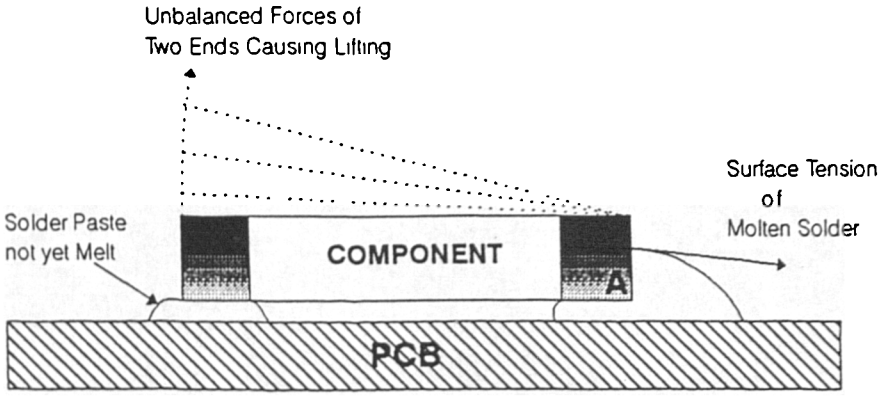

Fig. 3.2 Effects of unbalanced forces

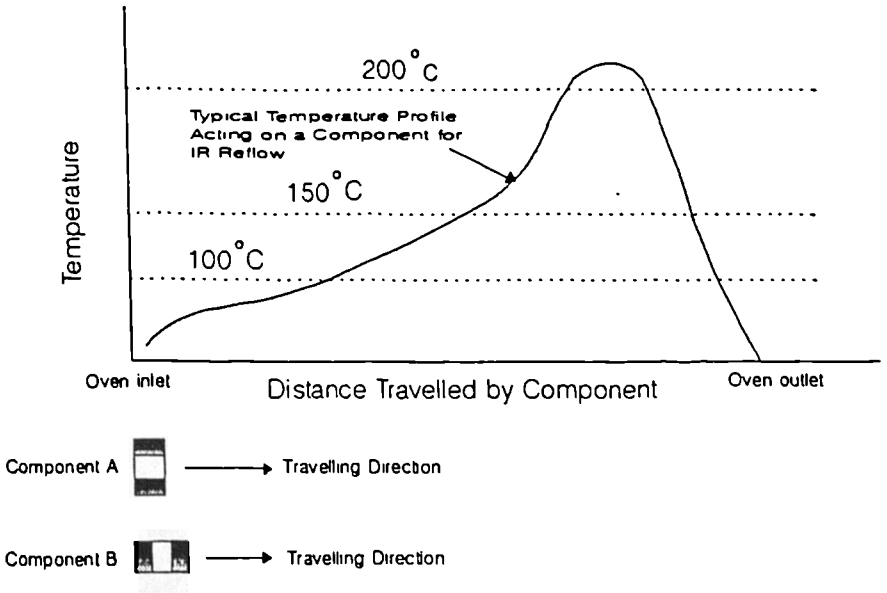

Fig. 3.3 Orientation of components

3.3 ANALYSIS

It is believed that the force sustaining the standing up of a leadless component during reflow comes from the surface tension of the molten solder [6,7,61,]. The present study emphasises the initiation of the lifting, since it is considered that once one end of the component is lifted up, regardless of the amount, its functional effect is lost as long as it has lost contact with the PCB land. Fig. 3.4 illustrates the conditions prevailing at the end where the solder first melts. When the temperature is high enough, the molten solder forms a curved surface and adheres to the end surface of the component. It was shown by Dupré [29,108] that the work of adhesion, w_a, between liquid and solid is

$$w_a \quad \gamma + \gamma_s - \gamma_{s/l}$$

and can be expressed as

$$w_a - \gamma(1 + \cos\theta)$$

where γ is the surface free energy of the liquid solder, γ_s is the surface free energy of the solid, $\gamma_{s/l}$ is the surface free energy of solid/liquid solder, and θ is the angle of contact between the liquid solder and the solid component. The combined effect of w_a, and γ creates an upward moment on the component. Referring to Fig. 3.5, the upward moment, T_l, about point 'A' due to the surface tension, γ, of the protruding solder from the end of the component is

$$T_l = \gamma.H.D.\sin\theta. \qquad (3.1)$$

The forces keeping the component in contact with the PCB come from the weight of the component, m.g, and the surface tension of the solder underneath the component, γ. The two downward moments T_g and T_s, about the point 'A', generated by these two forces, m.g and γ, respectively, are

$T_g = ½L.m.g$

and

$T_s = \gamma.H.W.\sin\alpha.$

Hence the total downward moment is

$T_2 = T_g + T_s = ½L.m.g + \gamma.H.W.\sin\alpha.$

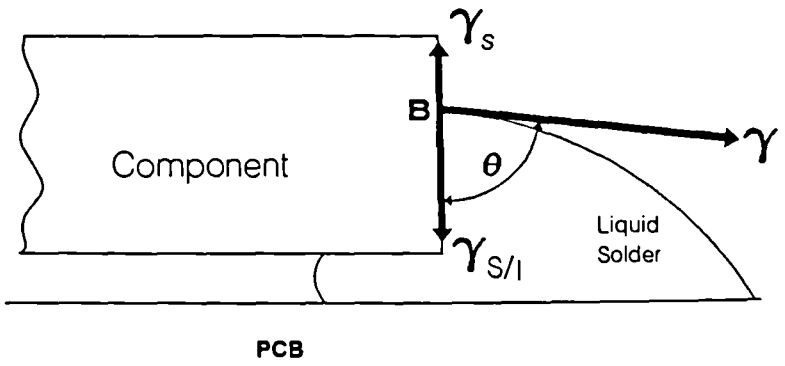

Fig. 3.4 Effect of surface tension

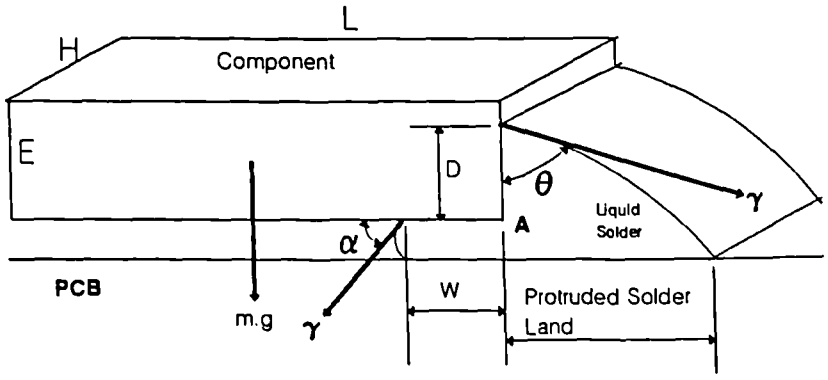

Fig. 3.5 Forces acting on the component

Notations for Fig. 3.5 are: E, height of the component; L, length of the component; H, width of the component; m, mass of the component; g, acceleration due to gravity; γ, surface tension (surface energy) of liquid solder; D, solder height, θ, angle of contact between liquid solder and component end surface; α, angle of contact between liquid solder and the component bottom surface; and W, liquid solder length underneath the component.

Figs. 3.6a - c, illustrate the changes of the solder meniscus shape when the component is being lifted up gradually. Fig. 3.6a represents the initial situation, in which the component is assumed resting freely on the molten solder. The meniscus curvature of the molten solder, which has a surface tension γ and forms a contact angle α with the bottom surface of the component, is convex. If a force F is applied, see Fig. 3.6b, which causes the component to rotate about point A, the value of α would increase and at the same time the curvature would decrease gradually. Letting the rotation continue, it would arrive at a situation where the meniscus curvature is at right angles to the bottom of the component ($\alpha = 90^0$), Fig. 3.6c. It is at this stage that the downward force created by the molten solder underneath is at its maximum. Since the tilting of the component, when $\alpha = 90^0$, is small, its effect on changing the value of the moment due to the component weight is considered insignificant. The total downward moment, T_2, reaches its maximum when the meniscus is perpendicular to the component surface (i.e. $\alpha = 90^0$, $\sin\alpha = 1$), and can be expressed as

$$T_2 = \tfrac{1}{2}L.m.g + \gamma.H.W. \qquad (3.2)$$

At the threshold of tombstone initiation, the total upward moment should be equal to the total downward moment, so that

$$T_1 = T_2$$

and approximately can be expressed as

$$\gamma.H.D.\sin\theta = \tfrac{1}{2}L.m.g + \gamma.H.W. \qquad (3.3)$$

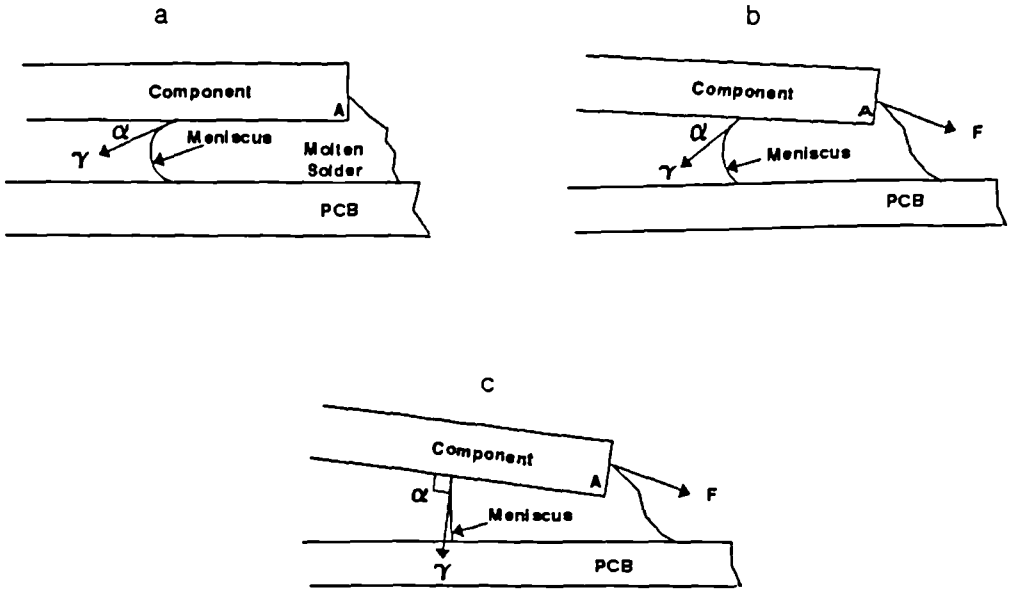

Figs. 3.6a-c Meniscus changes during lifting of component

3.4 INITIATION CALCULATION

The conditions underwhich tombstone initiation might be expected to occur for selected leadless chips were calculated. A summary of the features of the selected components are given in Table 3.1, with the notations referred to in Fig. 3.5. The weight of a component is the average weight from a sample of fifty. The results of these calculations are all shown in Figs. 3.7a-i. The following information is obtained from Fig. 3.7.

1. From Equation 3.1, the upward moments, T_1 ,at different contact angles, θ, and solder heights D, were calculated. The contact angle starts off from zero degrees, which occurs when no protruded solder is present, and finishes at a value of ninety degrees which occurs when the protruded solder has an infinite length. The solder heights, D, used were at a maximum which were equal to the heights of the components, and also with heights equal to 0.75, 0.5 and 0.25 of E.

2. From Equation 3.2, the total downward moments, T_2, were calculated for different magnitudes of W. T_2 is unchanged for a particular W, and is a straight line.
3. Any point where T_1 cuts T_2 gives the conditions at which lifting would take place.

Component	Weight m ($X 10^{-3}$kg)	Length L (mm)	Width H (mm)	Height E (mm)
RC 1206(1)	0.02383	3.20	1.60	1.00
RC 1206(2)	0.00931	3.20	1.60	0.70
CC 1206	0.02382	3.20	1.70	1.50
CC 1812	0.07828	4.50	3.20	1.70
RC 1210	0.01630	3.20	2.5	0.60
A 3216	0.02275	3.10	1.72	1.80
C 6032	0.13390	6.00	3.20	2.80
D 7243	0.27514	7.20	4.30	3.04
CC 0805	0.008266	2.00	1.25	0.7

Table 3.1 Features of calculated components

Apart from the conditions at which component lifting may occur, other information may also be deduced from these figures. It can be seen that the upward moments are effectively increased as the contact angles increase. The other factors which determine the probability of component lifting during reflow are the geometry and weight of the component. It can also be seen that the likelihood of having tombstone initiation depends on the relative positions of the straight lines T_2, and the curves T_1 for the component. Considering Fig. 3.7a as an example, length A-C is the difference between the maximum and minimum magnitude of T_2, where B-C is the length of part of A-C that falls inside the T_1 curve when D is a maximum. The higher the ratio of B-C:A-C, the higher is the likelihood of tombstoning. Thus when this ratio is equal to zero or negative, theoretically speaking no lifting should occur. The nine components on which calculations have been performed can be ordered as follows in terms of decreasing probabilities of tombstoning: CC 1206, CC 0805, A 3216, CC 1812, RC 1206(1), RC 1206(2), RC 1210, C 6032 and D 7243. In fact for D 7243, according to the calculations if reflowed under normal

conditions, such as free from vibration during transport, tombstoning or lifting should never occur. This is because, by referring to Fig. 3.7h, T_2 is greater than T_1 in all circumstances. Table 3.2 summarises the results of these calculations.

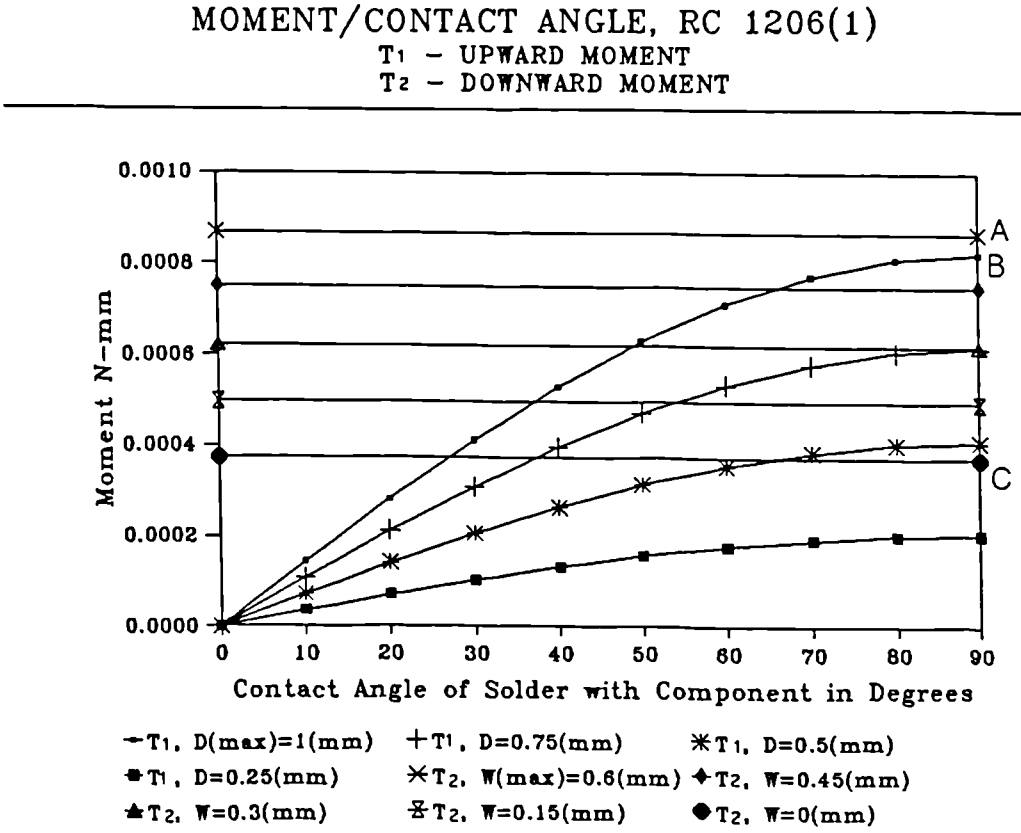

Fig. 3.7a Moments acting on RC 1206(1)

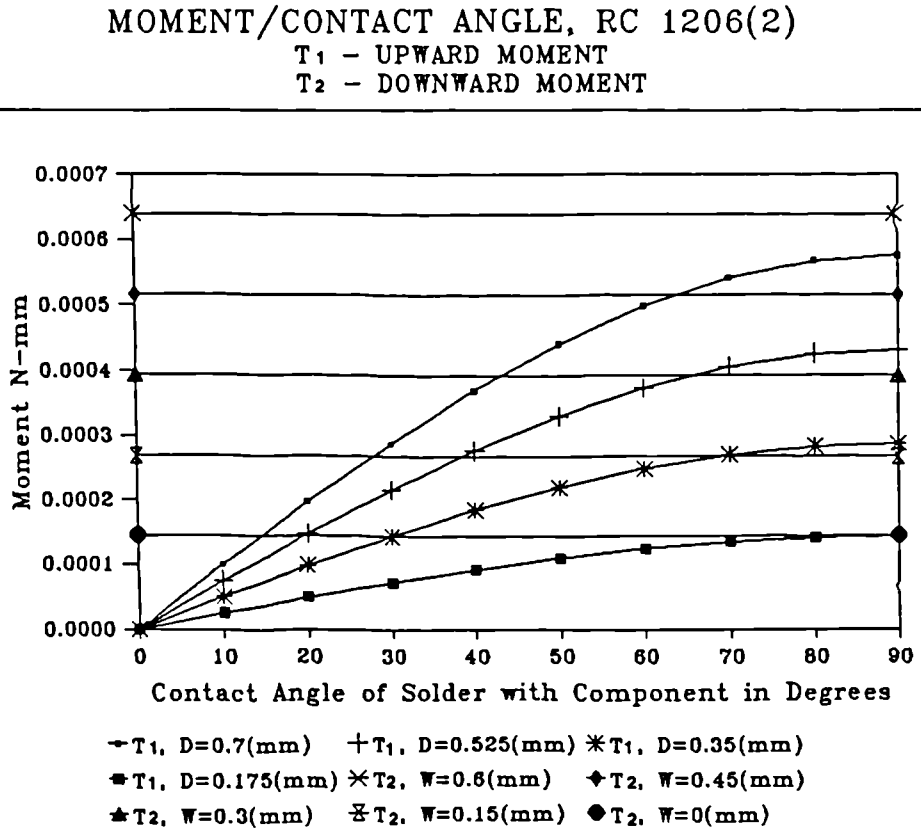

Fig. 3.7b Moments acting on RC 1206(2)

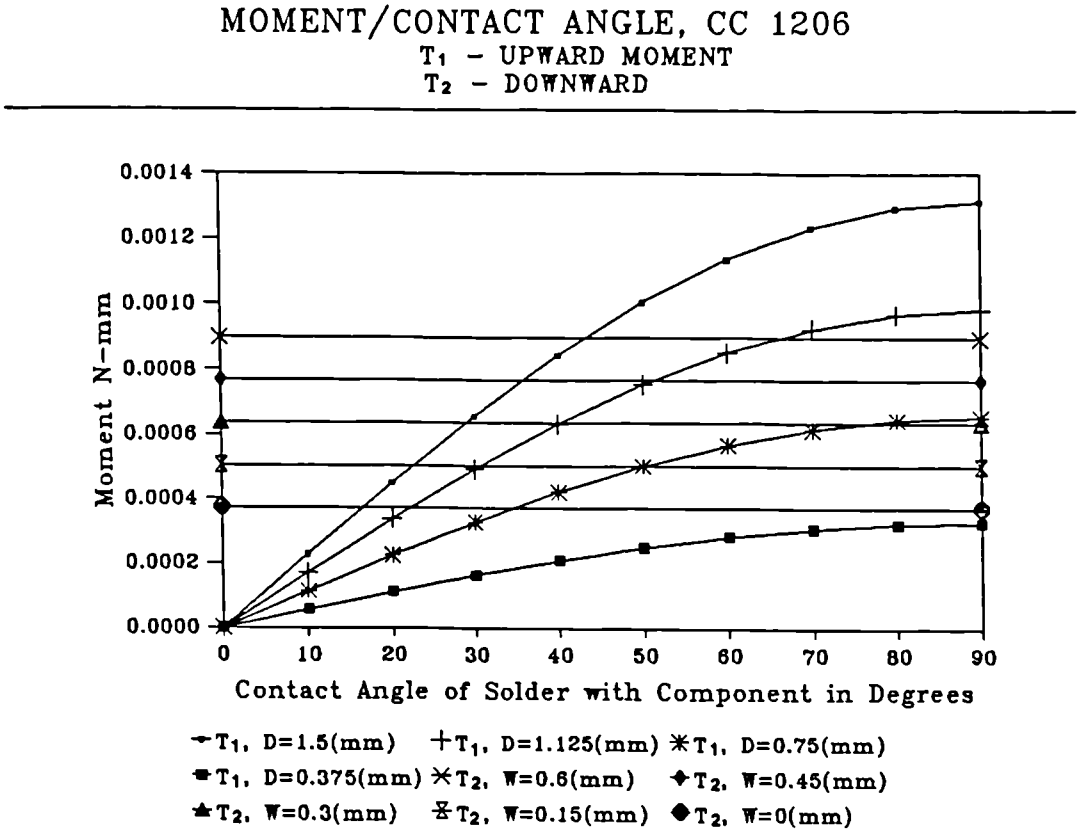

Fig. 3.7c Moments acting on CC 1206

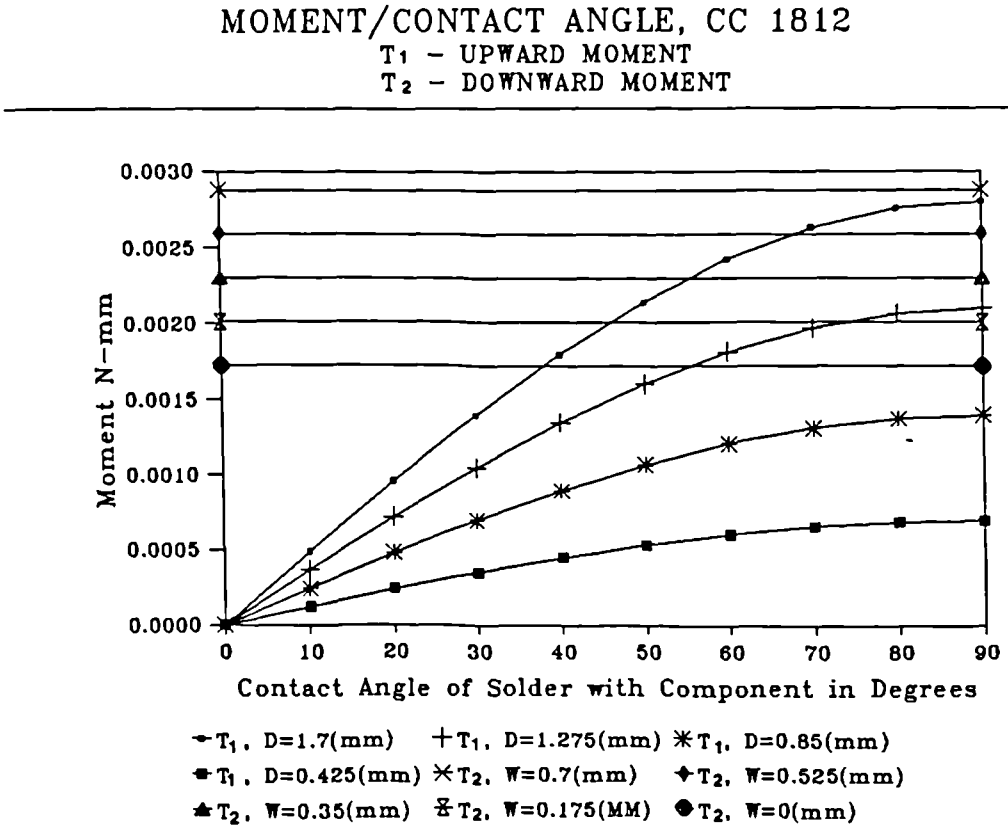

Fig. 3.7d Moments acting on CC 1812

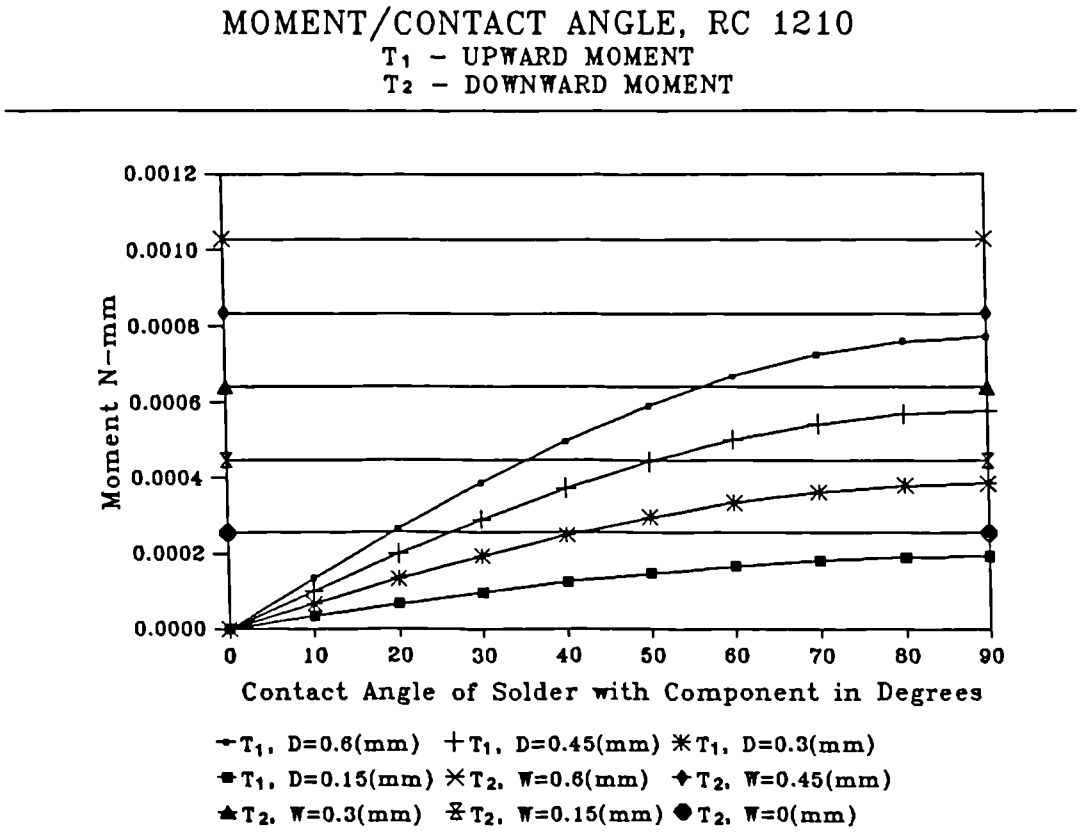

Fig. 3.7e Moments acting on RC 1210

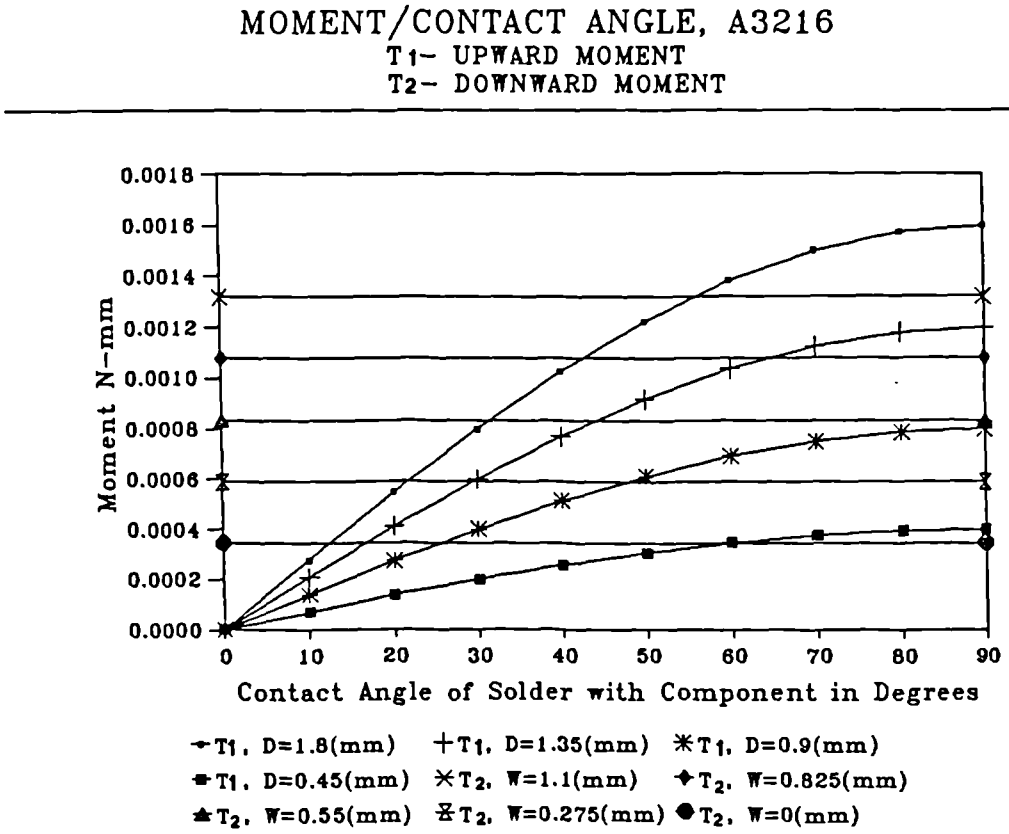

Fig. 3.7f Moments acting on A 3216

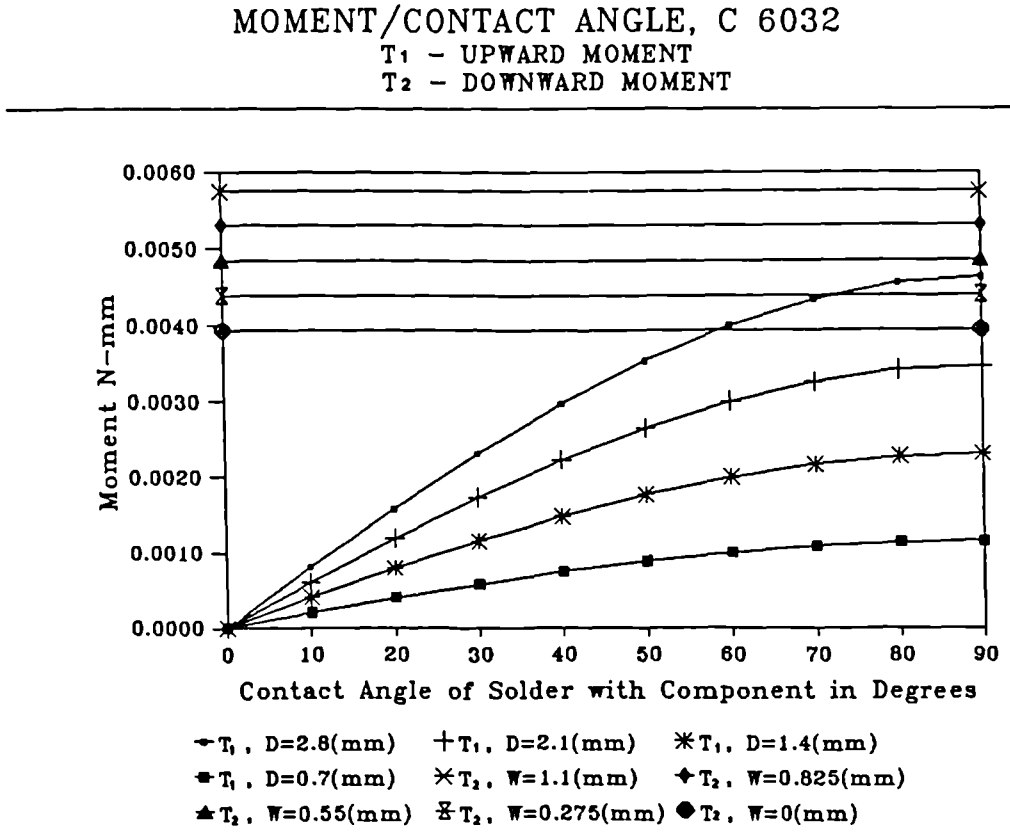

Fig. 3.7g Moments acting on C 6032

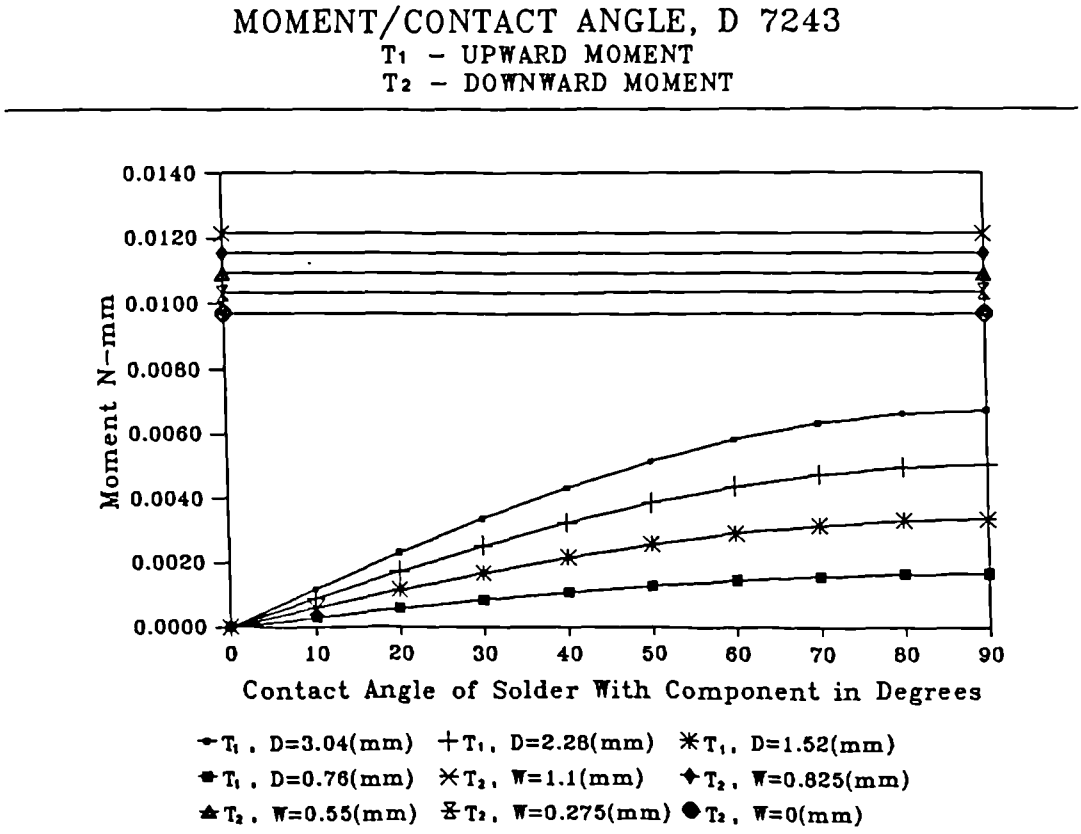

Fig. 3.7h Moments acting on D 7243

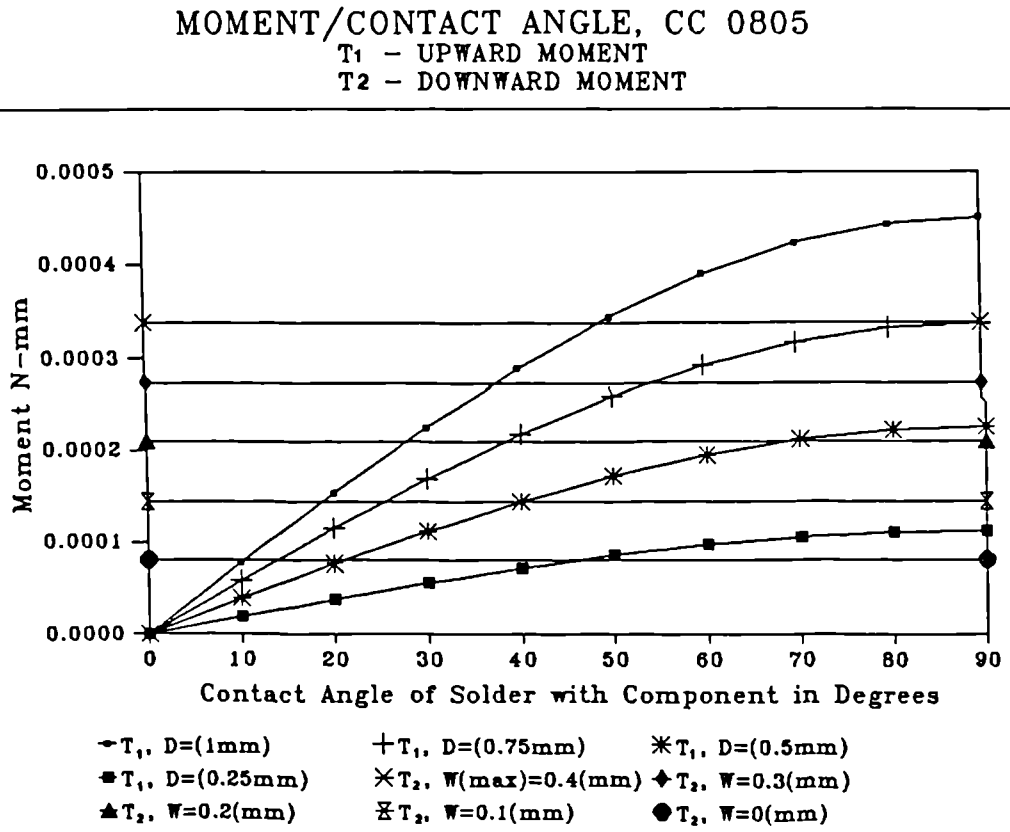

Fig. 3.7i Moments acting on CC 0805

Component	Ratio =B-C/A-C	Lifting Probability Rank
RC 1206(1)	0.911	5
RC 1206(2)	0.872	6
CC 1206	1.790	1
CC 1812	0.933	4
RC 1210	0.66	7
A 3216	1.280	3
C 6032	0.374	8
D 7243	-1.22	No chance
CC 0805	1.432	2

Table 3.2 Probability of tombstoning

From Equation 3.3, the liquid solder length underneath the component can be expressed in the form:

$$W = D.\sin\theta - L.m.g/2\gamma.H.$$

Since the parameters L, m, g, γ, and H are all constants for a particular component, then this can be simplified to

$$W = D.\sin\theta - C. \qquad (3.4)$$

Selecting RC 1206(1) as an example, and taking the most common solder height D as equal to E, the relation between W and θ at the threshold of lifting can be calculated from Equation 3.4, and is shown in Fig. 3.8.

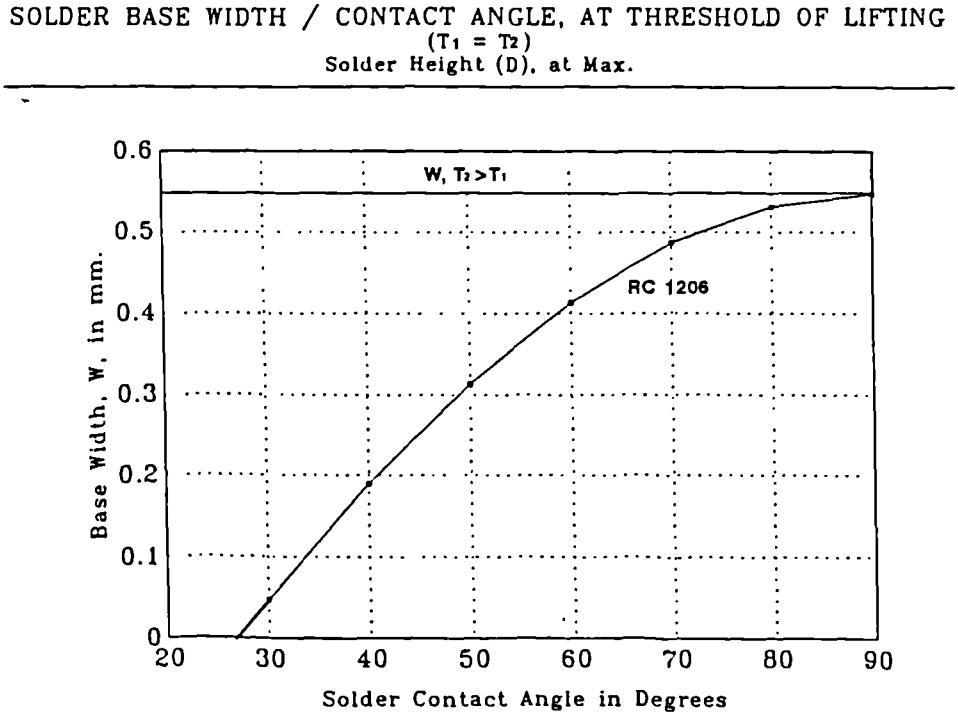

Fig. 3.8 W - θ relation at lifting threshold

3.5 EXPERIMENTS

Fig. 3.9a - c, show the configurations of the three types of board used in the experiments. The boards were single-sided with materials FR4 epoxy as base, and bare copper as solder land. Taking RC 1206(1) in Fig. 3.9a as an example, the dimensions of the pair of solder lands denoted by R100% on the board are in according with the IPC standard. For the rest, the solder land lengths on the right are increased gradually from lengths equal to 110% to 250% that of the R100%, and are denoted by R110% through R250%. The lengths of the lands on the left are kept unchanged, the same as that of R100%. The idea of this design is to provide different lengths of protruded solder, hence achieving different solder fillet shapes in the experiments.

Multicore RM92, (63Sn37Pb) solder paste was used. The solder paste was firstly manually screen printed onto the board, and then components were placed in position by hand. To simulate an unevenly heated condition during reflow, which would result in the paste at one end of the component melting before the other, solder paste was only printed onto the lands where the length varied. The lands on the other side of the components were unprinted. Taking RC 1206(1) as an example, the lands at the right were covered with solder paste, whilst the lands on the left were left clear. Thus the printed ends simulated the component ends where melting took place first, and the unprinted ends simulated the ends subjected to a slower heating rate thus remaining solid during the tombstone initiation.

To accommodate all the components to be tested, three types of boards were used. To maintain consistency in the heating process, the optimum temperature profile was firstly found for a particular board, and that profile was used throughout the tests on that type of board. The boards were reflowed in a HELLER 932 IR oven. After the reflow process, components were examined for evidence of lifting and tombstoning. Table 3.3 gives the results obtained in this part of the experiments.

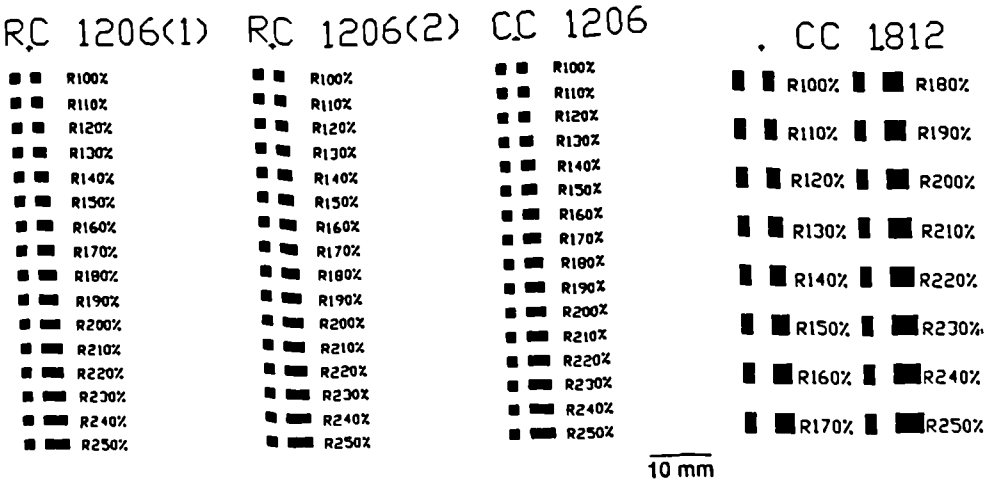

Fig. 3.9a Board configuration: Type 1

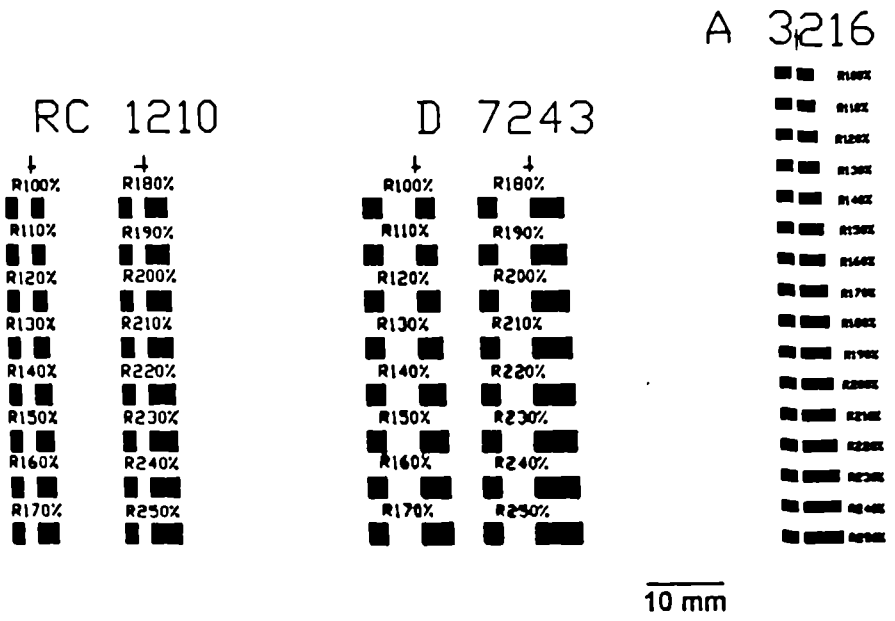

Fig. 3.9b Board configuration: Type 2

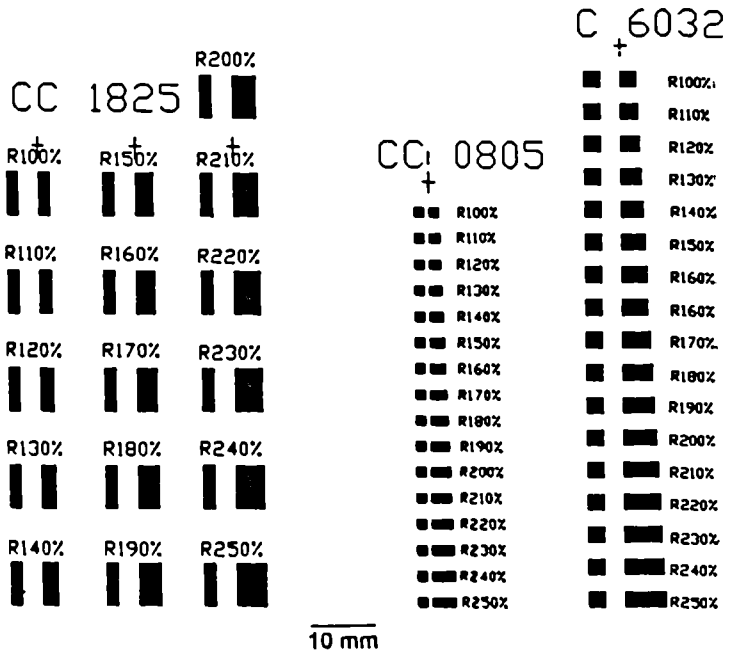

Fig. 3.9c Board configuration: Type 3

Component	Length of solder land 100 130% L	T	140 170% L	T	180 210% L	T	220 - 250% L	T	Sample size	Lift/ tombstone probability
RC 1206(1)	0	0	1	0	2	1	2	0	480	0.0125
RC 1206(2)	0	0	0	1	2	0	2	1	432	0.0138
CC 1812	0	0	1	0	1	0	2	0	320	0.0125
RC 1210	0	0	0	0	2	0	1	0	380	0.0079
A 3216	0	0	0	0	0	0	0	0	320	0
C 6032	0	0	0	0	0	0	0	0	320	0
D 7243	0	0	0	0	0	0	0	0	320	0
CC 0805	1	0	0	1	2	1	3	2	480	0.0208
Total No.	1		3		11		13		3052	

L--Number of components lifted up

T--Number of components tombstoned

Table 3.3 Effect of land length on tombstoning.

3.6 DISCUSSION OF RESULTS

Using the specially designed boards enabled us to carry out an investigation in which the solder length was the only variable affecting the tombstone initiation. It is generally known that to obtain a set of representative data in an investigation of the tombstoning process, a large sample size is necessary. Experiments of this type are basically probabilistic in nature. By leaving one end of the lands unprinted and at the same time with the length of the other end increased, it was, as expected, found that the chance of initiating the tombstone effect was increased. With reference to the results in Table 3.3, the following points can be made.

1. From the total number of liftings and tombstonings for different solder land lengths, there is strong indication that a longer land length results in a higher probability of lifting or

tombstoning of the component. This agrees well with the theory since Equation 3.1 suggests that a long land length would give a large contact angle θ and result in a large moment T_1 pulling the component upwards.

2. The component, which has the highest probability of lifting or tombstoning, is found to be the CC 0805. This again agrees very well with the prediction based on theory. Referring to Table 3.2, since no component tests were performed on CC 1206, CC 0805 ranks highest in terms of the probability of occurrence for this type of defect.
3. The configuration of the metal contact of a component can largely deter tombstone initiation. Among the components tested, RC 1206(1), RC 1206(2), CC 1812, RC 1210, and CC 0805 are all metallised as indicated by Fig. 3.10a which encourages the solder to wet to the top of the component. For components A 3216, C 6032 and D 7243, the configuration is quite different. As indicated in Fig. 3.10b, this has the effect of limiting the solder to a certain height, hence reducing the upward pulling moment generated by the surface tension of the molten solder. A configuration of this type largely reduces the occurrence of tombstoning or lifting. This explains why the experimental results on A 3216 do not match with the theoretical prediction in terms of probability ranking.
4. For components RC 1206(1), RC 1206(2), and CC 1812, there appear to be slight discrepancies between the experimental results and the theoretical predictions. However, on closer inspection, it can be seen that the values of their B-C:A-C ratios, as well as their experimental probabilities are almost equal to each other. Since the probabilities of initiating tombstoning are about the same for this group of components, it is considered unrealistic to expect the experimental outcome to be exactly the same as that calculated by theory. For RC 1210, both experiments and theory show that the probability of tombstoning falls below RC 1206(1), RC 1206(2), and CC 1812.
5. For C 6032 and D 7243, both experiments and theory indicate that they have the least probabilities of tombstoning or lifting. As mentioned above, the configuration of their contact metallisation (Fig. 3.10b) significantly deters the component lifting, hence, it is not surprising to see that, combined with their geometry and weight, both C 6032 and D 7243 give zero lifting and tombstoning values in the experiments.

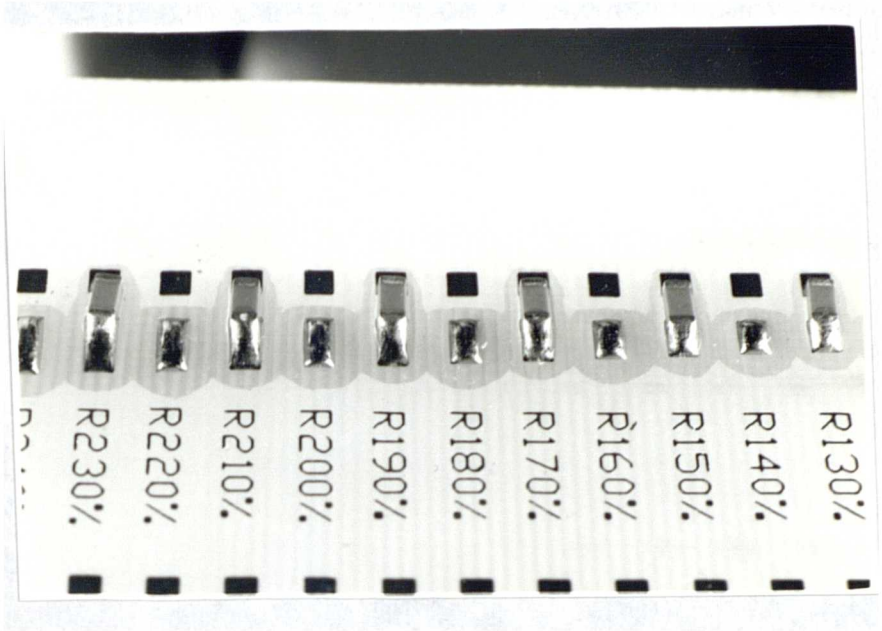

Fig. 3.10a Metal contact for RC 1206(1), RC 1206(2), CC 1812, RC 1210, and CC 0805

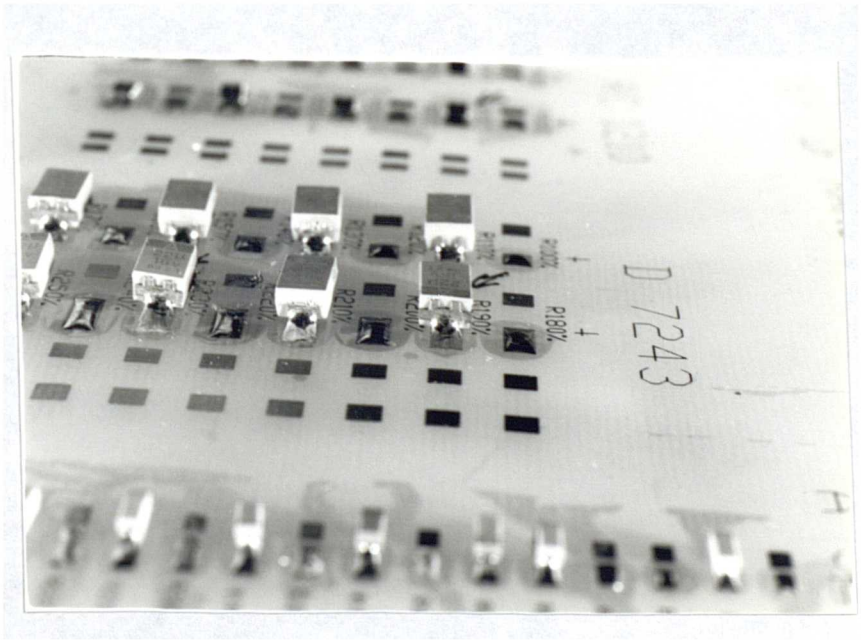

Fig. 3.10b Metal contact for A 3216, C 6032, and D 7243.

Chapter 4

Bond Strength and Effects of Solder Thickness

4.1 PULLING TEST

The reliability of a SMT joint is dependent on the operational quality at different stages of the soldering process. So far, there are no quick and objective methods for measuring the quality of a solder joint. The methods commonly used are either direct inspection by means of the naked eye, or metallography. However, both of these methods are very subjective. The latter method does provide an effective indication on the wetting quality, but its drawbacks are the fact that it is time consuming, requires well-trained personnel, and very often can only be performed in a laboratory environment. One of the objectives of the present study is to look into the feasibility of using a direct pulling test as a method for measuring the quality of a joint, so that a quick and quantitative method can be established, and more importantly, one that is applicable to the manufacturing environment.

4.1.1 Test Methodology

Components selected for the tests were all leadless chips which included RC1206, RC1210, CC1812, D7243 and CC1206. A test board which could accommodate all the selected component types was designed and fabricated. The pad sizes on the board were all in accordance with the IPC standard. A special component gripper which covers all the sizes of the

selected components was also designed and manufactured from tool steel, by machining, and heat-treatment. To enable a component to be held firmly in each test, fine teeth were produced on the gripper faces. At the same time, a fixture for holding the printed circuit board onto the test table was made. This fixture was designed to provide minimum movements to the board during testing. Fig. 4.1 shows the arrangement during testing. To allow solder paste to be printed onto the predetermined positions on the board, 0.15 mm thick stainless steel stencils were produced.

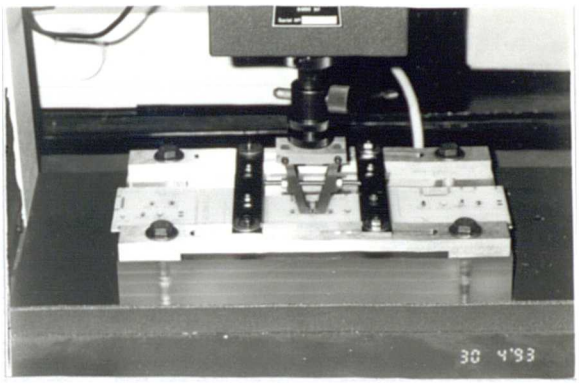

Fig. 4.1 Photograph showing the pulling test conditions

The first method employed for soldering components on the boards was the IR reflow process. Since different board configurations require different optimum reflow conditions, the optimum reflow temperature profile of the test board was found first (Appendix B). Components of all selected types were secured on the boards by going through the operations of screen printing of solder paste, placement of components, and infrared reflow. The type of solder paste used was Multicore RM92, 63Sn37Pb. The reflow process was performed in a Heller 932 IR oven.

The second method for soldering components was an adhesive wave soldering (WS) process. The components used were the same as those used in the first method, so that a direct comparison could be performed. To solder the components on the boards, this method consists

of operations of adhesive dispensing, placement of components, curing of adhesive by heat and ultra-violet (UV) light, and wave-soldering. Here, the amount of adhesive applied was just a tiny dot, always positioned at the centre a component. The adhesive used was Multicore SMD 881.

Pulling tests were performed on components that had been soldered onto the boards by the two methods mentioned above. The tests were carried out on a Hounsfield universal testing machine. The test speed used was 1 mm/minute. The force/extension curve of each test was stored in computer software then printed out at a later stage. The conditions of failure of all joints were recorded.

4.1.2 Findings and Results

It was found in the pulling tests that for D7243, CC1206, and components with similar metal connector configurations, the solder joint was stronger than the bonding of the metal connector to the component. Failures were in the form of the connector breaking off from the component body, as indicated in Fig. 4.2a. Accordingly, pulling tests for determining the quality of solder joints of components with this type of metal connector in the field were found to be unfeasible. Table 4.1 shows the summary of tests for these two types of components. Due to the mode of failure, an ultimate tensile force in the table is only an indication of the bond strength of the connector to a component, rather than the strength of the solder joint. However, for components RC1206, RC1210, CC1812, failures mainly occurred in the solder joints as shown in Fig. 4.2b, apart from a few with component breakage. So far, the adhesive strength between the copper pads and the epoxy was found acceptably strong; failures with copper pads peeling off the boards have not been encountered. From Fig. 4.3, it can be seen that the IR reflowed component with the largest average bond strength is CC1812, followed by RC1210 and RC1206. Only CC1812 and RC1206 components were employed for the WS comparisons. Although IR reflow and WS are two totally different soldering processes, comparing the ultimate tensile forces of components CC1812 and RC1206 soldered by these two processes, there is no evidence showing that one process produces higher strength joints than the other; it

varies with the component type. The results obtained here indicate that, for CC1812, WS gives a higher strength than IR soldering, whilst for RC1206 it is the opposite.

Component	Sample size	Mean ultimate tensile force (N)	Standard deviation	Failure mode
D7243	20	173 57	14.50	Metal connectors breaking off from the component bodies
CC 1206	20	45 44	7.87	Metal connectors breaking off from the component bodies

Table 4.1 Pulling test results for D7243 and CC1206

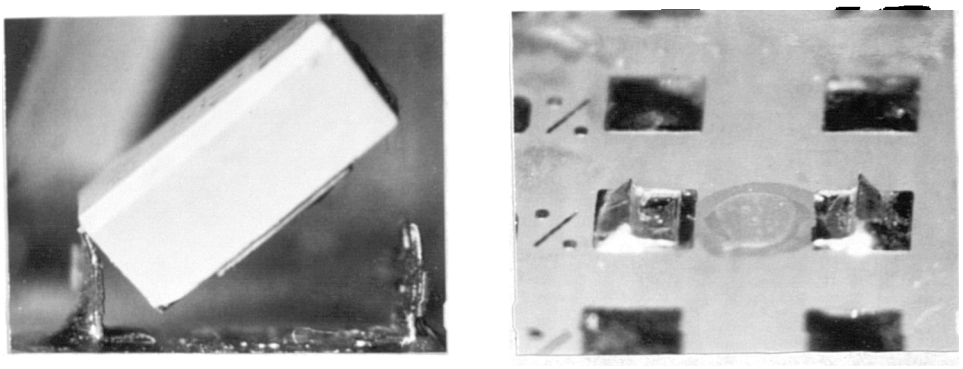

4.2a 4.2b

Figs. 4.2a-b Modes of failure

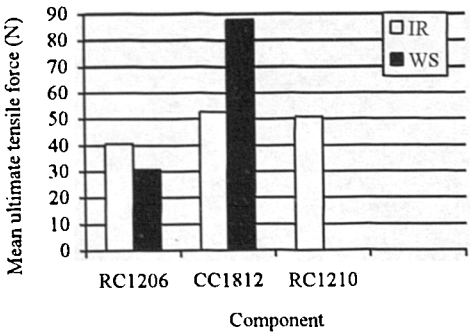

Fig. 4.3 Mean ultimate tensile force of tested components

4.2 FINITE ELEMENT ANALYSIS

With the advances in computers and their associated software, FEA is a flexible and convenient method for the computation and analysis of the stress/strain characteristics of complex physical objects. For intricate shapes and localised stress/strain analysis, very often, FEA is found to be the only viable method. In service, it is understood that solder joints are subjected to combined stress and temperature cycling conditions. With the FEA approach, to analyse the plastic deformation behaviour of each cycle and then to predict the fatigue life of a joint, requires a large amount of computation time, and is not an easy matter. Although it is realised that solder joints involve large plastic deformations during life cycling, straight linear elastic FEA provides a quick and effective way to compare the strength of joints with different configurations.

4.2.1 Analysis

RC1206 was selected as the component for a linear elastic FEA. The overall dimensions of this component were 3.12 mm long, 1.57 mm wide, and 0.61 mm high. The analysis assumed that the component was soldered on a printed circuit board with FR-4 epoxy as substrate material, then subjected to a pulling test. The physical and mechanical properties of the assembly are shown in Table 4.2a. The objective of these simulations was to study the relation between the bond strength and the joint geometry. The FEA package used was the Patran Plus, installed in a Sunsparc system. Table 4.2b summarises the configurations of the six cases for which analyses have been performed, and the joint geometry notations in the table are with reference to Fig. 4.4a - d. Fig. 4.5a shows a 3D finite element mesh model for Case 4, and Fig. 4.5b is the solid model base on which the 3D finite element mesh model was built. For all the cases analysed, plane strain was assumed in the 'Z' direction, and at the same time a constant tensile load equal to 30N was applied to the component, and this load was evenly distributed on eighteen nodal points along the two component sides. As a result, each nodal point was carrying a pulling force of 1.67N. From the stress and strain analysis, the bonding conditions of each case were interpreted.

Material	Young's Modulus (MPa)	Poisson's Ratio	Density (kgm^{-3})
Ceramic (RC 1206)	255,000	0.3	1830
Solder	30,000	0.4	8522
Epoxy (FR-4)	11,000	0.28	387

Table 4.2a Physical and mechanical properties of assembly

Case	Solder fillet height (mm)	Solder fillet shape	Standoff height (mm)
1	0	no fillet	0.051
2	0	no fillet	0.127
3	0	no fillet	0.203
4	0.61	concave	0.127
5	0.61	concave (left) convex (right)	0.127
6	0.61	convex	0.127

Table 4.2b Configuration of solder joints for finite element analysis

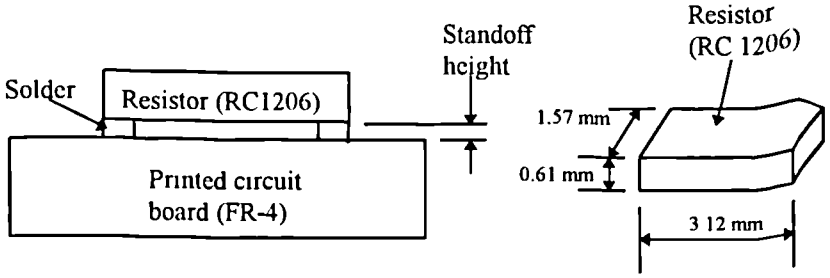

4.4a No fillet for Case 1, 2, and 3

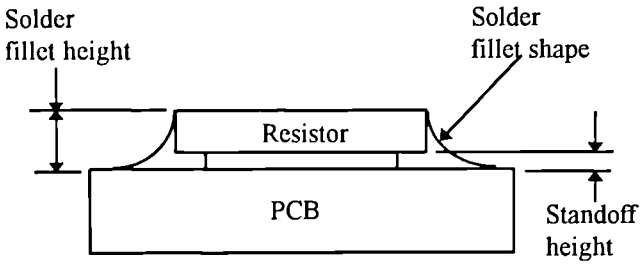

4.4b Concave fillets for Case 4

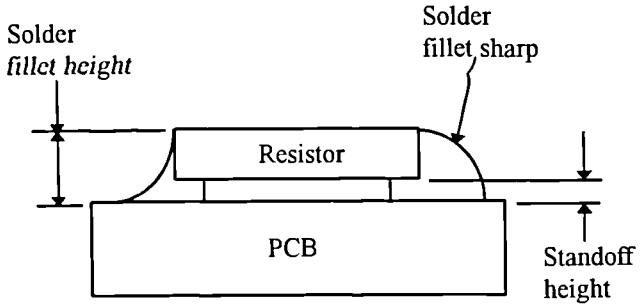

4.4c Left concave, right convex fillets for Case 5

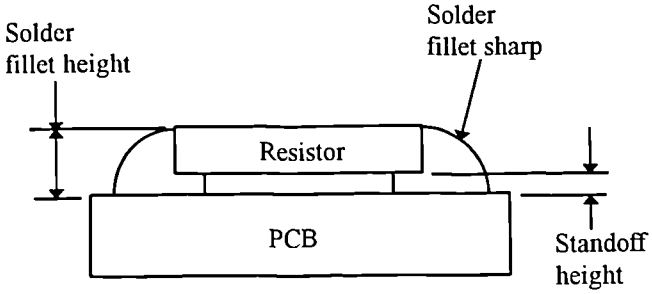

4.4d Convex fillets for Case 6

Figs. 4.4a-d Shapes of joints for finite element analysis

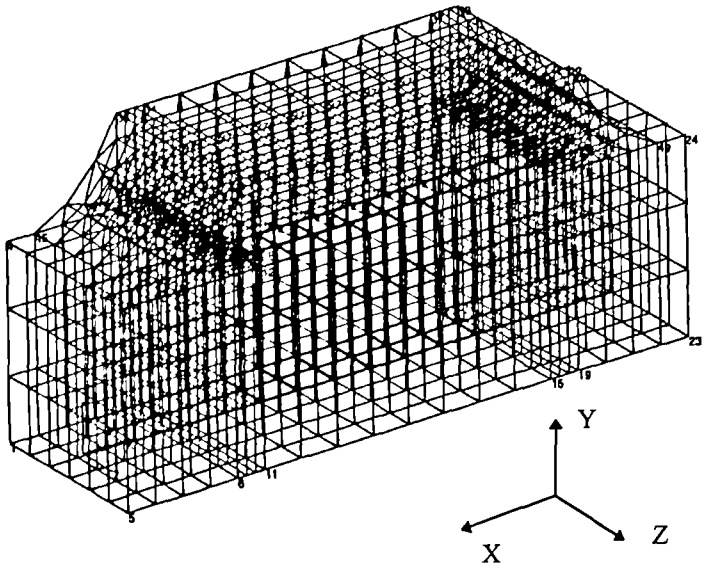

4.5a 3D finite element mesh model for Case 4

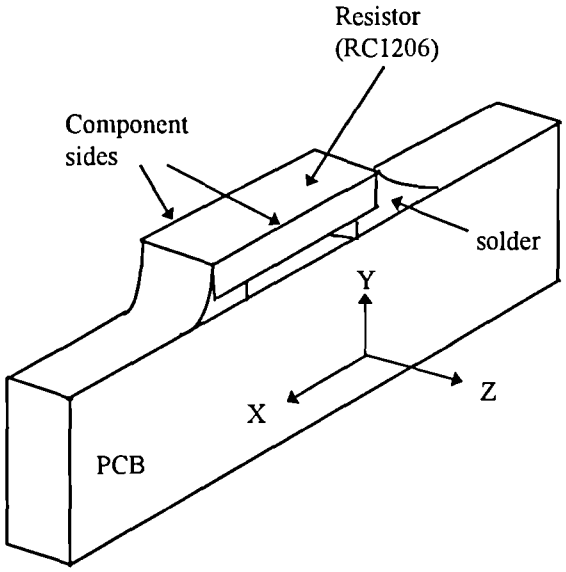

4.5b Solid model for Case 4

Figs. 4.5a-b Models for Case 4 finite element analysis

4.2.2 Results of the Analyses

In the finite element analyses, since a fixed pulling force was assumed to be applied to the components for all six cases, a comparison of their stress and strain concentrations, and their strain energy absorptions, were used for studying their bond strength differences. The maximum shear stresses and strains, and their locations for the six cases are shown in Fig. 4.6a and 4.6b. It can be seen, by comparing Cases 1, 2 and 3, which are joints without fillets but with different standoff heights, that both the maximum shear stress and strain decrease with an increase in the standoff height, and occur consistently in the same position on the joints. This indicates that, for the same tensile force, from the analysis point-of-view, a joint with a smaller standoff height is more susceptible to cracking. For Case 5, one end of it is concave and the other is convex, which represents typical conditions of a joint produced by WS. The finding shows that the concave end is subjected to slightly higher stress and strain concentrations, their values are 31.14 MPa and 2.91 x 10^{-3} respectively, as compared to that of the convex end which are 29.61 MPa and 2.76 x 10^{-3}. Fig. 4.7a and 4.7b show the solder joints for Case 4 and 6 respectively. Fig. 4.8a to 4.8d are the stress and strain contours of the joints for Case 4 and 6. Again, similar to Case 5, the concave joint has a resulting maximum stress and strain only slightly higher than that of the convex. The bonding conditions of concave and convex joints were further studied here by comparing their levels of strain energy absorption. From Fig. 4.7a, the solder plane which cuts through the line α_1-λ_1-β_1 is defined as Plane 1a, γ_1-σ_1-θ_1 as Plane 2a, and ρ_1-ϕ_1 as Plane 3a. Similarly, from Fig. 4.7b, the solder plane which cuts through the line α_2-λ_2-β_2 is defined as Plane 1b, γ_2-σ_2-θ_2 as Plane 2b, and ρ_2-ϕ_2 as Plane 3b. These planes are shown once again in Fig. 4.8b and 4.8d. The strain energy distribution along these planes for both cases are calculated and shown in Fig 4.9a and 4.9b. The average strain energy absorbed per unit volume of material of corresponding planes (e.g. Plane 1a and Plane 1b) from both cases are compared and shown in Fig. 4.10. This figure indicates clearly that the energy absorption level of all the three planes for a concave joint are higher than that of the convex. On the basis of the theory that a point in a material will fail when it has absorbed an energy equal to a critical value, W_c [109], and can be expressed as:

$$\int \sigma d\varepsilon = W_c$$

indicates that a convex joint is more robust.

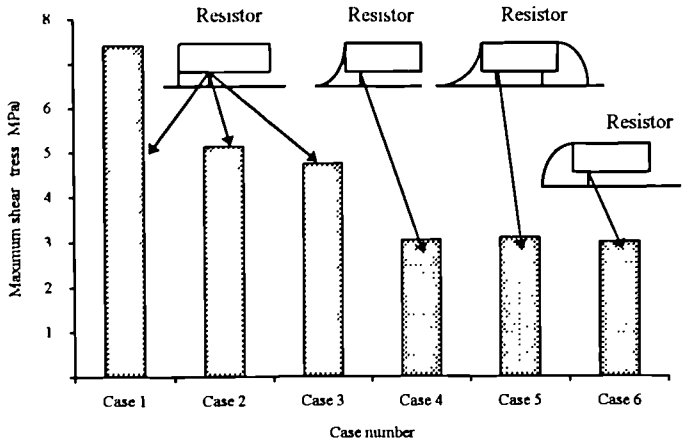

4 6a Maximum shear stress

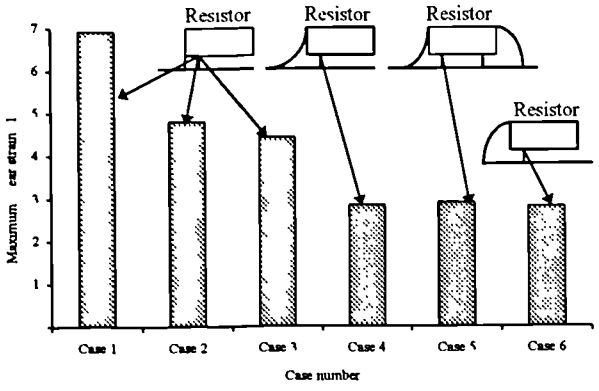

4.6b Maximum shear strain

Figs. 4.6a-b Value and position of maximum shear stress and strain for all cases

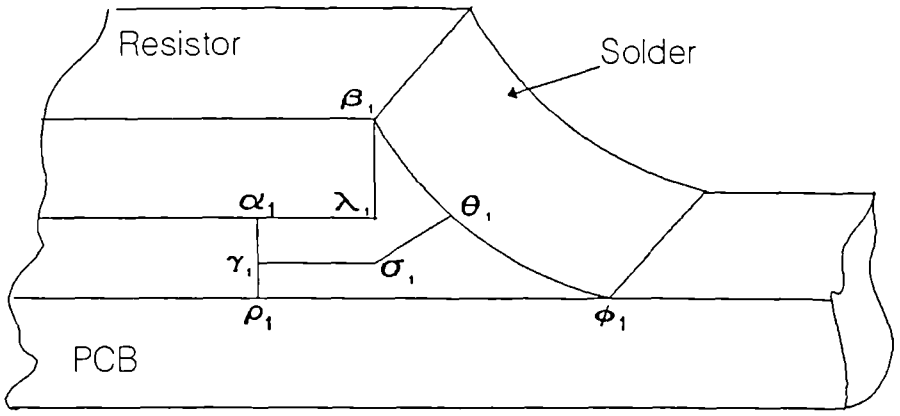

4.7a Concave joint

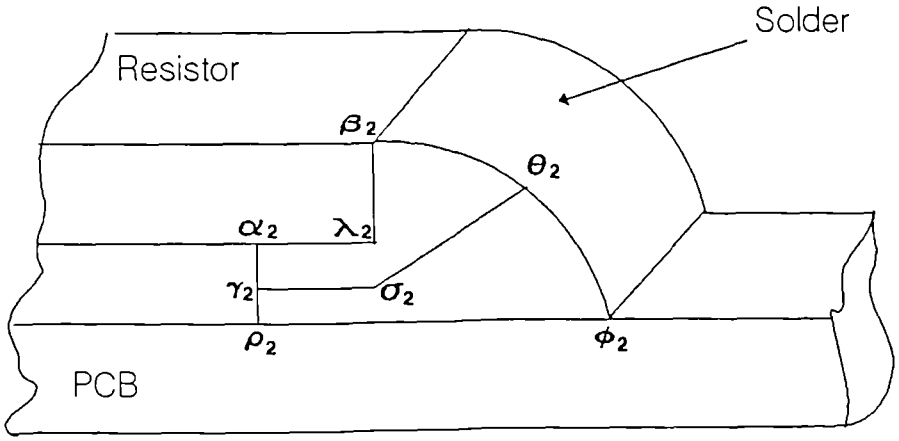

4.7b Convex joint

Figs. 4.7a-b Simplified joints for FEA

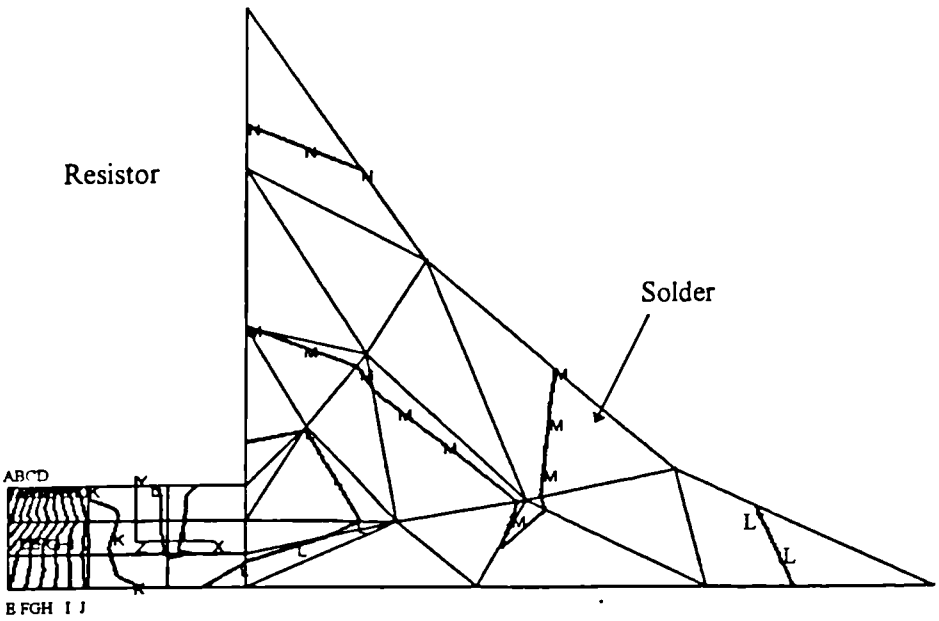

PCB

Contour	A	B	C	D	E	F	G	H	I	J	K	L	M	N	O
Shear stress MPa	30 57	28 74	26 91	25 07	23 24	21.41	19.57	17.74	15.91	14.07	12.24	10.41	8.57	6.74	4.91

4.8a Shear stress for Case 4

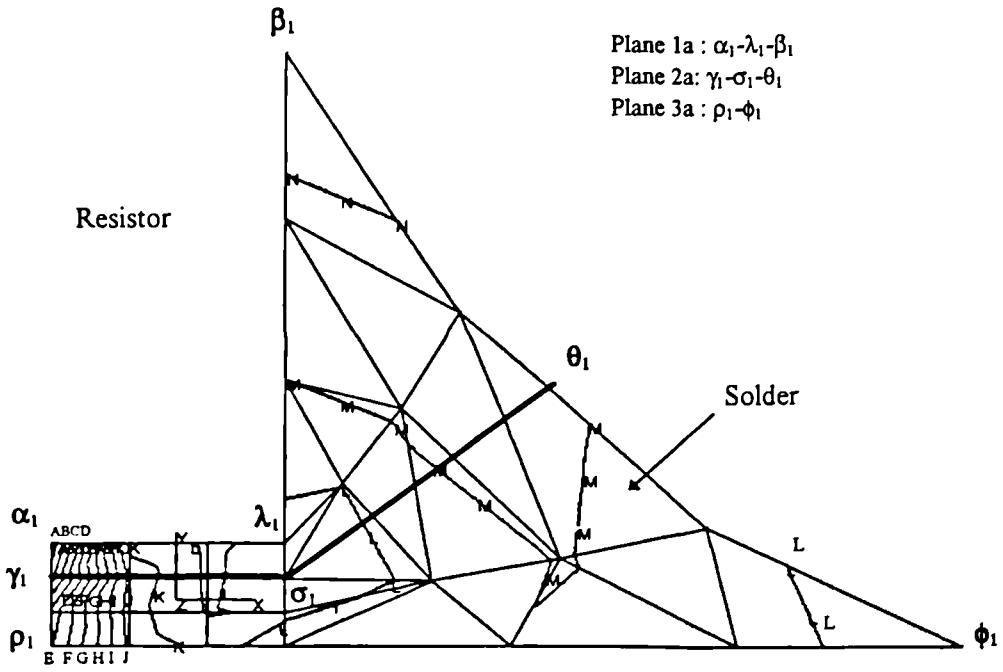

PCB

Contour	A	B	C	D	E	F	G	H	I	J	K	L	M	N	O
Shear strain 10^{3}	2 85	2 68	2.51	2.34	2.17	2.00	1 83	1 66	1.48	1.31	1 14	0 971	0.800	0 629	0.458

4 8b Shear strain for Case 4

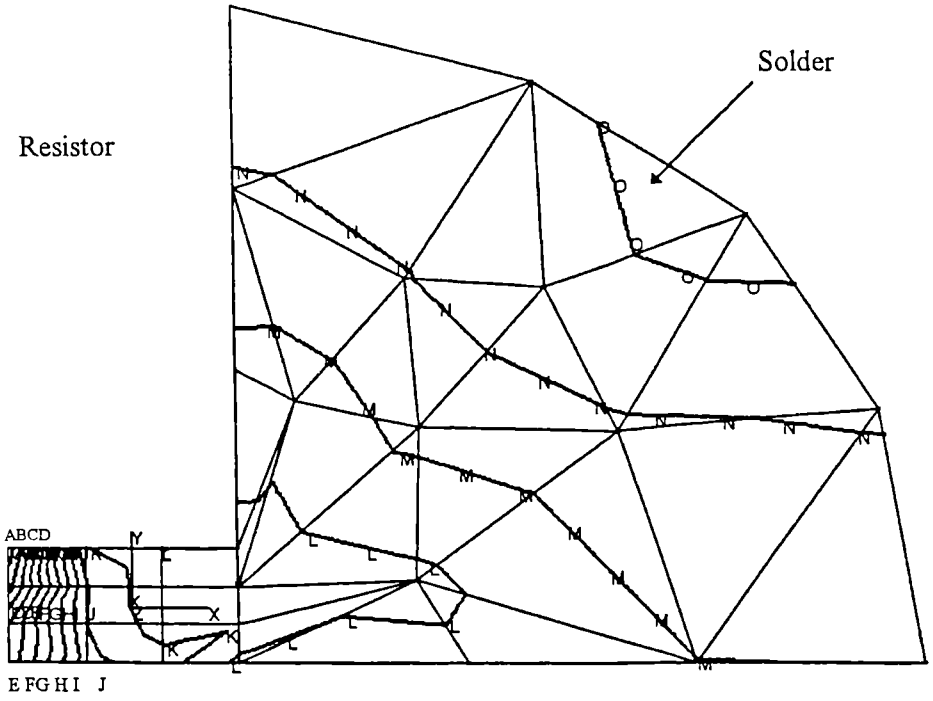

PCB

Contour	A	B	C	D	E	F	G	H	I	J	K	L	M	N	O
Shear stress MPa	30.15	28.23	26.32	24.41	22.49	20.58	18.67	16.76	14.85	12.94	11.02	9.11	7.19	5.28	3.37

4.8c Shear stress for Case 6

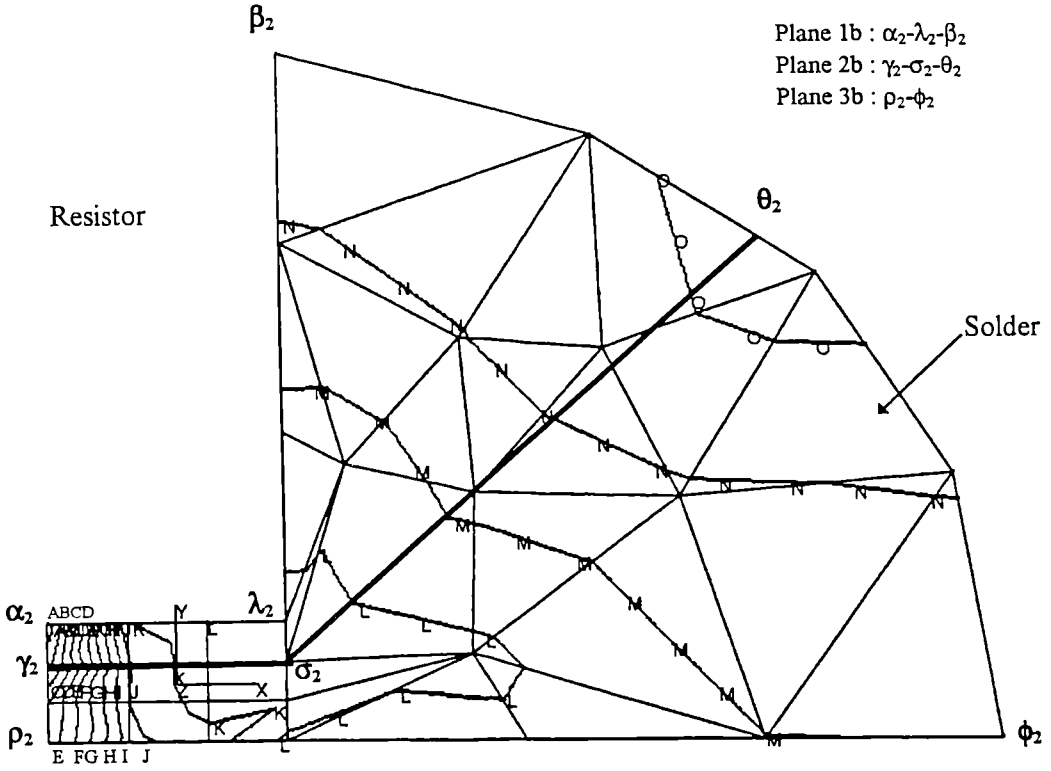

Contour	A	B	C	D	E	F	G	H	I	J	K	L	M	N	O
Shear strain 10^{-3}	2.81	2.64	2.46	2.28	2.10	1.92	1.74	1.56	1.39	1.21	1.03	0.85	0.672	0.493	0.315

4.8d Shear strain for Case 6

Figs. 4.8a-d Shear stress and strain contours
for Case 4 and Case 6

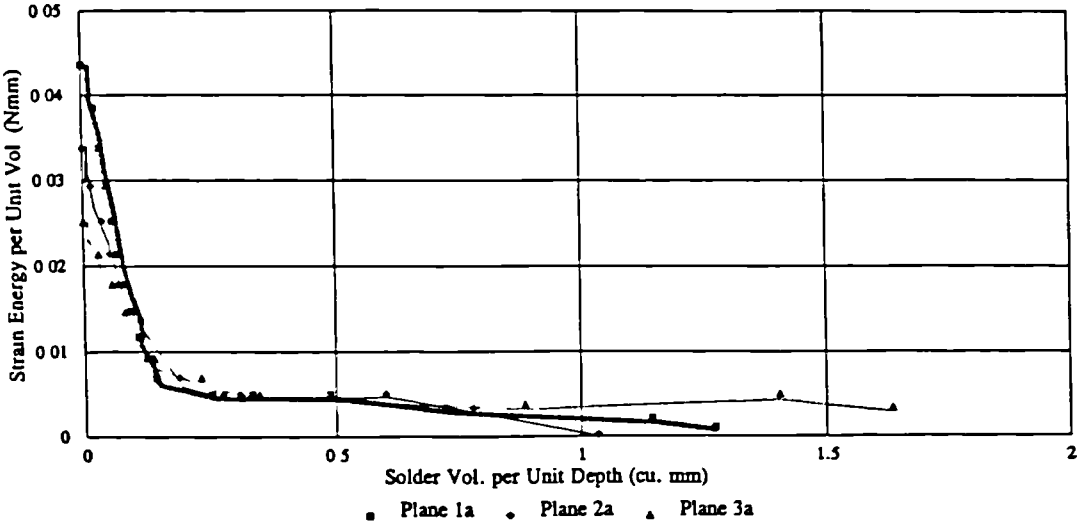

4.9a Concave joint

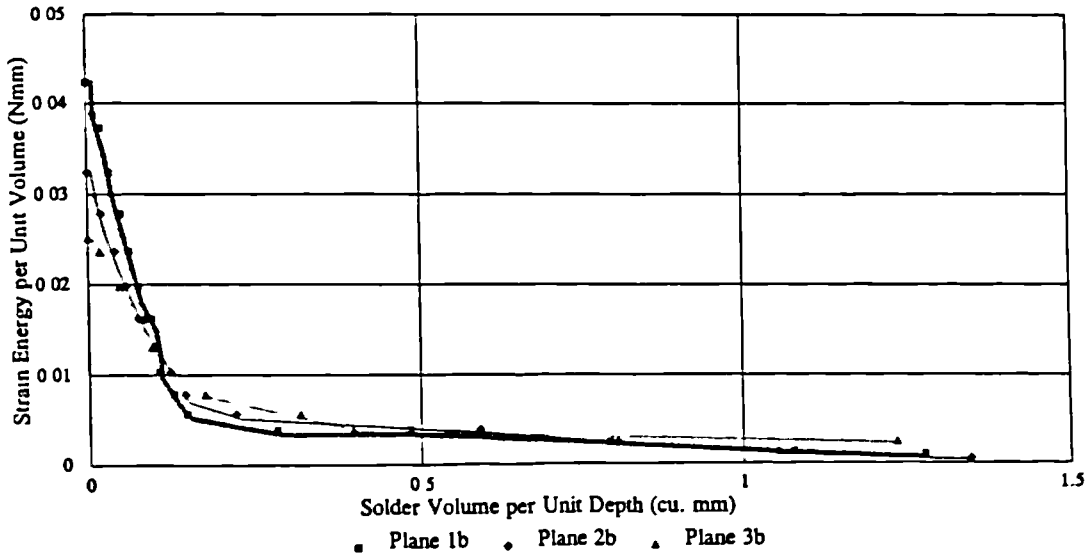

4.9b Convex joint

Figs. 4.9a-b Energy distribution of concave and convex joints

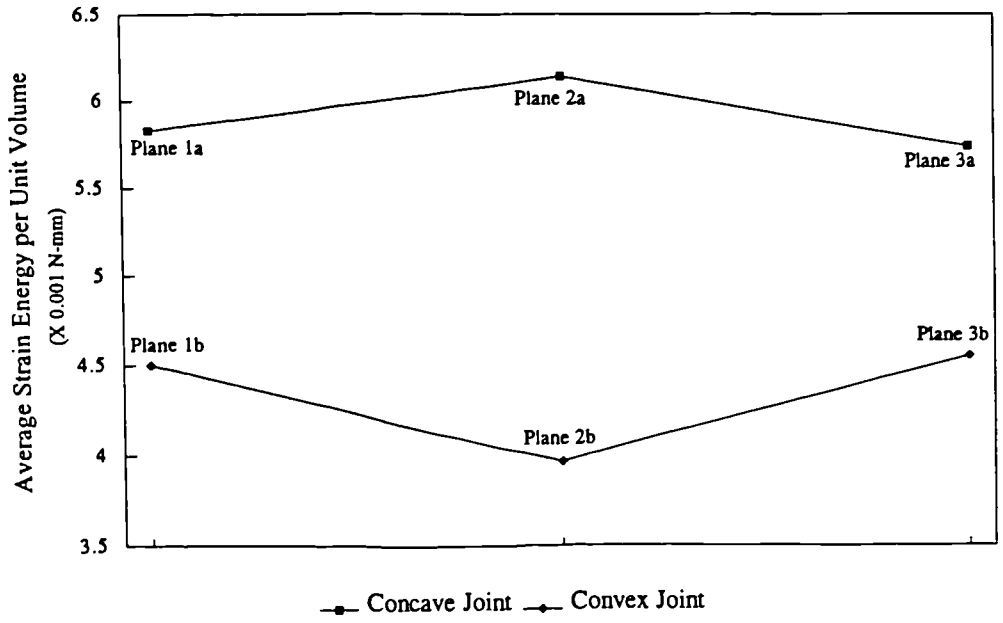

Fig. 4.10 Energy absorption of planes

4.3 SOLDER THICKNESS

Three aspects of the effect of solder thickness were investigated: the effects on the strength of the joint, the effects on the solder's ability to hold the component in position, and the effects on the final shape of the joint. Each of these was studied experimentally.

4.3.1 Methodology

From finite element analysis, it was found that a larger standoff height gives a smaller maximum shear strain when subjected to thermal fatigue, and based on the Coffin-Manson equation it is expected that such a joint can sustain a longer thermal fatigue life [73]. Here, it is also expected that the standoff height of a joint would also affect the pulling strength. To single out the solder thickness as the only parameter affecting the pulling strength of a joint, specimens as shown in Fig. 4.11, were produced. Over the two ends of a specimen were two copper strips. The size of the strips was standardised to the dimensions as indicated in the figure. The two copper strips of a test specimen were soldered together firstly by deposition of solder paste with

the aid of a syringe, then reflowed by the IR process To ensure alignment, the deposition of solder paste and the reflow process were all carried out with the specimen fixed onto a special jig made of thin epoxy strips. The excess solder sticking out of the specimen after reflow was removed by grinding The thickness of the solder was measured using a traveling microscope prior to the pulling test performed on a specimen Force/extension curves were recorded, and the tensile strengths were calculated for specimens with different solder thickness.

It was also found that defects such as misalignment, open, and tombstoning, are strongly correlated with the design of the PCB pads [9,61] The surface tension of the molten solder, relative to the weight and dimensions of the component, is considered to be the main source of component movement during soldering The soldered area underneath a leadless chip (overlap) directly affects its chance of resulting in all three types of defects A greater overlap decreases the chance of giving these defects. A longer solder extension from the end of a leadless chip increases the lifting moment, hence the likelihood of tombstoning occurring [110] It is expected here that the solder paste thickness also determines the ability of the molten solder to hold the component in its desired position. Components RC 1206 were used for this investigation. The pads of the test boards were designed in accordance with the IPC standard To provide a higher degree of movement of the components, solder paste was printed only on one of the two pads of a component. Different solder paste thickness was printed manually, and the thickness was measured using a Cyber Optics Laser Section Microscope. After reflowing in a Heller 932 IR oven, the number of misaligned components, as shown in Fig. 4.12, was counted.

For gull-wing components, it was found that the strength of a joint depends little on the shape of the lead but on the size and shape of the solder fillet [69] To optimise the strength of a joint, and at the same time to avoid excessive use of solder, a well-controlled solder paste thickness is considered critical. Components with gull-wing leads were placed on lands printed with different thickness of solder paste. After the reflow process, components were sectioned, ground, polished, then viewed under microscopes to detect the shape difference

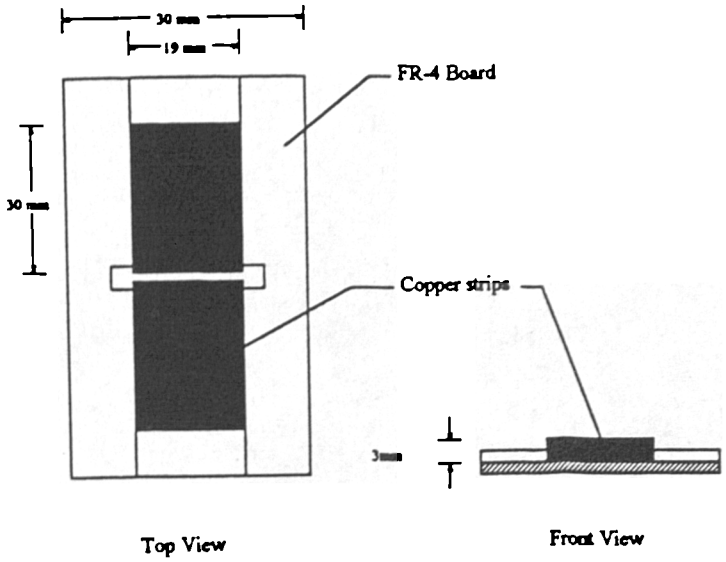

Fig. 4.11 The arrangement of the test strip in the fixture

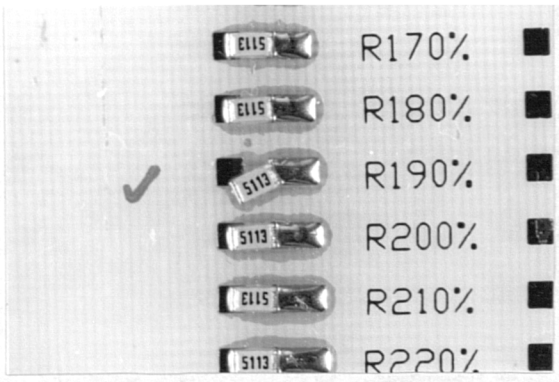

Fig. 4.12 Misalignment of component

4.3.2 Findings and Results

Referring to Fig. 4.13, it can be seen that within the range tested, the pulling strength of a joint varies with its solder thickness. Initially, the strength decreases with an increase in the solder thickness. This condition continues until the thickness is about 0.625

mm. The strength with a further increase in the solder thickness from this point remains almost constant

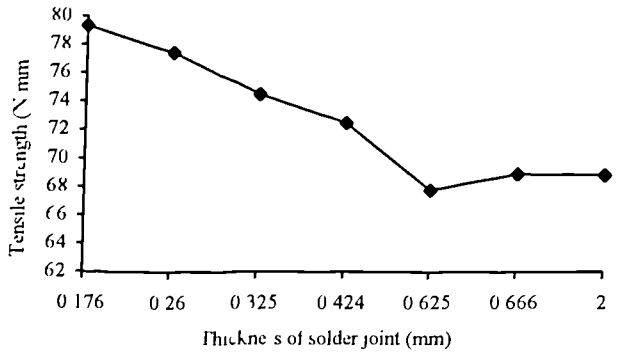

Fig. 4.13 Relation between strength and solder thickness of solder joints

Fig 4 14 gives the results of the misalignment test. Each thickness in the figure represents the average value of a sample of forty-eight components. The figure clearly indicates that a thick solder increases the probability of giving misalignments. No misalignments were detected for paste with thicknesses of 0.173, 0.231, and 0.243 mm. It was found that a thicker molten solder provides a larger degree of freedom of movement to the component

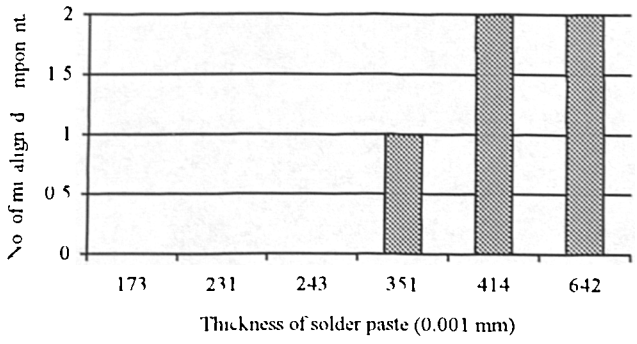

Fig. 4.14 Number of misaligned components solder thickness relation

Figs. 4.15a - c show that different paste thicknesses result in different shapes of gull-wing joint. Fig. 4.15a is the one with the least thickness, as can be seen there is little solder at the interface between the component lead and the PCB. The fillets formed both at the heel and the tip are small, and joints like this are weak. Fig. 4.15b was printed with a thicker paste, and is a better joint. As can be seen there is sufficient solder at the interface, and at the same time the fillets which are essential to the strength of a joint, are larger. Fig. 4 15c, is obviously from a joint with excessive solder. This resulted from unnecessary solder paste thickness. Excessive solder not only increases the material cost, but also increases the chance of giving defective products, such as by bridging or misalignment.

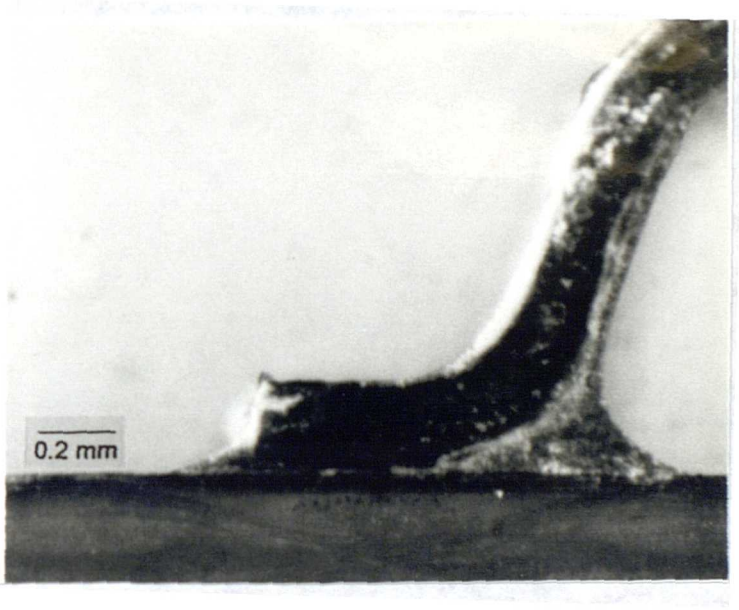

4.15a

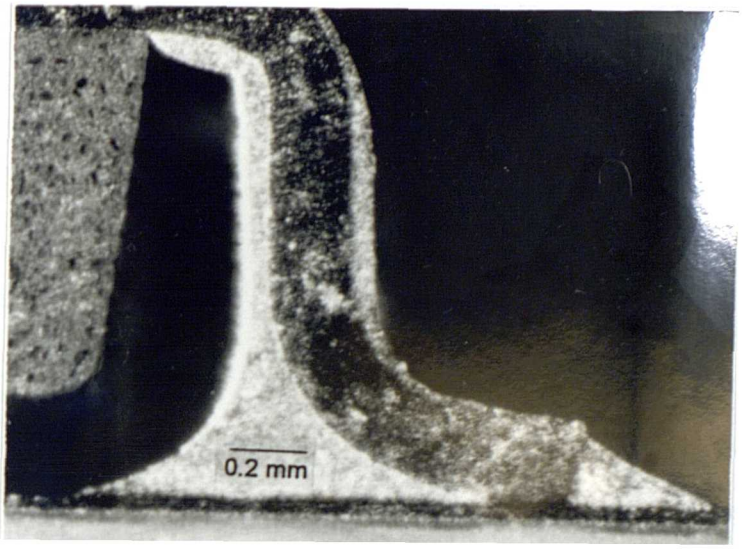

4.15b

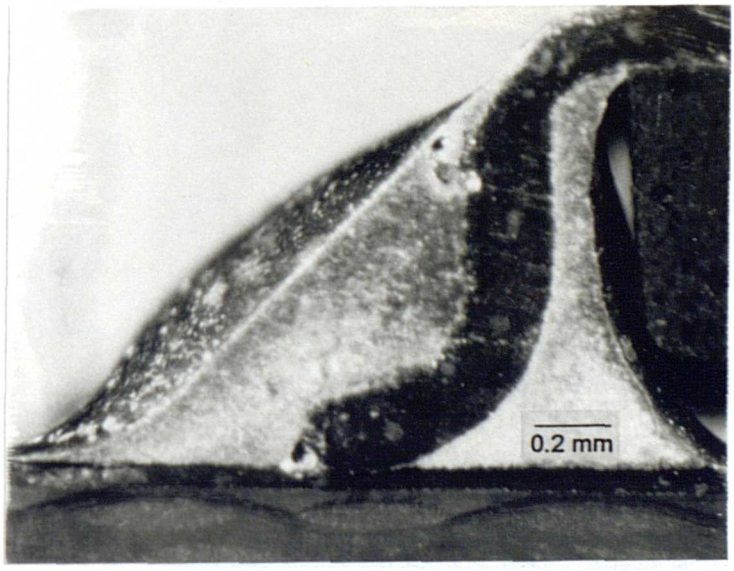

4.15c

Figs. 4.15a-c Gull-wing joints with different amount of solder

4.4 DISCUSSION

Very often in the manufacturing environment, a quick and non-subjective method is desirable to give an indication as to whether a particular process set-up in SMT is producing quality joints or not. Metallography does provide information about solder wetting, however, it is a slow process. Besides, the quality of a joint does not depend purely on the metallurgical aspects, the geometry of the solder joints also plays a significant role. The feasibility of using a pulling test for this purpose has been studied. It was found that with further development the mean ultimate tensile force from the pulling tests may be used as a parameter for measuring the quality of joints. It is known that, for a fixed pad size, the pulling strength of a solder joint basically depends on three factors, the solder wetting conditions, the fillet geometry, and the standoff height [70,111] If these three factors can be standardised for any one type of joint, a standard mean ultimate tensile force for that joint can be established. It is suggested here that this standard mean ultimate tensile force should be used as a quality assurance parameter for this type of SMT joint From the FEA, it was found that a smaller standoff height gives a higher stress concentration which leads to a higher chance of joint cracking during pulling. However, from the experiments described here, it was found that a smaller standoff height in fact resulted in a higher ultimate tensile strength. This contradiction is considered to be due to the fact that in the FEA the solder was assumed isotropic and the effects of the copper-tin intermetallic layer on the pulling strength were not taken into consideration. It is recognised that the presence of this intermetallic compound has effects on reducing the ductility, and hence the fatigue and creep endurance [37,94], but on the other hand increases the ultimate tensile strength of a joint, Fig. 4.13. The strength advantage of a convex joint over a concave joint found in the FEA is very marginal. In SMT reflow process, the solder thickness of a joint is determined by the thickness of solder paste printed. For gull-wing joints, it is believed that there is an optimum range of solder paste thickness which would give quality joints. This thickness range can be achieved by proper setting in the printing operation. Too thin a print would lead to insufficient solder and small fillets, but an unnecessary thick print not only is a waste of paste which increases the production cost, and it also increases the likelihood of resulting in various types of defects, such as misalignment which has been experimentally verified here.

Chapter 5

Infrared Reflow and Wave Solder Joints

5.1 INTRODUCTION

IR reflow and WS are found to be the most advantageous methods to meet the requirements of mass production Both methods are suitable for automation, and at the same time, provide a speedy through-put However, the formation of a SMT solder joint by means of these two approaches is completely different. The IR reflow process employs a solder paste printing operation with the aid of a stencil or screen. The thickness and the aperture of the stencil or the screen provide an effective control to the amount and position of the paste to be printed [31] The solder paste used basically includes the ingredients of solvent, flux, and alloy metal particles By going through a specific IR temperature profile, the flux and solvent are removed leaving the metal solder behind forming the solder joint The internal structure and the reliability of the joint depend very much on the composition of the solder paste and the reflow process [43,44,45,46]. As for a WS process, the fundamental operations include the adhering of components, preheating, fluxing and wave soldering In this process the surface tension of the molten solder plays a crucial role in determining the quality of the resulting joint [53]. For the same components, the mechanism of forming the joints by the IR reflow and WS processes differ significantly, here research was carried out to investigate the fundamental differences between joints produced by these two methods

5.2 SHAPE OF JOINTS

From both finite element analyses and experiments, there are strong indications that the thermal fatigue life, as well as the strength, of a solder joint are a function of the joint geometry [69,73,74,81]. The geometric parameters of a joint which are generally considered to have direct effects on the strength and fatigue life are the standoff height, fillet height, and fillet shape. It is expected that since the IR and WS are two processes employing completely different methods of depositing solder on the joints, the resulting solder shape and volume from the two methods would be different and this would have a direct impact on the reliability and functional ability of the joints. RC 1206 was the component used in this investigation.

5.2.1 Methodology

To study the effects of entry angle of components on the final shape of the joints in the wave soldering process, a test board as shown in Fig. 5.1 was designed. With the use of this test board, components would enter the bath at different angles. The angular difference between each adjacent pair of pads is 30^0. The board for the test was firstly cleaned with alcohol, then small dots of SMD 881 adhesive, supplied by Multicore, were dispensed at the mid-points of all pairs of pads. The sequence from adhesive dispensing to component placement is shown in Fig. 5.2. After placement of components the adhesive was cured by sending the board through the Heller 932 reflow oven, with the UV zone functioning. The combined UV and heat effect was used for the curing of the SMD 881 acrylic adhesive (for the temperature profile employed for the curing of the adhesive refer to Appendix C). The next step was the wave soldering of the board which was performed in an ARIES 300-C/SMT wave soldering machine, Fig. 5.3. Water soluble flux 864-1X, supplied by Alphametals, was applied to the board prior to the wave soldering. The solder composition was 63Sn37Pb (Appendix D gives a chart, provided by the wave soldering machine supplier, for the setting of the conveyor speed and preheat temperature of the machine once the required preheat temperature of the board is determined). It was determined that the boards had to be preheated to 95^0C. The setting of the machine for this experiment was as

follows:

Preheat temperature : 525^0C

Solder pot temperature : 235^0C

Speed of conveyor : 100 cm $minute^{-1}$

Inclination of conveyor : 4^0

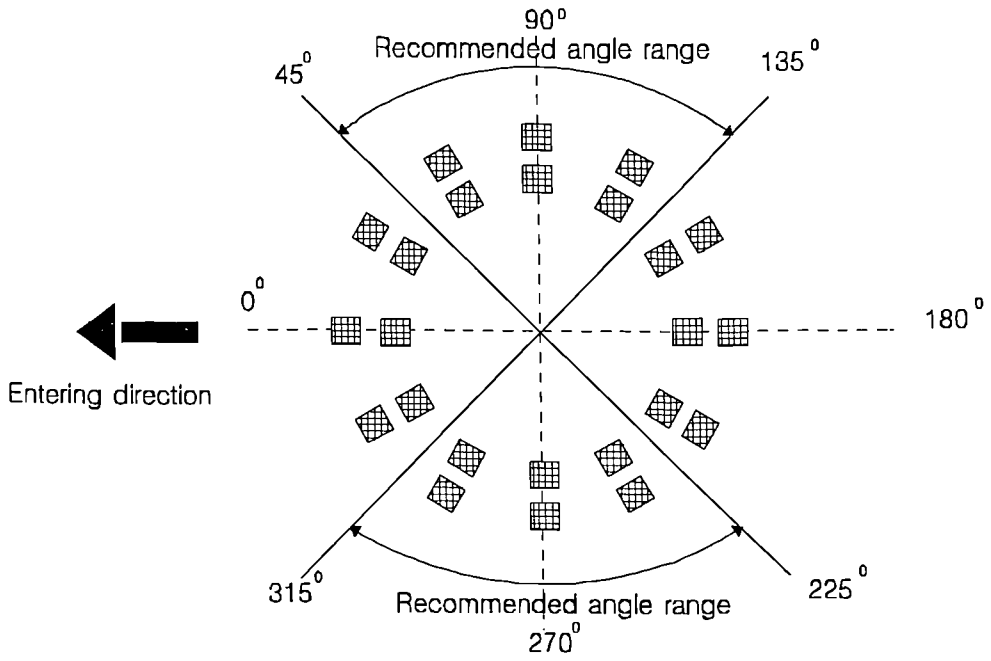

Fig. 5.1 Configuration of board for testing of entry angles

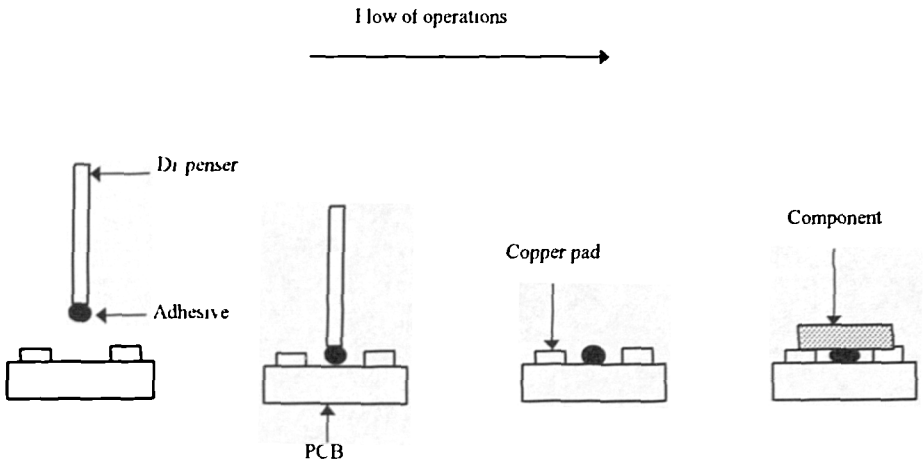

Fig. 5 2 Operation sequence for adhesive dispensing and component placement

Fig. 5.3 ARIES 300-C/SMT wave soldering machine

Wave soldered components with different entry angles were sectioned, ground, polished, and inspected by an x-ray real time radiographic inspection system. The geometry of their joints were compared and recorded. To enable a direct comparison, same components (i.e. RC 1206) were also used for the IR reflow. Multicore RM92 solder paste which has the same Sn/Pb ratio (i.e. 63Sn37Pb) as the wave solder was used. After reflow, the geometry of the joints were inspected and recorded with the aid of an optical microscope.

5.2.2 Inspection Results

With reference to the board shown in Fig. 5.1, due to symmetry, some component entry angles are in fact identical to each other, it was considered that sufficient information could be obtained by simply carrying out experiments on components in the first quadrant. WS components with entry angles 0^0, 30^0, 60^0, and 90^0 were chosen for shape investigation. Fig 5 4 a-d show their respective joint shapes. Joints on the left hand side of all the figures are the incoming joints, and joints on the right hand side are the outgoing joints It can be seen that the shape of the incoming joints do not change much with the entry angle, and this shape is always concave. However, the shape of the outgoing joints changes with the entry angle. The outgoing joints with entry angles of 0^0, and 30^0 are convex, and joints with 60 and 90 are concave. In summary, the resulting shapes of the WS joints with respect to their entry angles are as shown in Table 5.1.

Entry Angle	Incoming Shape	Outgoing Shape
0	Concave	Convex
30	Concave	Convex
60	Concave	Concave
90	Concave	Concave

Table 5 1 Shape of WS joints with different entry angles

In terms of the uniformity of joints over the two ends of a WS component, entry angles between 45^0 and 90^0 gave better results. Fig. 5.5 shows a component that was produced by IR reflow. Due to the nature of the process, the shape of the joints over the two ends are fairly uniform, both are concave The findings show that WS components with entry angles between 45^0 and 90^0 produced joints comparable to that of the IR reflow process, and components with entry angles between 0^0 and 45^0 gave different shapes of joints over the two ends.

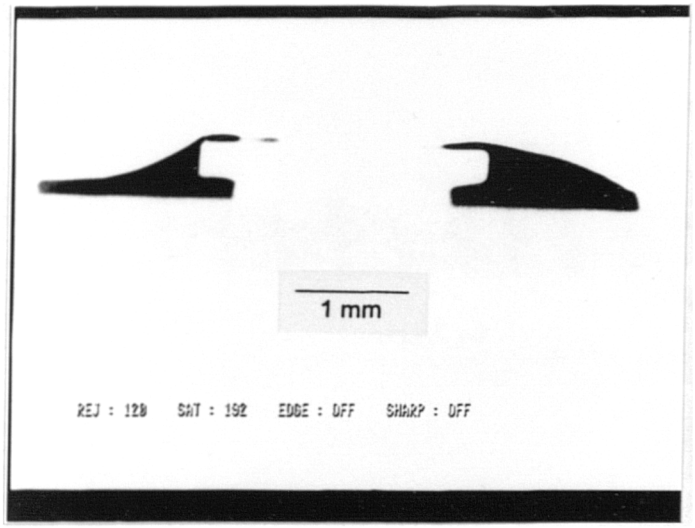

5 4a 0^0 entry angle

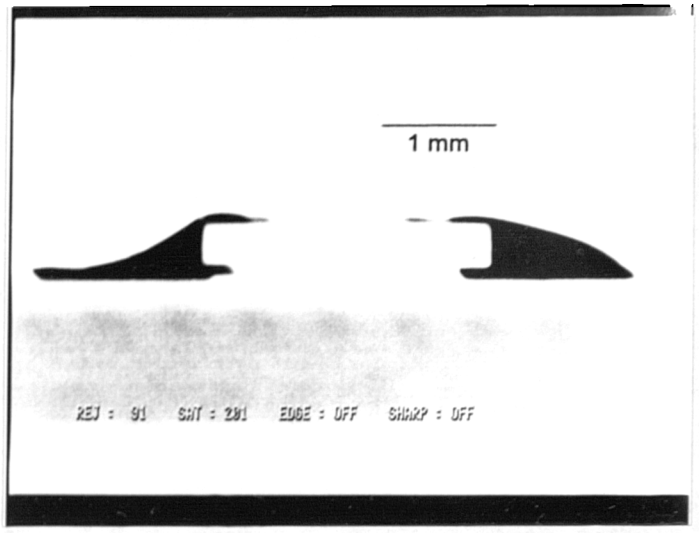

5 4b 30^0 entry angle

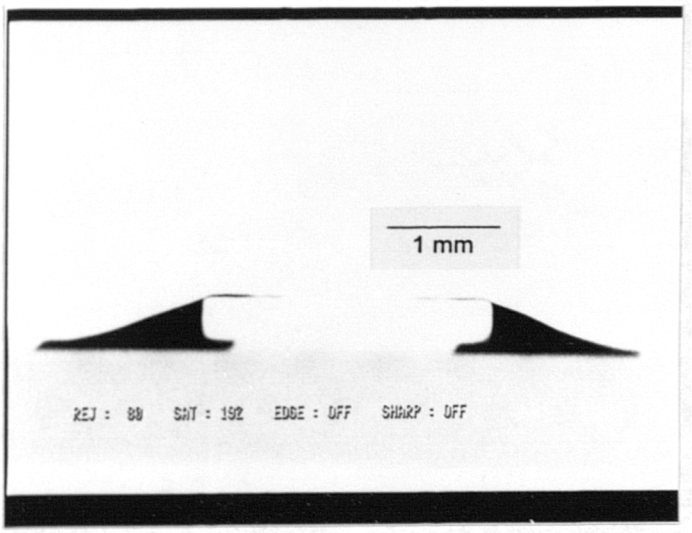

5 4c 60^0 entry angle

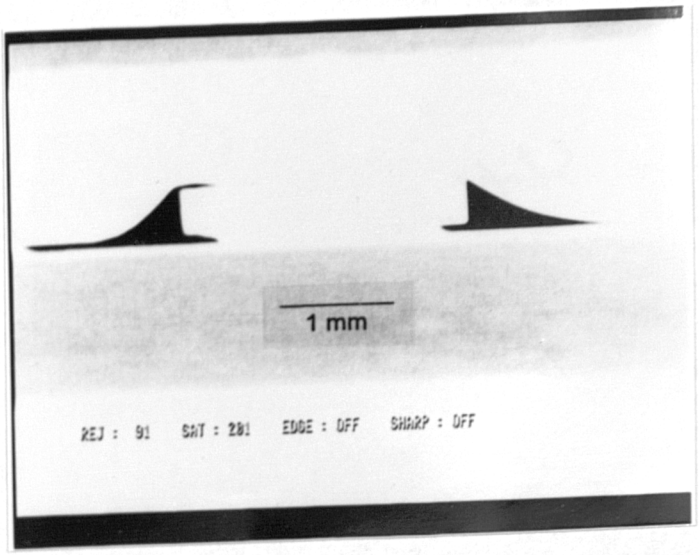

5 4d 90° entry angle

Figs 5 4a-d Shape of WS joints with different entry angles

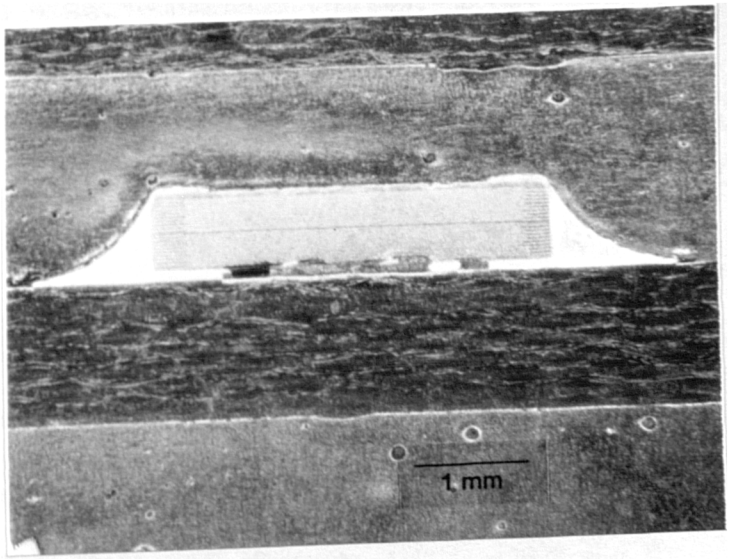

Fig. 5.5 Shape of joints produced by IR reflow

5.3 VOIDS

The amount and size of voids have significant effects on the reliability of the joints. The presence of voids deteriorates the mechanical properties in terms of strength, fatigue life, creep resistance, and ductility [63,64,65]. Based on the literature search, it was found that the formation of voids is related to the following factors [17,19,22,66]:

- the solderability
- the flux activity
- the alloy-to-flux ratio in the solder paste
- the size of alloy powders in the solder paste
- the heating process, which includes preheating, soldering, and cooling.

In view of the impact of voids on the reliability of solder joints, it was considered worthwhile to investigate the voiding difference between these two most commonly used methods, IR reflow and WS, in SMT

5.3.1 Methodology

By using the same specimens for shape investigations, the void content in the joints was inspected, and recorded The apparatus used for the void inspection was an x-ray system, model SOFTEX PRO-TEST 125, as shown in Fig. 5.6. The system allows real time inspection of voids At the same time a hard copy of the required image can be obtained. Components under investigation were viewed directly from the top. The scope of the investigation basically included the following:

1 compare the void differences between WS joints with different entry angles;

2 compare the void differences between the incoming and outgoing WS solder joints;

3 compare the void differences between joints produced by IR reflow and WS.

WS joints with different entry angles were first inspected. The angles selected for inspection were 0^0, 30 , 90 , and 120 The sample size for each entry angle was three, hence a total of twelve WS specimens were inspected. For the IR reflowed specimens, the sample size was ten Images for both WS and IR reflowed specimens were viewed at 100-

120 KV, 3 mA, and were adjusted to their best possible contrast. The images were recorded by taking photographs with the built-in camera in the x-ray system.

Fig 5 6 SOFTEX x-ray system for
void investigations

5.3.2 Findings

Fig 5 7a and Fig 5 7b show the typical results of the 0 , 30°, 90°, and 120^{0} WS joints From all the twelve samples inspected no voids were found. There were no indications that, for WS joints, the amount of voids was affected by the angle of entry of the component Neither were there indications that there were differences in void content between the incoming and outgoing joints. However, it was discovered that voids existed in all the IR reflowed samples Fig. 5 8a and Fig. 5.8b show typical results for the IR reflowed joints. The white areas are the positions of the voids. To obtain better views, enlarged results of WS and IR reflowed joints are shown in Fig. 5.9 and Fig. 5.10 respectively.

These findings show that resolvable voids were only found in IR reflowed specimens.

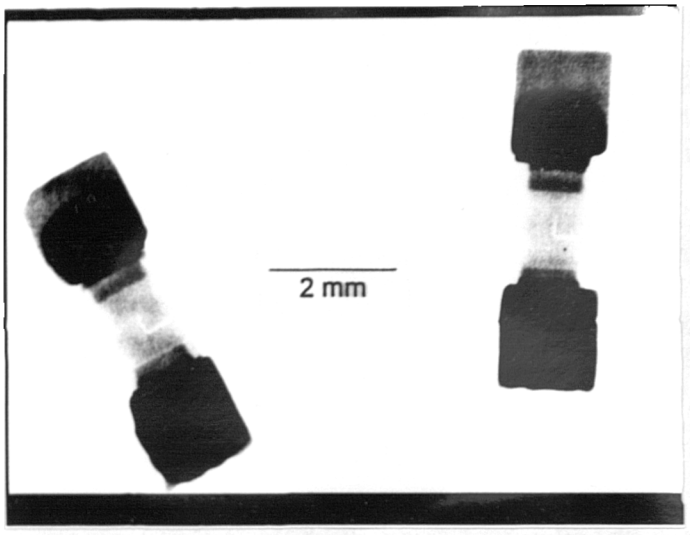

5 7a Right - 0^0, left -30^0

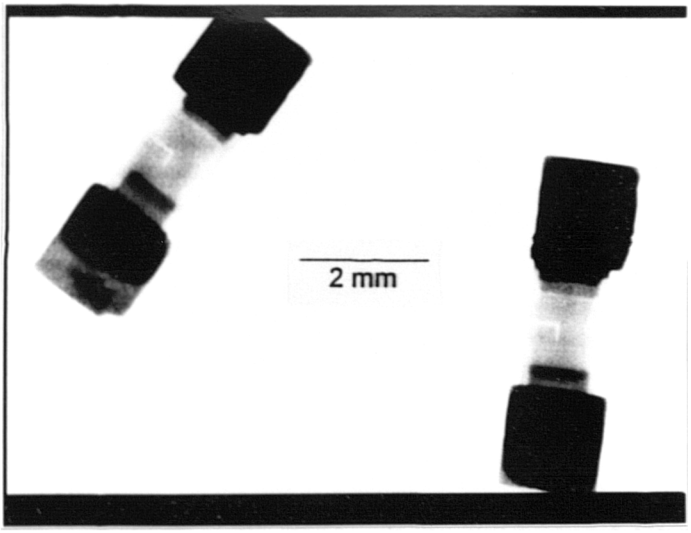

5.7b Right - 90^0, left - 120^0

Figs. 5.7a-b WS components taken by x-ray system with different entry angles

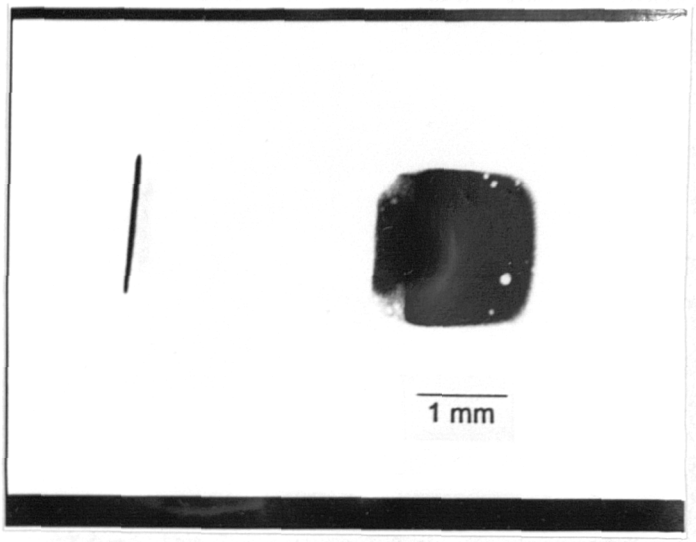

5.8a

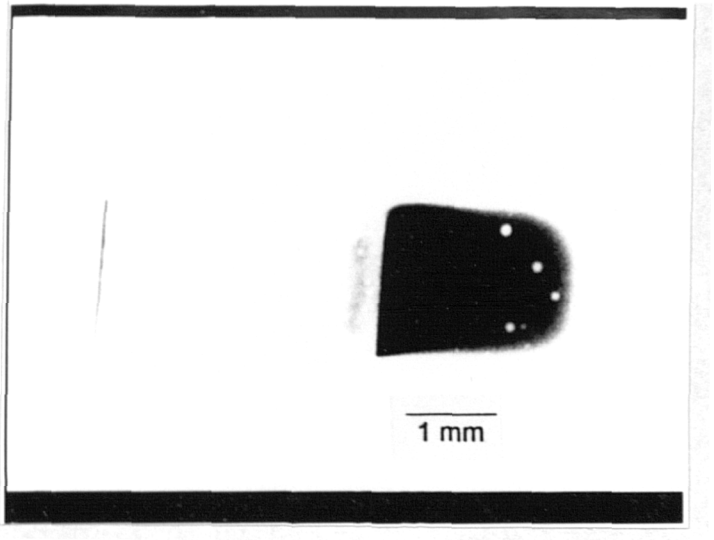

5.8b

Figs. 5.8a-b IR reflowed components taken by x-ray system

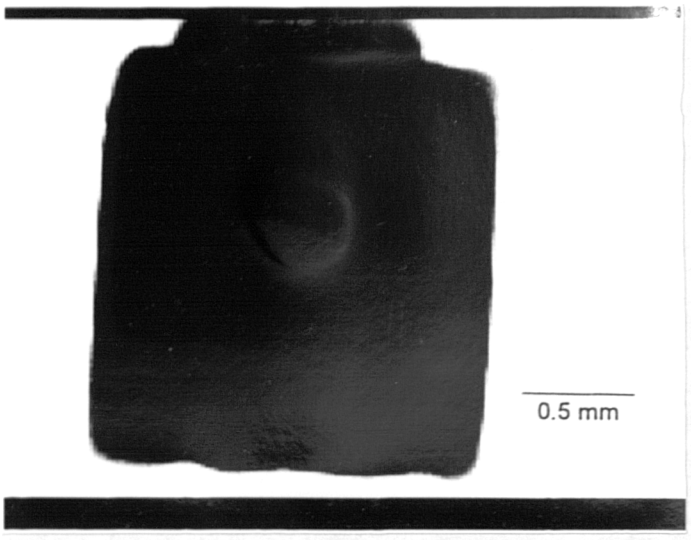

Fig 5 9 Enlarged WS component
taken by x-ray system

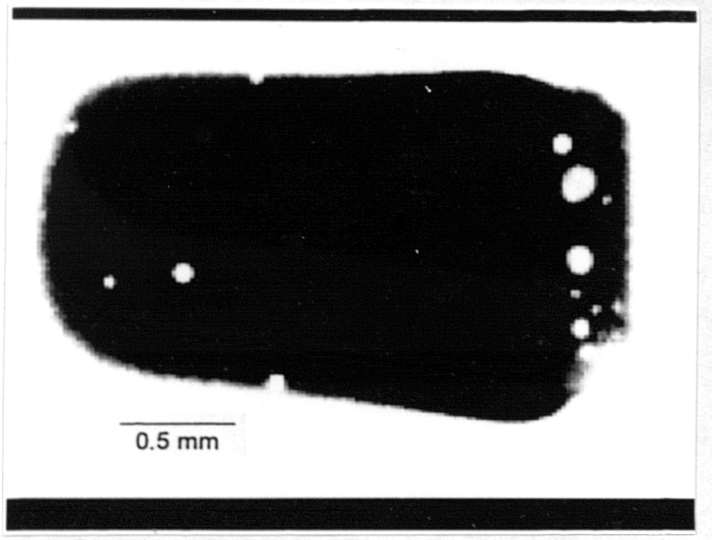

Fig. 5.10 Enlarged IR reflowed component
taken by x-ray system

5.4 HARDNESS AT THE INTERFACE

Evidence showed that a compound layer is formed at the interface of Cu/SnPb joints. This compound is primarily of copper/tin. Lead does not form compounds with copper, the function of lead in the solder is basically to reduce the solder's melting temperature. After soldering, the presence of a copper/tin compound in the joint indicates that the solder is properly wetted. A contaminated, or oxidised surface impairs soldering and prevents the formation of such a layer, and results in a weak joint. However, research results show that this layer affects the long term reliability [94,95,96,98,99,100,101] and the solderability of the joint [97]. A proper control and a better understanding of the layer are most desirable. Depending on the solder type and the conditions of aging, the compound layer can extend to a thickness of up to 30μm [102]. Due to its limited thickness, in the past, the effects of the layer on the bulk reliability and strength of the joint were the only issues investigated. Precise information about the properties and characteristics of the compound layer is very limited.

5.4.1 Methodology

There is a strong correlation between the strength and the hardness of a metal. It is found that the harder the metal is the higher its strength. For this reason, in many cases, a tensile test is substituted by a hardness test which is relatively a more convenient method for finding the strength information of a metal [112]. Further, a microhardness test allows measurements to be performed across a small region, and was used here to obtain information about the strength across the boundary between the copper and solder layer. It is expected that by means of this localised method of measurement, more precise information about the interface can be obtained.

A Matsuzawa Digital Micro Hardness Tester was used for performing the experiments. The system employs a diamond pyramid indentor. In the experiments, an indention load of 9.8×10^{-2} N was used. During testing, the lengths of the diagonals of the

impression are measured, and averaged. By referring to the table provided, the averaged diagonal length of the impression is converted into a Vickers hardness number. Specimens for the tests were prepared by going through the same procedure as those for shape inspection. Tests were carried out on both WS specimens with different entry angles, and IR reflowed specimens. One of the objectives of these experiments was to investigate the hardness in relation to the distance from the interface of the joints. To allow more space for indentation, and hence more measurements, the measuring points were lined-up at an angle as shown in Fig. 5.11 The hardness versus distance across the interface was then plotted. The point of origin was any point on the solder side with a distance far away from the interface, and was chosen arbitrarily. The microstructure of selected WS specimens was also inspected with an optical microscope.

5.4.2 Findings and Results

Figs 5 12a - h are the hardness distance graphs for the WS specimens. Their corresponding hardness/distance data are shown in Table 5.2a - h. The data from both the incoming and outgoing joints with different entry angles were plotted. It can be seen that the shape of all the graphs can be divided roughly into three sections. The first section represents the hardness of solder, the second section contains the effects of the intermetallic compound, the third is the section representing the hardness of the copper. It can be seen that as the first section gets near to the second section, the hardness increases gradually. This is due to the fact that the hardness is increased as a result of the increase in the compound content The hardness continues to increase until it has completely entered the intermetallic compound which gives a maximum hardness value. The hardness of the metal reduces gradually as one moves away from the second section, and eventually gives a value representing the hardness of the copper of the PCB. Figs. 5.13a - c are the resulting hardness distance graphs for the IR reflowed specimens, and their corresponding data are in Tables 5.3a - c. Similarly to that of the WS specimens, all the graphs have three sections. From both the WS and IR reflowed graphs, the existence of the compound layer is clearly shown, and its hardness is far greater than that of the two base materials; copper and solder. For the WS specimens, the average hardness of the compound is 143.12Hv as

compared to that of the copper and solder which are 95.05Hv and 14.8Hv respectively. The average largest hardness value of the compound of the three IR reflowed specimens, Figs. 5.13a - c, is 110.1Hv. The average copper hardness and average solder hardness are 92.2Hv and 9.91Hv respectively. Interesting information deduced from this investigation is that both the compound and the solder of WS specimens are in fact harder than that of the IR reflowed specimens, though their base materials have the same composition. The interface region where the hardness is affected by the compound spreads approximately across a width of 40 to 50μm for both the WS and IR reflowed specimens.

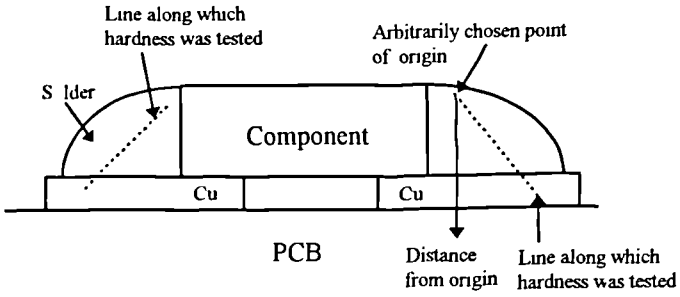

Fig. 5.11 Microhardness tested positions

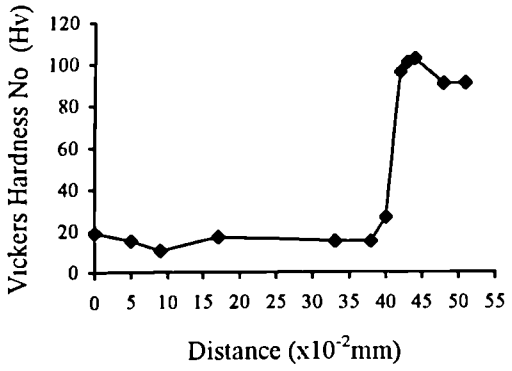

5.12a WS incoming joint at 0^0

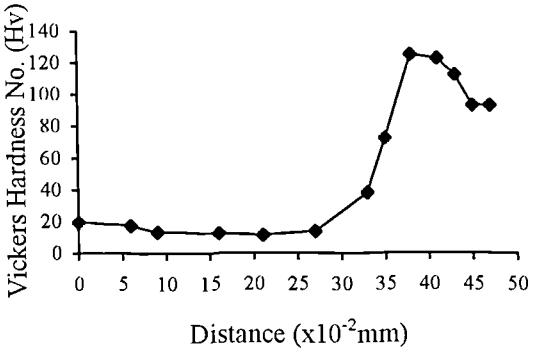

5.12b WS outgoing joint at 0^0

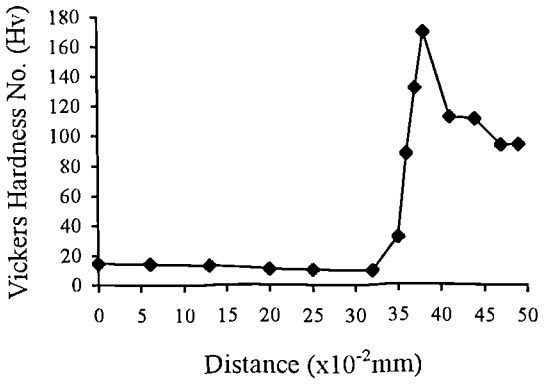

5.12c WS incoming joint at 30^0

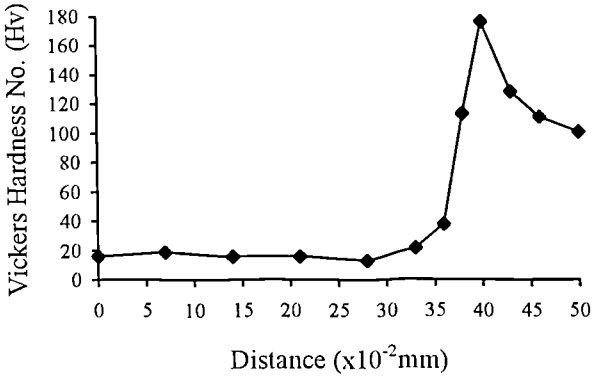

5.12d WS outgoing joint at 30^0

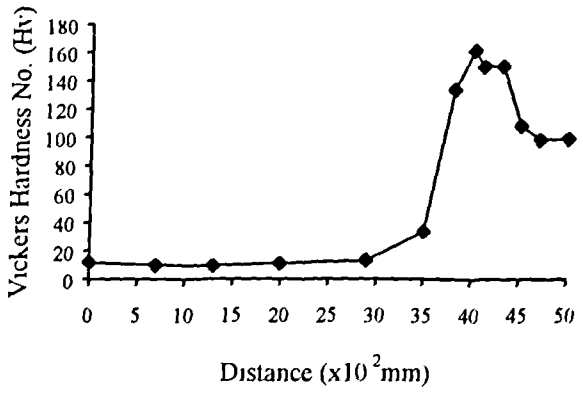

5 12e WS incoming joint at 60^0

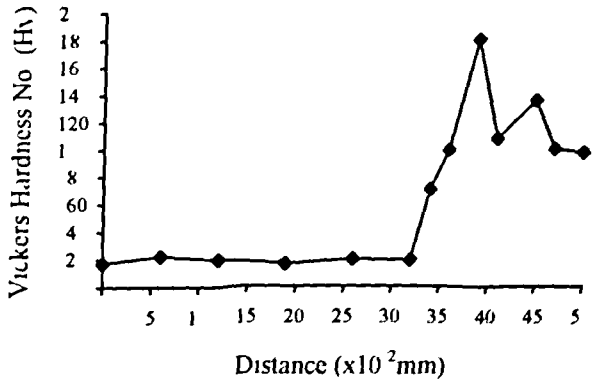

5 12f WS outgoing joint at 60

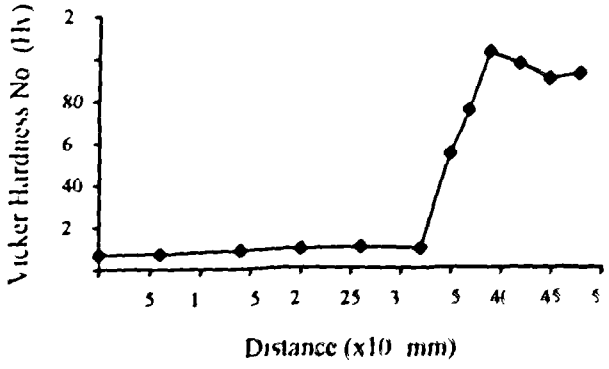

5 12g WS b ttom joint at 90

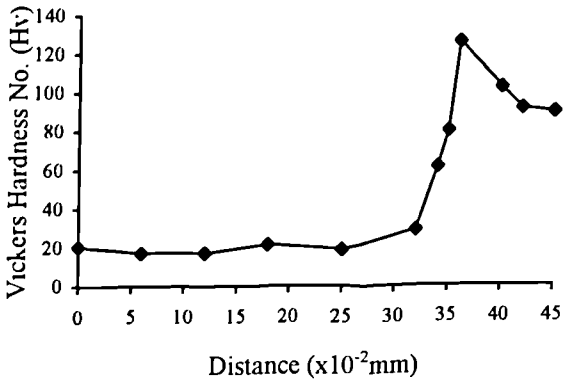

5 12h WS top joint at 90^0

Figs 5 12a-h Hardness/distance graphs for WS joints at different entry angles

Distance (x10 ^{2}mm)	0	5	9	17	33	38	40	42	43	44	48	51
Vickers Hardness (Hv)	18 9	15	1 3	17 3	15 2	14 9	26.6	96.6	1 1.3	1 3.2	90.6	90 7

Table 5.2a Data for Fig. 5.12a

Distance (x10 ^{2}mm)	0	6	9	16	21	27	33	35	38	41	43	45	47
Vickers Hardness (Hv)	19 5	17 5	13 4	12 5	11 3	13 8	38.1	72.8	125.6	123.5	113.1	97.8	93.5

Table 5.2b Data for Fig. 5.12b

Distance ($x10^{-2}$mm)	0	6	13	20	25	32	35	36	37	38	41	44	47	49
Vickers Hardness (Hv)	14.7	14.3	13.6	11	10.3	10	32	88.1	132	169.8	112.3	111.4	94.0	93.4

Table 5.2c Data for Fig. 5.12c

Distance ($x10^{-2}$mm)	0	7	14	21	28	33	36	38	40	43	46	50
Vickers Hardness (Hv)	15.7	19.1	15.7	15.8	13.3	21.4	37.7	113.1	176.5	128.7	111.4	101.2

Table 5.2d Data for Fig. 5.12d

Distance ($x10^{-2}$mm)	0	7	13	20	29	35	38	40	41	43	45	47
Vickers Hardness (Hv)	12	9.9	9.4	10.4	11.2	13.4	33.7	134.3	161.9	150.5	108.6	98.7

Table 5.2e Data for Fig. 5.12e

Distance ($x10^{-2}$mm)	0	6	12	19	26	32	34	36	39	41	45	47	50
Vickers Hardness (Hv)	17.1	22.4	19.9	16.4	19.7	19	70.6	100.2	181.7	108.8	136.6	101	98.4

Table 5.2f Data for Fig. 5.12f

Distance ($x10^{-2}$mm)	0	6	14	20	26	32	35	37	39	42	45	48
Vickers Hardness (Hv)	69	73	88	92	99	93	547	752	1026	973	90	925

Table 5 2g Data for Fig 5 12g

Distance ($x10^{-2}$mm)	0	6	12	18	25	32	34	35	36	40	42	45
Vickers Hardness (Hv)	26	174	172	215	191	289	612	797	1256	1025	913	894

Table 5 2h Data for Fig 5 12h

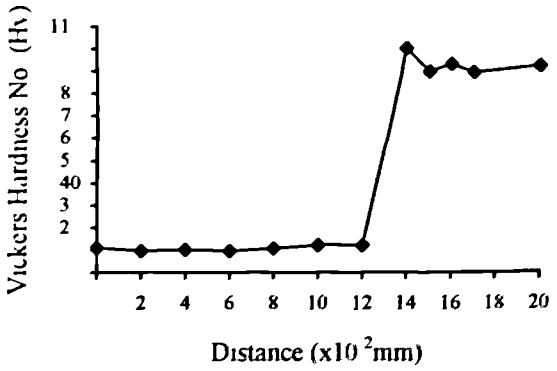

5 13a

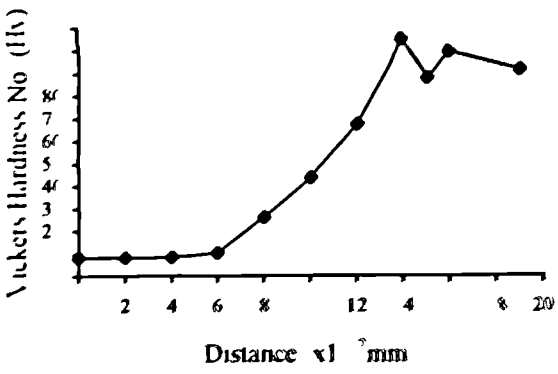

5 13b

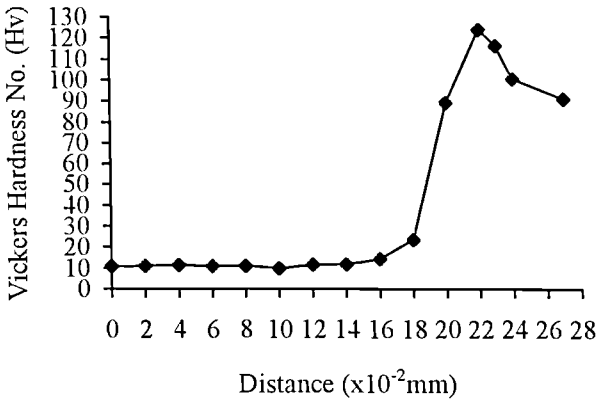

5.13c

Figs. 5.13a-c Hardness/distance graphs of IR reflowed specimens

Distance (x10 ^{2}mm)	0	2	4	6	8	10	12	14	15	16	17	20
Vickers Hardness (Hv)	11	9.6	10.4	9.7	10.9	12.3	12.2	100.2	90	93.2	89.4	92.3

Table 5.3a Data for Fig. 5.13a

Distance (x10 ^{2}mm)	0	2	4	6	8	10	12	14	15	16	19
Vickers Hardness (Hv)	8.1	8.1	8.5	10.5	26.1	44.1	68.1	105.6	88.7	100.2	92

Table 5.3b Data for Fig. 5.13b

Distance (x10 ^{2}mm)	0	2	4	6	8	10	12	14	16	18	20	22	23	24	27
Vickers Hardness (Hv)	10.9	11.2	11.4	11	11.1	10	11.7	11.9	14.6	23.9	89.4	124.5	116.8	101	91

Table 5.3c Data for Fig. 5.13c

Fig. 5.14 shows the microstructure of a WS solder joint. The figure clearly shows the layer of IMC, and also it can be seen that the grains of the solder are the finest in the region closest to the copper, and increase gradually as one moves away from the copper. This phenomenon indicates that the solder close to the PCB had a faster cooling rate so resulting in a finer grain size.

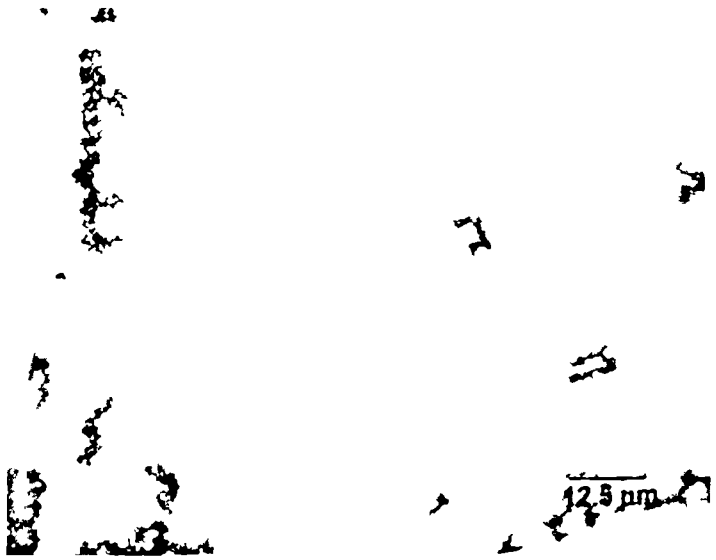

Fig. 5.14 Microstructure of WS joint

5.5 DISCUSSION OF RESULTS

Shape inspection experiments indicate that the IR joints are more uniform than the WS joints. Since the shape directly affects the reliability and the electrical conductivity of a joint, it is expected that the consistency over the two ends of an IR joint in terms of these properties is better. The outgoing joints of WS were found to change with the entry angles. This phenomenon is because the solder deposition mechanism over the two ends is different. Taking the 0^0 joint as an example, during wave soldering, the incoming end is always subjected to a compressive solder wave, and the joint is pushed through the entire process. On the other hand, at the outgoing end, the solder adhering to the end is always

subjected to tension. This tension is created due to the combination of the travel direction and surface tension of the solder. As a result, joints at the outgoing ends commonly have a convex profile. In principal, a convex joint may represent a stronger joint as it has more solder, but in fact most likely it is the weaker. Referring to Fig. 5.15, the contact angle determines the wetting ability. A properly wetted joint should have a small contact angle. In complete wetting, the contact angle in fact is zero [29]. A large contact angle indicates a low wettability which is usually caused by contaminated surfaces or high surface tension of the molten solder. The convex shape of an outgoing WS joint may mean an improperly wetted joint because of the resulting large contact angle which gives no guarantee that the bond between the solder and base metal is strong. Another drawback with the pulling back effects of the solder, especially during the exit of the outgoing joint from the bath, is that it may create a low pressure zone and lead to entrapment of gas in the joint.

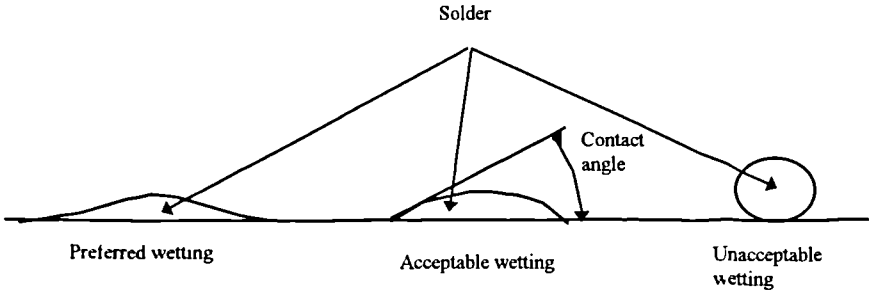

Fig. 5.15 Relation between wettability and contact angle

Alternatively, the formation of a joint over the two ends of a WS component may be looked at from a theoretical point-of-view. Since in wave soldering, say for a component with 0^0 entry angle, it is recognised that the solder at the incoming end is subjected to compression and that at the outgoing end it is subjected to tension, there would be a pressure differential across the two ends. This pressure difference would lead to different wetting conditions over the two ends. From the Young and Laplace capillary equation [55] (Appendix A), the pressure difference across the surface of meniscus can be expressed as:

$$\Delta P \quad \gamma\left(\frac{1}{R_1}+\frac{1}{R_2}\right)$$

where γ is the liquid surface tension

R_1 and R_2 are the radii of two surface planes which are perpendicular to each other

For a leadless chip R_2 is infinity, so the pressure difference of the meniscus becomes

$$\Delta P \quad \frac{\gamma}{R} \tag{5.1}$$

Under static conditions, which are similar to an assembly immersed in a solder bath and being held stable as shown in Fig. 5.16, the pressure head (Δh) of the molten solder is the only source giving ΔP. However, if the assembly is being moved forward along the direction as indicated, it would generate additional pressures over the two ends of the component. Assuming the increase in compressive pressure at the incoming end due to the movement is p_i, and the reduction in pressure at the outgoing end is p_o, Equation 5.1 for the incoming end then can be rewritten as:

$$\Delta P + p_i - \frac{\gamma}{R_i} \tag{5.2}$$

and the outgoing end can be rewritten as:

$$\Delta P - p_o = \frac{\gamma}{R_o} \tag{5.3}$$

Comparing Equations 5.2 and 5.3, since ΔP and γ are constants, it can be seen that to satisfy the basic requirements for proper wetting, the outgoing end demands a longer metallisation than the incoming end ($R_o > R_i$). Insufficient metallisation may lead to a convex joint profile. Based on the experiments conducted, it was found that to minimise the tension effects on the solder, and to provide uniform joints over the two ends of a WS component, the entry angle should be as recommended in Fig. 5.1.

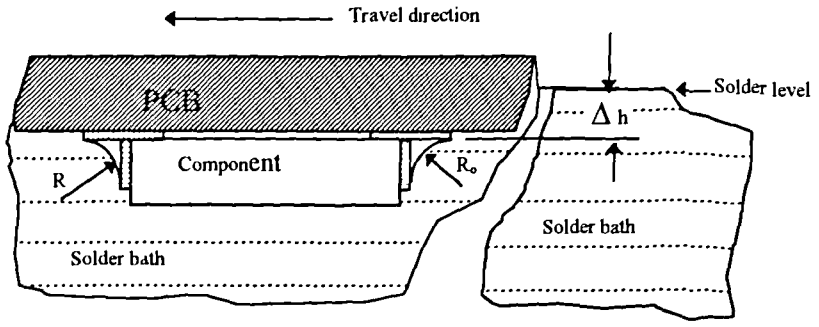

Fig. 5.16 Wave soldering of leadless chip

The amount of gas retained in a solder joint is related to the oxide content and the outgassing of the flux. By investigating the difference in nature between the solder paste and the solder bath it is not difficult to visualise the reasons why more voids were found in the joints produced by IR reflow. The surface area of the particles in the paste is the source of the large oxide content Since the solder paste is basically a mixture of the particles, solvent and flux, during reflow, gas is generated inside and finds it difficult to escape. This is particularly true if thick solder paste is printed, or an abrupt heating process is employed. The difficulty of gas escaping is further increased due to the fact that SMT components are placed on top of the paste. Comparing with the IR reflow process, the molten solder in WS does not have that large amount of internal oxide. The majority of the oxide formed flows on the surface and can be easily removed. Neither is the flux entrapped inside the solder, hence the chance of having gas entrapment due to outgassing of the flux is much less. The void differences are also believed to cause the hardness difference between the IR and WS joints. In the experiments, both the compound layer and the solder of IR joints were found to have hardnesses lower than that of the WS joints. The large amount of voids in the IR joints is considered to be the cause of the hardness reduction. It is also anticipated that due to the larger void content in IR joints, comparatively, WS joints will have better strength and long term reliability.

Chapter 6

Effects of Solder Paste Exposure

6.1 INTRODUCTION

A good SMT joint starts with the right type of solder paste. The properties of solder paste significantly affect the two pre-reflow processes, printing and component placement, and subsequently determine the quality of the joint. On the basis of the published information, the characteristics of solder paste are determined by the following factors [3,17,18,19,20,21,22,23,24,25,26,27]:

- powder content;
- powder morphology ;
- type of flux, solvent, and powders;
- flux/solvent/powder ratio.

Solder pastes with different specifications are used in different printing techniques in order to obtain the optimum results. Generally speaking, suppliers provide pretty comprehensive information for the selection of solder paste. Nevertheless, this does not guarantee the right selection at all times, because there are too many factors which need to be considered. In addition, the situation is further complicated by the fact that some of these factors contradict one another in terms of paste property requirements. Besides the specifications

provided by the vendor, the properties of a paste also vary with the shelf life and exposure time. Of these two, change of paste properties with exposure time more frequently comes into the user's considerations. Exposure time is defined as the time the paste is exposed to air waiting for the next process, or in the course of processing. Past research provides very little information about the effects of solder paste exposure. Suppliers usually suggest that a paste should be exposed to atmosphere for no more than four hours before reflow. However, this can only serve as a guideline, and the exact reasons behind this suggestion are far from adequately understood. It is considered here that detailed information as below should be made available to the users if quality joints are to be achieved:

1. the allowable exposure time of the paste before printing.
2 the allowable exposure time before component placement;
3 the allowable exposure time before reflow.

In view of the lack of information about the effects of solder paste exposure, a chapter is devoted to this part of investigation.

6.2 WEIGHT LOSS

To start off the investigation, experiments were performed to determine the quantity of substance lost with respect to different exposure times. Referring to the IR process in SMT, it can be seen that before reflow actually takes place, the solder paste has experienced an exposure time through the operations of paste mixing, printing, and component placement. It is anticipated that in this time of exposure, the predominant activity taking place in the paste is the evaporation of the volatile solvents with low boiling points [17]. The addition of solvents in the solder paste serves several functions; to control the rheology of the paste, to provide suitable tackiness to the paste, and to act as a flux activator [11,19,25]. However, no information, or very little, is given about the chemicals in these solvents. It is expected that the continuous evaporation of the solvents during exposure which causes changes in the properties of the paste would impose significant effects on the quality of the pre-reflow processes.

6.2.1 Experiments

Fig 6 1 shows the shape of the specimens used for the experiments. The specimens were cut to the required size from a double-sided copper bare-board. In the investigation, specimens were firstly cleaned then weighed individually. After weighing, solder paste was printed on the specimens with the aid of a 1.5 mm thick stainless steel stencil of the printed pattern given in Fig 6 1 The solder paste used in the experiments was RM92, supplied by Multicore, and had the following specifications

Metal content	90% ± 1%
Composition of particles	63Sn37Pb
Flux type	Mildly Activated Rosin
Mesh size	-300 + 500
Particle size	53 - 25 μm
Melting point	183 C

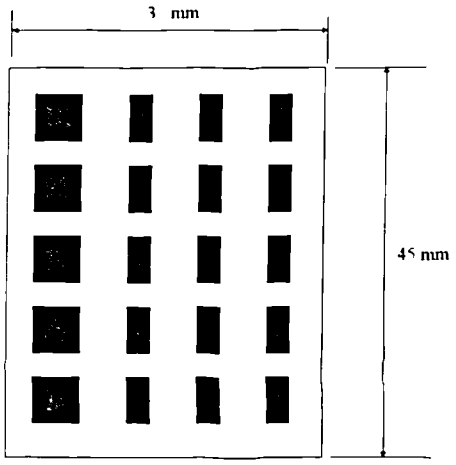

Fig 6 1 Specimen for weight loss and voids investigation

(dark patches are solder paste or solid solder)

This solder paste is formulated specifically for stencil printing. Immediately after printing, the specimens were individually weighted again. The following phase was to expose the specimens to the atmosphere for different durations. To obtain data for showing the weight loss/exposure time relationship, at every predetermined exposure interval, the specimens were weighted. The process of weighting at different intervals of exposure continued until arriving at a state where the weight change was unnoticeable. Two sets of weight loss data at different room temperatures and relative humidities were obtained. In addition, to obtain a better understanding of the changes taking place in the solder paste, some specimens at different intervals of exposure were reserved and viewed under the microscope. The state of the solder paste at different intervals of exposure were recorded in the form of micrographs.

6.2.2 Results

Weight loss experiments were performed on two sets of specimens. The first set consisting of three samples, was performed at an ambient temperature of 14^0C, and relative humidity of 50%. The second set consisting of four samples, was performed at an ambient temperature of 21^0C, and relative humidity of 80%. The percentage weight loss at every interval of exposure of every specimen in a set was firstly calculated using the following expression:

$$\text{The weight loss } \% = \frac{W_o - W_t}{W_o - W_i} \times 100$$

where W_o is the original weight of the printed board (i.e. at zero exposure time);
W_t is the weight of the printed board at exposure time t;
W_i is the weight of the bare-board.

Then, the average percentage weight loss of all the samples in a set at every interval was calculated. The results of the two sets of experiments are shown in Fig. 6.2. From the

figure it can be seen that the rate of solvent evaporation is a function of the ambient temperature and relative humidity. The curve plotted with the use of Set 2 data obviously gives a faster evaporation. Both curves indicate that the initial evaporation rate was greatest, then slowed down gradually until the rate of evaporation was almost zero. The curves show that almost all the solvent loss took place in the first two hours of the exposure, then the amount lost was insignificant. The total average percentage weight loss are 0.8 and 0.9 for Set 1 and Set 2 curves respectively. Analysis shows that the curves can be mathematically approximated to an exponential expression of:

$$Y \quad k(1-e^{-t/a}) \tag{6.1}$$

where Y is the average weight loss %

k is total average weight loss % (0.8 for Set 1 curve, and 0.9 for Set 2 curve)

a is the time constant

t is the exposure time

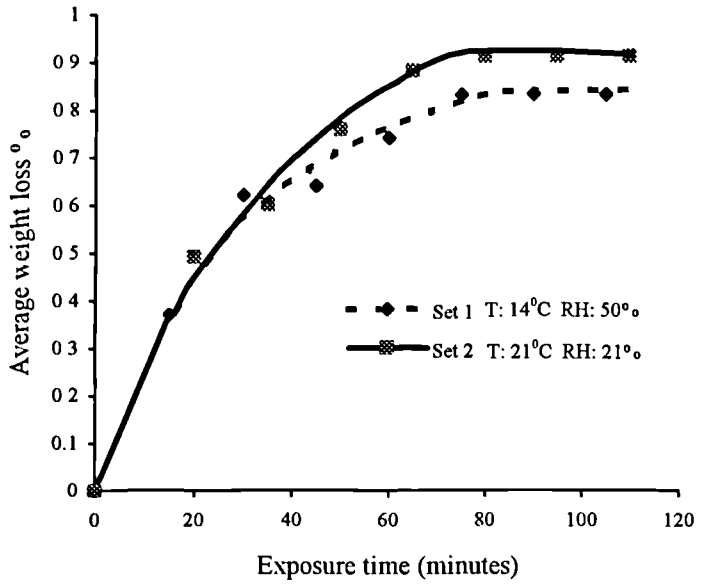

Fig. 6.2 Curves showing the weight loss % with respect to exposure time

The other part of the investigation was to monitor continuously the changes of the paste during exposure using an optical microscope. Figure 6.3a-f show the micrographs of the paste which had been exposed to atmosphere for different times. The spheres in the micrographs are the metallic particles, and are separated by the presence of the flux and solvents. Comparing the micrographs, it can be seen clearly that the fluid separating the particles gradually reduced as the exposure time increased. This has the effect of decreasing the distance between the metal particles, and causes the particles to become more closely packed It is evidence that certain properties of the paste change with exposure time. The immediate impact expected is on the rheology of the paste. Fig. 6.3f is a case where the paste was left exposed to the atmosphere overnight, and it shows that the paste completely dried-out

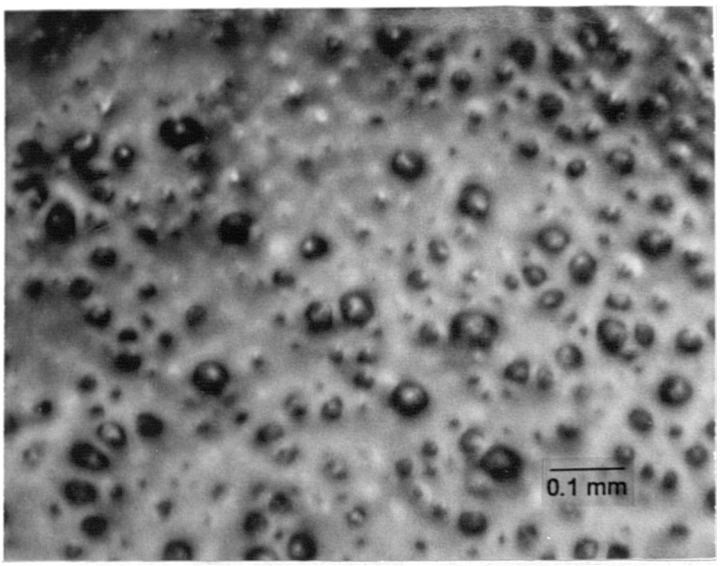

6.3a 0 minutes

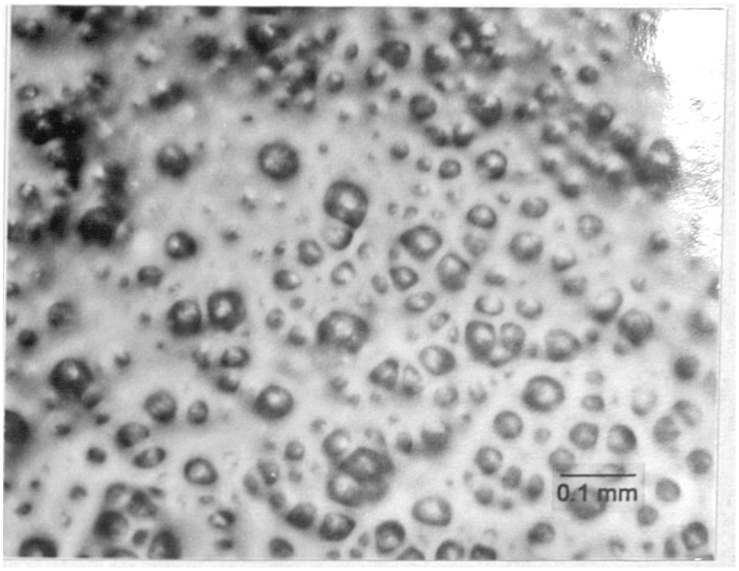

6.3b 30 minutes

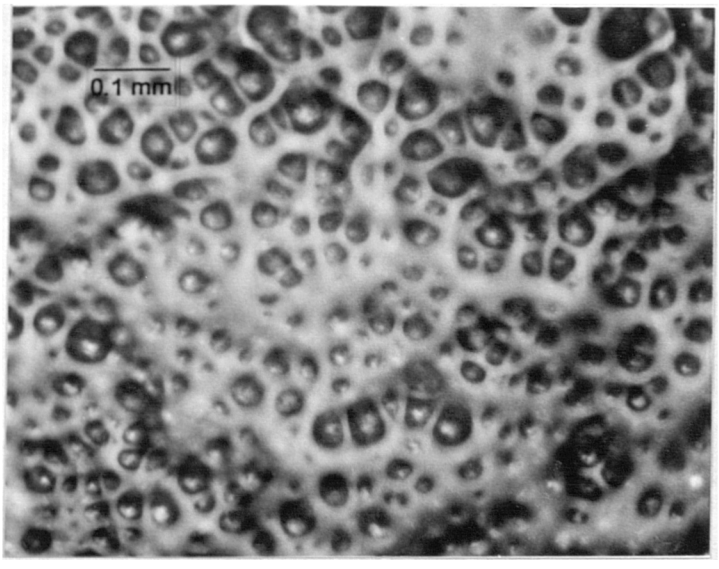

6.3c 60 minutes

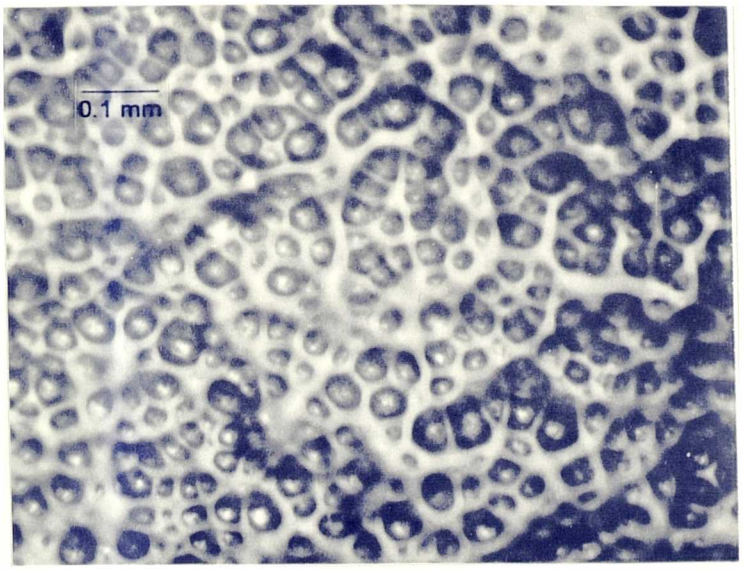

6.3d 1 hours 45 minutes

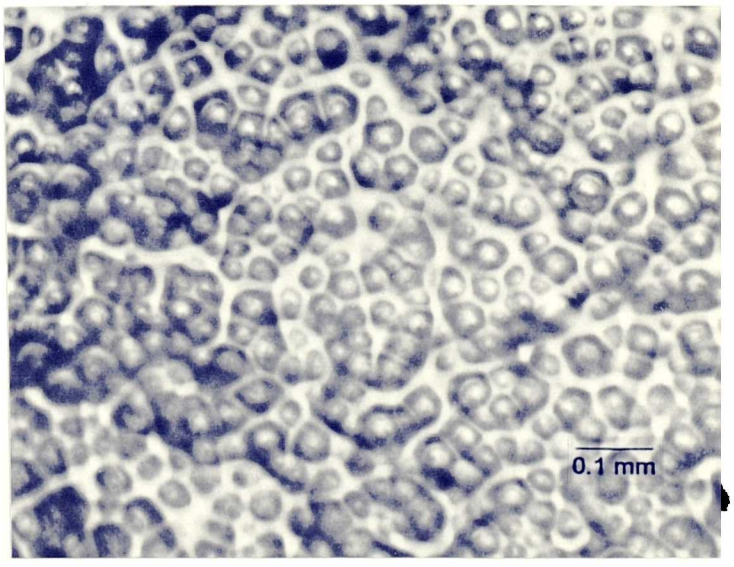

6.3e 2 hours 30 minutes

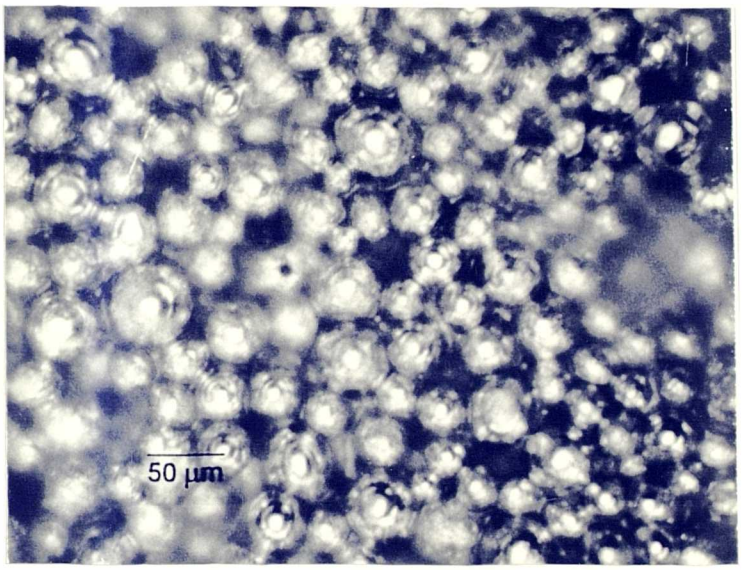

6.3f 24 hours

Figs. 6.3a-f Micrographs of solder paste
at different exposure times

6.3 VOID CONTENTS AFTER REFLOW

It was shown in Chapter 5 that an IR reflowed joint stands a very high probability of resulting in inclusion of voids. Some past research suggested that outgassing of the entrapped flux in the paste is the main cause of voiding. The void content ending up in a joint is determined by the oxide content in the paste, the rate of heating in reflow, flux strength, and soldering area. It is also very likely that voids impair the reliability of joints [64,65,66]. Although, flux outgassing is considered to be the major origin of voids, there is also a possibility that the resulting void content is related to the solvent content in the paste. and the solvent content varies with the solder paste's degree of exposure To verify this point, the void content present in joints at different times of exposure was measured

6.3.1 Experiments

Specimens used for the void measurements were the same as that used for the weight loss studies. The only difference is that after stencil printing, then exposing to atmosphere at specific time intervals, the specimens were also IR reflowed. The solder patches eventually end up as illustrated in Fig. 6.1. The specimens were then ground to flatten and smoothen the solder surfaces. This was intended to enhance the subsequent void detection process. The voids in the solder were detected by means of an x-ray system, model SOFTEX PRO-TEST 125, as described in Section 5.3.1. Radiographs showing the images of voids were taken with the use of the built-in camera in the x-ray system. To calculate the void content of a reflowed solder, the void images was first transferred to an image analysis system, then by using the Optimas software in the system the percentage of voids was calculated. Three sets of experiments with the same intervals of paste exposure were performed. The exposure intervals (at ambient temperature) were 30, 60, 90, 120, 270, 300, 330, 360, and 390 minutes.

6.3.2 Results

Figs. 6.4a-i are one of the three sets of radiographs showing the voiding conditions in the solder. The white areas in the radiographs represent the locations of the voids. Fig. 6 5 shows the average area of voids of the three sets of data plotted against the solder paste exposure time, and details of the three sets of measured data may refer to Table 6.1. Both this figure and radiographs show that the longer the solder paste was exposed the less is the resulting void content in the joints In addition, the radiographs show that the average size of the voids in fact decreases with exposure time.

6.4 TACKINESS ANALYSIS

One of the merits of solder paste is its "glue" characteristic that enables components to be held in position before the reflow operation. In fast manufacturing environments, the

assemblies after component placement are frequently subjected to acceleration and vibration prior to reflow The possession and maintenance of an appropriate tackiness in the paste determines its ability to secure continuously the components in their desired positions. The tackiness of a solder paste is found to be affected by many factors. The aim of this part of the work was to investigate the tackiness change with respect to the exposure time.

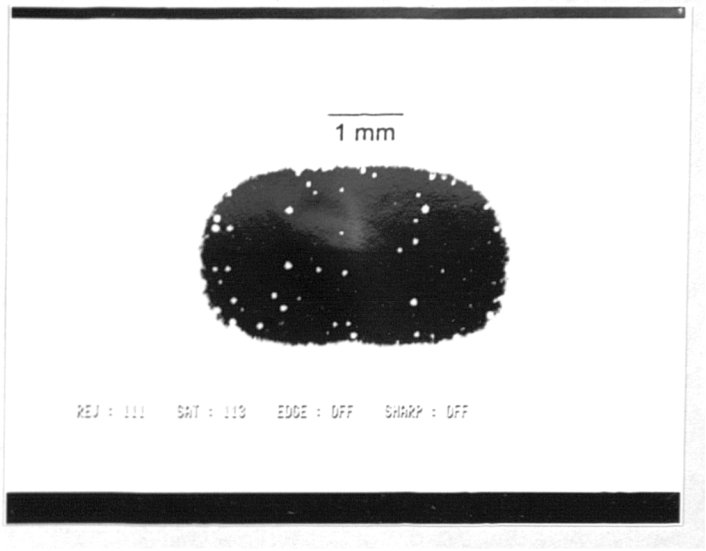

6.4a 30 minutes

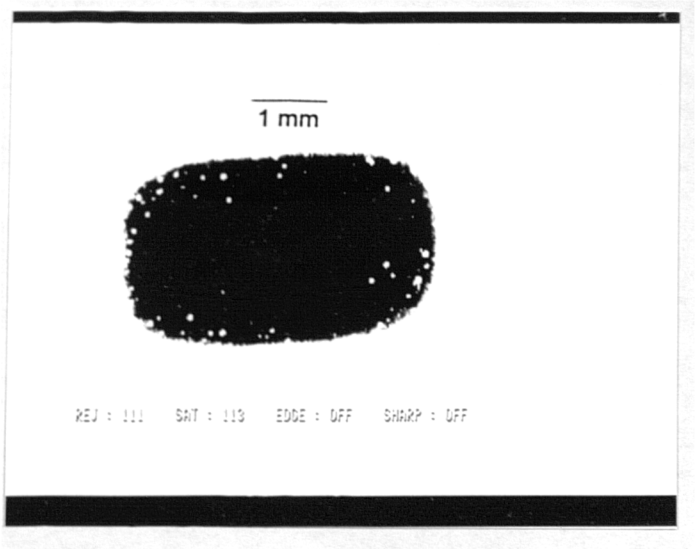

6.4b 60 minutes

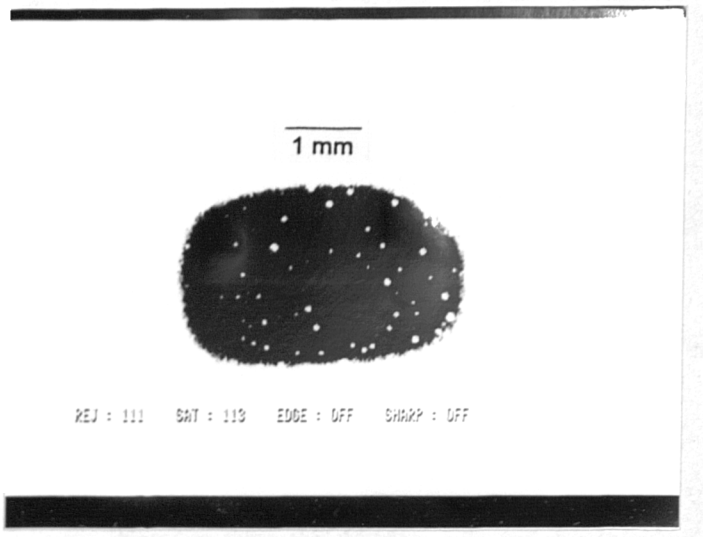

6 4c 90 minutes

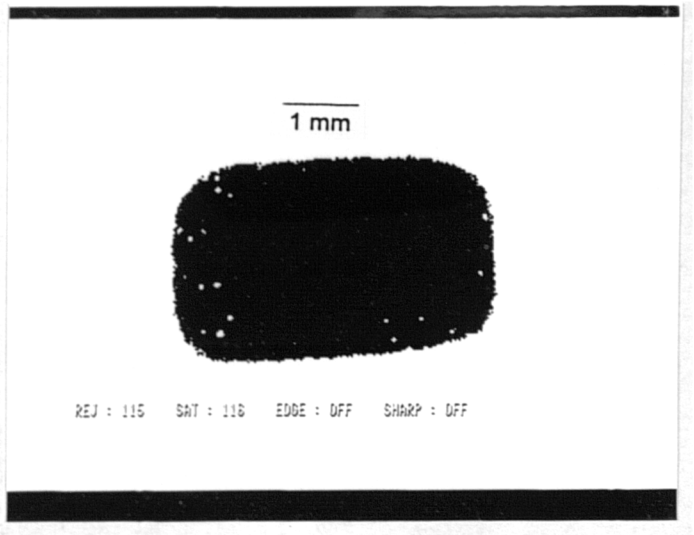

6.4d 120 minutes

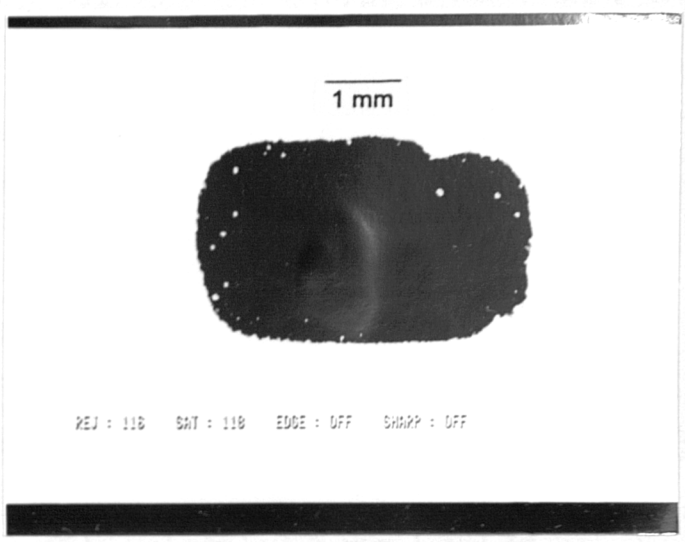

6 4e 270 minutes

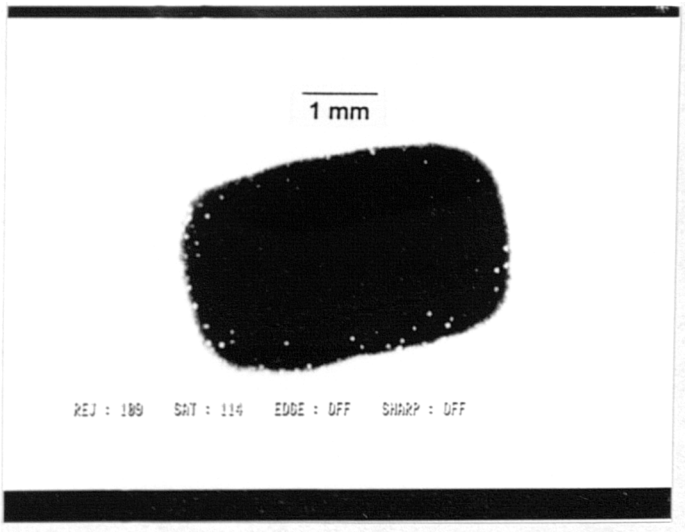

6.4f 300 minutes

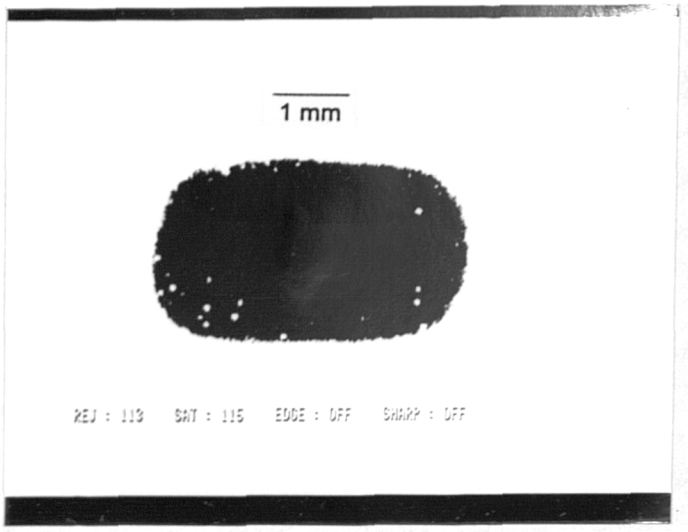

6 4g 330 minutes

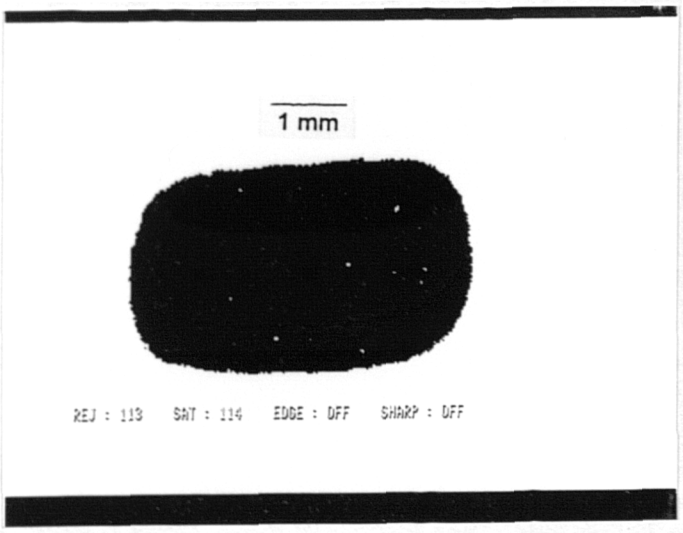

6 4h 360 minutes

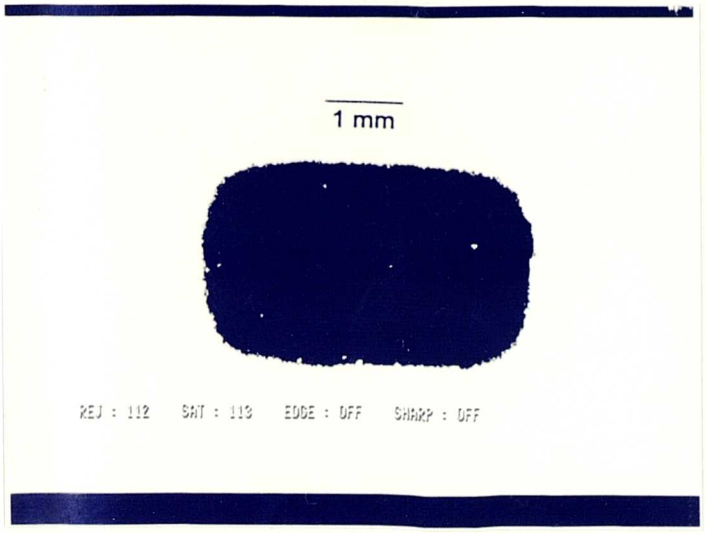

6.4i 390 minutes

Figs. 6.4a-i Radiographs showing the void contents in solder with the solder paste exposed for different times

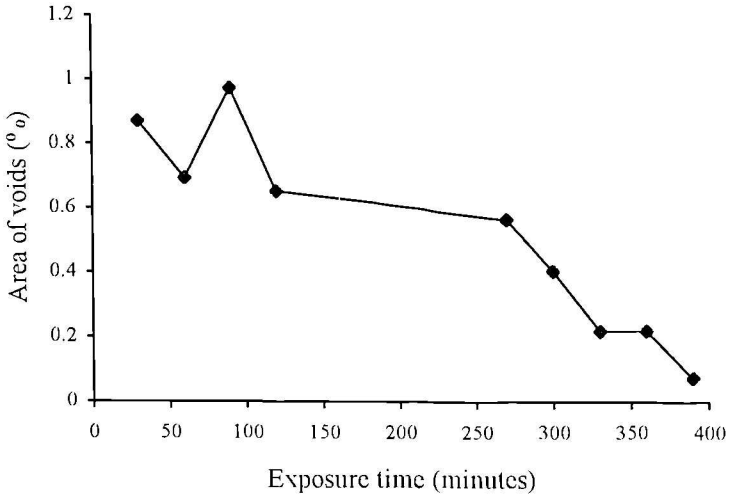

Fig. 6.5 Relation between percentage of voids and solder paste exposure time

Exposure time (minutes)	Area of voids (%) Set 1	Set 2	Set 3	Mean value
30	0.155	1 064	1.395	0 871
60	0.305	0 918	0.860	0.694
90	1.146	0.723	1.046	0 972
120	0.733	0.485	0.742	0 653
270	0.670	0.510	0.520	0 567
300	0.523	0 251	0.438	0 404
330	0.019	0.119	0.516	0 218
360	0.324	0 118	0.219	0 220
390	0.054	0 021	0.155	0 076

Table 6 1 Data for Fig. 6 5

6.4.1 Background Information

The tackiness of solder paste can be established by two methods. The first method is to preload a probe onto the printed solder paste then measure the tensile force required to extract the probe The tensile force is used as a measure of the tack force of the paste This method provides quantitative tackiness measurements with respect to the variables being investigated [15] However, these measurements can only be performed with special equipment. The second method is a qualitative approach, and is particularly suitable for tackiness comparisons This method involves the placement of components on the printed positions, then the entire board is inverted The elapsed time for a component to detach itself from the paste is noted and used as a means of measuring the tackiness of the paste [11] This method is fast and simple, but can only be used for comparative purposes The tackiness of a paste depends upon several factors, which include the [14 17 23 30]

- component preload value,
- tack age,
- solvent, flux, and particle size,

- temperature and humidity of the work environment.

Generally speaking, an increase in the preload results in an increase in the tack force. It was found that the tack force increases with tack age until arriving at a peak value, which is followed by a decrease [30]. There was a report that a decrease in the particle size gave a corresponding increase in the tack force, and that the tack force was independent of the age and metal content of the solder paste [23]. On the other hand, paste which is too tacky causes smear on the stencil and the board during printing. It was suggested by Gutllaume *et al.* [14] that the paste should maintain its tackiness for at least six hours after printing, to allow sufficient time whilst awaiting reflow.

6.4.2 Experiments

The qualitative method described above was employed here for analysing the tackiness of solder paste as a function of the exposure time. This approach works on the basis that if an article is placed on a printed paste pad and is inverted, the stronger the paste tackiness the longer the article would be held in position. The solder paste used for the analysis was the same as that used for the weight loss analysis, that was RM92 from Multicore. A brief description of the essential items used for the tackiness analysis is given below

1 a jar of new solder paste
2. two weights of 9.8g each
3 a stainless steel stencil with 10 circular apertures. Each aperture had a diameter of 6 mm.
4. 10 plastic nuggets, 10 mm in diameter and 8 mm high
5. bare copper boards
6 a squeegee
7. a stand for supporting the inverted board
8. a spatula for paste stirring
9. stop watches

For each experiment, a jar of new solder paste was brought out of the refrigerator one hour before the experiment. This ensured that the paste was brought to room temperature before application. To homogenise the paste, it was stirred for five minutes with a spatula Following this, an adequate amount of paste was spread on the stencil The printing of the solder paste onto the copper boards was performed manually, so, care had to be taken to keep the printing parameters consistent for all experiments After printing and removing of the board, the printed board was exposed to the atmosphere for a predetermined time When the required exposure time had arrived, the ten cleaned nuggets were placed on the printed positions of the board one by one. A weight of 9 8 g was put on top of each nugget with a dwell time of 5 seconds. Immediately after the completion of the above steps the entire board was turned up-side-down, and supported on a stand, as shown in Fig 6 6 The next stage was to record the time that each nugget dropped off Tack time was used for measuring the adhesive strength of the paste. Here, the tack time is the time required by a nugget to break the adhesive force, and is measured from the time of board inversion to the fall of the nugget A total of ten experiments but with different exposure times were performed The exposure time (at 26°C) of a board was counted from the moment the printing was finished to the moment when the placement of the ten nuggets commenced The exposure times for the ten experiments were 0, 0 5, 1, 1 5 2, 2 5 3 3 5 4 13 hours Since the tackiness was evaluated on comparative basis, the consistency of the weight of the nuggets was crucial Table 6 2 gives the whole picture about the weight of the ten nuggets used The table shows that the weight range of the nuggets is only 0 0253g and the standard deviation is only 0 0074g, therefore it is considered that the weight discrepancy factor of the nuggets is insignificant

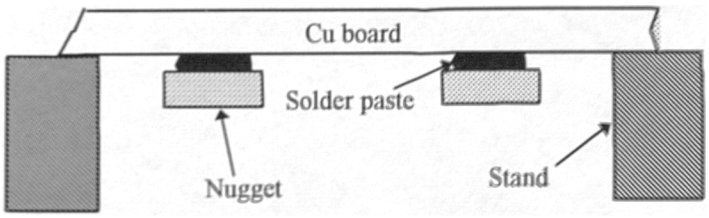

Fig 6 6 Board at inverted position for tack time measurement

Nugget No.	Weight (g)	Deviation from mean
1	3 8000	-0 0114
2	3 8031	-0 0083
3	3 8042	-0 0072
4	3 8108	-0 0006
5	3 8111	-0 0003
6	3 8115	0 0001
7	3.8125	0 0011
8	3 8138	0 0024
9	3 8214	0 0100
10	3.8253	0 0139
Mean	3.8114	
Range	0.0253	
Standard deviation	0.0074	

Table 6 2 Weight information of nuggets used for the tackiness analysis

6.4.3 Results

Table 6 3 shows the overall results of the tackiness analysis The tack time in the table is in minutes unless specified in seconds ("). Where the nuggets did not fall off over the entire test period, which was 3 hours, these are denoted by the symbol (-) The average tack time against the exposure time was plotted, and is shown in Fig 6 7 The graph gives an impression that the tack time and the exposure time may follow a power law relationship To test this, the data were plotted on a log-log scale, as shown in Fig 6 8 This time, the graph shows a strong linear correlation between the tack time and the exposure time The equation of the best fit line, Fig 6 8 as can be seen is in the form of

$$\log T - \log k - a \log t \qquad (6\ 2)$$

where T is the average tack time

t is the exposure time

k is the point of interception between the fitted line and log t 0 (i e. t 1)

a is the slope of the line

So, Equation 6.2 can be transform into a general equation as:

$$T \quad kt^{-a} \tag{6.3}$$

A (0.5, 1.33) and B (13, 0.005) are the two points arbitrarily selected on the straight line, Fig. 6.8, for calculating the slope of the line:

$$a \quad \frac{\log 1.33 - \log 0.005}{\log 0.5 - \log 13}$$

$$- - \frac{2.3979}{1.4149}$$

$$= - 1.69.$$

Then, Equation 6.2 can be further rewritten in the form of :

$$T \quad kt^{-1.69} \tag{6 4}$$

Again, by using any point on the line, say point A (0.5, 1.33), and substituting these co ordinates into Equation 6.4, the value of k can also be calculated as follow:

$$1.33 - k.0.5^{-1.69}$$

$$k - 0.413$$

The above shows that the tack time and exposure time relation, based on the experimental results, can be expressed by a power law equation in the form:

$$T - 0.413t^{-1.69}$$

Exposure time (hours)	0	0.5	1	1.5	2	2.5	3	3 5	4	13
Tack time in minutes unless specified in second (")	40	20	12	15"	17'	5"	15"	15	14	5
	55 '	83	20	12	55"	15"	20	16	15"	5'
	63	90	23	16	4	20"	30 '	35 '	31"	10"
	-	98	28	25	4	2	2	36'	35"	11"
	-	112	28	28	5	2	2	40"	55	15
	-	-	32	28	6	3	3	2	2	17 '
	-	-	34	30	8	3	4	3	2	21 '
	-	-	35	32	10	3	4	4	4	30 '
		-	40	-	-	4	7	6	4	40
	-	-	-	-	-	5	9	6	7	40
Average tack time (minutes)	-	80	28	21.4	4.8	2.3	3.2	2.3	2	0 32
Average tack time (hours)	-	1.333	0.467	0.3567	0.080	0 038	0.053	0.038	0 033	0.00 5

Table 6.3 Results of tack time against exposure time

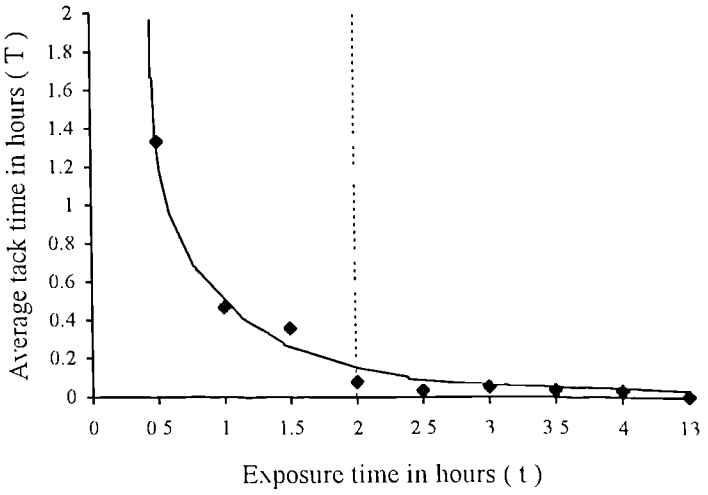

Fig. 6.7 Plot of tack time against solder paste exposure time

6.5.1 Background Information

The printability of a solder paste can be understood by a study of the paste's rheological properties. There are different systems available for performing this type of study, such as the Brookfield, Malcom, Ferranti-Shirley, and Haake [17]. The measurement technique of these systems is either of capillary, cup, falling ball, or rotational viscometry. Rotational viscometry is the most common technique used for solder paste measurements. The Malcom system used in the present investigation is of this type Several parameters are used to define the rheology of solder paste, among them, the most important one is the viscosity. Viscosity is a characteristic property which determines the flow of a paste or liquid. It may be defined as the internal friction or resistance to flow of the paste or liquid. Mathematically, viscosity (η) is defined as the ratio between the shear stress (τ) and the shear rate ($\dot{\gamma}$), and is expressed in the form [27]:

$$\eta \quad \tau \dot{\gamma}$$

The thixotropic nature of solder paste causes its viscosity value to change with shear rate. In effect, the pre-reflow processes, which subjects the paste to varying degrees of shear would change the viscosity of the paste over time. To allow a better understanding of this aspect, the relation between viscosity and shear rate is commonly plotted on a log-log scale In such a scale, it was found that viscosity and shear rate exhibit a straight line relation [17] The slope of the straight line, which describes the thinning characteristics of the paste, is the thixotropy index (T), and can be calculated by the following expression:

$$T \quad \log\left(\frac{\text{viscosity at } 1\ 8\ s^{-1}}{\text{viscosity at } 18\ s^{-1}}\right) \tag{6.5}$$

In the printing operation of SMT, a suitable thixotropy index is essential. Both too high and too low a value of the thixotropy index would cause printing problems. The other aspect of

the paste needed to be defined is the ability of the paste to repeat or maintain its rheology properties after shearing. A non-recovery rate, R, is commonly used to characterise the hysteresis loop of the shear stress/shear rate curve. In the Malcom system, the R valuc is calculated by the following expression, and the shear rate at 6 s^{-1} is only arbitrarily selected [23]:

$$R = \frac{\text{viscosity at 6 } s^{-1} \text{ (increasing shear) - viscosity at 6 } s^{-1} \text{ (decreasing shear)}}{\text{viscosity at 6 } s^{-1} \text{ (increasing shear)}} \qquad (6.6)$$

The model used for this investigation was a Malcom PCU-200 viscometer. The main part of the unit is the viscosity sensor, as shown in Fig. 6.9 [113]. The sensor consists of two major parts, an internal spiral screw and an external cylinder. During measurement, the external cylinder rotates while the internal spiral screw remains stationary. The rotation of the external cylinder combines with the spiral effects of the internal screw to turn the unit into a pump. Solder paste located at the inlets of the sensor would move upwards gradually while the external cylinder rotates. Eventually, the paste comes out of the outlets when it has arrived the top of the sensor. The internal spiral screw apart from working as a pumping unit, also acts as a torque sensor. From the torque sensed, the shear stress to which the solder paste is subjected is computed. The shear rate can be adjusted by changing the rotation speed of the external cylinder. In fact, at a particular rotation speed, values for both the viscosity in Pascal seconds (Pa.s) and shear rate in per second (s^{-1}) are calculated automatically by the built-in system, and a print-out can be obtained conveniently. Table 6.4 shows a print-out example of a test.

116.1	Pa.s
25.3	^{0}C
6.0	s^{-1}
10	RPM
13:13	Time
1955.02.23	Date

Table 6.4 Example of a print-out from the Malcom viscometer

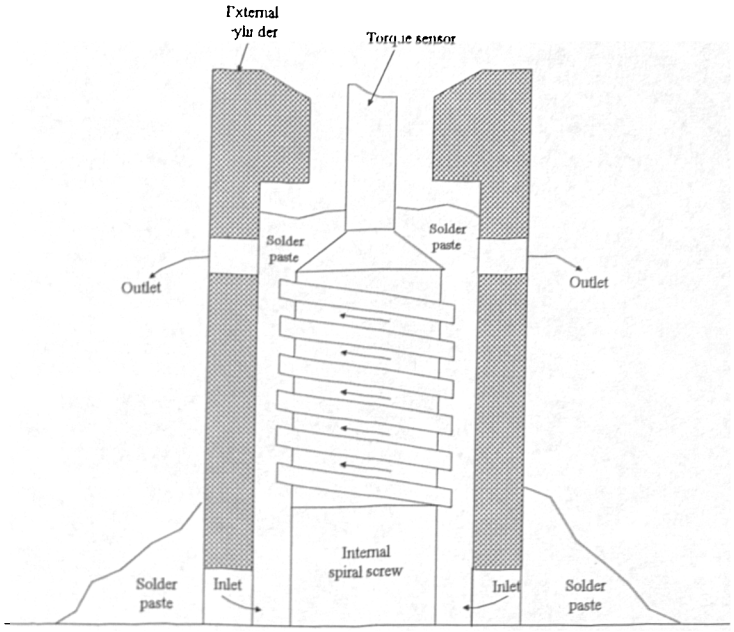

Fig 6 9 A cross-section view of the
Malcom PCU-200 viscometer sensor

6.5.2 Experiments

Viscosities of solder paste after exposing to ambient temperature for different times were measured The exposure times on which investigations had been performed were 0, 20, 40, 60, 80, 100, 120, 150, and 180 minutes. A glossary of the equipment and materials for the experiments is give below·

Raw material . RMA solder paste from Multicore contained in 250g jars.

Equipment: Malcom PCU-200 viscometer
2 empty RMA solder paste containers
3 plastic exposure plates (each marked with an area of 150 x 70 mm)
A stirrer

In performing each measurement, a new jar of solder paste must be used. The solder paste after removing from the refrigerator was allowed to come to room temperature. To ensure consistency in every experiment, the waiting time was standardised to one hour. When the waiting time had arrived, the cover of the jar was opened and the paste stirred. The stirring operation continued for five minutes to ensure homogeneity. The paste was then spread onto the marked off area of the plastic exposure plate. The marking, which was by means of four acrylic strips with a thickness of 3 mm, Fig. 6.10, was to ensure a controlled exposure area for every experiment. After the spreading of the paste, a steel rule was used to level off the excess paste and to even out the thickness. The solder paste was then exposed for a predetermined duration. When it had reached the desired exposure time, the paste was transferred into an empty jar, and the viscosity measurement was started immediately. The viscosity for every exposure was measured by following the standard steps recommended for the Malcom system, and the temperature was set to 25^0C. The standard operation sequence of the system is:

Mix mode : 5 minutes

Start mode :

Speed (RPM)	Shear rate (s^{-1})	Time (minutes)
10	6.01	3
3	1.81	6
4	2.41	3
5	3.01	3
10	6.01	3
20	12.01	1
30	18.01	1
10	**6.01**	**1**

As recommended, the last measured viscosity value from the standard steps is the one with a shear rate of 6.01 s^{-1} for every exposure and this was used for comparison.

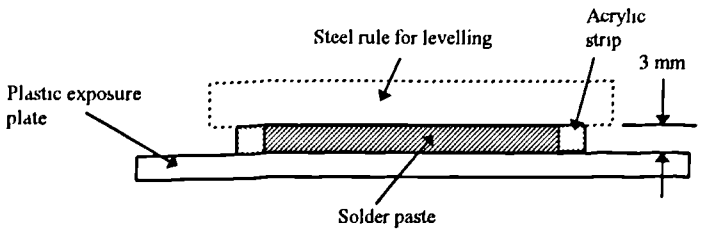

Fig 6 10 Diagram showing the solder paste at exposure

6.5.3 Results and Findings

Table 6 5 summarises the overall results of the investigation The Malcom viscometer used provides a print-out for each shear rate. As shown in Table 6 4, the information that can be deduced from the print-out include the viscosity value, test temperature, shear rate, external cylinder rotation speed, test time, and test date The effects of exposure time on the viscosity are illustrated in Fig 6.11. The viscosity value corresponding to each exposure time in the figure is the last measured viscosity value of the standard Malcom test Based on the results shown in this figure, it can be seen that the viscosity has increased from an initial value of 86.9 Pa s to 123.4 Pa s over an exposure time of 180 minutes The graph shows that there is a rapid increase in the viscosity at the initial stage, which then becomes more gradual. The increase in the viscosity suggests that exposure time might impair the flow characteristics of the paste, and hence affects its printability The viscosities at different shear rates for solder paste with 0 20, 40, 60, 80, 10 , 12 , 150, and 18 minutes exposure times were plotted on a log-log scale as shown in Figs 6 12a-i The figures show that on a log-log scale the viscosity and shear rate have a linear relationship In fact this linear relationship is shown in all these figures apart from Fig 6 12g which exhibits a slight scatter Fig 6 12a-i also show clearly the thixotropy property of the solder paste Fig 6,13 illustrates the thixotropy indices of paste calculated by using Equation 6 5 f r all exposure times This graph shows that the thixotropy index decreases only at a very slow and insignificant rate with the time of exposure That is to say the rate of thinning more r less would remain the same even if there is a change in the

shear rate. The ability of the paste to recover its rheological properties is indicated by its non-recovery rate R. The R values of solder paste with different exposures were calculated by using Equation 6.6, and the results were plotted and shown in Fig. 6.14. The curve in this figure shows that at the initial stage there is a rapid decline in the paste's recovery ability, and then the rate of decline slows down and eventually becomes stable.

Shear rate s^{-1}	VISCOSITY (Pa.s) Exposure time in minutes								
	0	20	40	60	80	100	120	150	180
6 01	93 0	111 4	111.4	116.6	112.5	110.7	111.5	124.3	132.6
1 81	221 6	246.2	247.2	245.2	243.7	240.7	203.6	262.4	267.6
2 41	169 4	210 4	209 2	209.0	205.2	206.8	152.9	225.8	213.2
3 01	147 7	179 7	178.5	179.4	177.4	179.4	138.7	194.2	196.3
6 01	104 3	118 5	116.1	119.7	117.7	120.1	128.3	130.3	133.4
12 01	61 7	82 0	78 1	84.1	82.2	84.7	52.4	92.0	95.0
18 01	49 6	64 7	62 4	68.1	66.7	67.8	66.7	75.2	77.1
6.01	**86.9**	**107.5**	**107.8**	**110.4**	**109.1**	**108.8**	**121.1**	**121.9**	**123.4**

Table 6 5 Viscosities of solder paste at different exposure times measured by the Malcom viscometer

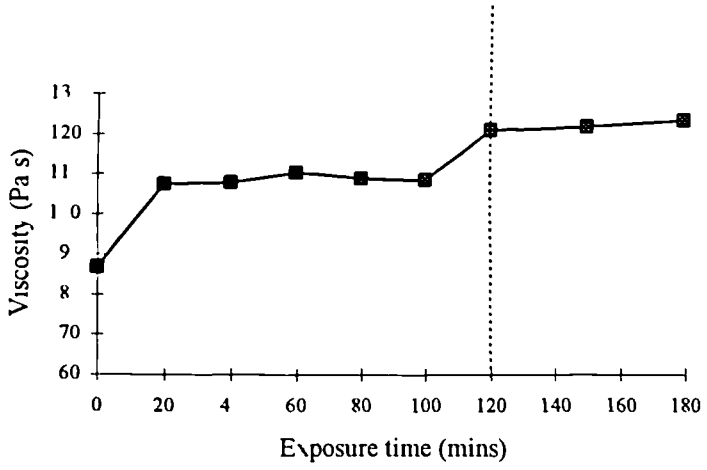

Fig 6 11 Effects of exposure on viscosity of solder paste

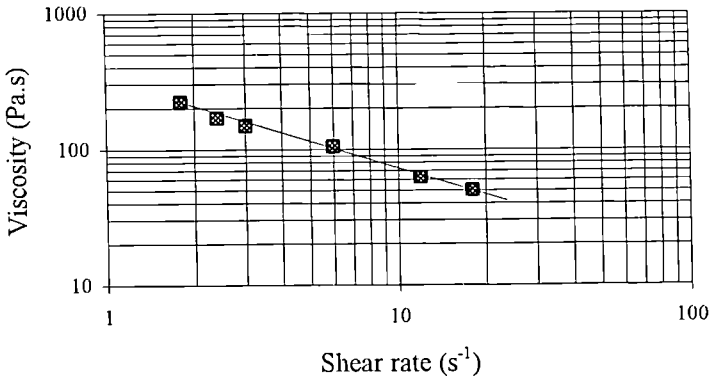

6.12a 0 minutes exposure time

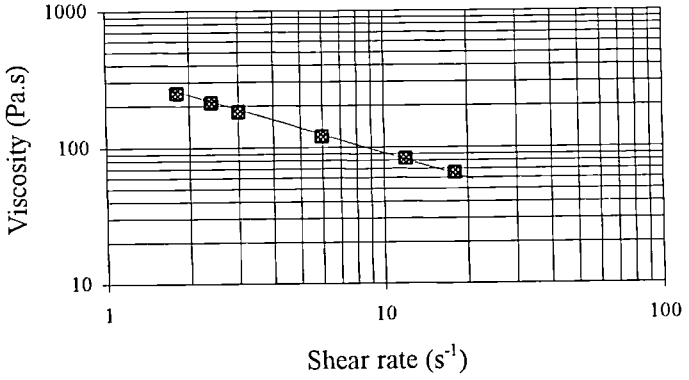

6.12b 20 minutes exposure time

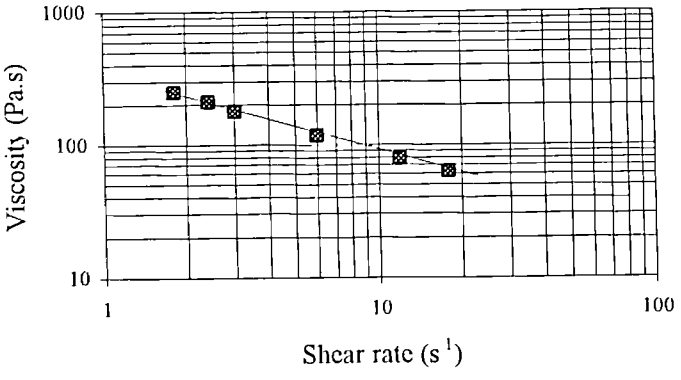

6.12c 40 minutes exposure time

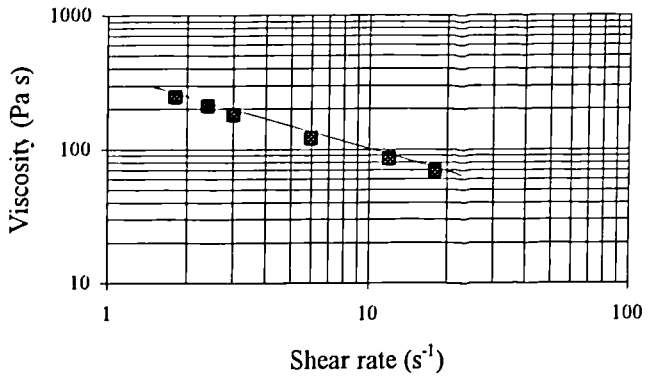

6 12d 60 minutes exposure time

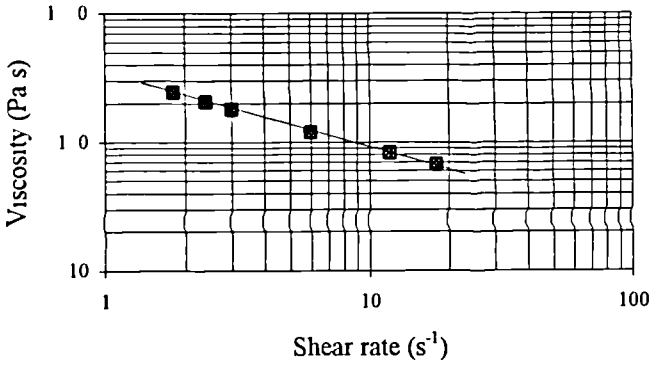

6 12e 80 minutes exposure time

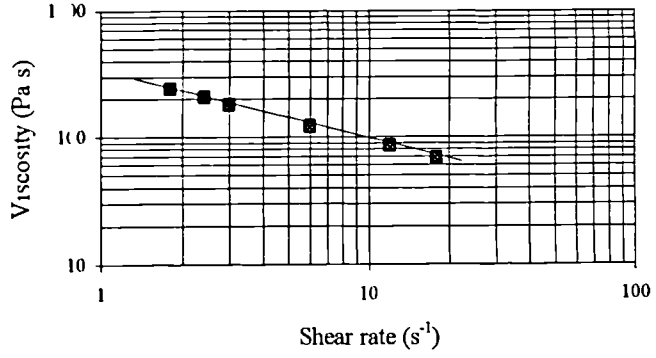

6.12f 100 minutes exposure time

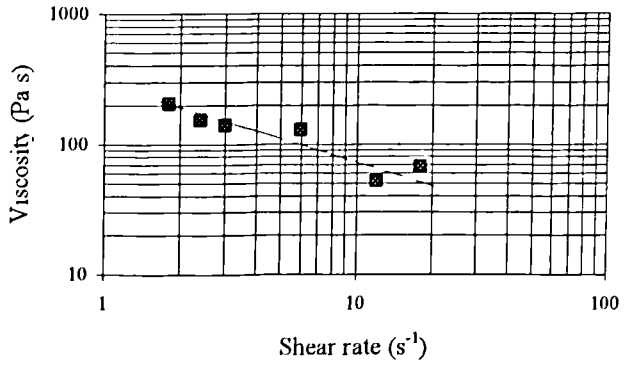

6 12g 120 minutes exposure time

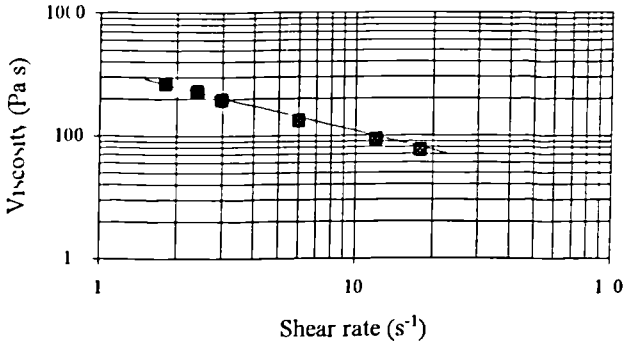

6 12h 150 minutes exposure time

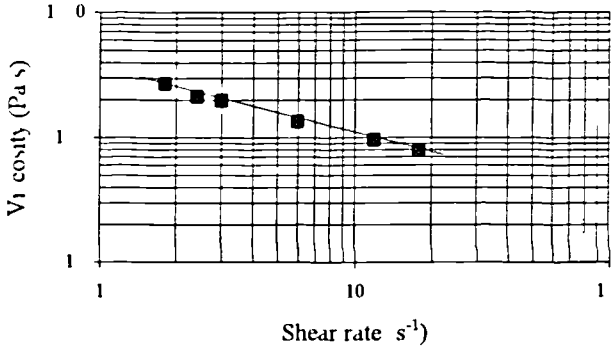

6 12i 180 minutes exposure time

Figs 6 12a-i Relation between viscosity and shear rate of pastes exposed for different times

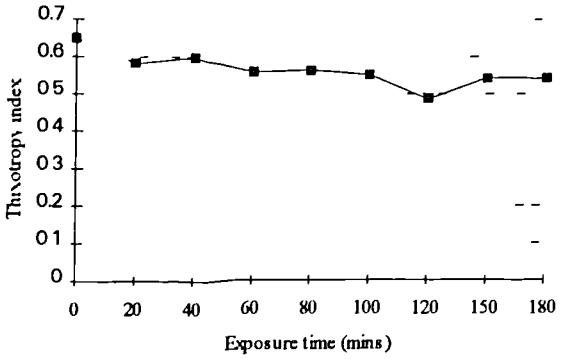

Fig. 6.13 Effects of exposure time on thixotropy index

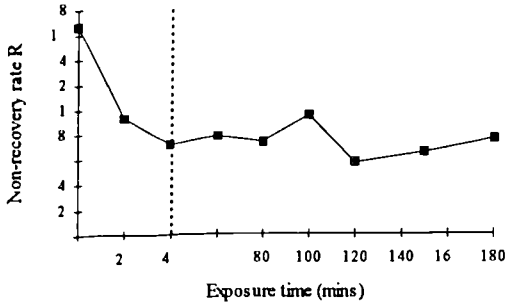

Fig 6.14 Non-recovery index plotted against exposure time

6.6 DISCUSSION

There are two factors governing the properties of a solder paste, the paste's ingredients and the working conditions. The ingredients determine the as-manufactured properties of the paste and gives a specification. The working conditions generally include the environment under which the operations of component placement, printing, and reflow are performed. Solder paste properties are complex and susceptible to the environment. They change with temperature, humidity, time, and shear rate. Since the birth of SMT,

research has touched upon most of these major areas. However, there is one which is very important which has been neglected and this is the effect of paste exposure. The presence of solvents in the paste is as important as the presence of flux and metal particles. Solvents are volatile, and their content also directly determines the characteristics of the paste. When a paste is exposed to the environment, solvents would be expected to evaporate. This Chapter has demonstrated that exposure has significant effects on the properties of the paste.

It is considered that the evaporation taking place at room temperature is largely of the solvents with low boiling points [17]. Evaporation mainly affects two aspects of a paste. The first is the ability of the paste to hold the components in position and to sustain the paste in its desired shape This part was covered by the study of the change in tackiness of the paste in this Chapter The second is the printability of the paste. It is known that the main function of the low boiling point solvents in a solder paste is to facilitate and control the flow Here, the change in the printability of the paste due to exposure was investigated through a study of the change in the rheology. To start off the investigation in this Chapter, a weight loss was performed first in order to demonstrate and measure the loss of substance through evaporation In this part of study, it was found that evaporation basically arrived at a steady state in the first two hours for this solder paste, and the weight loss percentage expressed as a function of the exposure time was in the form of an exponential increase as shown in Fig 6 2, and Equation 6.1. Although the finding was based on a single paste supplied by Multicore, it is expected that this phenomenon generally applies to all solder pastes with differences only in the 'k' and 'a' values. From Fig. 6.2, it can be seen that for a particular type of paste, the total amount of weight loss at steady state (equal to 'k'), and the time constant (equal to 'a'), in fact, are functions of the humidity and temperature to which the paste is exposed Provided that more information is available about 'a' and 'k' values, Equation 6 1 is a viable means for estimating the weight loss at different stages of exposure Figs 6 3a-f show that the amount of solvent in the paste progressively reduces. This continuous drying out phenomenon definitely makes the ease of flow of the paste more difficult. It is anticipated that at a certain stage of exposure, the lubricating effects from the solvents may have reduced to an extent that the particles do not slip over each

other, instead, movement is through the plastic shear plane, during the printing operation. When this stage arises, solder paste would move in lumps and this would lead to various sorts of problems.

Void entrapment in a joint made of solder paste, to certain extent, is unavoidable. This is due to the fact that liquid solutions, mainly flux and solvents, are impregnated in the paste When heat is applied to turn the paste into solder, there is no guarantee that all the liquids would escape, and as a result the entrapped liquids are turned into gas, forming voids in the joints Although it is considered that flux outgassing is the main source of voids, it was found in this Chapter that an increase in the solvent content also increases the size and volume of the voids This was substantiated by the finding that an increase in the exposure time which had the effects of reducing the amount of solvents, decreased both the size and volume of the voids in the resulting joints. During the time when a paste is exposed to atmosphere, it can be postulated that solvents near to the surface are far more easily evaporated. On this basis, it is logical to believe that higher void contents are expected in the inner part of a joint

The tackiness study provides clear information that tack time decreases rapidly with exposure With reference to Fig 6 7 it can be seen that the tackiness of the paste declines at a very high rate in the first two hours This timing is in agreement with the weight loss finding, that is most of the solvents evaporated in the first two hours. The power law expression, Equation 6 3 provides a means to estimate the decay in tackiness over a particular exposure time So, if the initial tackiness is provided as a specification of the paste, the loss in the tackiness over time can then be calculated. From the tackiness point-of-view, it can be concluded that the sooner the component placement operation is performed the less is the chance that components may be shaken off.

The printability of a paste is mainly determined by its rheological characteristics Neither too high nor too low a viscosity is desirable In screen or stencil printing, the solder paste is simultaneously subjected to shear and exposure This, combined with the thixotropic property of the paste, would effectively change the viscosity value of the paste

with time. Fig. 6.11 shows that the increase in the viscosity due to exposure can be very significant; the increase within 180 minutes was as much as 42 percentage (from 86.9 Pa.s to 123.4 Pa.s). This gives a message that if the paste is exposed for too long it would thicken up and lead to printing problems. Incidentally, Fig. 6.11 also indicates a more significant increase in the viscosity after two hours. Although, the solder paste on which these investigations were performed dried up rapidly, its rate of thinning which is measured by the thixotropy index, was not being affected significantly by the effects of exposure. This implies that the viscosity of the paste is not that susceptible to the speed of printing Fig 6 14 shows that the reproduction ability of the paste deteriorates rapidly in the initial exposure, and then becomes stable after approximately 40 minutes.

Chapter 7

Cu/Sn Intermetallic Compounds

7.1 BACKGROUND INFORMATION

When two pieces of metal are joined together by a filler metal, a good joint would consist of an interfacial layer which is an alloy of the base and the filler metals Typical examples are joints found in the electronic industry with copper as the base metal and solder as the filler metal This interfacial layer, which only occupies a very thin region is fundamentally made up of Cu Sn_5, Cu_3Sn, and other solder products. The compounds of copper and tin here referred to as intermetallic compounds (IMC) can be distinguished from the other alloys because these compounds have a fixed stoichiometric composition whereas the composition of other alloys can change within a small range without significant change of their crystal structure [114]. IMC is formed through mutual diffusion of atoms between the base and the filler metals both in the liquid and solid states. In a copper/solder system, the thickening of the IMC layer through solid diffusion of copper tin atoms at room temperature is almost negligible. However, with sufficient heat and time, the growth of this IMC in the solid state could be substantial [37,102,103,104]. This thin layer of IMC is an indication of proper wetting, yet on the other hand, its composition and thickness have profound effects on the reliability of the joints [94-101]. SMT joints are commonly designed to withstand thermomechanical cycles. During service, vibration of the electronic device in most circumstances is the only source of mechanical cycling, and the stress generated in a joint is usually very small. Relatively speaking, the thermal effects when

electric currents pass through the joint are more damaging. The electric current, and hence the heat, passing through an electronic device can be in various cyclic patterns. The heat cycle plus the fact that materials of the substrate assembly have different thermal coefficients of expansion would subject the joint to a continuous thermo-fatigue. If this condition persists, the heat would continuously increase the IMC thickness, so the embrittlement by the IMC, and as a result, the likelihood of cracks being initiated in the IMC would also increase In view of the significance of the IMC layer to the fatigue resistance, this chapter is specifically devoted to studying the IMC of IR reflowed joints which in the past has rarely been investigated SEM with energy-dispersive x-ray analysis EDX) was used to reveal the chemical distributions along the copper solder interface of joints that had been soldered and aged at different conditions

7.2 IMC COMPOSITION

This part of investigation makes use of the secondary electrons SE) and EDX to give a detailed study of the composition across the boundary between the copper and solder Predominantly, it was intended to explore the capability of SEM when applied to the study of this boundary region It is expected by going through a detailed study of the composition changes across this interface, the formation and properties of IMC can be more comprehensively understood The other objectives are to find out if the solder paste exposure has any effects on the interface thickness, and how aging may change the structure of the IMC

7.2.1 Methodology

The specimens used were prepared and reflowed in the same way as those used for the void investigation Section 6 3 After IR reflow the resulting geometry of the specimens is illustrated in Fig 6 1 To prepare the specimens for the SEM investigations, they were cut to an appropriate size and embedded in epoxy The epoxy was cured under vacuum condition to remove the gas entrapped The moulded specimens must be of a size that can

be handled within the SEM chamber which in this case is approximately 20 mm diameter, and 10 mm height. To achieve the best possible effects in the SEM examination, the specimens were ground, polished, then coated with a layer of carbon or gold. Coating is necessary because insulating materials, or even nonconducting particles, when dispersed in a metallic matrix build up a space charge by accumulation of absorbed electrons. This charge interferes with the incident beam of the SEM and leads to image distortion. The conductive coating here was gold at a thickness of about 10 nm.

The SEM model used for this investigation was a JSM-820, in which there is a built-in EDX. EDX is an attractive tool for quantitative x-ray microanalysis. In this investigation, SE were used for the microstructural study, and EDX was used for the compositional study. The collecting and the processing of the data were performed by an AN10000 analyser. In order to establish the composition distribution across an interface, point-by-point measurements were performed. Referring to Fig. 7.1, measurements always initiated at a point on the specimen well within the copper region of the substrate, and were finished at a point that was well inside the solder region. To show the trend of variation in composition across the interface region, the weight percentage of all elements was plotted against the distance. The arbitrarily chosen starting point was taken as the point of origin. The procedure adopted followed the following lines[115].

1. With the SE imaging technique, focus and locate the interfacial layer. The image on the screen may look like the micrograph shown in Fig. 7.2.
2. Select a point of interest by using the pointer, and record its position.
3. Display the x-ray spectrum, which is a count-rate against the energy, to identify all the elements present. An example of an x-ray spectrum is shown in Fig. 7.3.
4. Using EDX in conjunction with the Link AN10000 analyser programme, determine the energy shells (i.e. K, L, or M) to be used for working out the weight percentage for all elements. For the 63Sn37Pb solder being investigated, K is for Cu, L is for Sn, and M is for Pb.
5. Print out the results of the analysis, one form of which is the weight percentage of individual elements, Table 7.1.

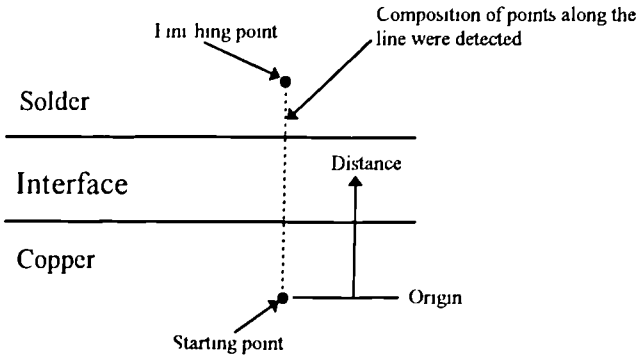

Fig 7 1 Diagram showing the positions where composition were detected.

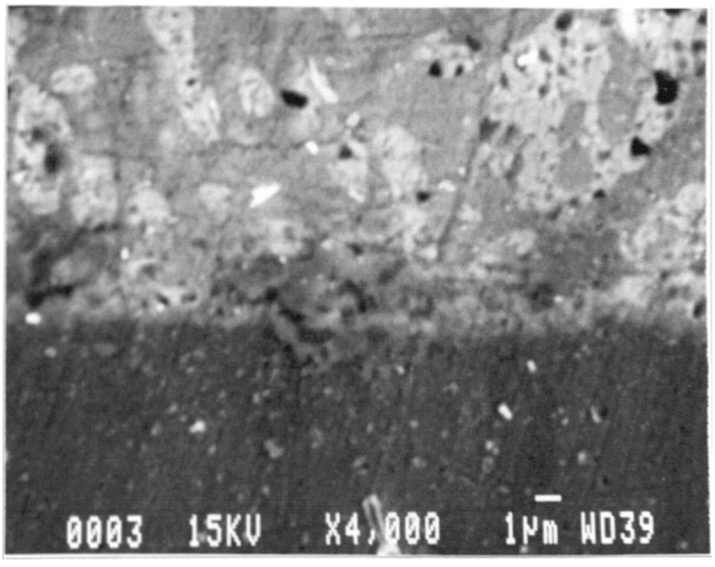

Fig 7 2 A micrograph showing the interface of copper and solder

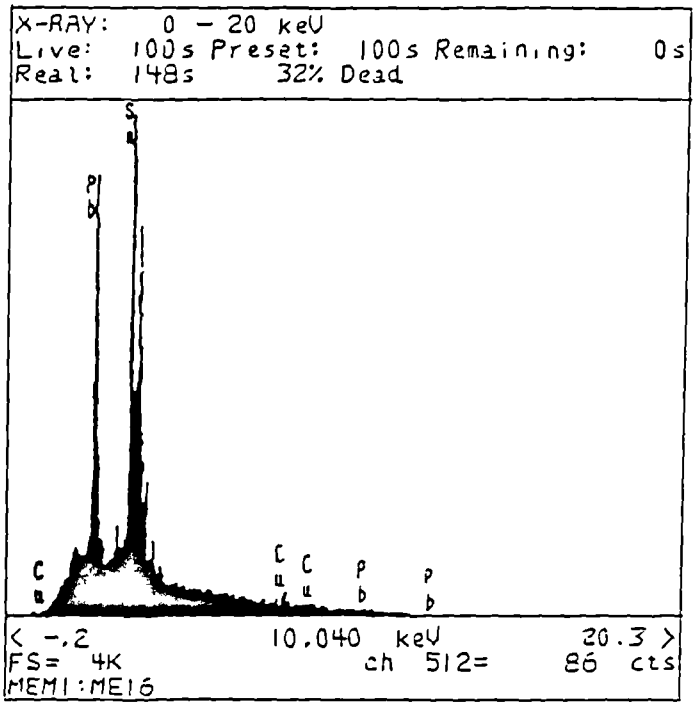

Fig. 7.3 X-ray spectrum showing the elements present

ELMT	ZAF *	ATOM %	WEIGHT %
CuK : 1	1.021	68.557	80.555
SnL : 1	.873	30.205	19.000
PbM : 1	.740	1.236	.445
TOTAL		99.997	100.000

* ZAF is an acronym from the three separate effects; atomic number (Z), absorption (A) and fluorescence (F), which the method compensates for.

Table 7.1 An example showing the result print-out of an EDX analysis

7.2.2 Results and Discussion

The compounds at the interface of a copper/solder joint can possibly be in the forms of Cu_3Sn, Cu_6Sn_5, $Cu_{20}Sn_6$, or $Cu_{31}Sn_8$ [114]; since Pb does not form compounds with either Cu or Sn. However, the predominant compounds constituting the IMC layer are believed to be the Cu_3Sn and Cu_6Sn_5. With reference to the phase diagram of Cu and Sn, Fig. 7.4, and making use of the calculated Cu and Sn weight percentages for various compounds in Table 7.2, it can be seen that Cu_3Sn is the ε phase, and if present, it is trapped in between the Cu and the Cu_6Sn_5 (η) layer. Knowing the atomic ratio of a Cu/Sn compound one can actually calculate the weight percentage of the Cu and Sn elements present, or in reverse, if the weight percentage of the elements of a point is measured, say by using EDX, the compound at that point can be determined. Taking Cu_3Sn for instance, its Cu to Sn atomic ratio is 3 to 1.

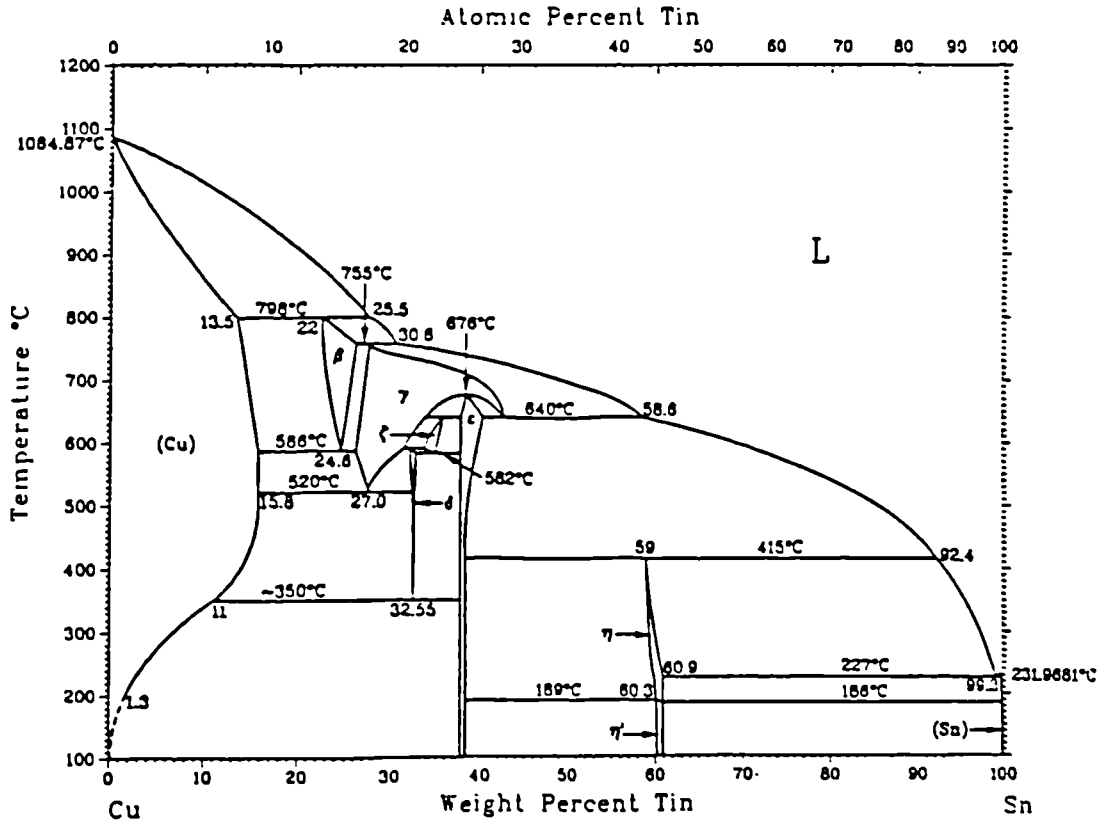

Fig. 7.4 Copper/tin phase diagram

COMPOUND	Wt % (Cu)	Wt % (Sn)
$Cu_{31}Sn_8$	67.5	32.5
Cu_2Sn_6	64	36
Cu_3Sn (ε phase)	62	38
Cu_6Sn (η phase)	39	61

Table 7 2 Weight percentage of Cu and Sn in various copper-tin compounds

In Chapter 6, it was found that the void size and content of a reflowed joint decrease with the solder paste exposure time. Such a phenomenon is explained by the fact that the longer the exposure, the more the solvent is evaporated, and the less is there a chance of gas entrapment, and as a result less voids are formed. The formation of IMC in copper solder joints is through the diffusion of Cu and Sn atoms. It is anticipated that the void content, which is one of the factors governing the grain boundary conditions may affect the solid diffusion mechanism, and hence the IMC growth rate.

Specimens with solder paste exposed to room temperature for 0, 5, and 24 hours were analysed and compared on the basis of their compositions across the copper/solder interface The solder paste used was again the 63Sn37Pb from Multicore. Basically two types of graphs were plotted to help in the interpretation, i) concentration of all elements (i e Cu, Sn, and Pb) versus distance, and ii) concentration of Cu and Sn (Cu plus Sn equal to 100%) in the alloys versus distance. These graphs with different exposure times are shown in Figs. 7 5a-b, 7 6a-b, and 7.7a-b. Figs. 7.5a, 7.6a, and 7.7a show the distribution of elements across the interface These graphs, not only illustrate the interrelation in content of the three elements (Cu, Sn, and Pb), from which the interface thickness in each case can also be determined The interface thickness is measured from the point of a graph where the Cu starts to drop from 100%, to a point where Cu becomes zero. Since copper solder IMC is formed only between Cu and Sn, a graph showing the fraction of Cu and Sn of the interfacial alloys would assist in defining the type of compounds spreading

over the entire boundary. Figs. 7.5b, 7.6b and 7.7b are graphs of this type for joints which have had their solder paste exposed to room temperature for 0, 5, and 24 hours respectively. With reference to any of these graphs, for instance Fig. 7.5b, the distance between points A and D represents the overall thickness of the interface. A is a point at which interfacial alloys have started to form. If there is any compounds at this point, they would be with very minimal amount of Sn, and the amount of Cu is near to 100%. Any alloy, which may be in the form of solid solution or compound, at a distance between A and D can easily have its Cu and Sn percentage read off directly from the curves. Since compounds are with a fixed stoichiometric composition, theoretically, if a particular compound is present and extends for a certain thickness, this thickness would be shown by a section with both Cu and Sn constant on the graph. For example, if there is a thickness of Cu_3Sn existing, the Cu curve at 62% and the Sn curve at 38% would both appear flat (parallel to the x-axis) over the thickness. So, in this case, the thickness of the Cu_3Sn layer can be found by simply reading off the length of this section from the graph. The possible Cu Sn compounds, shown in Table 7 2, when arranged in descending order of Cu content, or ascending order of Sn content, are $Cu_{31}Sn_8$, $Cu_{20}Sn_6$, Cu_3Sn, and Cu_6Sn_5. Since the Cu and Sn percentages of each compound are known (Table 7.2), with the aid of the graphs Fig 7 5b, 7 6b, and 7 7b, the thickness of all these compounds can be identified.

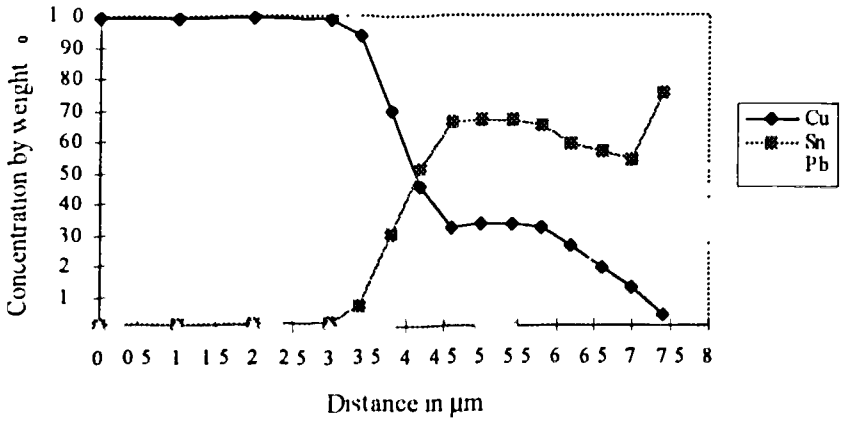

Fig 7 5a Percentage of elements versus distance
for a specimen with the solder paste exposed for 0 hour

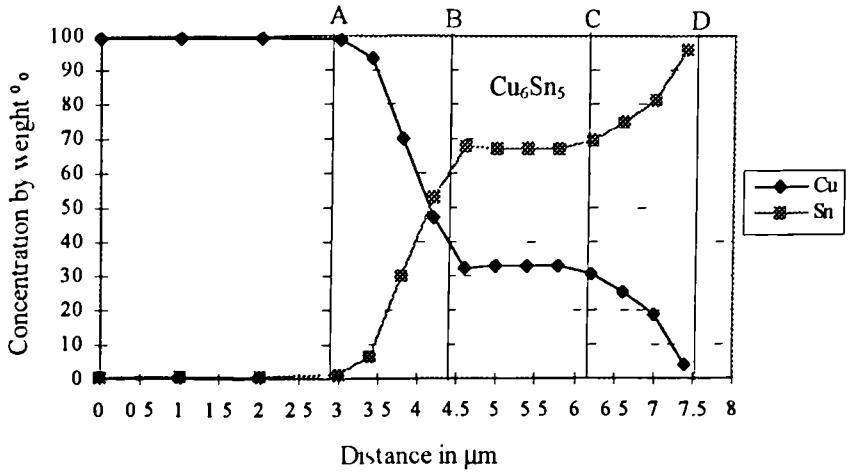

Fig 7 5b Percentage of Cu and Sn versus distance
for a specimen with the solder paste exposed for 0 hour

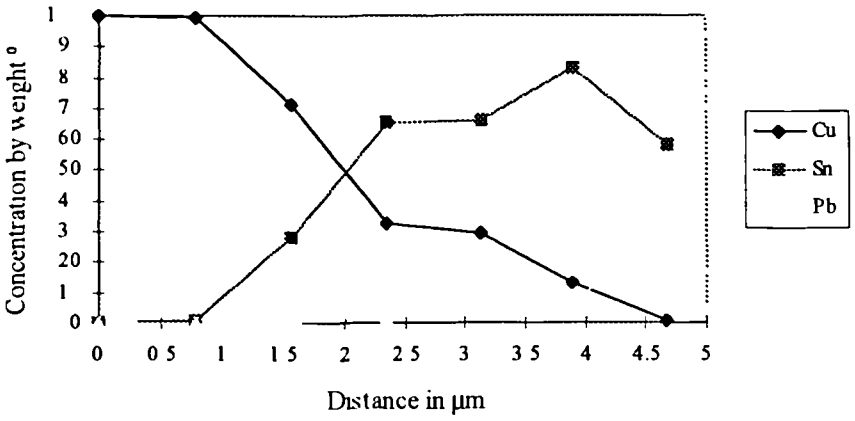

Fig 7.6a Percentage of elements versus distance
for a specimen with the solder paste exposed for 5 hours

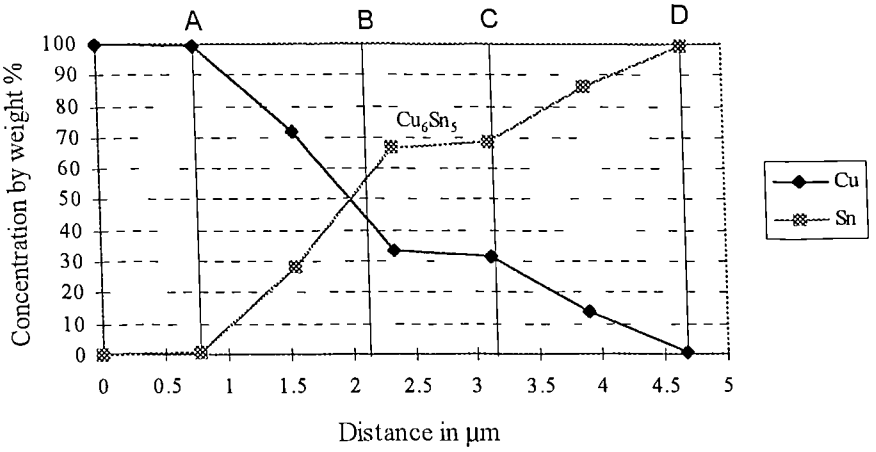

Fig. 7.6b Percentage of Cu and Sn versus distance
for a specimen with the solder paste exposed for 5 hours

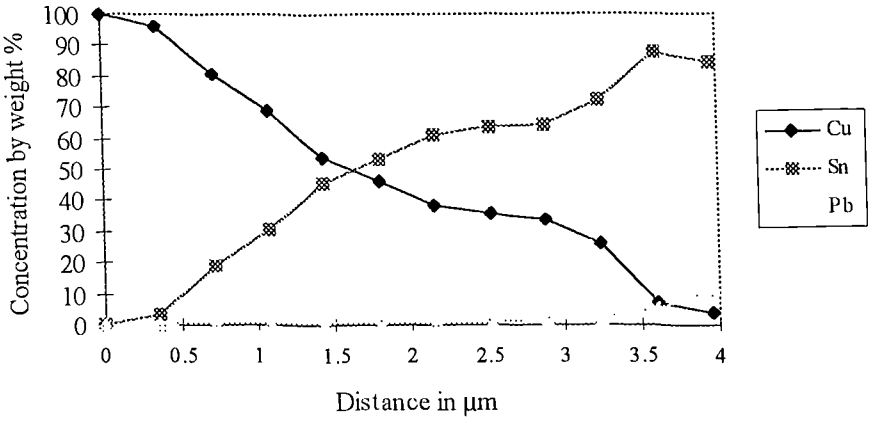

Fig. 7.7a Percentage of elements versus distance
for a specimen with the solder paste exposed for 24 hours

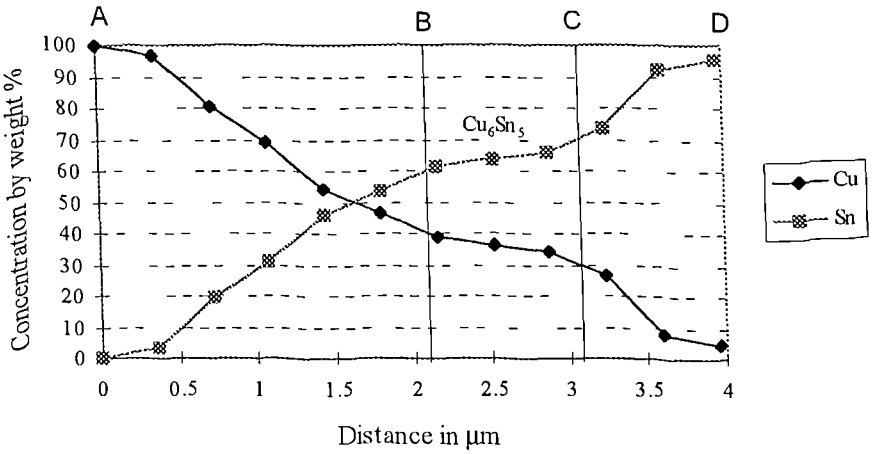

Fig. 7.7b Percentage of Cu and Sn versus distance
for a specimen with the solder paste exposed for 24 hours

With reference to anyone of Figs. 7.5b, 7.6b, or 7.7b, and working based on the calculated Cu percentage of the compounds shown in Table 7.2, it can be seen that compounds $Cu_{31}Sn_8$, $Cu_{20}Sn_6$, and Cu_3Sn, if they exist, should appear in the region between points A and B. However, within this region there is no evidence of any flat sections along the Cu curve. This shows that none of these compounds are present as detectable or resolvable layers. The Cu_3Sn commonly found in the conventional soldering process did not actually exist in the as-processed SMT 63Sn37Pb solder joints. The overall interfacial thickness is represented by the distance between A and D of the graph. Fig. 7.8 shows the overall interfacial thickness of the three cases in which their solder paste had been exposed for different times. The chart indicates no evidence that the overall interfacial thickness is influenced by the solder paste exposure time at all. The region defined by points B and C in Figs. 7.5b, 7.6b, and 7.7b represents the Cu_6Sn_5 layer. In fact, in all the three graphs, this region defined by the Cu content from 30 to 40 percentage (39% is the theoretical figure as shown in Table 7.2) appears reasonably flat. Taking into consideration the accuracy in measurement, it is believed that this section reflects the approximate thickness of the Cu_6Sn_5 layer. Fig. 7.9 shows the relation between the thickness of Cu_6Sn_5 compound and

the solder paste exposure time Once again, it does not give any indication that the thickness of the Cu_6Sn_5 layer correlates with the time of exposure of the solder paste The findings hint that the limited amount of void differences created by the different time of solder paste exposure are *insignificant to affect* the diffusion process in the formation of the IMC layer.

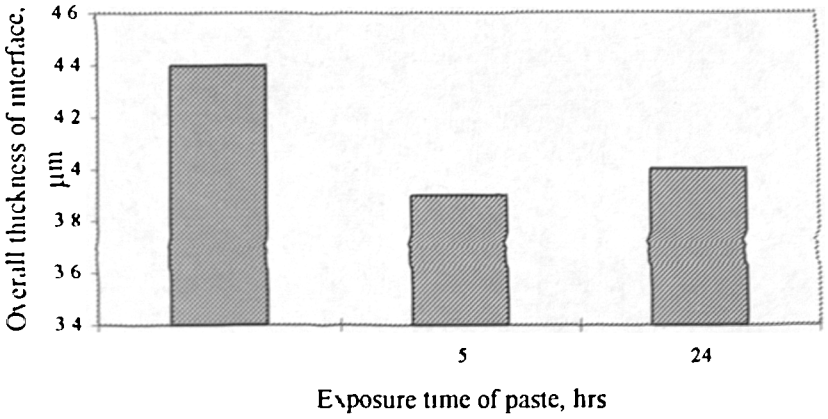

Fig 7 8 Chart sh wing the relation between overall thickness f nterface and solder paste exposure time

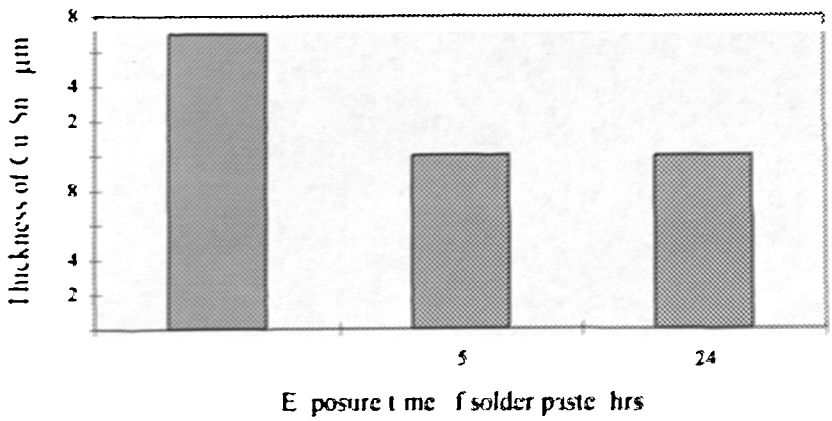

E posure t me f solder paste hrs

F g 7 Chart wing t e relation between the thickness f t e Cu Sn ver and lder pa te exposure t me

Solid diffusion of atoms plays a significant role in the growth of the copper/solder interface and copper/tin IMC in solder joints. Reflowed specimens aged for 0, 40, and 120 hours at 100^0C were used to study these two growth aspects. Fig. 7.10a and Fig. 7.11a are graphs showing the elements distribution of the interface layer for specimens aged for 40 and 120 hours respectively. Fig. 7.10b and Fig. 7.11b are graphs showing the changes in Cu and Sn (Cu plus Sn equals to 100%) over the interface for specimens aged for 40 and 120 hours respectively. As before, Fig. 7.10b and Fig. 7.11b enable an interpretation of the thickness of various compounds over the analysed region. Working on the basis of the Cu curve of these graphs, referring to the region covered by the points A and B, no obvious layers of $Cu_{31}Sn_8$, $Cu_{20}Sn_6$, and Cu_3Sn are again detectable. On the other hand, for both graphs, in the Cu range between 40 to 30 percent, the curve appears to be relatively flat which is an indication of the existence of the Cu_6Sn_5 layer. Making use of the information deduced from Fig. 7.10b and Fig. 7.11b, plus that from Fig. 7.5b, the overall thickness of the interface (points A - D) and the thickness of Cu_6Sn_5 (points B - C) aged at 100^0C for durations of 0, 40 and 120 hours can be obtained and plotted as shown in Fig. 7.12. Fig. 7.12, clearly shows that aging time increases both the overall interfacial as well as the Cu_6Sn_5 layer thickness. Since no Cu_3Sn are shown in all circumstances, which indicates the

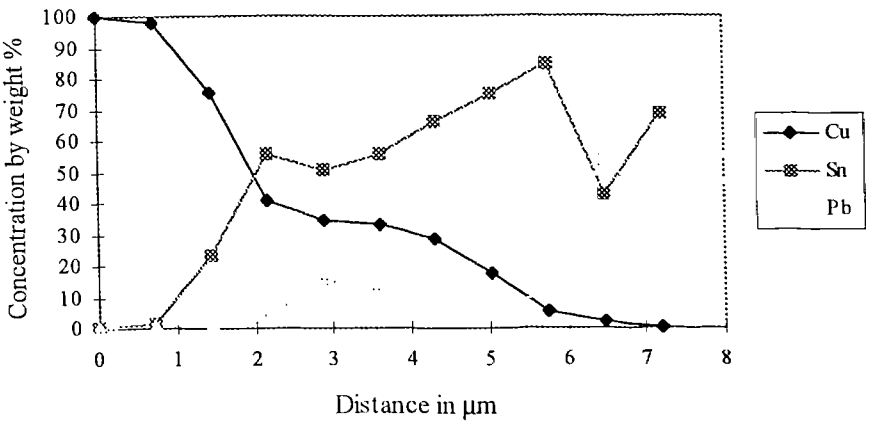

Fig. 7.10a Percentage of elements versus distance for a specimen aged for 40 hours at 100^0C

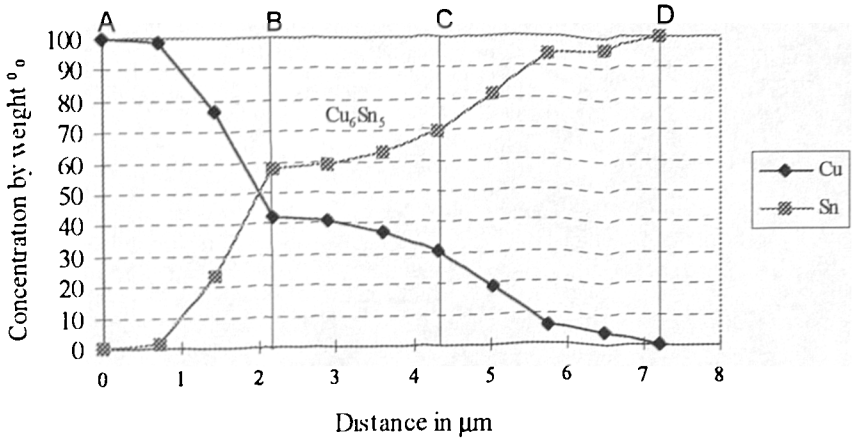

Fig 7 10b Percentage of Cu and Sn versus distance
for a specimen aged for 40 hours at 100^0C

growth of the IMC was mainly due to the growth of the Cu_6Sn_5 during aging. Broadly speaking, it is expected that Cu_3Sn is not present in the as-processed or aged at low temperatures 63Sn37Pb joints However, Cu_6Sn_5 is present at all times and it grows with aging time Since it is found that Cu_6Sn_5 is more susceptible to cracking during thermal cycling [95,97], aging time is directly impairing the reliability of the joint. Further, Figs 7 13a-b are two optical micrographs substantiating the existence of and the growth of the interfacial layer in the two specimens aged under the specific conditions.

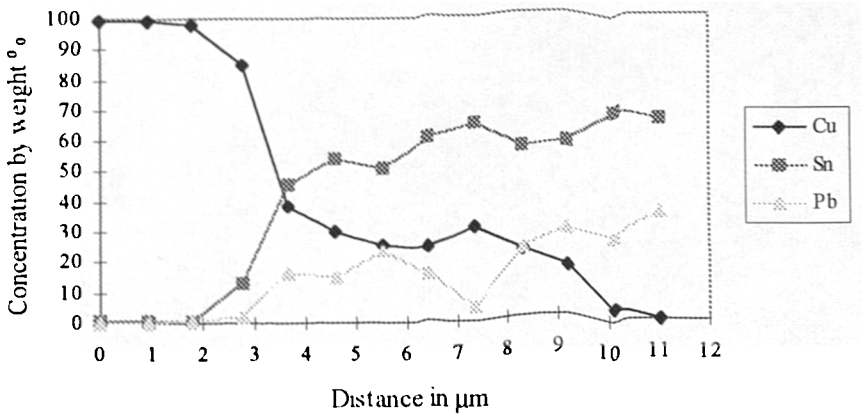

Fig. 7.11a Percentage of elements versus distance
for a specimen aged for 120 hours at 100^0C

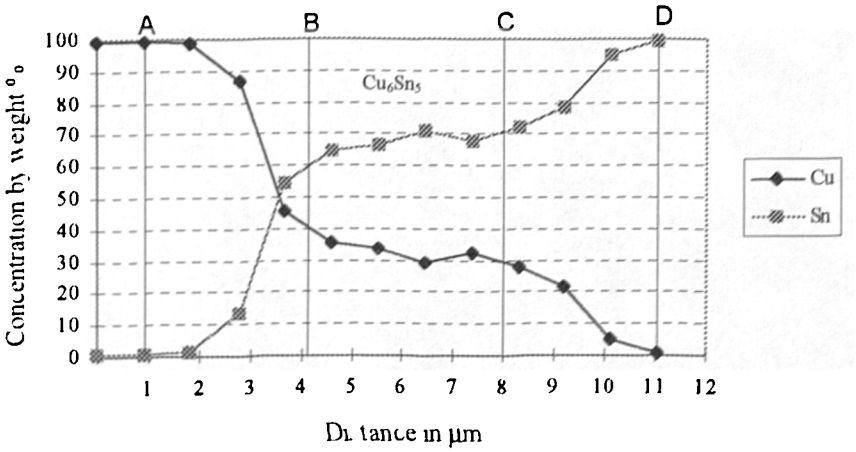

Fig 7 11b Percentage of Cu and Sn versus distance for a specimen aged for 120 hours at 100 C

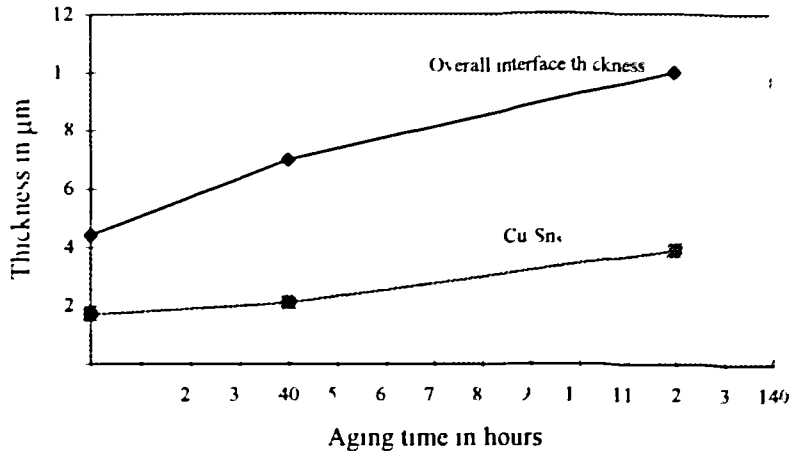

Fig 7 12 Effects of aging time on interface and Cu_6Sn_5 layer thickness at an aging temperature of 100 C

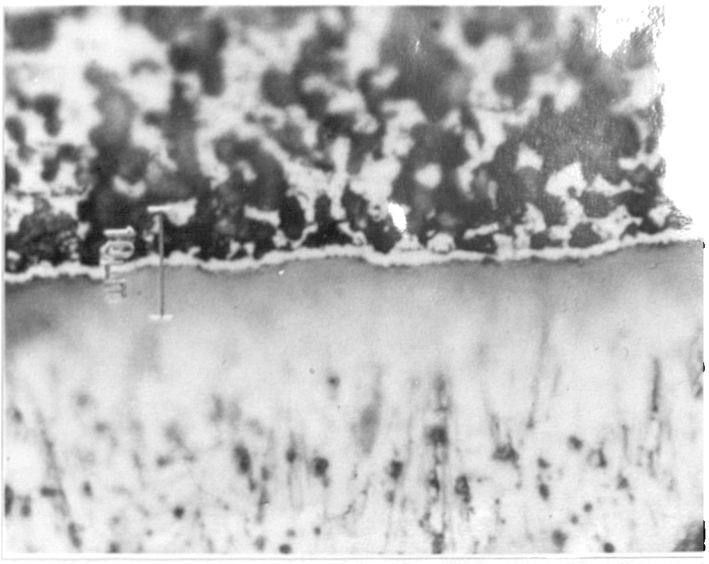

Fig. 7.13a Optical micrograph of a specimen aged for 40 hours at 100^0C

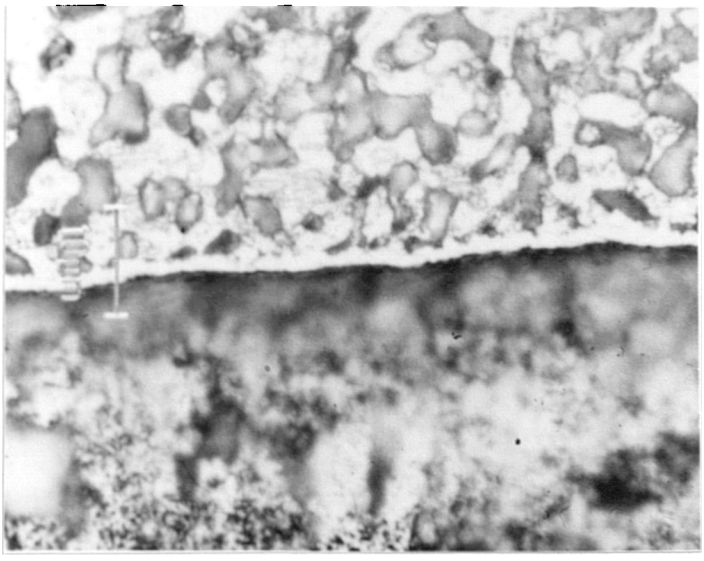

Fig. 7.13b Optical micrograph of a specimen aged for 120 hours at 100^0C

Chapter 8

Overall Discussion

8.1 INTRODUCTION

The tasks of quality inspection and cleaning in SMT, as compared to that in conventional through-hole technology, are far more difficult and costly. The narrow gap between the components and the PCB, and the closely packed leads of components, create cleaning and inspection difficulties. Difficulties in this respect are further intensified for some packages like the plastic leaded chip carrier (PLCC), with its leads bent towards the bottom of the component bodies in order to save space. Research has been going on to find ways to give effective inspection and cleaning methods for SMT assemblies. Different methods such as the x-ray approach to enable the inspection of the hidden parts have been developed and are being used However, a quick and cost-effective inspection method has still not yet surfaced The abolition of chlorofluorocarbons (CFCs) by the year 2000 as a cleaning fluid in the electronics industry, for environmental reasons, imposes even more difficulties in the cleaning process. This has sparked ideas to substitute the use of CFCs by water-based liquids Some people take an alternative approach, that is rather than concentrating on the method of cleaning, water soluble solder paste and solder paste not requiring cleaning were developed. However, so far, the application quality of these pastes is not very satisfactory Re-work is another area in SMT which is very costly and time consuming Components like PLCC, and QFP are particularly tedious from this point-of-view. The difficulties lie in the fact that, during re-work, heat has to be applied evenly to

the leads along the four sides of the component, so as to cause all the solder to melt at the same time. When the solder is molten a device must be available to extract the component from the board; this is usually performed by means of a vacuum sucker. The residual solder after the defective part has been removed must be cleaned thoroughly, to ensure that the new component will sit squarely on the pads and no bridges result. The replacement of a component, in common practice, is carried out manually. This entire removal and replacement operation must be carried out in a dedicated and well-controlled manner. Any deviation may result in defects such as bridges, or even damage to the PCB pads.

Repair or re-work is undesirable. It is expensive because it requires additional labour, space, and equipment. The interruptions caused by carrying out the repair work also slow down production. Defects which require subsequent repairs may originate from the manufacturing process. Humans and machines are the two factors responsible for creating the majority of these defects. The sources of this kind of defect are comparatively easier to eliminate. The other type of defects are those that result from defective design, and their sources are more difficult to identify and remove. These manufacturing problems due to wrong design can be largely minimised if the concept of "design for manufacture" is implemented. Traditionally, the role of design and manufacturing are looked at as two separate entities. A designer performs his function by designing a product to satisfy the aesthetic, functional and safety requirements. If he is good, he may be also conscientious in the economic selection of material. However, little or no consideration is usually given to the manufacturability of the product. The designer might be involved in the monitoring of the prototype production, but his main concern at this stage is to ensure that the prototype made performs in accordance with what he has put down on paper. Manufacturing engineers, on the other hand, are usually never involved at the product design stage to give advice on manufacturing aspects. The design and manufacturing functions are always performed in a serial manner, one seldom gives advice to the other. The concept of "design for manufacture" emphasises that, at the stage of design, manufacturability of the product should have been taken into consideration. It is anticipated that only by incorporating the manufacturing factors into the design of the product can the amount of subsequent defects be substantially reduced. Equally important in terms of achieving defect-free and reliable

products is the process selection and the setting of process parameters. Different processing methods, or different settings of a process, result in different configurations of joints. The implication of joint configurations on joint quality demands more comprehensive studies. SMT is a relatively young technology, and there is plenty of room for quality improvement which can be achieved through continuous research to establish better design and assembly guidelines.

8.2 TOMBSTONING

Chapter 3 looks at the tombstoning problems which are commonly encountered by leadless chips The analysis given shows that the initiation of tombstoning is a result of the combined effects of the PCB pad design and the processing conditions. It is believed, with confidence, that tombstoning of a chip occurs only if the forces over the two ends of the component are unbalanced. The unbalanced forces can be created due to different heating rates at the two ends of the chip, or sometimes, from vibrations during transportation. To minimise uneven heating over the two ends of chips, there are three criteria to bear in mind, i) design the PCB in such away that the chips are orientated with their axes perpendicular to the direction of travel, Fig. 3.3, ii) distribute the chips so that they would not cast shadows on one another, and iii) design the metallisation of PCB pads on which the two ends of components are soldered to have equal heat absorption rates.

With vibration free conditions, referring to Equation 3.3, the analysis shows that initiation of tombstoning is a function of the solder surface tension γ, contact angle θ, component weight, and component dimensions. Assuming other conditions are fixed, it can be seen that extended PCB metallisation would lead to an increase in the value of θ, and hence an increase in the opportunity of tombstoning. On the other hand, if the metallisation for both the chip and the PCB remain unchanged, the value of θ then is a function of the temperature and the cleanliness of the solder. A clean and high temperature solder has better wettability, and sustains a smaller contact angle with the metal. Over the extremes, a wettable solder would give a concave shape and a non-wettable solder a convex shape, as

shown in Figs. 8.1a and 8.1b. Applying the two conditions, concave and convex, in Equation 3.1, it can be seen that the larger the contact angle θ the larger is the value of the upward moment imposed on a component. This induces the belief that a clean and high temperature solder is preferable as it lowers the chance of tombstoning. The theoretical calculations predominantly shown in Figs. 3.7a-i, are the first step taken into consideration of all the factors involved to provide design guidelines in tombstoning prevention. Overall, as has been discussed in Section 3.6, the results of the experiments subsequently performed, are in fact in-line pretty well with the theoretical predictions.

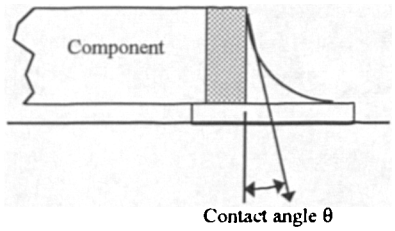

Fig 8 1a Wettable solder

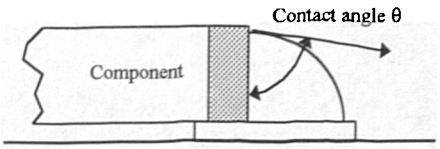

Fig. 8.1b Non-wettable solder

Figs 8 1a-b Difference in contact angle between wettable and nonwettable solder

Looking from the design point-of-view, tombstoning can be reduced through an increase in the weight of the component, a decrease in the height of the component, a shortening of the protruding PCB metallisation, and an increase in the metallisation underneath the component. However, in reality, some of these may conflict with other criteria, for instance a short PCB metallisation may give the danger of insufficient solder; a decrease in the height of the component would lead to an increase in the floor space on the PCB On the other hand, the weight of a component is predetermined by its type and amount of material used, and therefore there is not much room for change. All these may impose, in one way or the other, restrictions in the design. In view of this, and still on the basis of the theory developed in Chapter 3, two positive as well as practical approaches are

suggested here Fig 8 2 shows the one which takes the principle of reducing the pulling up moment generated by the surface tension of the molten solder. The figure proposes that instead of adopting a traditional approach of having the component metallisation covering the entire height A-B, metallisation is restricted to a suitable height A-D. It is by shortening the distance between the point at which the surface tension is applied and the pivot point, which is at point A, that tombstoning can be drastically reduced. Fig. 8.3 shows another proposition, which works on the principle of increasing the downward moment on the component A lead is introduced at both ends of the component. Under the pull of the surface tension from the molten solder, the total downward moment which has to be overcome in order to lift the component up can be effectively increased by shifting the pivot position originally at point A to a new position point C after the introduction of the lead, as illustrated in the figure With the same PCB design, taking this approach, the chance of tombstoning can be reduced to a large extent.

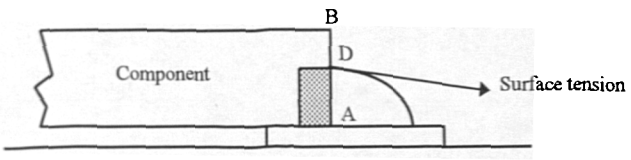

Fig 8 2 Shortening the metallisation of component
to reduce the up pulling effects from the surface tension of molten solder

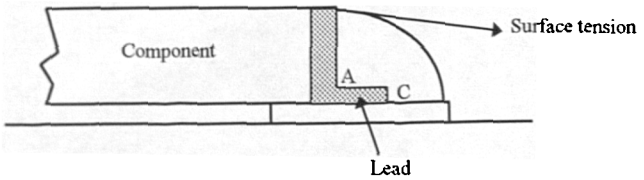

Fig. 8 3 Introduction of component lead to
give hindrance in the lifting of the component

8.3 THICKNESS

The thickness of the solder has long been a concern for SMT joints where solder paste is used. Surveys indicate that, on a per joint basis, the amount of solder used in SMT is far more than that in the through-hole technology. This, together with the fact that solder paste is more expensive than the solid solder used for through-hole technology, the material used in SMT joints is much more costly. Part of Chapter 4 looks at the effects of solder thickness. Demands on solder thickness in fact contradict with each other. In this chapter (4) it was found that for joints subjected to pure tensile forces, a thin solder joint is stronger. Experimental results given in Fig. 4.13 show that, within the thickness range tested, the solder joint with 0.176 mm thickness gives the maximum tensile strength. The tensile strength drops continuously until the solder thickness is approximately 0.6 mm. The hardness measurements in Section 5.4, show explicitly that the IMC at the interface is the material in the joint with the maximum hardness, and hence the maximum strength. Figs. 5.12a to 5.13c, all substantiate this. The peak values in these graphs are virtually representing the hardness - tensile strength, of the copper-tin compounds. It is believed that for joints with a thin solder layer, the IMC strength has a larger effect, and therefore leads to a joint with higher strength. Thin solder joints have advantages in other respects as well. Thin solder, when it is in a molten state, allows smaller degree of movement and pull from surface tension to the components, and therefore is less likely to result in misalignments as shown in Fig. 4.14. However, joints with little solder do not necessary produce advantages in all circumstances. One typical condition is that the amount of solder may not be sufficient to give a strong bond. Particular attention should be noted for factories producing small batches of products where hand-soldering is still being used. In hand-soldering of SMT components, since solder is applied from the top, there would be little, or in most cases no, solder at the interface between the lead and the PCB pad, as illustrated in Fig. 8.4. A joint soldered in this manner is much weaker than one which is reflowed by machines. For QFP, PLCC, SOT, SOIC, etc. if there is insufficient printed solder paste, the most likely results are joints without, or no, fillets which greatly reduce the overall bond strength of the joints, as shown in Fig. 4.15a. Thin solder joints are also undesirable from the thermal-fatigue endurance-point-of view. Joints with increased solder thickness reduce the brittle effects of

the copper-tin compounds, and increase the volume of ductile material which has effects of eliminating or slowing down crack propagation. The effects of solder standoff height (solder thickness) for leadless chips were analysed by FEA and experimentally tested in Chapter 4. In fact contradictory results were obtained. The reason has been discussed in Section 4.4, and is mainly due to the fact that in the FEA materials were assumed to be isotropic, but in reality they are not. Based on the results of the investigation, it is recommended that for leadless chips, to ensure a quality joint, the thickness of the solder should be in the range of 0 05 to 0.3 mm, and the fillet height should be at least equal to 1/3 of the height of the component

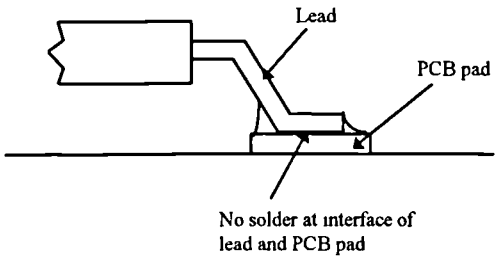

Fig. 8 4 A typical hand-soldered joint
with no solder at lead and PCB pad interface

8.4 FINITE ELEMENT ANALYSIS

One of the merits of FEA is that the part, or the structure, to be analysed can be configured into any desired shape. For this reason, the geometrical effects of the part can then be analysed easily. Section 4.2, makes use of this advantage of FEA to analyse and compare the bond strength of solder joints with different geometries, which if performed experimentally is almost impossible. The FEA performed basically has covered two areas, the effects of solder standoff height, and the effects of fillet shape. Interpretation of the resulting stress and strain, and strain energy values, were the two methods used to compare their bond conditions. The findings and the discussion of the results are covered in Section

4.2.2, and Section 4.4 respectively. It should be emphasised here that the FEA performed was on a very simplified case. In a realistic situation, materials do not behave in a linear elastic manner. In fact, when a solder is subjected to a mechanical load, or a thermal-fatigue stress, it would go through a large plastic deformation before failure occurs. Also, the properties of solder change with temperature. The difference in thermal coefficient of expansion of materials, and the difference in the heat absorption and heat the dissipation rates in different regions, will generate residual strains inside the joints. PCBs are basically copper with epoxy substrates and will deform when under stress. Materials making up the joints are anisotropic, and with directional properties. All these factors mentioned actually have not be taken into consideration in the FEA described in Section 4.2. The argument is that, since the main purpose of the analysis is to compare the bond strength of joints with different geometries, and there is no intention to calculate the absolute strain/stress values, nor to predict the endurance life of the joints, simplified conditions as described in Section 4 2 should serve this objective With reference to Fig. 4.6a and 4.6b, comparing Cases 1, 2 and 3, the FEA shows that an increase in the standoff height has the effect of increasing the crack resistance of the joint Again, referring to the same figures, and comparing Cases 2, 4, and 6, those are the cases with the same standoff height but varied fillet configurations, the FEA shows clearly that Case 2 which is the one without fillets is the weakest joint, where as Cases 4 and Case 6 are joints with about the same bond strengths. These findings also reveal that the presence of the fillet can significantly increase the bond strength of a joint, whilst a change in the shape of the fillet or the standoff height can only slightly affect the bond strength of a joint.

8.5 WAVE-SOLDERING/IR REFLOW

Wave-soldering and IR reflow are the two processes most commonly employed for soldering of SMT devices IR reflow has lots of advantages over wave-soldering. The limitations and problems with the wave-soldering process have been discussed in Section 2.4.1.3. Nevertheless, the fact that wave-soldering still has not been phased out is mainly due to the following three reasons:

1. a mixture of through-hole technology and SMT devices is possible;
2. provided that all the devices on the board are able to be soldered by this method, wave-soldering is easier to set-up and control;
3. compared to IR reflow, it requires less capital investment and is cheaper to operate.

In the past, in comparing these two processes, most were based on the visible defects of their resulting joints [10,11,42,53]; little had touched upon the bond strength. Chapter 5 is designed to make up for this deficiency by giving a comprehensive study on the quality implications in between the choice of IR reflow and wave-soldering. Based on the findings in this chapter, there is strong evidence showing that the shape of a WS joint is very much dependent on the orientation of the component on the PCB. The shadow of the component during wave-soldering can result in totally different shapes between the incoming and outgoing joints of a component. It is expected that this difference would be intensified if the height of the component is increased. The reasons for forming different shapes for different entry angles have been explained in Section 5.5. This section further discusses and analyses the wetting conditions of joints. It gives strong indications that a convex joint is undesirable as it, in most cases, represents improperly wetted conditions. The results of this part of the study allow the PCB designer to realise the importance of component orientation relative to the soldering direction in WS, and hence to suggest he takes this factor into account in his design. It was found that the IR reflow soldering method enables the production of more uniform joints, and the shape is usually concave. The FEA in Chapter 4, shows that a convex joint is only marginally more robust than a concave joint. It is necessary to point out that FEA is only a pure mathematical stress/strain approach, the metallurgical factors of the joints have not been taken into consideration at all. However, if the wetting condition, which is a crucial factor in determining the bond quality of solder, is also to be taken into account, a concave joint is actually more desirable.

To provide further understanding about the IR reflowed and WS joints, the voiding conditions and the hardness across the copper/solder boundary were studied. The findings in Section 5.3.2, show no evidence that the void content in a WS joint is affected by the component's orientation. In fact, just based on the number of experiments conducted, no

voids were detected in any of the WS specimens. However, IR reflow gave the opposite behaviour, voids were detected in every specimen. The reasons that IR reflowed joints always showed the presence of voids have been discussed in Section 5.5. Voids have long been recognised as detrimental to the fatigue resistance of a joint. When a joint is under repeated stress, voids are the areas that are subjected to stress concentrations. At a certain stage, a localised and highly stressed region near a void may be responsible for crack initiation. Once the crack is initiated, it will propagate. Stress concentration by voids, and preferential crack paths through the voids, greatly increase the rate of crack propagation. When the crack has propagated to an extent that the remaining material in the joint is insufficient to withstand the cyclic stress, fracture occurs. In reflow, the heat profile can influence the resulting void population greatly. Section 2.4.1.2, has given a relatively detailed description of the requirements of a temperature profile for IR reflow. Heating time and rate can do much to reduce the void content in an IR reflowed joint. In an ideal situation, which gives the minimum void content, the rate and time of heating should meet the fluxing requirements at different stages of the joining process and while doing so would not cause any volatile outgassing of the solvents in the flux. All the flux should have evaporated or emerged on the surface when solidification of the solder commences. It is believed that thick solder joints are more likely to result in large voids. This is because, during reflow, applying the principle of surface energy, there is a tendency that adjacent voids would coalesce This coalescence causes small voids to shrink and large voids to grow, and in a thick solder joint there is a larger source of voids and therefore a greater chance of producing large voids. It was found that an increase in the void size has a larger impact on the strength than an increase in the void/volume fraction [64].

Both the parent solder and the compound at the interface of the copper/solder in WS joints were found harder than in IR joints, although both joints used the same solder composition, i e 63Sn37Pb It is believed that void content is the prime factor in lowering the hardness of IR joints A secondary factor may be due to the reason that the WS and IR solders were processed by two different heat profiles. The difference in the heat-up and cooling rate may give different grain structures, and result in different hardnesses of the joints

8.6 INTERMETALLIC COMPOUNDS

Organisations like the International Tin Research Institute have published some useful reference data on solders. However, data specifically directed to IR reflowed solder is still very limited. Since IR reflowed solder starts as a solder paste with a structure totally different from that of conventional solid solder, its subsequent properties after solidification may end up modified. For instance, as discovered and described in Chapter 5, its resulting void content and hardness of the IMC layer differ significantly from that produced by wave-soldering Study of the compounds at the boundary between the base metal and the solder of joints has aroused interest for some time. In particular, studies of the copper/tin compounds are popular, mainly because copper is commonly used as the base metal for electronic joints Research based on the conventional soldering approach found that the copper/tin IMC is mainly made up of two layers, Cu_3Sn and Cu_6Sn_5. The reliability as well as the solderability of the joints were found to be closely related to the thickness and type of the copper tin IMCs present The copper/tin IMC layer is hard and brittle, as found in Chapter 5 For near eutectic solder, cracks are most likely to be initiated at the Cu_6Sn_5 layer When the IMC is subjected to heat, it will grow in thickness with time. The thickening of it would further lower the fatigue endurance of the joint. It was found that Cu_6Sn_5 contributes mainly to the brittleness of the IMC. When heat is applied, both Cu_3Sn and Cu_6Sn_5 grow, and the growth of Cu_3Sn is at the expense of the Cu_6Sn_5 [103]. It appears that previous publications have not produced a consensus on the fracture path in solder joints The mode of fracture was found to depend on two factors, composition of the solder and the rate of deformation [99]. A slow deformation rate usually results in a crack through the bulk of the solder and is associated with extensive plastic deformation, whilst, a fast deformation rate causes fracture through the IMC and in a brittle mode. Chapter 7 of the thesis employs the SEM technique to study the copper/tin IMC for a number of IR reflowed joints The composition plotted against distance across the copper solder interface was found to be another viable means to give an interpretation of the IMC structure. One of the discoveries in this chapter is that for an eutectic solder processed by IR reflow, the type of IMC which can sustain a detectable thickness is only the Cu_6Sn_5. Unlike reports for

conventional soldering, Cu_3Sn was not found at all. This discrepancy may be attributed to two reasons, i) for conventional methods, e.g. hand-soldering or wave-soldering, the solder is usually being heated up to a higher temperature, say 250^{0}C, ii) the time which the solder stays at elevated temperature is longer for conventional soldering methods. Fig. 8.5 shows an imaginary sequence in the formation of the Cu_6Sn_5 and Cu_3Sn. It is believed that when the heat applied has arrived at a temperature higher than the eutectic temperature (183^{0}C), solder starts to melt and wet the copper surface. The first layer of compound formed is the Cu_6Sn_5. Since in the IR reflow process, because quite a number of the SMT components (e g. QFP, PLCC, and SOIC etc) are very sensitive to heat, the peak temperature is usually limited to approximately 215^{0}C, and this for a short time of no more than 50 seconds Because of the low temperature and time in the IR reflow process, the resulting IMC would be free from Cu_3Sn On the other hand, the conventional soldering process provides sufficient heat and time for the growth of the Cu_3Sn after the appearance of the Cu_6Sn_5 Since Cu_3Sn is formed and located in between the copper and Cu_6Sn_5 layers, its formation needs the diffusion of Sn atoms from the solder through Cu_6Sn_5, or directly from Cu_6Sn_5. The formation of the Cu_3Sn layer is relatively a much longer and more difficult process It may become visible by optical microscopy only after longer aging times at higher temperature (e g 150 - 170^{0}C). Considering the low temperatures at which IR reflowed joints are used, it would take a very long time before the nucleation of the Cu_3Sn layer, or possibly, the Cu_3Sn layer would never appear over the joint's entire working life.

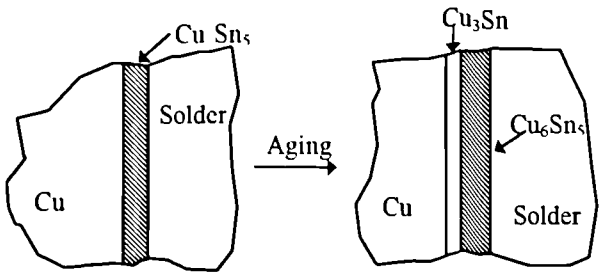

Fig. 8.5 Formation sequence of Cu_6Sn_5 and Cu_3Sn

8.7 SOLDER PASTE EXPOSURE

The yield of SMT depends heavily on three factors: PCB design, solder paste characteristics, and process set-up. Choosing the right solder paste is the first criterion for providing a reliable product. Literature covering the characteristics of solder paste has been dealt with in Section 2.2. Generally speaking, to facilitate selection, manufacturers would provide the necessary information on the characteristics of solder paste in the form of specifications. Chapter 6 covers the study of more information which is also crucial and should be provided to the users of solder paste, that information is on the effects of solder paste exposure. Solder paste is exposed to ambient temperature due to the pre-reflow requirements. A component present in the solder paste is the solvents. The functions of solvents are for controlling the rheology, tackiness, and flux activities [11,19,25]. Solvents may be divided into two groups, those with high and low boiling points. The proportion of these two groups of solvents affects the characteristics of the solder paste. Different groups of solvents evaporate at different temperatures. A paste with too high a concentration of high boiling point solvent will remain tacky for a long time, but with the danger of resulting in spatters after reflow. A paste with too high a concentration of low boiling solvent will dry-out quickly. Exposure of solder paste at the pre-reflow stage is anticipated to produce the following; i) evaporation of the low boiling point solvent and ii) oxidation of the alloy particles. It is expected that the consequence of increased exposure would affect the solder characteristics with respect to the following:

1. void content and wettability;
2. tackiness;
3. printability.

To identify the evaporation rate of solvents, a weight loss analysis was performed and is described in Section 6.2. The weight loss against exposure time was found to follow an exponential expression, Equation 6.1. As discussed in Section 6.6, the 'k' can be looked at as a paste characteristic constant representing the total amount of solvent which could possibly be evaporated at room temperature. 'k' then is the amount of low boiling point

solvent added and expressed as a fraction of the paste weight. Ideally, the value of 'k' should be supplied by the manufacturer as he is the person who knows exactly how much low boiling point solvent has been added. Alternatively, this can be evaluated by finding the weight loss of a printed solder paste after exposing it to atmosphere for a prolonged period, say 24 hours, to allow the paste to dry-out completely. The constant 'a' in the equation is in fact a function of the combined effects of the temperature and humidity. Fig. 6.2 strongly suggests that the value of 'a' is environmentally dependent. A hot working environment gives a larger 'a' value; that is to say the paste would dry-out at a faster rate.

Studies in Chapter 5 found that voids are always present in IR reflowed joints. In Section 6 3, it was discovered further that other than the flux, entrapped solvent is also responsible for the formation of voids. Fig. 6.5 shows the effects of exposure time, and hence the residual solvent, on void content. There is a drastic drop in the void content over a range of exposure times from 0 to 400 minutes. The drop is approximately from 1% at 0 minutes to 0% at 400 minutes. The high solvent content at 0 minutes can be attributed to the large resulting void content. This demonstrates that the more the solvent is evaporated *the less is the resulting void content. Although, long exposure reduces the void content,* this advantage is most likely off-set by its adverse effects on other properties, mainly the printability Referring to Figs. 6 4a-i, there are also hints showing that the void size is related to the exposure time, that is the longer the exposure time the smaller is the average void size

The tackiness of the solder paste can be defined as its ability to hold the components securely before reflow. In the manufacturing environment, frequently there is a time lag between the printing and the component placement operations, and between the component placement and the reflow operations. The overall waiting time from printing to reflow can be as long as 72 hours. Over this waiting time, the assembly is most probably subjected to accelerations and vibrations due to transportation. Insufficient tack force from the solder paste may allow the components to shift away from their designated positions creating various defects, such as misalignments and opens. In view of the importance of the tackiness, and with the anticipation that tackiness is related to the solvent content, a study

of the tack time and exposure time relation of solder paste was performed and described in Section 6.4. With reference to Fig. 6.7, the finding gives a clear trend that tackiness deteriorates with exposure time. Surprisingly, the curve shows that the tackiness dropped at a very rapid rate in the first two hours, and then stayed almost at a steady state over the rest of the exposure. The tack time had dropped from infinity at 0 hour exposure to 0.2 minutes at 2 hours exposure. After this initial rapid fall, the tackiness then stayed at low values and gradually reached its zero value. All this occurred over a range of 13 hours of exposure. The curve suggests that to achieve a good tackiness, the component placement must be completed in the first two hours. This finding corresponds well with that in Fig. 6.2 which shows that almost all the low boiling point solvent was evaporated in the first two hours, and this provides strong grounds for the belief that the loss of solvent is the main cause for the deterioration of the tackiness property. The decay in tackiness as a function of exposure time can be expressed in a form of a power law as in Equation 6.3. The 'a' in the equation is a characteristic constant of the solder paste defining the response of tackiness to exposure time It is expected that the value 'k' would change with the ratio of preload printed area The preload in this case is equal to the sum of the weight of the nugget (3 8114 g) and the weight that is put on top of the nugget (9.8 g), and the printed area is equal to the 6 mm diameter aperture of the stencil. Both the preload and printed area in the experiments were arbitrarily chosen. This part of the study has proved that the exposure time has profound effects on the tackiness, and is an area that cannot afford to be ignored. It is suggested that by standardising the preload/printed area ratio, the quality approach adopted in this study is a feasible method for defining the change in tackiness characteristics of solder paste with respect to exposure time.

The process immediately being affected by the characteristics of solder paste is the printing operation. The quality of print is determined by various factors and their interrelations The literature search, Section 2.3, has dealt with this topic. The printability of a solder paste can be determined directly by examining the quality of print in specific patterns [33], or indirectly, by measuring the rheology of the paste. There are numerous types of SMT devices, ranging from chips without leads to chips with lead pitches of 0.3 mm. Different fineness of stencil aperture imposes different demands on the characteristics

of the solder paste. Whilst selecting the solder paste with the right characteristics is crucial, controlling the consistency of the characteristics over the entire operation is equally important. Rheology of solder paste depends on i) the mix ratio of alloy particles, solvents, and flux, and ii) the alloy particle morphology. However, the rheology consistency at room temperature is considered to be a function of the solvent content, which changes with time of exposure of the solder paste. The experimental results in Section 6.5, substantiate this statement. Fig. 6 11 shows clearly the phenomenon that the longer the paste is opened to the atmosphere, the more viscous is the paste. It can be seen from the figure that in just three hours, the viscosity has increased from 86.9 Pa.s to 123.4 Pa.s, representing an increase of more than 40°o Viscosity is a measure of the flow characteristics of the solder paste. When it is too high it would definitely create difficulties in printing, especially in passing through fine stencil apertures The common defects resulted from solder paste with high viscosity value are skips. The curve in Fig. 6.11 further shows that there is a rapid increase in the viscosity in the first 20 minutes. After that, the viscosity remains almost unchanged until the exposure hits 120 minutes. After 120 minutes, there is another increase in the viscosity value. Based on these results, it is anticipated that if a paste is continuously being used by exposing it to atmosphere, at a certain stage the paste would become too viscous to give a fine print. These findings strongly suggest that to maintain the fluidity, the paste should not be exposed for more than 2 hours. Figs. 6.12a-i show the thixotropic nature of the solder paste For all cases of exposure, the viscosity is very responsive to the shear rate, viscosity decreases as shear rate increases and is in the form of a linear relation when on a log-log scale. The slope of the curves is an indication of the rate of thinning, or shear sensitivity, of the paste when subjected to shear, and is known as the thixotropy index The change in the thixotropy index after different exposures can be found from Fig. 6 13 The figure shows that the thixotropy index is almost unchanged throughout the test range From this, it is reasonable to believe that the exposure time has little effects on the shear sensitivity of the paste In printing, if the solder paste is too sensitive to shear, it would thin down rapidly and increase the chance of cold slumps and bridges. It is crucial to control the thixotropy index so that it is within a certain range if consistency of print is to be maintained. The thixotropic property of solder paste is considered to be primarily related to the heat generated during shear. Under continuous shear, say in printing, because of the

friction, there would be a rise in temperature within the paste. The rise in temperature in effect raises the fluidity of the solvent and flux, and as a result would reduce the overall viscosity of the paste. Fig. 6.14 illustrates that the ability of the paste to recover its characteristics after the removal of shear is also impaired by the time of exposure. The non-recovery rate R has dropped from an initial value of 0.165 to 0.075 over an exposure time of 3 hours. The drop is at its fastest in the initial 40 minutes.

The findings in Chapter 6 strongly recommend that, in addition to the conventional data, manufacturers should also provide information about the change in solder paste properties due to exposure. Relevant information, such as the constants in Equations 6.1 and 6.3, would enable a customer to choose the most suitable conditions for his application, and thereby to optimise the yield in the processing of SMT.

Chapter 9

Conclusions

CONCLUSIONS

"Popping up" of leadless components is mainly due to two reasons, either vibration or because the heat applied to the two ends of the component is not uniform during the reflow process. An analysis based on the belief that the surface tension of the molten solder is the main cause of lifting under uneven heating conditions has been presented. The moment lifting the component is generated by the surface tension and varies with the solder height and contact angle. Both theoretical predictions and experimental results have shown that an increase in the contact angle results in an increase in the lifting moment. The upward moment increases with the length of the PCB land that protrudes from the end of the component, and decreases with the cleanliness and temperature of the molten solder. To reduce the chance of lifting, it is recommended that, in the design, the protruding PCB land length should be limited. The forces holding the component downward come from the weight of the component and the molten solder underneath the component. The present work has confirmed a previous suggestion [9] that a large solder length underneath the component (W) would result in less chance of lifting. It is possible to calculate the soldering conditions contributing to the initiation of lifting merely from a knowledge of the dimensions and weight of the component. The two parameters, T_2 at minimum and T_1 at maximum, may be used for determining the weight and dimensions of the component in a design when the factor of lifting is also to be considered. The configuration of the metal contact of a component also affects the likelihood of lifting or tombstoning. Not all

commercially available leadless chips would lead to the phenomenon of tombstoning or lifting.

The pull test conducted has a large potential as a means for providing quick answers to questions on quality of leadless joints. This requires the establishment of a standard mean ultimate tensile force database for different types of joints, and the availability of testing facilities which should be located adjacent to the production line. The pull test designed here for measuring the bond strength is applicable to leadless chips only; chips with leads such as the QFP, PLCC, and SOIC are not suitable. Contradictory results were found in FEA and experimental tests regarding the effects of solder thickness on bond strength. Based on the experimental results, it is believed that the bond strength of thin joints is significantly affected by the strength of the intermetallic compound. Considering the brittle nature of the IMC in which cracks are more likely to initiate, and the plastic nature of tin-lead solder which would act as a crack stopper, when the joint is subjected to thermal-cycles, a certain thickness of solder in the joint is always necessary A compromised solder thickness in the range of 0.05 to 0.3 mm is suggested. Special attention should be paid to hand-soldering because in this process solder is applied at the top of the leads, whereas little or no solder is trapped in between the lead and the PCB pad, therefore there is always a danger of insufficient solder in the joint. The FEA found that, an introduction of a solder fillet can significantly increase the joint strength, and an increase in the solder thickness can only slightly increase the bond strength of a joint. Stress-strain analysis shows that a convex joint is only marginally more robust than a concave joint.

The two most commonly used soldering methods, WS and IR reflow, in SMT actually produce joints with geometries substantially different from each other. The uniformity of joints from IR reflow is much better, and they are usually concave in shape. For WS, the shape of an incoming joint may differ totally from that of an outgoing joint, depending on the orientation of the component relative to the assembly travel direction. A convex shape, which is the common shape of an outgoing WS joint, is undesirable from the quality point-of-view. It represents a joint not properly wetted, and contains more internal defects. For WS, if uniform joints over the ends of a leadless chip are desirable, the angle of entry of the component has to be controlled and should be taken care of at the PCB design stage. To obtain a reasonable uniformity, the pads for the components should be orientated as recommended in Fig. 5.1. Pull tests performed

on WS and IR joints drew no conclusion on which of the soldering methods produces stronger joints; it all depends on the component type. Internally, and under normal circumstances, little or no voids were found in WS joints. One of the factors determining the void content in an IR joint is the time the solder paste has been exposed to atmosphere before the solder paste is reflowed into solder. Both the IMC and solder in WS joints have hardness values higher than that of the IR joints. This difference is due to the difference in the heating history and void content of these two types of joints. From the fatigue reliability point-of-view, a concave shaped WS joint should be better than an IR joint.

The influence of the IMC layer on the quality of a solder joint has initiated the studies described in Chapter 7 of the thesis. The use of the EDX in an SEM system enabled more detailed studies of the compounds across the copper-solder interface. The thickness of each compound can be more accurately worked out based on the plot of composition against distance. The findings show no correlation between the solder paste exposure time and the resulting Cu/Sn IMC thickness Due to the fact that the temperature used for reflowing of 63Sn37Pb solder is low, and the reflow process takes place in a short time, the only IMC with a detectable thickness is the Cu_6Sn_5 The other IMC, Cu_3Sn, is virtually non-existent in an eutectic solder copper reflowed system. Since the formation of Cu_3Sn in the solid state is through diffusion of atoms, and occurs only at comparatively high temperatures over long times [104], and the service temperatures of SMT devices are usually below 120^0C, it is expected that Cu_3Sn compound would not form over the life time of the joints at all. The overall copper/solder interface and the Cu_6Sn_5 thicknesses of an IR joint both grow at elevated temperatures. It was found that at 100^0C, the overall interface thickness grew at a rate faster than that of the Cu_6Sn_5.

Investigation results show clearly that the characteristics of solder paste change with the solder paste's exposure Based on the solder paste used in this investigation, it was found that the resulting void content and void size, and the tackiness and rheology of solder paste, are all functions of the exposure time The evaporation of the low boiling point solvent is the predominant contribution to the change in the paste's characteristics. The weight loss due to solvent evaporation, which may be used as a measure of the degree of changes in the solder paste, can be expressed as Equation 6.1. It was found that the temperature and humidity affect

the evaporation rate of the solvent; and this would be reflected by the value of the constant 'a' in the equation. The other constant 'k' in the equation represents the total weight of the low boiling point solvent in the paste. To enable the calculation of the amount of solvent evaporated at a particular time of exposure, the manufacturer should provide both the 'a' and 'k' values of each solder paste. Exposure directly determines the size and amount of voids in the resulting joints. It was found that long exposure results in less and smaller voids. The decay in tackiness can be expressed as Equation 6.3. With reference to Fig. 6.7, this indicates that the tackiness of the solder paste falls dramatically in the first hour, and remains almost unchanged after two hours Purely from the tackiness property view point, one may conclude that it is best to perform the component placement as soon as possible. However, in manufacturing, due to machine layout or production schedule, immediate component placement after printing may not be possible If the 'a' and 'k' values in Equation 6.3 of a solder paste are provided, the customer can effectively work out an exposure time frame within which the tackiness still meets his requirements.

The change in the solder paste characteristics resulting from exposure changes the printability of the solder paste Different aperture fineness, or printing method, demands a solder paste with different rheology. Broadly speaking, stencil printing with fine apertures and screen printing require solder paste with low viscosity, low yield strength, and high thixotropic index. In a similar way to that suggested above, the solder paste manufacturer should also provide information about how the rheology of a solder paste would change with exposure time, based on which the user can optimise his printing operation. It was found that the loss of solvent imposes direct effects on the viscosity. There is an obvious trend that the longer is the exposure the more viscous the solder paste becomes. It is anticipated that the longer the solder paste has been exposed, the less suitable it is for fine stencil or screen printings. If the paste is left exposed to the atmosphere for too long the solder paste would dry-out completely and this definitely would result in printing defects. It is crucial for the supplier to provide a graph indicating the viscosity changes against exposure time, so that the user can make the choice accordingly. Other information which could usefully be provided is the exposure life of the paste to define the longest time that the paste can be exposed before it should be obsolete. It is suggested here that the exposure life of a paste is determined by the time over which 90% of the low boiling point

solvents have been evaporated. For the solder paste used in this part of investigation, it was found that it has a very short exposure life, which is approximately equal to two hours. This investigation shows clearly the thixotropic nature of solder paste. When plotted on a log-log scale, the viscosity decays linearly with shear rate for all exposures, as shown in Figs. 6.12a-i. There is no obvious indication that the thixotropic index of solder paste is being affected by exposure time. This implies that the sensitivity to shear rate or shear time of the solder paste more or less remains unchanged for all exposures, Fig. 6.13. In other words, the exposure time has little effect on the thinning rate of the solder paste. In addition, it was found that exposure lowers the non-recovery rate of the solder paste. Fig. 6.14 shows that the non-recovery rate R decreases rapidly in the first 40 minutes, and then becomes almost unchanged afterwards. A lowered non-recovery rate means that the ability of the solder paste to regain its viscosity after the removal of the shear is impaired. In a practical sense, this means that the ability of the solder paste to recover its viscosity after stopping stirring or printing is reduced.

Chapter 10

Further Work

10.1 RELIABILITY

IR reflow is the method used for soldering the majority of the SMT components on PCBs The research here discovered that joints produced by this method in fact contain a substantial void content Past data, especially that published by the International Tin Research Institute, has provided relatively detailed information about the properties and reliability of solder. However, the drawback of this data is that the effects of voids have not been taken into consideration. In service, SMT assemblies are continuously subjected to thermal fatigue. The temperature cycle may come from the power on/off, cyclic functioning, or change in environmental temperatures. This temperature cycle together with the thermal expansion mismatch of the materials involved generate a cyclic stress-strain pattern in the assembly. On rarer occasions, the assemblies may also be simultaneously subjected to vibrations. This stress-strain cycle, in most circumstances, is the factor determining the reliability of a joint. Empirical formulations were established for predicting the fatigue life of conventional solder joints. The most well known one is the Coffin-Manson equation [37,81,82]. The complexity of fatigue life prediction for IR joints is increased due to the presence of voids. To develop an analytical model for IR joint fatigue life prediction is almost impossible because of the large number of variables involved. However, an empirical approach is visualised as a viable alternative for establishing such a model. Here it is suggested that a conventional S-N curve approach is adopted. Specimens

used for the fatigue tests should contain different void contents, and the void content could be controlled by adding different amount of solvents to the solder paste, or, by exposing the solder paste to the atmosphere for different times. Shear or tensile specimens as shown in Fig. 10.1 can be used for carrying out these tests. Before every test, the void fractions must be measured quantitatively. It has been reported that S-N curves on log-log scale of conventional solder joints were straight lines [81]. Whether this trend would remain the same for IR reflow soldered joints is an area of investigation that should be performed. The aim of this proposed investigation is to establish a model expressing the fatigue lifetime (N_f) as a function of the cyclic stress (σ), temperature (T), and void volume fraction (v), as follows

$$N_f \quad f(\sigma, T, v)$$

To speed up the test, low cycle accelerated fatigue testing is considered adequate. Data extrapolation techniques can be used for predicting thermal fatigue life at higher number of cycles To simulate the service conditions better, stress cycling and temperature should be applied simultaneously This requires the fatigue tests to be carried out in a temperature controlled chamber

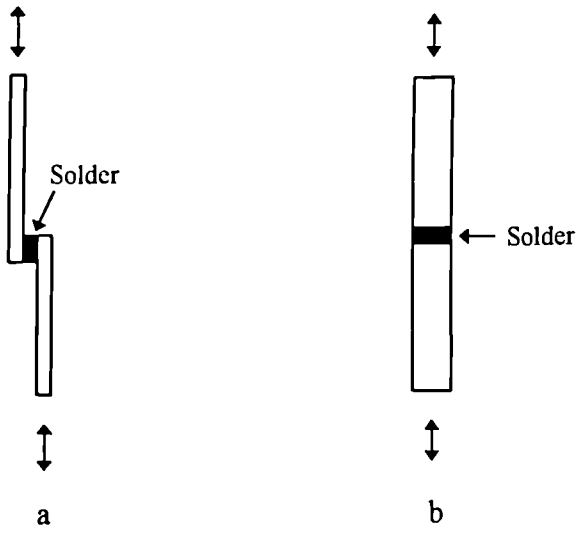

Fig. 10 1 Geometry of specimens for
a) shear fatigue test, and b) tensile fatigue test

10.2 PRINTABILITY

In the past, printing quality was understood mainly either from experience or from experiments. The theories behind have never been investigated in detail. Because of this, the ability of bringing the variables together so as to provide useful guidelines for setting up a quality print is very low. Since a printing operation is very deterministic in terms of the subsequent joint quality, there is a great demand to perform a more detailed theoretical analysis on this operation. The ultimate objective of this analysis is to develop a model so that the interrelations of the variables can be more fully understood, and also based on the developed model suitable printing parameters can be chosen for a particular application. Fig 10 2 is a schematic diagram representing the stencil printing operation. Assuming that in printing, the squeegee is inclined and fixed at an angle θ. The printing force F allows the squeegee to move forward at a speed V. At position A, which is any point on the squeegee in contact with the solder paste, a vector diagram A-B-C can be drawn. Vector AB is the printing energy per unit time, directly from the moving squeegee and is equal to F times V. In these circumstances, the vector AB would exert a couple of energy vectors onto the solder paste One is vector AC, which has an effect of pushing the solder paste downward through the stencil apertures forming the registrations on the PCB. It can be seen that vector AC cannot be too large or too small. If it is too large it may result in smearing, or if too small it may not allow the solder paste to go through the stencil apertures properly and result in skips, especially for fine apertures. Vector CB would have the effect of pushing the solder paste upward. Whether the solder paste would flow smoothly or not depends very much on the viscosity of the solder paste. If the solder paste is too viscous, the flow curvature may break down. Since solder paste is made up of loose particles, when it is being forced, just like the compaction process in powder metallurgy, a point that is closest to the force source would be subjected to the largest compaction value, say point A, and a point further away would be subjected to a lower compaction value, say point Z. The decreased force area value at a point away from the force source is a result of the weakened compaction energy which has to be transmitted through the particles. This results in the phenomenon that for more viscous solder paste, less volume of solder paste

would be sheared up forming the flow curvature. However, for less viscous solder paste, a larger volume of solder paste would be sheared up. If the solder paste has a high fluidity, at a particular squeegee angle and speed, a smooth curvature might not be formed at all, instead the entire solder paste surface would swell up in lump and move forward along the V direction. A solder paste flowing as lumps or in a broken down manner is undesirable. Since viscosity is defined as shear energy per unit time, it is expected that for a particular solder paste viscosity value, there should be an optimal set of θ and V values to give the best results in printing Developing the theory mentioned above, a model defined by the variables of F, V, θ, and the viscosity of solder paste for calculating suitable printing conditions can be produced

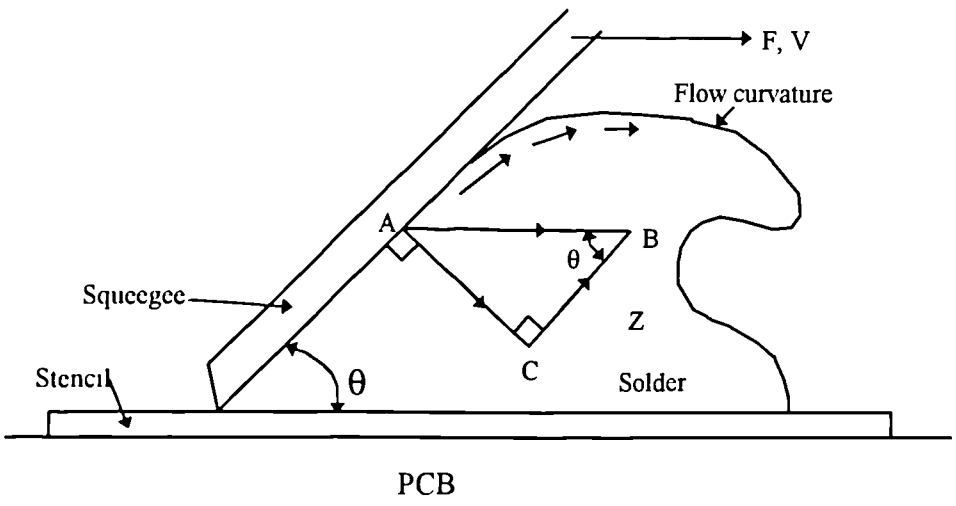

Fig 10 2 Schematic diagram of printing operation

Chapter 6 has looked at the solder paste rheology changes due to exposure. At the same time through interpretations of these changes the effects of exposure on printability of solder paste was understood indirectly. To supplement the work of Chapter 6, a direct measure of the effects of exposure on printability is considered necessary. Fig. 10.3 are patterns proposed for this measurement The patterns are designed to have varied aperture fineness and pitches, with the intention to provide as much printing quality information as possible. A sample of prints must be performed for each exposure. After printing, the

following information, or data, can be obtained:

- squareness of the print from sides and top;
- fineness of print;
- bridges and slumps;
- skips and scoops.

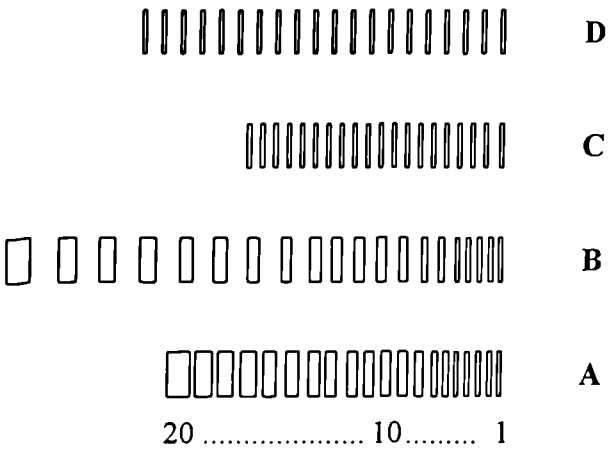

D — Constant Aperture · 0 8 mm
Constant Pitch : 0 3 mm

C — Constant Aperture . 0 8 mm
Constant Pitch : 0 2 mm

B — Increasing Aperture (mm) ·

0 3	0 4	0 6	0.7	0 8	1.0	1.1	1.2	1.4	1.5
1 6	1 7	1 9	2 0	2.1	2.3	2.4	2.5	2.7	2.8

Increasing Pitches (mm) :

0 3	0 4	0 5	0 55	0.6	0.65	0.7	0.75	0.8	0.9
0 95	1 0	1 05	1.1	1.15	1.2	1.3	1.35	1.4	

A — Increasing Aperture (mm) .

0 3	0 4	0 6	0 7	0 8	1.0	1.1	1.2	1.4	1.5
1 6	1 7	1 9	2 0	2 1	2.3	2.4	2.5	2.7	2.8

Constant Pitch : 0 3 mm

Fig. 10 3 Patterns for printability analysis

10.3 EXPOSURE

The results presented in Chapter 6 were based on one type of solder paste only. This solder paste was supplied by Multi-core. To increase further the confidence in the understanding of the effects of exposure established here, it is suggested that the same investigations should be performed on other solder pastes. Whether Equations 6.1 and 6.3 are applicable to other solder pastes and can be treated as generalised models, and whether the rheology changes discovered here would be the same for other solder pastes, all need to be verified The preload printed area ratio in the method used for measuring the tackiness here was chosen arbitrarily. It is obvious that different preload/printed area ratios would give different 'k' values in Equation 6.3. In view of this, work is recommended to standardise this ratio, so as to enable the use of Equation 6.3 for calculating the tackiness of different pastes, or paste under different conditions.

10.4 NEW APPROACH

The invention of SMT has given one big step forward to the miniaturisation of electronic packaging In the period from 1980 to 1990, this technology basically had been able to meet the interconnectivity needs of the electronics industry. However, the striving for miniaturisation is a continuous process; it does not stop at any particular stage. Since the start of this decade, SMT in many circumstances is unable to satisfy every requirement. The demands for miniaturisation very often require lead pitches to be less than 0.3 mm, and more components need to be placed in a given board area. Current SMT will find it increasingly difficult to deliver these requirements. Therefore, it is time to modify the current SMT process, so as to make it more capable.

Current SMT requires the printing of solder paste and the placement of components. It is these two operations which very often lower the quality consistency of the product Misprints are the most common defects found in printing, and the causes of these are numerous and difficult to control. Solder paste is complex, finding a suitable

solder paste for the job adds another dimension to the difficulties of producing quality prints. After printing, components have to be placed into position without deviations. The ever increasing component lead density actually imposes great difficulties in meeting this requirement. It is considered here that if these two operations can be eliminated or replaced the capability and yield of SMT can be largely improved. Fig. 10.4 represents an idea to modify the current SMT. Of course, its viability needs verification and further investigation. The primary difference of this proposition is that no solder paste is to be used, instead, the PCB pads on which the components are to be placed are pre-coated with a layer of solder. This solder coating technique is in fact available and being used for some PCBs nowadays, it is only that a thick layer of solder is necessary so to provide sufficient subsequent bonding To ensure that the component would sit squarely in position, it is suggested that the pre-coated solder is pressed to convert the curved surface of the solder into a flat one. Further, it is suggested that component leads are pre-coated with a layer of flux of a controlled stickiness, so that when they are placed in position they would stick to the PCB pads After the placement of the components, the whole assembly is then heated up to the required temperatures by reflow to produce the desired joints. The advantages of this proposed approach include.

1 solder paste is not used, so that material cost is reduced;
2 the solder paste degradation problem is completely eliminated;
3 the printing operation is removed, as a result the overall processing time is shortened;
4 variables and uncertainties in the printing and component placement operations of current SMT are removed so that better control is possible.

It is expected that the key to make this suggested approach successful depends on the development of a flux with suitable stickiness and viscosity, which can be coated onto the leads of components. The pressure to be used to convert the pre-coated solder into flat surfaces can only be determined by trial and error. As for the thickness of the solder pre-coat, that should be standardised after detailed investigations.

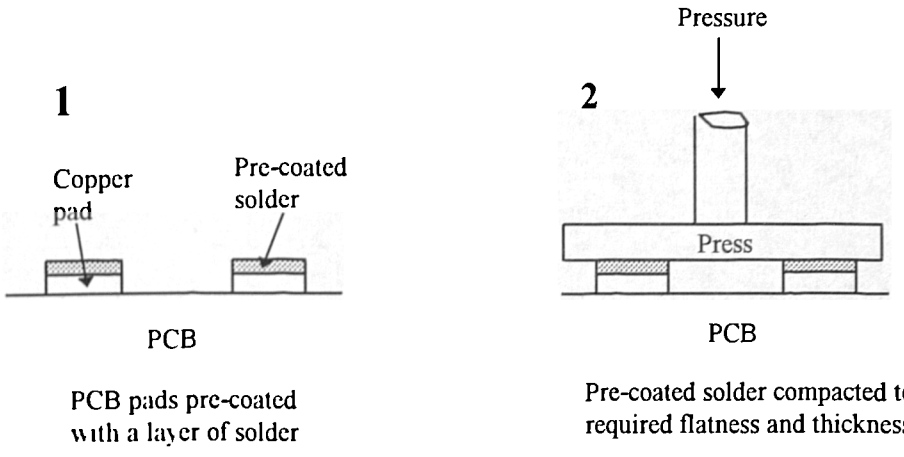

Fig. 10.4 Sequential diagrams showing the new approach

References

1. T. L. Landers, W. D. Brown, E. W. Fant, E. M. Malstrom, and N. M. Schmitt, Electronics Manufacturing Processes, Prentics Hall Inc.,1994.

2 C. F. Coombs, Jr , Printed Circuits Handbook, 3rd. Edition, McGraw-Hill, Inc. 1988.

3 A Stein, How to Choose Solder Pastes for Surface Mounting - Part 1, ELectronics, Vol. 31, No 6, June 1985, pp. 57-59.

4 P P Conway, D J Williams, A C.T. Tang, P. M. Sargent, and D. C. Whalley, Process Variables in the Reflow Soldering of Surface Mount, IEEE Cat. n. 90 CH2833-2, pp 385-394

5 R P Anjard, Sr , Quality Solder Paste Systems for Use in Microelectronic Applications, Solid State Technology, October 1983, pp. 183-189.

6 S W Hinch, Handbook of Surface Mount Technology, Longman Scientific & Technical, 1988.

7 K Hollomon, Jr , Surface-Mount Technology for PC Board Design, Howard W. Sams & Co. a Division of Macmillian Inc. 1989.

8 IPC-SM-782, Surface Mount Land Patterns, Lincolnwood, IPC, IL., April 17, 1987.

9 E A Kress, Solder Pad Geometry Studies for Surface Mount of Chip Capacitors, IEEE Trans on Components, Hybrids, and Manufacturing Technology, Vol. Chmt-8, No. 4, December 1985, pp. 505-509.

10. D. Elliott, How to Avoid Problems with Wave Soldering and IR Reflow, Surface Mount Technology, October 1989, pp. 47-54.

11. D Elliott, Wave Soldering Concerns for Surface Mount Assemblies, Circuit World, Vol. 15, No. 4, 1989, pp. 25-27.

12. J. S. Hwang, Solder Paste in Electronics Packaging, Van Nostrand Reinhold, New York, 1989.

13 W L. Archer, and T. D. Cabelka, Behavior of Rosin Fluxes and Solder Paste during Soldering Operations, Proceeding of the Technical Program, National Electronic Packaging and Production Conference, 1987, pp. 829-850.

14 B Gutllaume, J Guinft, and J. Hubert, Solder Paste Tackiness: The Influence of the Process Atmosphere and of the Test Method, IEEE/ISHM '90 Symposium, pp. 375-384

15 IPC-SP-819, General Requirements and Test Methods for Electronic Grade Solder Paste, IPC, Lincolnwood, IL., October 1988.

16 R P Prasad, Surface Mount Technology, Van Nostrand Reinhold, New York, 1989.

17 C Parekh, Quality of Solder Paste, Surface Mount Technology, Vol. 4, No. 4, April 1990, pp. 40 43-45

18 C.. A MacKay, Solder Creams and How to Use Them, Electronic Packaging and Production, Vol. 21, No. 2, February 1981, pp. 116-133.

19. J Tom, Solder Paste (English), Electronikcentralen (Report) ECR, No. 222, January 1989, pp. 1-65.

20. M. A. Stein, L. Spadafora, and D. Patel, Solder Paste: Powders Affect Performance, Circuits Manufacturing, Vol. 25, No. 11, November 1985, pp. 37-38, 40,42.

21. M. A Stein, Solder Paste for Reliable Surface Mount Assemblies, Hybrid Circuit Technology, Vol. 5, No. 9, September 1988, pp. 8-12.

22 J. W. Evans, and J. K. Beddow, Characterization of Particle Morphology and Rheological Behavior in Solder Paste, IEEE Trans. on Comp, Hybrids, and Manuf. Technology, Vol. Chmt-10, No. 2, June 1987, pp. 224-231.

23 M Warwick, and H Steen, The influence of Solder Powder on the Properties and Storage Performance of an RMA Solder Paste, Soldering and Surface Mount Technology, No. 9, October 1991, pp. 16-18, 24.

24 D H Daebler, Specifying solder Paste Materials for Stenciling Applications on Thick Film Circuits, Electronic Packaging and Production, April 1981, pp. 99-106.

25 B Roos-Kozel, Designing Solder Paste Materials to Attach Surface Mounted Devices, Solid State Technology, October 1983, pp. 173-178.

26 M L Martel, A Paste Primer, Circuits Manufacturing, Vol. 28, No. 4, April 1988, pp 54, 57,58

27 M A Stein, How to Choose Solder Pastes for Surface Mounting - Part 2, Electronics, Vol 31, No. 8, July 1985, pp. 28-32.

28 J S. Hwang, Considerations for Surface Mounting Solder Paste, Brazing and Soldering, No. 14, Spring 1988, pp. 13-21.

29 Z. D. Jastrzebski, The Nature and Properties of Engineering Materials, John Wiley, New York, 1977.

30. J. R. Morris, Jr., Solder Paste Tackiness Measurement, Brazing and Soldering, No. 14, Spring 1988, pp. 34-37.

31. H. W. Markstein, SMT - Meeting Requirements of Fine Pitch Printing, Electronic Packaging & Production, March 1993, pp. 34-39.

32 C Missele, Stencil Printing Solder Paste, Surface Mount Technology, Vol. 7, No. 4, April 1993, pp. 21-24.

33 J R Morris, Stencil Printing of Solder Paste for Fine-Pitch Surface Mount Assembly, IEEE Trans. on Components, Hybrids, and Manufacturing Technology, Vol. 14, No. 13, September 1991, pp 560-566.

34 S H Mannan, N N Ekere, I. Ismail, and E. K. Lo, Squeegee Deformation Study in the Stencil Printing of Solder Pastes, IEEE, Trans. on Components, Packaging, and Manufacturing Technology, Part A, Vol. 17, No. 3, September 1994, pp. 470-476.

35 S H Mannan, N N Ekere, E K. Lo, and I. Ismail, Predicting Scooping and Skipping in Solder Paste Printing for Reflow Soldering of SMT Devices, Soldering and Surface Mount Technology, No. 15, October 1993, pp. 14-17.

36 D Landis, and J. Notman, PWB Surface *Finishes for COB, Circuit World, Vol. 20,* No 2, 1994, pp. 5-7.

37 D R Frear, and F G. Yost, Reliability of Solder Joints, MRS Bulletin, December 1993, pp. 49-54.

38 D L. Linman, Vapour Phase Applications, Proceeding of the Technical Program National Electronic Packaging and Production Conf., by Cathen Exposition, Vol. 1, February, 1991, pp. 341-144.

39. R. K. Merle, Update: Vapour Phase Comes of Age, Circuits Manufacturing, Vol. 29, Part 3, March 1989, pp. 32-33.

40. J. Maxwell, Temperature Profiles: The Key to Surface Mount Assembly Process Control, Surface Mount Technology, Vol. 4, Part 7, July 1990, pp. 22-26.

41. C. L. Hutchins, SMT/FPT Soldering Problems and Solutions, Surface Mount Technology, Vol. 4, No 7, July 1990. pp. 37-40.

42 T J Beck, Surface Mount Soldering Techniques, Assembly Engineering, Vol. 30, No 5, May 1987, pp 40-42.

43 K Philip, Consistent Thermal Profiling: Meeting ISO 9000 Soldering Standards, Vol. 7, No 2, Feb 1993, pp 23-25

44 F J de Klein, Important Issues in Reflow Soldering, Soldering $ Surface Mount Technology, No. 16, February 1994, pp. 26-30.

45 M R Kalantary, F Sarvar, P. P. Conway, D. J Williams, and D. C. Whalley, Observed Phenomenology of the Interaction between Solder Paste and Soldering Processes, Soldering $ Surface Mount Technology, No. 18, October 1994, pp. 8-11.

46 N R Cox, Infrared Solder Reflow of Surface Mounted Devices, Hybrid Circuit Technology, March 1985, pp 37-41.

47 L Headrick, SMT Reflow· How to Select the Right Process, Surface Mount Technology, Vol 2, No. 5, October 1988, pp. 22-25.

48 A. C. T. Tang, and P. M Sargent, Differential Scanning Calorimetry Studies on Eutectic (Sn63 Pb37) Solder Paste and Powder for Surface Mount Technology, Electronics Letters, Vol. 27, No. 22, 24th October 1991, pp. 2018-2020.

49. C. Lowell, and J. Sterritt, Why reflow ? Circuits Assembly, October 1990, pp. 46-48.

50. R. M. Botham, R. A. Burke, C. R. Lowell, and J. R. Sterritt, SMT Wave Soldering Techniques, Proceedings of the Technical Program of the National Electronics Packaging and Production Conference - NEPCON WEST, Vol. 1, 1991, pp. 1717-1727.

51. W. H. Schwartz, Wave Soldering Roundup, Assembly Engineering, No. 2, 1989, pp. 23-25.

52. M. Judd, Electrovert, SM Wave Soldering - The Single Wave Solution, New Electronics, Vol. 20, No. 7, 31 March 87, pp. 22-24.

53. C. L. Hutchins, Reducing Wave Soldering Defects, Surface Mount Technology, Vol. 7, No. 9, September 1993. pp. 10-11.

54. G. Schouten, Wave Soldering of SMDs - A Smart Approach From Science to Practice, Circuit World, Vol. 14, No. 3, 1988, pp. 41-44.

55. W. Adamson, Physical Chemistry of Surfaces, John Wiley & Sons, Inc., 1990.

56. P. E. Liedtke, S. M. Heinrich, A. F. Elkouh, N. J. Nigro, and P. S. Lee, Prediction of Wave-soldered Fillet Geometry in SMT Applications, Manufacturing Processes and Materials Challenges in Microelectronic Packaging, Vol. 131, ASME 1991, pp. 65-72.

57. J. Clements, Tombstoning Prevention and Surface-Mount Production, Electronic Packaging and Production, Vol. 27, No. 4, April 1987, pp. 82-83.

58. D. Buckley, Surface Mount Forum, Electronic Production (London), Vol. 15, No. 4, April 1986, pp. 32-33.

59. B. R. Cobb, Tailor-Made Soldering, Circuits Manufacturing, Vol. 28, No. 7, July 1988, pp 52-56.

60. J. Guinet, X. Lambert, and D. Bono, Study of the Corrosivity of Solder Pastes, Soldering & Surface Mount Technology, No. 16, February 1994, pp. 11-14.

61. R. J. Klein-Wassink, and M.M. F. Verguld, Drawbridging of Leadless Components, Hybrid Circuits, No. 9, January 1986, pp. 18-24.

62. J. R. Ellis, and G. Y. Masada, Dynamic Behavior of SMT Chip Capacitors During Solder Reflow, IEEE Trans. on Components, Hybrids, and Manufacturing Technology, Vol. 13, No. 3, September 1990, pp. 545-552.

63. S. Liu, and Y. H. Mei, Effects of Voids and Their Interactions on SMT Solder Joint Reliability, Soldering & Surface Mount Technology, No. 18, October 1994, pp. 21-28.

64. W. B. Hance, and N.C. Lee, Voiding Mechanisms in SMT, Soldering and Surface Mount Technology, No. 13, February 1993, pp. 16-21.

65. D. J. Xie, Y. C. Chan, and I. K. Hui, Porosity Formation and Its Effects on Mechanical Properties of SMT Solder Joints, Proceedings of 44th IEEE Int. Conf. on Electronics Component and Technology, Washington D.C. USA, 1-5 May, 1994, pp. 590-595.

66. J. Barrett, C. O. Mathuna, and R. Doyle, Case Studies in Quality and Reliability Analysis of Fine Pitch Solder Joints, Soldering & Surface Mount Technology, No. 13, February 1993, pp. 4-11.

67. S. M. Heinrich, P. E. Liedtke, N. J. Nigro, A. F. Elkouh, and P. S. Lee, Effect of Chip and Pad Geometry on Solder Joint Formation in SMT, Trans. of the ASME, Journal of Electronic Packaging, Vol. 115, December 1993, pp.433-439.

68. N. J. Nigro, S. M. Heinrich, E. F. Elkouh, X. Zou, R. Fournelle, and P. S. Lee, Finite Element Method for Predicting Equilibrium Shapes of Solder Joints, Trans. of the ASME, Journal of Electronic Packaging, Vol. 115, June 1993, pp. 141-146.

69 J Hoyt, Influence of Leg Shape and Solder Joint Metallurgy on Surface Mount Solder Joint Strength, Brazing & Soldering, No. 13, Autumn 1987, pp. 10-19.

70 S P Hawkins, C J. Thwaites, and M. E Warwick, The Mechanical Properties of Soldered Joints to Surface Mounted Devices, Brazing & Soldering , No. 10, Spring 1986, pp 4-6

71 Y Nakaoka, J Hirota, and K Machida, Mechanical Properties of Solder Joints in Surface Mounting, 6th IEEE Chmt. Int'l Electron. Manuf. Technology Symp. 1989, pp 117-120.

72 E L Epping, MSC/NASTRAN Transient Thermal and Thermal Stress Analysis of a Surface-Mounted Chip Capacitor, MSC/NASTRAN Users' Conference, Los Angeles, CA, March 1986, pp. 21-35.

73 J H Lau, and D. W. Rice, Effects of Standoff Height on Solder Joint Fatigue, Proceedings of NEPCON, WEET 86, Anaheim, February 1986, pp. 437-454.

74. J H. Lau, D. W. Rice, and P. A. Avery, Elastoplastic Analysis of Surface-Mount Solder Joints, IEEE Trans. on Components, Hybrids, and Manuf. Technology, Vol. Chmt-10, No. 3, September 1987, pp. 346-357.

75. J. . Lau, G. Harkins, D. Rice, J. Kral, and B. Wells, Experimental Analysis of SMT Solder Joints Under Mechanical Fatigue, Proceedings IEEE 37th Electronic Components Conf., May 1987, pp. 589-597.

76. J. Lau, G. Dody, W. Chen, M. McShane, D. Rice, S. Erasmus, and W. Adamjee, Analytical and Experimental Studies of 208-pin Fine Pitch (0.5) Quad Flat Pack Solder-joint Reliability, Circuit World, Vol. 18, No. 2, 1992, pp. 13-19.

77 J H Huang, and H. Z. Li, The Influence of Metal Plating of Chip Carriers on Reliability of Solder Joints Under Thermal Cycling, Soldering & Surface Mount Technology, No 15, October 1993, pp. 18-20.

78 J H Huang, J Y Pei, Y. Y. Qian, and Y. H. Jiang, Life Prediction of SMT Solder Joints Under Thermal Cycling, Soldering & Surface Mount Technology, No. 16, February 1994, pp. 31-32, 50.

79 Z Guo, and H Conrad, Fatigue Crack Growth Rate in 63Sn37Pb Solder Joints, Trans of the ASME, Journal of Electronic Packaging, Vol. 115, June 1993, pp. 159-164

80 P M Hall, Solder Attachment of Leadless Ceramic Chip Carriers, Solid State Technology, March 1983, pp. 103-107.

81 J H Lau, and D W. Rice, Solder Joint Fatigue in Surface Mount Technology: State of the Art, Solid State Technology, October 1985, pp. 91-104.

82 W. Engelmaier, A reliability Test, A solder joint reliability test for actual use conditions, Circuits Manufacturing, June 1988, Vol 28, No. 6, pp. H2-H10.

83. R. Dudek, and B. Michel, Thermomechanical Reliability Assessment in SM- and COB- Technology by Combined Experimental and Finite Element Method, CH3332-4/94/0000-0458 IEEE/IRPS 1994, PP. 458-465.

84. P. Sarbach, L. Guerin, A. Weber, M. Dutoit, and P. Clot, Stress Analysis and Reliability of Chip On Board Encapsulation Technology, 1993 IEEE/CHMT Int'l Electronics Manufacturing Technology Symposium, pp. 82-86.

85 S Suresh, Fatigue of Materials, Cambridge University Press, 1991, New York.

86 M F. Ashby, and D R. H. Jones, Engineering Materials, Pergamon Press Ltd., England, 1980.

87 J Lau, T. Marcotte, J. Severine, A. Lee, S. Erasmus, T. Baker, J. Moldaschel, M. Sporer, and G Burward-Hoy, Solder Joint Reliability of Surface Mount Connectors, Journal of Electronic Packaging, Trans. of the ASME, Vol. 115, June 1993, pp. 180-188

88 S E Yamada, and Y Watanabe, The Inverted T-Joint for Surface Mount Connectors, IEEE Trans on Components, Hybrids, and Manufacturing Technology, Vol 13, No. 2 June 1990, pp 397-400.

89 L W Condra, G. M Johnson, M. G, Pecht, and A. Christou, Evalutation of Manufacturing Variables in the Reliability of Surface Mount Capacitors, IEEE Trans. on Components, Hybrids, and Manufacturing Technology, Vol. 15, No. 4, August 1992, pp 542-552.

90 T Yamada, J. Barrett, R. Doyle, and A. Boetti, Quality Optimisation of Fine Pitch Surface Mount Solder Joints Using Taguchi Experimental Design Techniques, Soldering & Surface Mount Technology, No. 16, February 1994, pp. 15-20.

91. H. N. Keller, Significant Features of Solder Connections to Gold-Plated Thin Films, IEEE Trans. on Components, Hybrids, and Manufacturing Technology, Vol. Chmt-5, No. 4, December 1982, pp. 408-419.

92 J Glazer, P. A. Kramer, and J. W. Morris, Jr., Effect of Gold on the Reliability of Fine Pitch Surface Mount Solder Joints, Circuit World, Vol. 18, No. 4, 1992, pp. 41-46.

93 C J. Thwaites, Some Metallurgical Aspects of SMD Technology, Brazing & Soldering, No. 10, Spring 1986, pp. 38-42.

94 C J Thwaites, Some Metallurgical Studies Related to the Surface Mounting of Electronic Components, Circuit World, Vol. 11. No. 1, 1984, pp 8-12.

95 J O G Parent, D D. L. Chung, and I. M. Bernstein, Effects of Intermetallic Formation at the Interface Between Copper and Lead-tin Solder, Journal of Materials Science, 23, 1988, pp 2564-2572.

96 L Quan, D. Frear, D. Grivas, and J. W. Morris Jr., Tensile Behavior of Pb-Sn Solder Cu Joints, Journal of Electronic Materials, Vol. 16, No. 3, 1987, 203-208.

97 P L Blum, J Pelissier, and G. Silvestre, An Investigation of Soldered Copper-Tin Bond Brittleness by Electron Microscopy, Solid State Technology, March 1973, pp. 55-59

98 S Kang, N. D. Zommer, D. L. Feucht, and R. W. Heckel, Thermal Fatigue Failure of Soft-Soldered Contacts to Silicon Power Transistors, IEEE Trans. Parts, Hybrids, Packaging, Vol. PHP-13, 1977, pp. 318-321.

99. H. N. Keller, Temperature Cycling of HIC Thin-Film Solder Connections, IEEE Trans. on Components, Hybrids, and Manufacturing Technology, Vol. Chmt-4, No. 1, March 1981, pp. 132-139.

100. D. Frear, D. Grivas, and J. W. Morris, Jr., Parameters Affecting Thermal Fatigue Behavior of 60Sn-40Pb Solder Joints, Journal of Electronic Materials, Vol. 18, No. 6, 1989, pp. 671-680.

101 D R Frear, and P. T. Vianco, Intermetallic Growth and Mechanical Behavior of Low and High Melting Temperature Solder Alloys, Metallurgical and Materials Transactions A, Vol 25A, July 1994, 1509-1523.

102 P T Vianco, P F. Hlava, and A. C. Kilgo, Intermetallic Compound Layer Formation Between Copper and Hot-Dipped 100In, 50In-50Sn, 100Sn, and 63Sn-37Pb Coatings, Journal of Electronic Materials, Vol. 23, No. 7, 1984, 583-594.

103 K N Tu, and R D Thompson, Kinetics of Interfacial Reaction in Bimetallic Cu-Sn Thin Films, Acta Metall., 30, 1982, pp. 947-952.

104 Z Mei, A. J Sunwoo, and J. W. Morris Jr., Analysis of Low-Temperature Intermetallic Growth in Copper-Tin Diffusion Couples, Metallurgical Transactions a, Vol 23A, March 1992, pp. 857-863.

105 K C Liu, J G Duh, Microstructural Evolution in Sn/Pb Solder and Pb/Ag Thick Film Conductor Metallization, IEEE Trans. on Components, Hybrids, and Manufacturing Technology, Vol. 14, December 1991, pp. 703-707.

106 T. Yamada, R. Doyle, and J. Barrett, Procedures for Metallographic Examination and Mechanical Strength Testing of Fine Pitch Surface Mount IC Package Solder Joints, Soldering & Surface Mount Technology, No. 19, February 1995, pp. 26-31.

107. Karlheinz G., S., and Manfred G, Methodology of Investigating Structural Modifications in Solder Joints of TAB Component, Prakt. Metallogr. 30, 1993, pp. 162-171.

108. J F. Lancaster, The Metallurgy of Welding Brazing and Soldering, George Allen and Unwin Ltd, London, 1970.

109 A Nadai, Theory of flow and fractures of solids, Vol. 2, McGraw Hill, New York, 1963.

110 I K Hui, and B. Ralph, A Study of the Initiation of the Tombstoning Effect on Leadless Chips, Int Journal of Machine Tools and Manufacture, Vol. 35, No. 9, pp. 1251-1268.

111 I K Hui, and B Ralph, A Study of the Effects of Solder Paste Thickness in SMT, Proceedings of the IEEE Third International Symposium on Consumer Electronics, Hong Kong, November 1994, pp. 405-410.

112 A G Guy, Physical Metallurgy for Engineers, Addison-Wesley Publishing Co. Inc., 1962

113 Manual of Malcom Viscometer

114 L Giovanni, Handbook of Printed Circuit Design, Manufacturing, Components and Assembly, Ayr. Scotland. Electrochemical, 1981.

115 AN1000 X-ray Analyser Operatior's Manual.

Appendix A

With reference to Fig. A1, due to the effects of the surface tension of the bubble, the pressure against the concave interface is greater than that of the convex. If the inside pressure is P_1 and the outside pressure is P_2, and the bubble has increased its radius by dr, then, the work done on the concave interface is

$$P_1 \; 4\pi r^2 dr$$

and the work done on the convex interface is

$$P_2 \; 4\pi r^2 dr$$

The difference in work done due to the pressure difference is balanced out by the increase in surface energy of the bubble, and is in the form of

$$(P_1 - P_2)\, 4\pi r^2 dr \quad d(A\gamma)$$

$$\Delta P \; 4\pi r^2 dr \quad \gamma \, dA$$

$$\gamma \, d(4\pi r^2)$$

$$-\gamma \, . \, 8\pi r$$

$$\Delta P \quad \frac{2\gamma}{r} \qquad \text{(A1)}$$

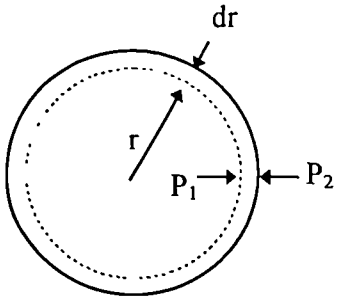

Fig. A1 Expansion of a spherical bubble

where γ is the surface energy per unit area (surface tension), A is the surface area, and ΔP is equal to $(P_1 - P_2)$.

Equation A1 shows that the smaller the bubble the greater is the pressure of the inside air compared to the outside. When two bubbles, one large and one small join together, the air from the smaller bubble will diffuse into the larger one.

Fig. A2 represents an arbitrarily selected curved surface. R_1 and R_2 are the radii of curvature perpendicular to each other. Now if the surface is displaced outward by an amount dz, the change in area will be

$$\Delta A \quad (x + dx)(y + dy) - xy$$
$$xdy + ydx$$

The work done in creating the additional surface is

$$w_1 \quad \gamma (xdy + ydx)$$

The work done due to the pressure difference across the surface (ΔP) moves the xy surface through a distance dz, and is

$$w_2 \quad \Delta P \, xy \, dz$$

Since, w_1 and w_2 are equal to each other, therefore

$$\Delta P \, xy \, dz \quad \gamma (xdy + ydx) \qquad (A2)$$

From a comparison of similar triangles, it follows that

$$\frac{x + dx}{R_1 + dz} \quad \frac{x}{R_1}$$

or

$$dx \quad \frac{xdz}{R_1} \tag{A3}$$

and

$$\frac{y + dy}{R_2 + dz} \quad \frac{y}{R_2}$$

or

$$dy \quad \frac{ydz}{R_2} \tag{A4}$$

Substituting Equations A3 and A4 into Equation A2, leads to

$$\Delta P \quad \gamma \left(\frac{1}{R_1} + \frac{1}{R_2}\right) \tag{A5}$$

Equation A5 is known as the Young and Laplace Equation of capillarity It can be seen that for a spherical surface R_1 is equal to R_2, in which case, Equation A1 and A5 will be identical

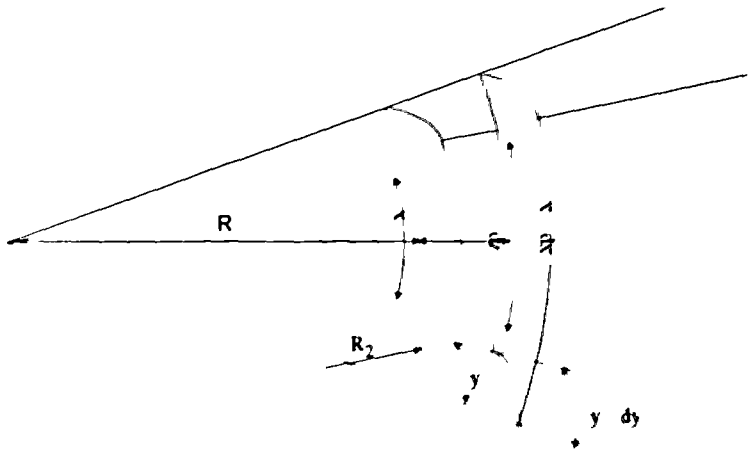

Fig A2 Equil brium c ndition of a curved surface

Appendix B

Temperature profile of boards for pulling test:

Preheat	Ramp-up	Lower Ramp-up	Forced air	Reflow	Lower Reflow	Belt Speed
330°C	310°C	300°C	190°C	355°C	340°C	9.2

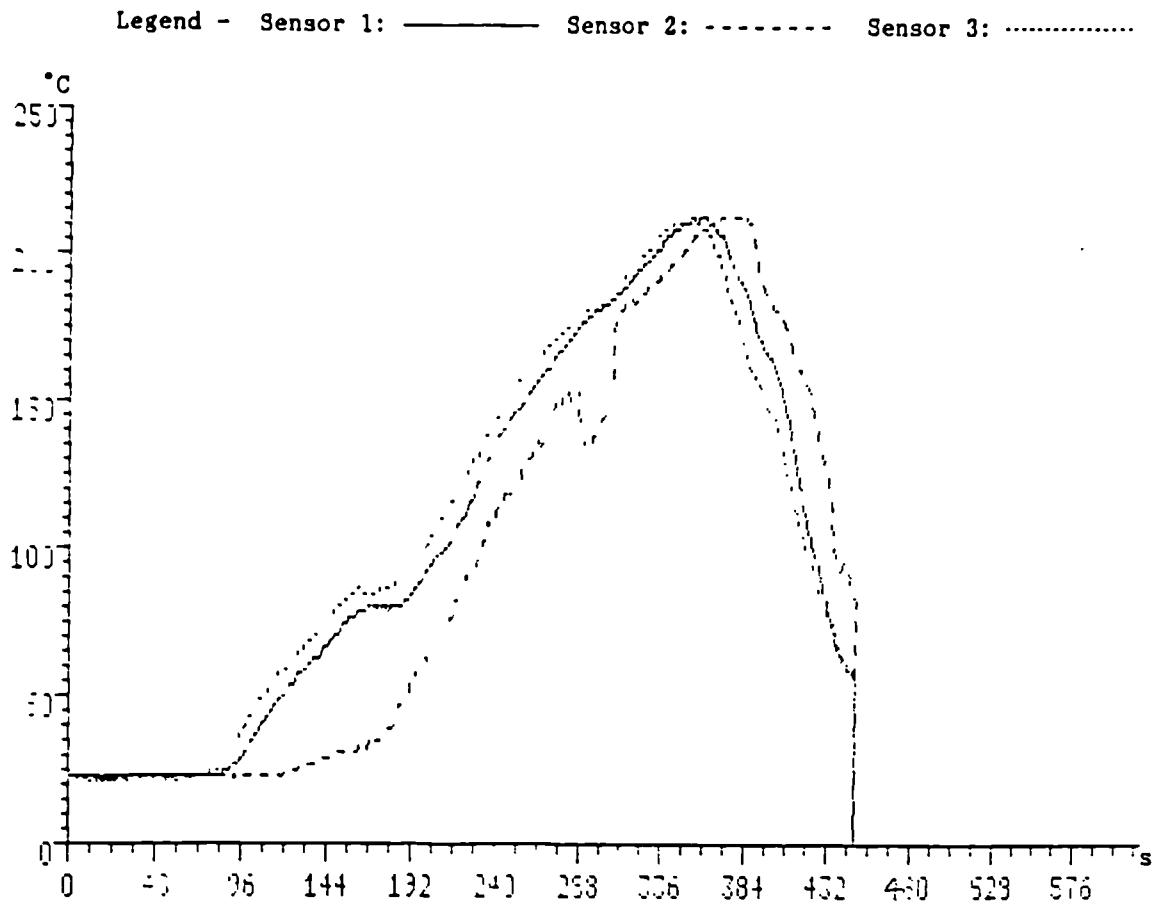

Number of readings - 1119
Interval between readings - 0.4s
Maximum internal temperature - 21C
Battery voltage - 8.6V
Maximum temperature on Channel 1 - 214C after 348s
Maximum temperature on Channel 2 - 214C after 364.8s
Maximum temperature on Channel 3 - 212C after 338.4s

Appendix C

Temperature profile for curing of SMD 881(Multicore):

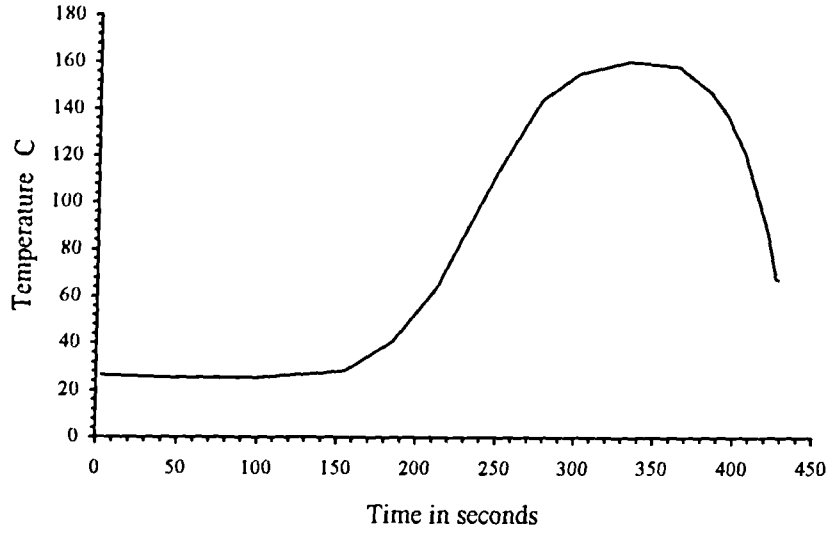

Appendix D

Chart for ARIES 300-C/SMT wave-soldering machine conveyor speed selection:

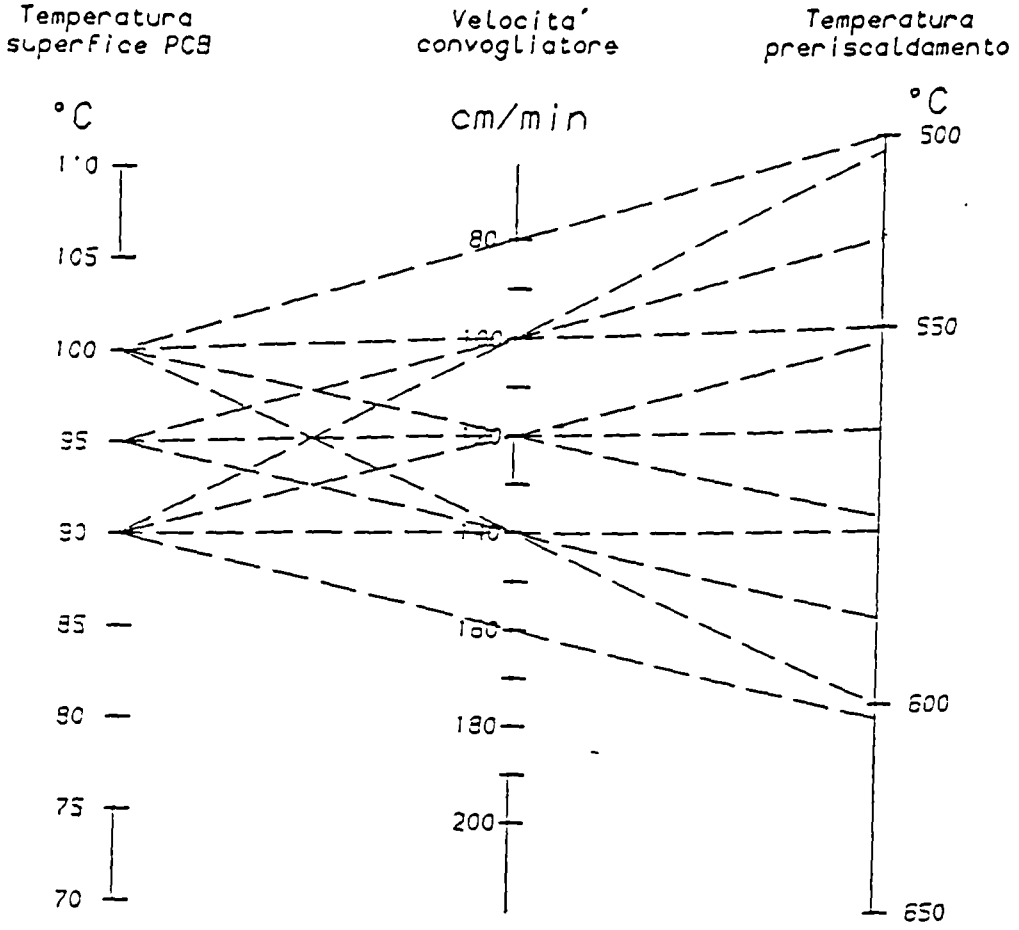

* *extracted from Catalogue*

Publications

1. **Hui I. K.** and **Ralph B.,** A study of the initiation of the tombstoning effect on leadless chips, International Journal of Machine Tools and Manufacture, Vol. 35, No. 9, Sep. 95, pp 1251-1268.

2 **Hui I. K.** and **Ralph B.,** Pulling strength and geometry of SMT leadless chip solder joints, Proceedings of the IEEE Int. Conf. on Industrial Technology, Guangzhou, China, 5-9 Dec 1994, pp 395-400.

3 **Hui I. K.** and **Ralph B.,** A study of the effects of solder paste thickness in SMT, Proceedings of the IEE Third International Symposium on Consumer Electronics, Hong Kong, 14-16 Nov 94, pp 405-410.

4 **Hui I. K.** and **Ralph B.,** A study of the strength and shape of SMT leadless chip solder joints, Journal of Engineering Manufacture, Proceedings of the Institution of Mechanical Engineers, Part B (accepted for publication).